UNIVERSITY OF WARWICK
EngD (International)

INNOVATION REPORT

Characterising the Effects of Vibration on the Durability of Electric Vehicle Batteries

James Michael Hooper

Student ID: 1360248

15th September 2017

This work is submitted in partial fulfilment of the requirements for the degree of Doctor of Engineering (International)

Abstract

Vehicle electrification is a technology pathway being adopted by original equipment manufacturers (OEMs) to either reduce or eliminate tailpipe emissions. However, electric vehicles (EV's) that employ a rechargeable energy storage system (RESS) still face significant barriers within the marketplace when compared to incumbent internal combustion engine (ICE) vehicle technology. One of these barriers is ensuring that the RESS lasts the life of the product or maintains customer satisfactory performance over a warranted life (such as 10 years or 100,000 miles of customer usage). There has been comparably little published research critically examining the effect of vibration on high voltage (HV) batteries within battery electric vehicles (BEV) and hybrid electric vehicles (HEV). Subsequently the effects of vibration on RESS components and subsystems are potentially a major cause of in market durability failures.

The following thesis presents the findings from an International Engineering Doctorate (EngD (int.)) investigating factors influencing the vibration durability of HV batteries and components. This research programme has the objective of providing the underpinning knowledge that allows manufacturers to improve the mechanical durability and performance of EV battery assemblies with respect to vibration.

This objective has been achieved through several novel studies within three primary areas of investigation. Firstly, the research focused on defining the "in-service" vibration environment of BEV components and assemblies through the analysis of vibration measurements from contemporary BEVs. This study was the first to synthesise a vibration profile that is representative of a durability life of 100,000 miles of UK customer usage from multiple real world BEV measurements. The presented profile can be employed by academics and engineers to underpin future vibration durability assessments of BEV battery components. The second avenue of investigation was to characterise the natural vibration and modal response of EV components and assemblies. This was to determine their susceptibility to vibration excitation, as identified from measurements of the in-service environment. It was also the first of its kind to fully characterise the natural vibration characteristics and mode shapes of lithium-ion pouch cells via modal analysis techniques. The final objective was to determine the durability behaviour of EV components and assemblies, by subjecting them to vibration, via state of the art single and multi-axis test techniques, which were the equivalent of a typical vehicle life (10 years) or customer mileage (100,000 miles). As well as defining the degradation characteristics of a contemporary BEV module and multiple EV cells, the impact of packaging variation and state of charge (SOC) on cell ageing was also determined.

In conclusion, this research thesis defines innovative testing techniques and characterisation data, which can be employed by engineers to predict the warranty performance, with respect to the effects of in-service vibration, of future EV battery assemblies.

Acknowledgements

I would like to express my sincerest gratitude to a number of individuals who have helped me over the past four years. Firstly I would like to thank my supervisor, Dr James Marco, for his advice and direction with the doctorate. At WMG I would also like to thank Mark Amor-Segan, Dr Yue Guo and Dr James Taylor for their expertise and advice on conducting my experimental research in a safe and professional manner. I would also like to thank fellow researchers Tom Bruen, Simon Brook, Phil Davies and Limhi Somerville for their friendship during the doctorate. I would also like to thank Tom and Limhi for allowing me to collaborate with them on projects investigating how vibration degraded cells can impact the battery management strategy of EV's and how the surface films of battery cells are impacted by vibration.

I would also like to acknowledge the generosity of HBM for the in-kind funding in the form of the nCode Glyphworks software which supported the analysis of electric vehicle vibration standards and the synthesis of the BEV vibration profile proposed in Chapter 3. I would also like to thank Mark Embra, Dr Andrew Halfpenny and Rob Plaskitt for helping me understand the theory behind the calculation of fatigue damage and shock response spectrum data.

At Millbrook Proving Ground, I would like to thank Julian Cantwell, Darren Williams, Simon Jenkins, Alan Smith, Lyndon Harris, Alan Thompson, Chris Felce, Mick Wood and Derrick Wiltshire for their support with the testing discussed in Chapters 5 and 6, and for the kind use of their facilities.

At Sound and Vibration Technology, I would like to thank Peter Holden and Richard Johnson for the kind use of the modal analysis equipment within the investigations presented in Chapters 4 and 6.

I would also like to recognise the support of Dr Gael Chouchelamane, Dr Chris Lyness, Jason Page, Shivali Pai, Julie Chevalier and Paul Haney at Jaguar Land Rover (JLR). I would also like to thank JLR for being the industrial sponsor of this research project and also for providing additional funding for the testing activities discussed in Chapters 5 and 6.

I would like to thank John Gaffey, Graham Cavendish and Howard Cross at Abtech Precision Engineering Ltd and Simon Hooper and Tom Busfield at Guttridge Ltd for the excellent service and delivery of machined and sheet metal fabrications for the test fixtures and rigs used within the studies presented in Chapters 5 and 6.

I would like to acknowledge that the research presented within this report was supported by the Engineering and Physical Science Research Council (EPSRC - EP/I01585X/1) through the Engineering Doctoral Centre in High Value, Low Environmental Impact Manufacturing.

Finally I would like to thank my Mum and Dad for all the love, encouragement and support they have given me over years.

Contents

Section **Page Nos.**

List of Figures

List of Tables

Nomenclature

Abbreviation / Nomenclature	Term
6DOF	Six Degrees of Freedom
ASTM	American Society of Testing and Materials
BEV	Battery Electric Vehicle
BMS	Battery Management System
BS	British Standard
CAE	Computer Aided Engineering
CC	Constant Current
CC-CV	Constant Current Constant Voltage
CID	Current Interruption Device
CT	Computerised Tomography
CV	Constant Voltage
DFT	Discrete Fourier Transform
DOD	Depth of Discharge
DOF	Degree of Freedom
DUT	Device Under Test
ECE	Economic Commission for Europe
ECM	Equivalent Circuit Model
EIS	Electrochemical Impedance Spectroscopy
EMS	Electro-Magnetic Shaker
EngD (int.)	International Engineering Doctorate
EOT	End of Test
EPSRC	Engineering and Physical Sciences Research Council
ERS	Extreme Response Spectrum
Euro NCAP	The European New Car Assessment Programme
EV	Electric Vehicle
FDS	Fatigue Damage Spectrum
FEA	Finite Element Analysis
FFT	Fast Fourier Transform
FRA	Frequency Response Analyser
FRF	Frequency Response Function
FT	Fourier Transform
GM	General Motors
g_n	Gravity (9.81 m/s)
GPS	Global Position Sensor
Grms	Root-Mean-Square Acceleration
GVW	Gross Vehicle Weight
HBM	Hottinger Baldwin Messtechnik GmbH
HEV	Hybrid Electric Vehicle
HSC	High Speed Circuit

HV	High Voltage
ICE	Internal Combustion Engine
ICEV	Internal Combustion Engine Vehicle
ICV	Internal Combustion Vehicle
IMechE	Institution of Mechanical Engineers
iMiEV	Innovative Mitsubishi Electric Vehicle
IP	Intellectual Property
ISO	International Organisation for Standardisation
ISR	Individual Sample Reference
JLR	Jaguar Land Rover
LCO	Lithium Cobalt Oxide
LDS	Ling Dynamic Systems
LFP	Lithium-ion Phosphate
LMO	Lithium Manganese Oxide
LTI	Linear Time Invariant
LTO	Lithium Titanate
MAST	Multi-Axis Shaker Table
MPG	Millbrook Proving Ground
MPH	Miles Per Hour
NCA	Nickel Cobalt Aluminium Oxide
NHTSA	National Highways Traffic Safety Administration
NMC	Nickel Manganese Cobalt Oxide
NVH	Noise Vibration and Harshness
OCV	Open Circuit Voltage
OEM	Original Equipment Manufacturer
PLC	Programmable Logic Controller
PLM	Polarised Light Microscopy
PSD	Power Spectral Density
PT	Part Throttle
R_{CT}	Charge Transfer Resistance
R_{DC}	DC Resistance
RESS	Rechargeable Energy Storage System
R_i	Relative Resistance
RMS	Root-Mean-Square
R_O	Ohmic Resistance
S&VT	Sound and Vibration Technology Ltd
SAE	Society of Automotive Engineers
SDOF	Single Degree of Freedom System
SEM	Scanning Electron Microscopy
SIMO	Single Input Multiple Output
SISO	Single Input Single Output
Smart ED	Smart Electric Drive
SOC	State of Charge

SOT	Start of Test
SRS	Shock Response Spectrum
SUV	Sports Utility Vehicle
UK	United Kingdom
UL	Underwriters Laboratories
UN	United Nations
USABC	United States Advance Battery Consortium
VAG	Volkswagen Audi Group
WMG	Warwick Manufacturing Group
WMG-MPG	Warwick Manufacturing Group - Millbrook Proving Ground
WOT	Wide Open Throttle
WVTR	Water Vapour Transmission Rate
X	X-Axis
X:X	Vehicle X Axis, Cell X Axis
X:Y	Vehicle X Axis, Cell Y Axis
X:Z	Vehicle X Axis, Cell Z Axis
Y	Y-Axis
Y:X	Vehicle Y Axis, Cell X Axis
Y:Y	Vehicle Y Axis, Cell Y Axis
Y:Z	Vehicle Y Axis, Cell Z Axis
Z	Z-Axis
Z:X	Vehicle Z Axis, Cell X Axis
Z:Y	Vehicle Z Axis, Cell Y Axis
Z:Z	Vehicle Z Axis, Cell Z Axis

Mathematical Notation

Symbol	Description	Unit
	Capacity	Ah
R_{CT}	Charge transfer resistance	Ω
R_{DC}	DC resistance	Ω
R_O	Ohmic resistance	Ω
R_i	Relative resistance	Ω
f_n	Natural frequency	Hz
ω_n	Natural frequency	$rads^{-1}$
C	C-rate	Ah
L	Length	mm
t	Temperature	°C
E	Young's modulus	GPa
K	Stiffness	Nm^{-1}
S	Stress	N/m^2
T	Time	Seconds
f	Frequency	Hz
ρ	Density	g/cm^3
ς	Damping coefficient	Nm/(rad/s)
ω	Frequency	$rads^{-1}$
$\sum_x$	Sum of all the data values	-
$C_{xy}(\omega)$	Coherence function	-
$G_{xx}(\omega)$	Auto-spectral density of x signal	-
$G_{xy}(\omega)$	Cross-spectral density between signal x and y	-
$G_{yy}(\omega)$	Auto-spectral density of y signal	-
x_k	A complex frequency-domain data set	-
x_n	A complex time-domain data set	-
$H(j\omega)$	System transfer function (frequency domain)	-
$H(s)$	System transfer function (Laplace domain)	-
$X(s)$	System input (Laplace domain)	-
$Y(s)$	System output (Laplace domain))	-
H_m	Hammer mass	kg
I_{max}	Maximum applied current pulse	A
N_f	Number of cycles to failure	-
V_{10s}	Voltage at the end of 10 second current pulse at I_{max}	V
V_{OCV}	Voltage prior to the application of maximum	V

	applied current pulse	
f_{max}	Maximum frequency	Hz
k_c	Cell stiffness	Nm^{-1}
k_p	Tip stiffness	Nm^{-1}
m_c	Cell mass	kg
$\Delta\omega$	Width of the range of frequencies for which the energy within the system output is at least half of its peak value	$rads^{-1}$
$A(f_n)$	Amplitude of the sine sweep at f_n.	g_n
BW	Bandwidth	Hz
C	Basquin coefficient	-
D	Total damage	-
$G(f_n)$	PSD of acceleration at f_n	g_n^2/Hz
N	Size of data sets	-
PSD	Power spectral density	g_n^2/Hz
Q	Quality-factor	-
b	Basquin exponent material parameter	-
n	Number of values	-

List of Equations

1 Introduction

1.1 Motivation for the Research

The automotive industry is under increasing pressure from political, social and economic factors to develop powertrain systems which continue to deliver improved vehicle performance and refinement whilst simultaneously offering a significant reduction in emissions and overall environmental impact [1].

Within the United Kingdom (UK), one of the chosen technology pathways to meet this environmental challenge is to reduce the consumption of liquid fossil fuels through the development of battery electric vehicle (BEV) and hybrid electric vehicle (HEV) powertrains [1]. These two approaches to vehicle electrification require a form of on-board rechargeable energy storage system (RESS). The current favoured method of electric vehicle (EV) RESS by original equipment manufacturers (OEMs) is the installation of large battery packs, assembled from modules of battery cells. Figure 1 presents the example of a Nissan Leaf RESS and Illustrates the assembly stages of cell, module and battery (pack).

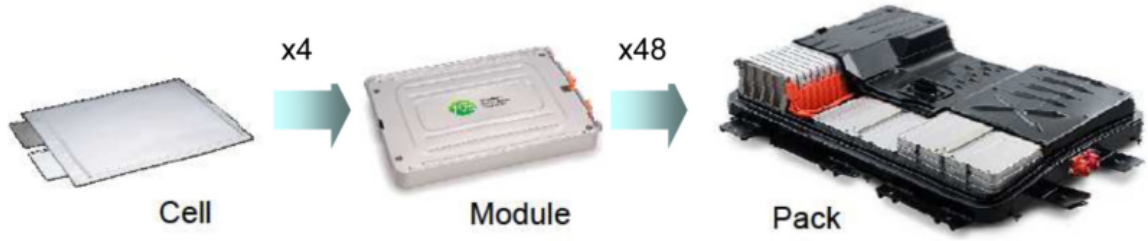

Figure 1: Stages of a Battery Pack Construction – Example Shown is the RESS from a 2012 Nissan Leaf [2]

To ensure in market reliability and safety of components and assemblies, it is often necessary for automotive manufacturers to obtain characterisation data from physical components, or to undertake “life representative” durability tests to ensure that they are fit for purpose. This warrants that any design or integration issues can be resolved prior to the release of the product to the public [3-5].

Within the context of cells utilised for the fabrication of EV battery assemblies and on-board energy storage systems, a significant body of research exists into mechanical characterisation of cells via physical “quasi-static” (a test where dynamic forces are assumed to be negligible and the desired test forces are applied at slow rates) and “dynamic” (a test where the forces are applied using accelerations representative of in-service conditions) techniques. These are often performed to provide baseline data to corroborate computer aided engineering (CAE) designs, concepts and simulations.

When critically reviewing the body of research relating to quasi-static testing, there has been a focus on obtaining cell material data such as mechanical strain and

bending [6-9], force displacement [6-10], creep [9] and tolerance changes during charge-discharge [11] on cylindrical, prismatic and pouch cell assemblies. There is also another large group of studies that have the objective of obtaining mechanical crashworthiness and robustness data (via both “quasi-static” and “dynamic” means) via methods such as mechanical crush [6, 10, 12], penetration [8, 13], impact resistance [6, 12], mechanical shock [6], degradation associated with climatic changes [14] and finally atmospheric pressure decompression for air transportation safety validation [15]. The need to conduct the latter group of studies has been driven by an industry need to meet whole vehicle crash homologation [16, 17], consumer focused accreditation (such as euro NCAP [18]) and mandatory shipping legislation (such as UN38.3 [19]). All of which, involve the compulsory evaluation of production intent EV battery assemblies. However these assessments are typically performed via CAE prior to physical certification to manage development costs and the need for expensive prototype assemblies.

With regard to “dynamic” testing which, is focused towards defining the mechanical durability and vibration response of cells, there is limited data that defines their behaviour or aging characteristics when subjected to the vibration energy levels experienced within a typical EV installation. A possible explanation why there is limited research data for this form of mechanical ageing is; that traditionally battery cells have been developed for applications where the product has a limited service life (such as 2 to 3 years) or the battery cells are consumer replaceable. Subsequently the device or batteries are exchanged before vibration has an effect [20]. For this reason, it has been unnecessary for battery cell suppliers to undertake expensive and costly vibration ageing studies to satisfy niche markets, which only until recent years has included EV’s [21]. Due to the limited knowledge within this area with respect to batteries aimed at an automotive application, manufacturers entering the EV marketplace face a significant challenge when trying to predict the durability performance of a given RESS to road induced vibration excitation. Therefore, the scope of this research is to create new experimental techniques and characterisation data to determine how vibration, that is representative of a desired durability life (such as 10 years or 100,000 miles), affects the performance of EV batteries.

1.2 **Research Objective and Aims**

The research objective of this doctorate is to provide knowledge that allows manufacturers to understand the mechanical durability and performance of automotive battery assemblies and their sub components, with respect to vibration.

To achieve this objective, the doctorate has three primary aims. Firstly, the research focuses on understanding the “in-service” vibration environment of EV components and assemblies through the analysis of vibration measurements from contemporary BEV products and current state of the art legislative and “best practice” test

standards. The second aim is to characterise the natural vibration and modal response behaviour of EV components and assemblies to determine their susceptibility to vibration. The final aim is to determine the durability behaviour of EV components and assemblies by subjecting them to vibration that is representative of a typical vehicle life or customer mileage.

1.3 The Sponsoring Company and their Relevance to the Direction of the Research

The direction of the research was considered from the perspective of the sponsoring company Jaguar Land Rover (JLR). JLR are the largest automotive manufacturer in the UK, specialising in the production of luxury saloons, sports utility vehicles (SUV) and sports cars. JLR products accounted for more than 30% of all domestic car production in 2016 and their product lines are among the top ten best-selling British manufactured vehicles [22, 23].

Like many of their competitors, JLR have been adopting a vehicle electrification strategy to help improve fuel economy and reduce exhaust emissions so that future homologation requirements can be achieved. This approach is evident with the launch of HEV variants of their Range Rover and Range Rover Sport models and the recently announced BEV Jaguar i-Pace [24, 25]. With any new product, JLR have to ensure the product is fit for purpose and will operate both reliably and safely in the marketplace. However, knowledge surrounding the mechanical susceptibility of battery cells, modules and assemblies with regard to road induced vibration inputs is limited within published industry and academic research [26]. Subsequently the prediction of in-market warranty faults of this new powertrain technology is of concern to the organisation.

Through experimental evaluation of battery cells and modules, this project quantified the vibration energy that a battery system will be exposed too over the warranty lives of 100,000 miles and 10 year customer use. In addition, new insights have been gained into the complex relationships between battery system vibration and performance degradation, failure modes and system efficiency. This research has focused on delivering testing solutions, methodologies and data that will help support the development of future electric JLR products and life-cycle warranty cost models.

Whilst this research has conducted experimentation on both pouch and cylindrical cells, its main focus has been on the definition of the vibration durability behaviour of 18650 lithium-ion cylindrical cells, as per the request of the sponsoring organisation. However much of the test methodology and safety protocols developed within this research program could be transferred to other cells forms and modules employed by JLR, in future validation activities. The presented experimental practises and characterisation data are also applicable to other organisations developing EV products or legal authorities defining new BEV vibration test standards.

1.4 Scope of Thesis

The scope of this thesis is towards providing knowledge of novel experimental methods which allow for the accurate characterisation of the effect of vibration on EV batteries. It also presents electromechanical data from battery cells and modules which have been exposed to vibration that is commensurate with European and North American operation, typical of 100,000 miles or 10 year customer operation. It identifies trends in battery performance resulting from vibration excitation; however it does not identify specific changes in material or chemical properties of the test samples.

It must be noted that within this thesis the term “durability testing” is used to describe a validation method which has been correlated to a pre-determined service life such as 100,000 miles or 10 years operation. It is a test that has the objective of understanding the performance of a component when subjected to “normal customer” daily operation [3, 27-29]. The term “robustness testing” is used to describe a test that is devised to assess a components integrity when subjected to a single abusive load case [30, 31]. This event may result in component replacement or vehicle loss. Examples of robustness load cases are; a vehicle crash event or an item being dropped from a significant height during shipping [31].

1.5 Summary of Innovation and Impact

The presented research “characterising the effects of vibration on the durability of EV batteries” has resulted in the following innovations.

Innovation 1: Defines a new vibration test profile and methodology for single axis testing which is representative of 100,000 miles of UK BEV durability.

Unlike contemporary standards this research programme has derived a vibration test profile from real world BEV measurements (presented in Chapter 3) and BEV customer usage data. Unlike current test standards, it is not excessively compressed with respect to time. Subsequently the presented profiles replicate the shock loading and fatigue damage, associated with 100,000 miles of UK customer driving. The derived profile and methodology employed to synthesise this new test method are published within [32-34].

Whilst developing the new test profile and testing methodology, a series of recommendations were also defined (in Chapter 2, Table 3), to improve the repeatability and accuracy of future EV test standards. These recommendations have been adopted by a number of organisations in the development of future vibration test standards and procedures, including JLR and National Highway Traffic Safety Administration (NHTSA). A significant number of these recommendations have been published within [32-34].

Innovation 2: Applied state of the art modal analysis testing techniques to mechanically characterise lithium-ion pouch cells and a contemporary battery module

The research has applied state of the art modal analysis testing techniques to the mechanical characterisation of lithium-ion pouch cells (presented in Chapter 4) and a Tesla model S module (presented in Chapter 6). This research has also defined the effect of SOC on the stiffness, damping, natural frequencies and mode shapes of lithium-ion pouch cells. The information from these studies has the potential to support future battery characterisation and simulation activities. It has also been utilised by JLR in the mechanical modelling of EV battery assemblies. These studies are the first to define the mode shapes, natural frequencies, stiffness and damping of EV RESS components via impact excitation modal analysis. It has also proven that this measurement technique can be applied to the assessment of pouch cells and battery modules. The results from the characterisation of the lithium-ion pouch cells are published within [35].

Innovation 3: Characterised the electromechanical changes within 18650 cells and a Tesla Model S module when exposed vibration that is representative of 100,000 miles / 10 years BEV service

This research programme has investigated the effect that vibration has on the electromechanical performance of two different lithium-ion chemistries of 18650 cells and a Tesla Model S module (presented in Chapters 5 and 6). Within these investigations, statistically significant electromechanical degradation from vibration applied via both uniaxial and multiaxial (in six degrees of freedom (6DOF)) techniques are quantified for both of 100,000 miles and 10 years of customer use. The effect of SOC and cell packaging orientation on the susceptibility of the 18650 cell form to vibration is also ascertained. As discussed within Chapter 2, prior to these investigations, published research has failed to correlate electrical and mechanical decay resulting from vibration excitation, in cells or modules, to vehicle mileage or time in service. The study presented in Chapter 6 is the first to characterise the effect of multi-axis vibration on 18650 cells and a contemporary BEV module. The results from the single axis studies have been published within [36-38].

Innovation 4: Defines novel vibration testing practices to allow for the safe and repeatable evaluation of battery cells and modules

As well as providing mechanical and electrical data on the effect that vibration has on cells and modules, this research programme has provided significant impact in the form of new experimental techniques. It has devised novel multi axis vibration durability processes for the evaluation of EV battery cells and modules. It presents repeatable test processes that can be employed by research and development engineers in future EV battery vibration durability studies. It has also identified industry best practice with regard to the design, fabrication and assessment of vibration fixtures, and applied these requirements to the construction of rigs for the vibration durability evaluation of battery cells and modules. It also identifies health and safety requirements for conducting high voltage battery vibration on modern

shaker table facilities and provides practical solutions to meet these considerations. Many of the testing practices developed during this research programme have been published within [32-40] and have been adopted by JLR.

In summary, these innovations are significant for both industry and academia as they have the potential to improve the safety, reliability and ultimately, the customer satisfaction of future EV products.

1.6 Structure of the Portfolio

This innovation report is derived from a series of research Submissions based on studies and investigations conducted during the tenure of the EngD (int.), which studied the effects of vibration on the durability of HV batteries. The portfolio structure is presented in Figure 2. The chronological order of the Submissions is not reflective of the structure of this innovation report. Therefore it is recommended that the portfolio supporting this thesis is reviewed in the order defined in Figure 2.

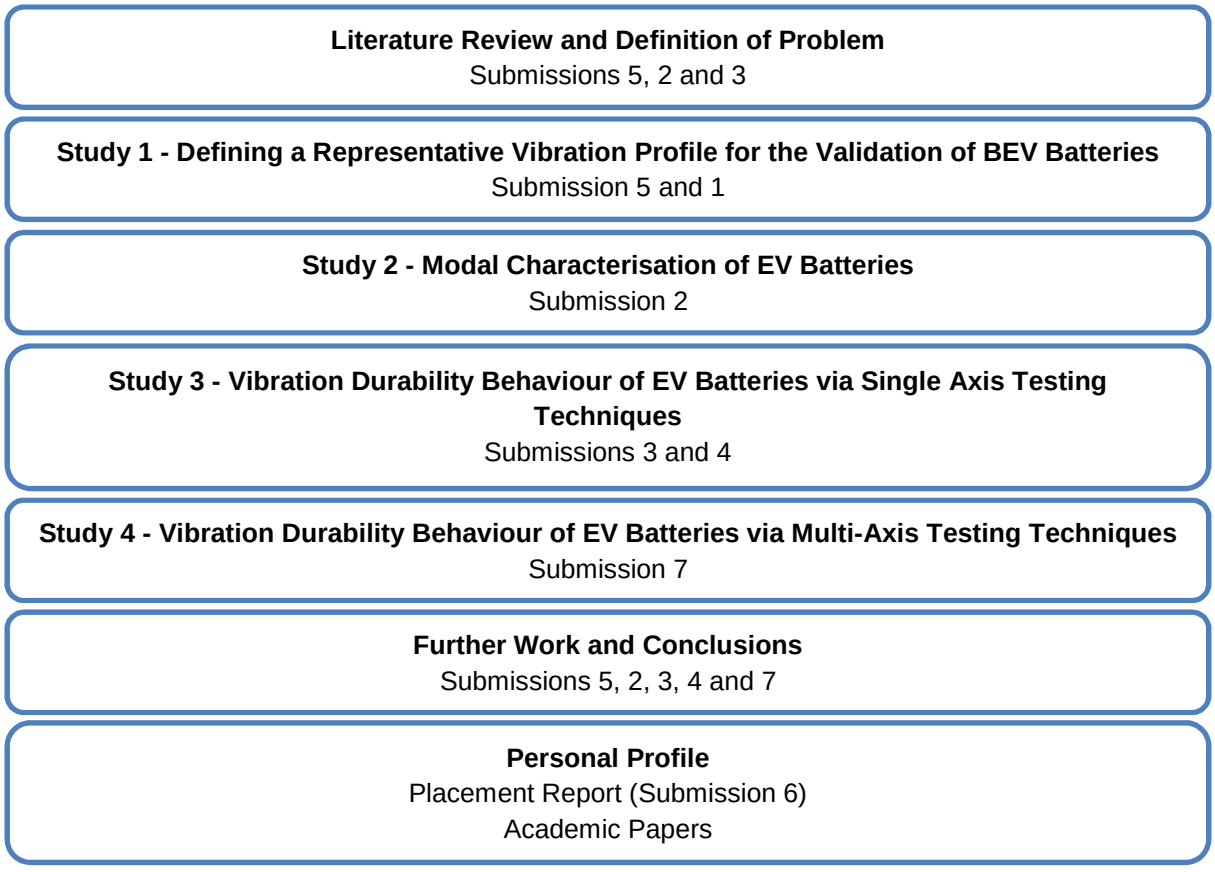

Figure 2: Portfolio Structure

The research within this EngD focused on the three key subject areas that define the vibration durability of components. These three influencing factors were; the definition of the vibration environment of EV batteries, so that a suitable vibration tests could be synthesised or selected, the definition of the natural vibration

characteristics of EV batteries so that the susceptibility of EV cells to vibration excitation could be quantified, and finally the determination of the effect of vibration on EV batteries. A definition of the problem and a critical review of the current research within each of these three subject areas are presented within Chapters of Submissions 5, 2 and 3 respectively.

Following the review of these Chapters, the first study investigating the vibration environment of BEV batteries and the development of a representative BEV vibration profile is defined in Submission 5. Theory supporting this investigation is presented in Chapters 4 to 5 of this Submission.

The author also recommends that Submission 1 is read following Submission 5. Submission 1 is a report that was written by the author on behalf of the NHTSA and Society of Automotive Engineers (SAE). This submission critically reviews a future EV RESS vibration standard to the vehicle measurement data discussed in Submission 5. However, due to confidentially agreements associated with this project, the assessment of this future unpublished procedure has been omitted from innovation report. Therefore submission 1 has been included within the portfolio as evidence of impact of the EngD to future legislation.

Following Submissions 5 and 1, the study investigating the natural vibration characteristics of EV battery cells, as well as the theory behind the measurement of automotive components via modal analysis is presented in submission 2.

Finally Submissions 3, 4 and 7 present innovative studies that investigate the effect that vibration has on the performance of lithium-ion 18650 cells and modules via single and multi-axis vibration testing techniques.

Other Submissions to the portfolio include all assignments from the six modules undertaken, the international placement report (Submission 6), published journal and conference papers from this research project [32-40] and copies of certificates from training courses and professional accreditation from the Institution of Mechanical Engineers (IMechE). A summary of the main competencies developed or enhanced through the activities and research completed with the EngD(int.) is also presented in the personal profile.

1.7 **Structure of the Innovation Report**

This thesis defines the research undertaken and demonstrates the connection between projects that have all contributed to the requirements of the Engineering Doctorate.

Chapter 2 critically reviews the current state of the art with regard to previous research that has investigated the vibration robustness of EV components. This review focuses on three classifications of EV vibration literature. Firstly it defines and analyses studies that have attempted to define the vibration environment of EV batteries and assemblies. It also defines and critically reviews current vibration standards available to engineers for the validation of EV components. Chapter 2

continues to outline research that has investigated the natural vibration characteristic and natural frequencies of EV components. Finally it presents research that has investigated the effect of vibration on EV batteries. Chapter 2 concludes by presenting limitations and research gaps within the current published literature.

Chapter 3 defines the process taken to synthesise a random vibration profile for the assessment of RESS on modern shaker table systems. A BEV vibration profile for the three main axis of the vehicle is subsequently presented. The defined profile is representative of 100,000 miles of UK customer usage and is created from real world BEV measurements. The shock and fatigue loading of this derived profile is compared to contemporary EV vibration standards (as defined in Chapter 2). Limitations with existing vibration test methodology when compared to measurements from the operational environment of BEV batteries are presented. This Chapter concludes with recommendations for future researchers on how to develop and conduct EV vibration tests which have a higher degree of correlation to the in-service environment and can be conducted in a more repeatable manner.

Chapter 4 presents a novel study to define the natural vibration characteristics of lithium-ion pouch cells using contemporary modal analysis testing practices. It outlines the test methodology, test considerations and theory associated with this testing technique. It presents the results of the modal analysis investigation on 15 samples of lithium-ion polymer pouch cell and identifies the effect that SOC has on the stiffness, damping and natural frequency response of this cell type.

Chapter 5 defines the effect that vibration which is representative of 100,000 miles of customer usage has on the ageing of two chemistries of 18650 cylindrical cells. The studies presented within this Chapter apply vibration using single axis vibration durability testing techniques and employ the test profiles identified or developed within Chapter 3. As well as presenting a new vibration durability test methodology, it defines the effect that vibration has on the impedance, capacity, open circuit voltage (OCV) and mechanical characteristics of the cells. The statistical significance of the effect of vibration is determined and the impact of cell orientation and SOC on the witnessed degradation is also established.

Chapter 6 introduces an innovative vibration study on 18650 Nickel Manganese Cobalt Oxide (NMC) cells and a Tesla Model S module via state of the art multi axis vibration durability testing techniques and real world vibration measurements applied to the test items in the time domain. This Chapter presents the test method and test requirements developed for this study.

The effect of vibration that is representative of 10 year European customer usage is presented and the impact of the vibration on the test items electromechanical performance is corroborated with statistical analysis to 95 % certainty.

Chapter 7 confirms the innovation and discusses areas of further work with regard to the definition of vibration durability of high voltage batteries. Finally Chapter 8 presents a summary and the conclusions from this research project.

2 Literature Review

2.1 Introduction

This literature review assesses the published research in the three areas that define the impact of vibration on EV RESS (as illustrated in Figure 3). Firstly, it outlines and evaluates studies which have defined the vibration environment that EV batteries are exposed to prior to defining the current state of the art with regard to vibration test procedures. It identifies research that has investigated the natural vibration characteristics of EV batteries. It also discusses the current state of the art with respect to studies investigating the effect of vibration on EV batteries, modules and cells. Subsequently this chapter identifies gaps within the current published knowledge and distinguishes areas for further investigation within these three research subjects.

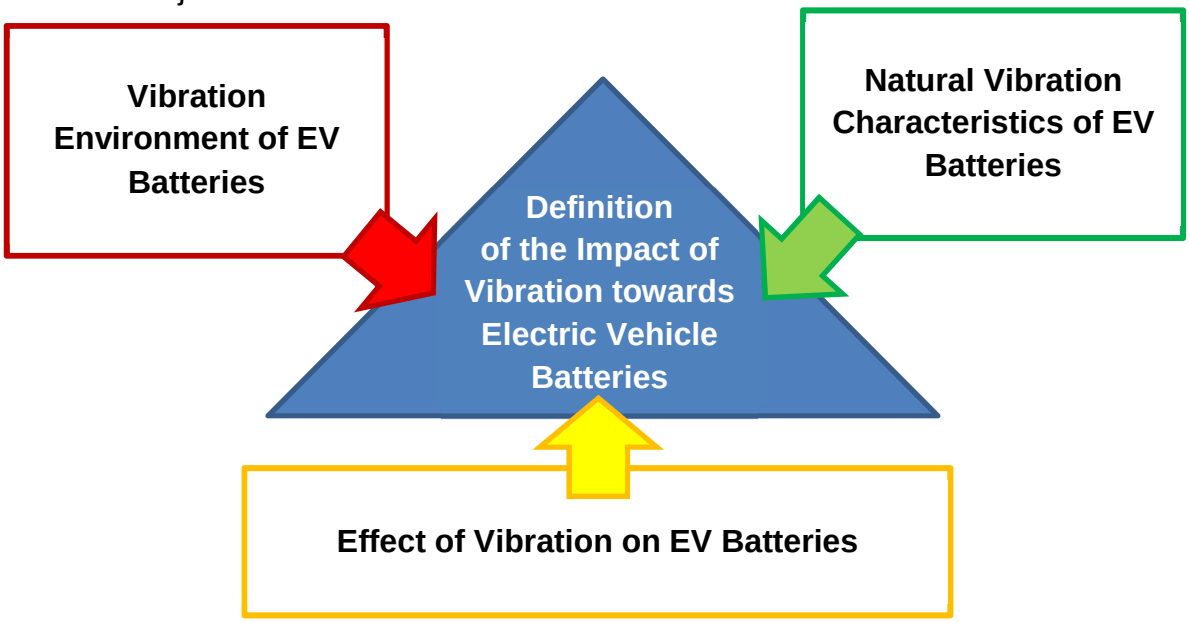

Figure 3: Illustration of the Three Areas which Define the Vibration Robustness of Electric Vehicle Components

Throughout this thesis the Society of Automotive Engineers (SAE) J670e (as presented in Figure 4) is used to define the axis convention for the vehicle measurements and presented vibration profiles.

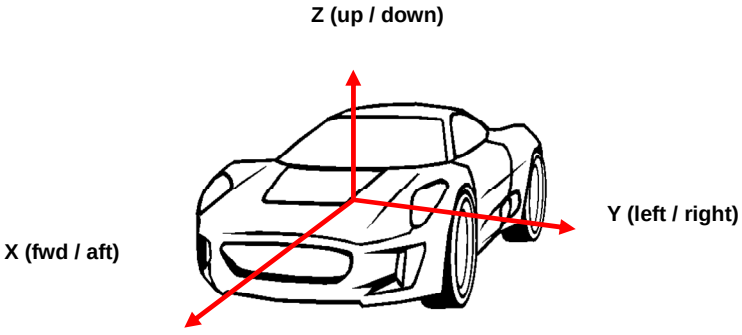

Figure 4: Vehicle Axis Convention in Accordance with SAE J670e [36, 41]

2.2 Critical Review of Vibration Test Standards of EV Batteries and Literature Investigating the Vibration Environment of RESS

The current state of the art vibration tests, which have been developed specifically for the assessment of EV RESS, are defined and analysed. Prior to the critical review of established standards, the theory behind the types of vibration profile within these standards is presented. Finally, existing research with the objective of defining the vibration environment of EV batteries is also critiqued.

2.2.1 Introduction to the Types of Vibration Profiles within Standards

Vibration can be measured in the "real world" and then replicated using shaker systems in a laboratory [42]. Whilst vibration measurements can be reproduced in the time domain on a shaker system, test standards typically specify tests that are applied to the DUT in the frequency domain for purposes of standardisation and repeatability. There are typically two categories of frequency domain vibration profiles suitable for the assessment of components fitted to wheeled road vehicles; they are sinusoidal vibration and random vibration.

2.2.1.1 Sinusoidal Vibration

Typically, sine waves are defined by a frequency or frequency range in Hz and acceleration. The acceleration is defined with respect to the gravitational constant g_n ($9.81ms^{-1}$). With sinusoidal tests, both the frequency and acceleration can vary with time. A common sine vibration test is to sweep from a low to a high frequency with fixed or varying acceleration [43]. The speed that a sine wave can change in frequency is defined by a sweep rate. This can be either a linear sweep rate that is expressed in Hz / second or a logarithmic sweep defined in octaves / minute [42]. An octave / minute sweep has the advantage of applying the same number of sinusoidal cycles per frequency. However, sinusoidal vibration profiles do not represent accurately the in-service vibration witnessed by chassis mounted automotive components [42, 43]. However, they are often used for simple robustness evaluations at fixed frequencies or via resonance dwell (where the test purposely tracks and excites the natural frequency of the test item to determine its resistance to fatigue when forced into a resonance condition).

2.2.1.2 Random Vibration

For a more realistic simulation of a real life automotive environment, engineers can choose to apply a broad band random vibration to a test item which is controlled to predetermined criteria to ensure test repeatability. Random vibration is defined as noise whose instantaneous amplitude is not specified at any instant of time [44]. A true random signal will have a frequency content that varies in acceleration and never repeats with time. It could therefore be said that; unlike a swept sine test, which influences individual frequencies, a random vibration test will influence many frequencies simultaneously. Because random vibration excites a defined band of frequencies, resonant frequencies within the item under evaluation are excited

regularly and together, subsequently causing interactions which typically would not occur within a sine vibration test [42]. Random vibration testing is also more representative of road surface induced vibration phenomena on wheeled vehicles and therefore are more desirable for accelerated life testing of chassis mounted automotive components [42]. In simple terms, random vibration profiles are generated via applying a fast Fourier transform (FFT) to the measured vibration signal to convert it from the time domain to the frequency domain. The process of synthesising a random profile is discussed in greater detail in Section 3.3.

To reproduce a random signal on a shaker table it is necessary to define parameters that are representative of the operational environment of the item. The profile itself must also replicate the vibration energy within the frequencies witnessed within service. Random test profiles are defined as amplitude against frequency which will have an upper and lower frequency restriction (such as 5 Hz to 190 Hz).

With random vibration profiles, because the acceleration is applied over a spectrum of many frequencies, the level is expressed as the quantity of g_n rms^2 in a 1 Hz bandwidth or $g_n rms^2$/Hz [44]. However, within test standards it is more commonly expressed as g_n^2/Hz. The unit of g_n^2/Hz describes the average power seen in a 1 Hz bandwidth, i.e. the power spectral density (PSD). The area below the curve is the energy content of the test profile and is a combination of an average level over the test bandwidth and represents the g_n rms or more commonly referred to as the Grms. The Grms can be calculated using equation 1 where the bandwidth in Hz is defined by BW and the g_n^2/Hz value by PSD.

$$Total\ Grms = \sqrt{BW \times PSD}$$

Equation 1

It must be noted that whilst the Grms level can be an indication of the severity of the test profile, it cannot be used as a comparative measure of how aggressive a random test is against another. This is illustrated in Figure 5 where a simple test profile that requires 2.0 g_n^2/Hz to be applied to the device under test (DUT) over a bandwidth of 10 to 20 Hz, has the same Grms value (4.471 Grms) to a profile that requires 0.5 g_n^2/Hz to be applied over a bandwidth of 120 Hz to 160 Hz [45].

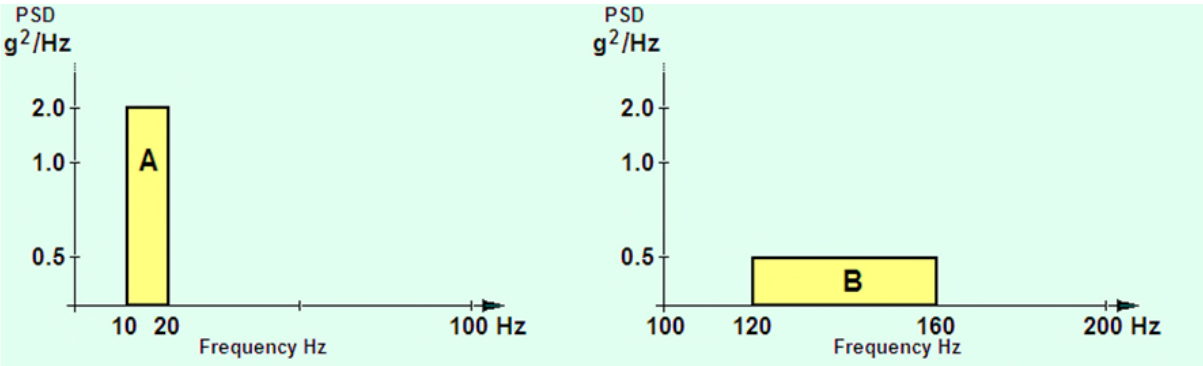

Figure 5: Example Showing Two Different Vibration Test Spectra with Same Grms [44]

The example shown in Figure 5 highlights that the frequency content is a significant factor in understanding the test profile severity [45].

2.2.2 Existing Vibration Standards for the Evaluation of EV Cells and Battery Assemblies

In this section, current vibration standards available for the validation of lithium-ion EV cells and battery packs in the context of RESS durability are defined. Whilst twenty-three standards were identified that are currently in use for the validation of passenger vehicle EV cells, modules and packs, many of them referenced other vibration standards. Therefore, this review has been rationalised to nine key test procedures. Table 1 presents these nine procedures and the associated standards, whilst Figure 6 and Figure 7 illustrate the profiles contained within these specifications. Whilst it is acknowledged that other vibration standards exist which could be employed to validate the resistance of RESS to mechanical excitation (such as MIL-810-F, DEF STAN 0035 or ISO-16750-3), these have been omitted, as they have not been specifically developed for battery systems.

All EV RESS vibration standards apply component excitation via either a sinusoidal or random vibration methodology. These test standards are divided into two classifications of: duty of care and legislative. Duty of care standards have no legal mandatory requirement associated with their application to validate the performance of a given automotive component or vehicle. It is at the manufacturers discretion to request that these tests are included as part of a design validation program. These standards are often referred to as “voluntary” within text books and academic studies.

Legislative standards are typically associated with vehicle and component certification or homologation programs, such as European Type Approval. Examples of these classifications of standards within the vibration testing of RESS are UN38.3 Test 3, ECE R100 and AIS-048. It is a legal necessity for these standards to be performed and passed during the product development programme prior to the legal authority being granted for a given market, region or application.

Table 1: Summary of Test Standards [17, 19, 46-69]

Specification / Standard	Type of Vibration Test	Other Standards Referencing this Specification	Application Level	Test Axis	Test Frequency Range (Hz)	Peak g_n	Voluntary or Legislative Requirement	Profile Created From EV Data?	Durability Test or Robustness Test?
UN38.3 – Test 3	Swept Sine	BATSO 01 (UN38.3 – Test 3 Revision 4) IEC62133 - Pack Testing IEC 62281 J2929 NEMA / ANSI C18.2m-Part 2 – 2007.	Cell, Module and Battery Assembly	X, Y and Z Axis	7 to 200 Hz	8 g_n (50 to 200 Hz) for Small Cells or Battery Assemblies 2 g_n (25 to 200 Hz) for Large Battery Assemblies	Legislative	No – Based on Aircraft Data	Robustness
USABC Procedure 10	Choice of Swept Sine or Random	SAND 123 SAEJ2380 UL2580	Module and Battery Assembly (However also in use as a Cell Assessment Specification)	X, Y and Z Axis	10 to 190 Hz	0.1 $(g_n)^2$/Hz at 10 Hz to 20 Hz or 3 g_n from 10 to 20 Hz	Voluntary	Evidence to Suggest Generated from Lead Acid EV Data	Durability – 100,000 miles
ISO12405	Random	None at time of writing	Module and Battery Assembly	X, Y and Z Axis	5 to 200 Hz for part 1 and 10 to 2000 Hz for part 2	0.06 $(g_n)^2$/Hz at 10 Hz to 20 Hz for test 1 and 2.05 $(g_n)^2$/Hz at 10Hz or test 2	Voluntary	No	Robustness
ECE R100 – Appendix 8a	Swept Sine	None at time of writing	Battery Assembly	Z Axis Only	7 to 50 Hz	1.02 g_n from 7 to 18Hz	Legislative	No	Robustness
GB/T31486-2015	Swept Sine	None at time of writing	Battery Assembly	Z Axis Only	10 to 55 Hz	3.05 g_n from 10 to 55 Hz	Legislative	No	Robustness
India AIS-048	Swept Sine	None at time of writing	Module	Z and Y Axis Only	30 to 150 Hz	3 g_n from 30 to 150 Hz	Legislative	No	Robustness
UL1642	Swept Sine	UL2054 IEC62133 – Cell testing	Cell	X, Y and Z Axis	10 to 55 Hz	4.87 g_n at 55 Hz	Legislative (Voluntary for Automotive Cells)	No - Consumer Electronics	Robustness
UL2271	Swept Sine	IEC61959	Cells and Battery Assemblies (Less than 60 V)	X, Y and Z Axis	10 to 500 Hz	5.09 g_n from 85 to 500 Hz	Voluntary	No	Robustness
BS62660	Random	ISO12405 – uses BS62660 for Part 2 of its Vibration Validation.	Cell	X, Y and Z Axis	10 to 2000 Hz	2.05 $(g_n)^2$/Hz at 10 Hz	Voluntary	No	Robustness

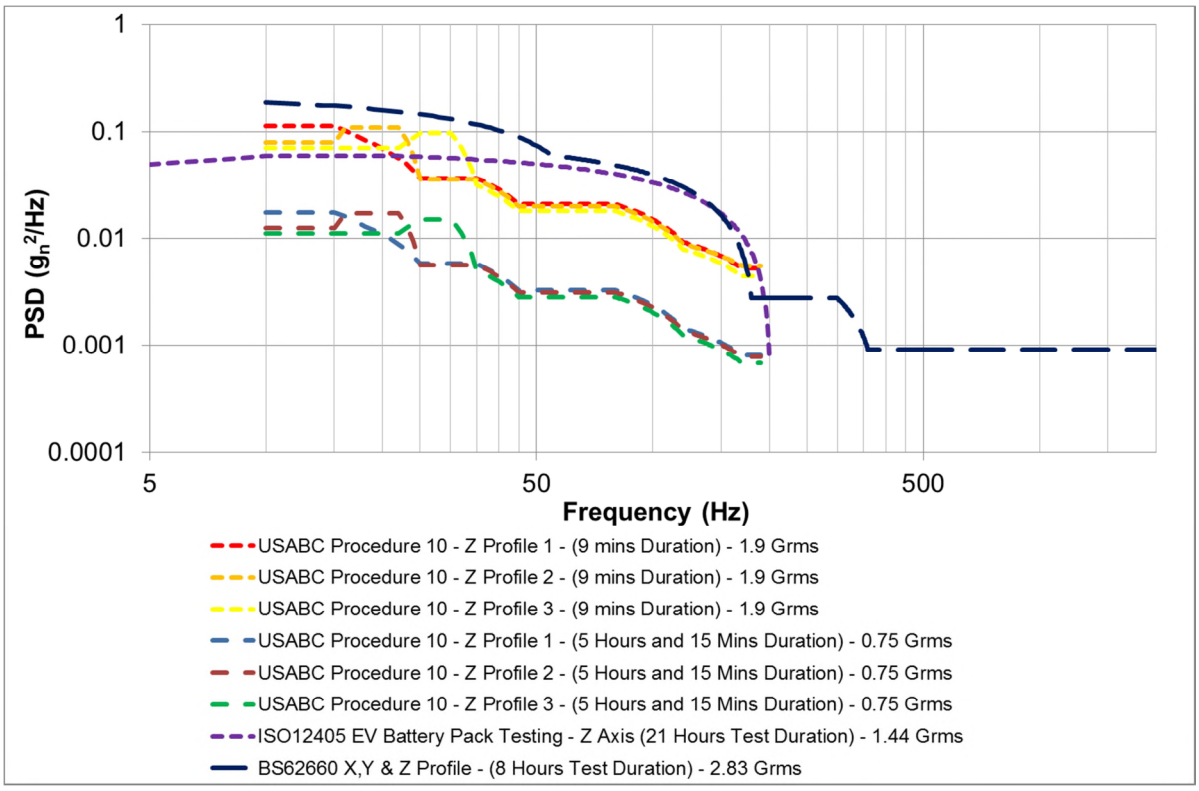

a)

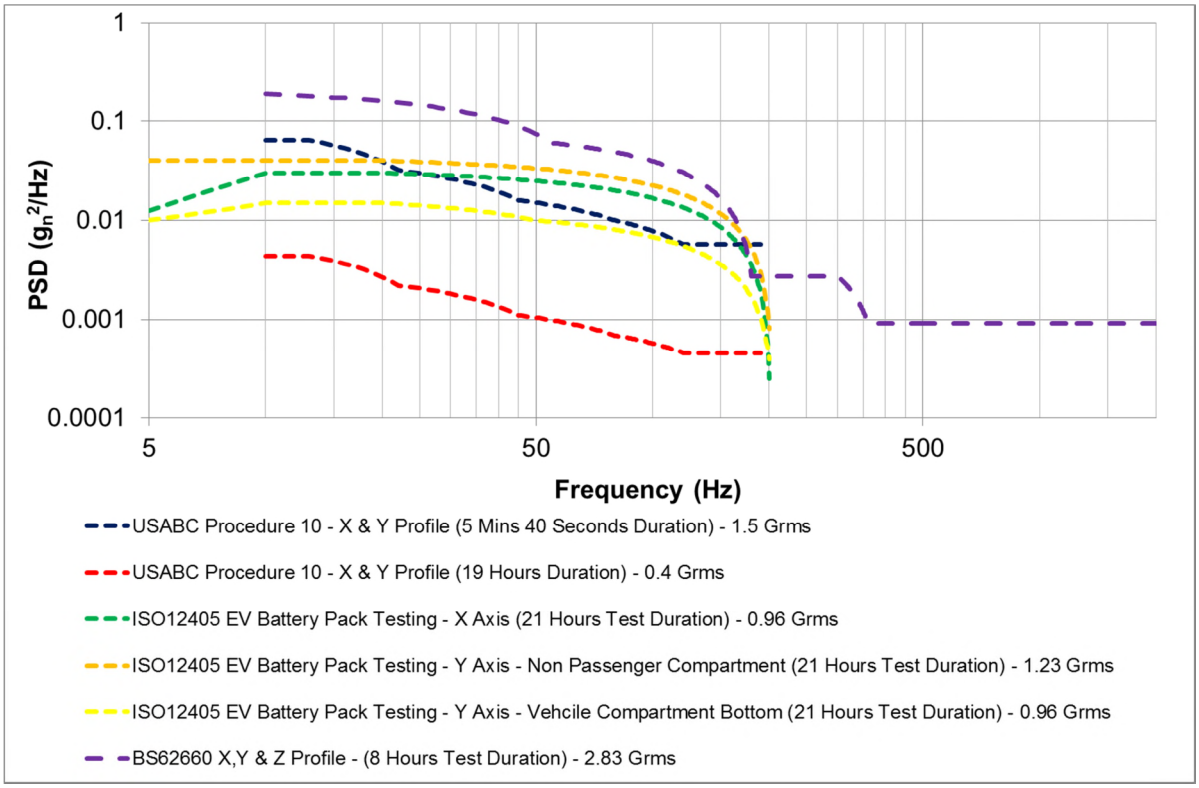

b)

Figure 6: Comparison of Acceleration Content of Standards that Utilise a Random Vibration Methodology – a) Vertical (Z Axis) Excitation, b) Horizontal (X and Y Axis) Excitation

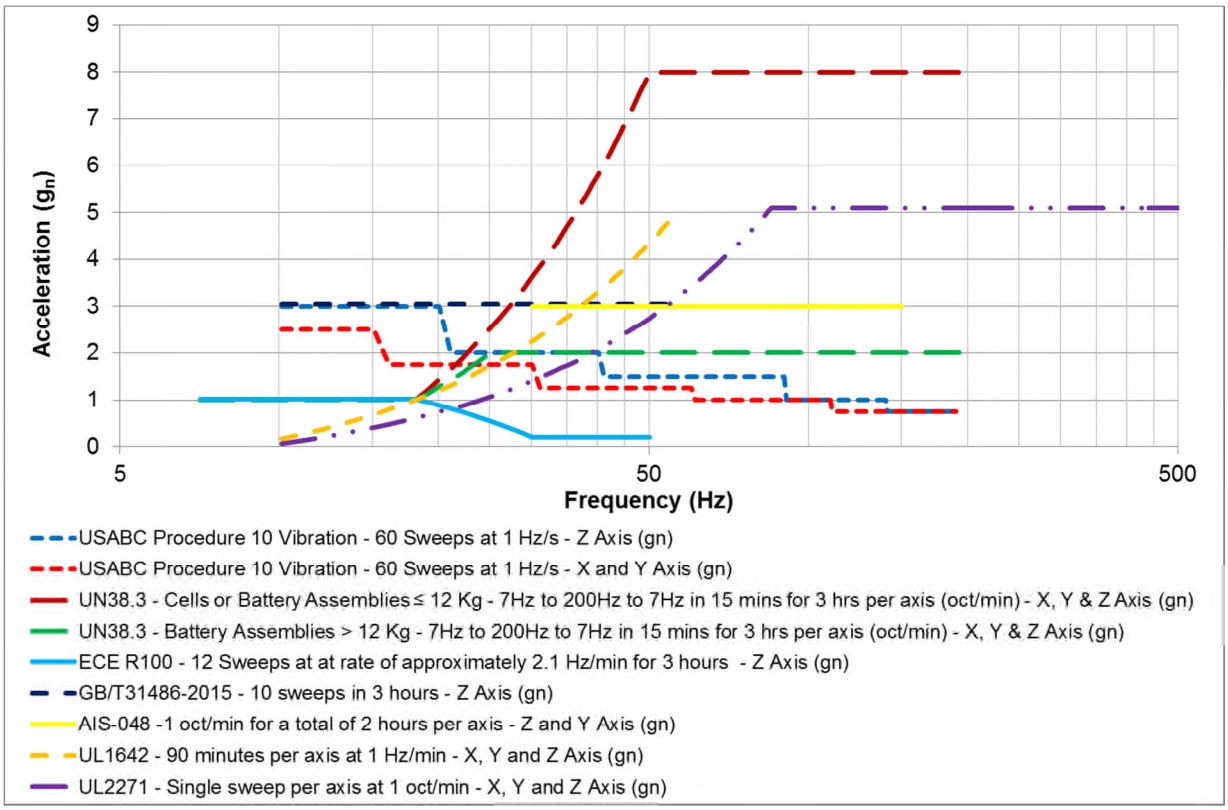

Figure 7: Comparison of Acceleration Content of Standards that Utilise a Swept Sine Vibration Methodology

A full critical review of each test specification is presented in Submission 5 [70] however the overall findings from this critique are presented here for completeness. The first major concern with existing test standards is the appropriateness of the data that these specifications have been derived from. Many of the test standards have evolved from legacy procedures which have been generated from consumer electronics. If the baseline data of the test standard is not representative or relevant to the item being tested, it can result in the product being over tested [26]. This could lead to a product that is over engineered to compensate for the test method which may lead to a heavier and more expensive pack assembly [26]. Conversely the item could be under tested, resulting in a product that has an increased risk of in market failure due to poor design robustness [26]. The concern over the provenance of the baseline data that the test procedures are derived from is illustrated by comparison of the different test standards presented in Figure 6 and Figure 7. Whilst the profiles in these figures are not normalised for test duration, and therefore are not optimised for a comparative study, this basic comparison highlights the lack of consistency in the application of vibration testing to EV components for both robustness and durability testing. This concern is enforced by the fact that the majority of these standards fail to offer a summary or objective of the in-service condition that the profile is replicating or even a test scope.

Another factor impacting the accuracy of contemporary RESS vibration procedures is that only a third of these standards evaluate using a random vibration

methodology. Out of the 9 key vibration standards available or required by engineers to validate EV battery assemblies, 7 define the test spectra via a swept sine methodology. Also, all legislative tests utilise swept sine profiles. As highlighted in Section 2.2.1.1, swept sine profiles are not representative of the vibration loading experienced within a chassis mounted component that is excited by road induced vibration (such as that of a EV RESS). It is therefore recommended that in the development of more representative vibration tests that the focus is towards producing random vibration test spectra.

Submission 5 [70] defined several other recurring concerns which needed to be addressed in the development of new EV RESS vibration test specifications. The main concern is that only USABC Procedure 10 has been correlated to a specified design life of 100,000 miles durability. It is also the only standard that is scoped for durability testing and not robustness validation. However there is evidence to suggest within [71] that this specification is overly compressed, thus resulting in unrepresentative loading of the test specimens.

With regard to the standards that utilise a random vibration methodology, only ISO12405 defines a set of control tolerance parameters (presented in Table 2). No swept sine tests define control tolerance parameters. To ensure test repeatability and accuracy, it is recommended that in the development of future EV vibration test standards that specific vibration tolerances are stated.

Table 2: Vibration Control Parameters Defined in ISO12405 [66, 72]

Control Parameter	Control Tolerance
Delta frequency	1.25 +/- 0.25 Hz
Inner range of tolerance	+/- 3 dB
Outer range of tolerance	+/- 6 dB

Current test standards do not define the accelerometer control methodology (such as averaging via a minimum of two accelerometers). As discussed within [45] there are three key control strategies available to engineers when conducting vibration testing (average, maximum and minimum). Each method can have the potential to influence the peak loading that the DUT will be subjected to. Therefore, it is recommended that in future EV vibration standards the control method is defined.

With regard to test conditions tolerances, few standards specify a temperature tolerance. Whilst some specify ambient test conditions, this is not necessary specific enough to ensure test repeatability or consistency. Therefore, it is desirable in future specifications and durability studies that a temperature tolerance is specified (such as 21 °C ± 3 °C) to improve test consistency and minimise effects of temperature variation.

Research conducted by Moore et al. with regard to UN38.3, highlighted that test specifications generally do not define how the DUT should be attached to the shaker facility or whether the DUT is evaluated with respect to gravity (i.e. DUT remains in vehicle orientation for duration of test and the shaker is moved in relationship to the

DUT) [73]. Ideally, for a test that simulates the life of a battery assembly within the vehicle installation, the item should be tested with respect to gravity to ensure that no unrealistic loading conditions are generated. It should also be installed to the facility via a means that emulates the vehicle to DUT interface and mounting condition. There are also no test fixture requirements defined in contemporary battery vibration standards. Whilst it may be unrealistic to define specific guidelines, a standard such as BS EN 60068 [74] which defines vibration test fixture requirements could be referenced within future vibration test procedures.

Surprisingly, many of the tests which have been devised with the purposes of robustness and safety testing of EV RESS's only test the DUT in a single axis. As a result the horizontal and longitudinal axis are not assessed. Subsequently there is a risk assembly issues are not captured during sign off testing and are allowed to enter the market place. The majority of standards assessed that do offer vibration loading for all three axis often do not differ the loading between the horizontal and longitudinal axis, resulting in unrealistic test loading conditions.

Many standards scoped for the vibration validation of lithium-ion EV batteries and cells do not combine attributes such as charging-discharging, vibration and climatic conditioning in a single test. In-fact no standard currently exists that replicates via rig testing a complete set of conditions that an EV RESS, cell or module would witness during its design intent service life. Whilst GB/T31486-2015 is unique in the fact that is requires a transient discharge with vibration being applied simultaneously, the DUT is not subject to transient charging loads. It also highlights that sub components are not "aged" using representative "in-vehicle" conditions and potentially result in tests that lack accuracy of the service environment, which is undesirable from both a robustness and durability perspective. Within all specifications, no acknowledgement of the thermal management systems is made and how this would be impacted by vibration. However, some specifications such as ECE R100 allow the option of the DUT to be evaluated with the battery management system (BMS) installed so that its functionality during vibration testing is also assessed. This highlights that these specifications have not been written to consider current advances in EV battery technology.

Another noteworthy finding from the critical review of existing test standards are that all standards assessed treat BEV and HEV battery packs the same, with the exception of BS62660, which mandates different states of charge (SOC) based on vehicle application. With regard to vibration inputs, there is a possibility the battery pack in a HEV might be subjected to vibrations from an on-board power generator such as an ICE. Whilst BEV battery assemblies are traditionally mounted in the underfloor area of the vehicle, HEV assemblies have been mounted in between the D pillar and boot (trunk) bulkhead. In the research conducted by [71], increase vibration loads were witnessed when accelerometers were placed in this region of the vehicle, indicating that different vibration profiles may have to be developed for

different generic mounting locations within passenger vehicles for RESS due to the change in structural stiffness and vehicle geometry.

A noteworthy observation is that some specifications have started to distinguish between the loads applied to cells and battery assemblies (such as UN38.3 and ISO12405). This is either via the sample definition or the weight of sample. However at the time of writing, no specification (or study) has defined separate or specific vibration criteria for modules other than AIS-048.

Finally, many of the testing regimes either ignore any form of pre and post-test measurement of cell electrical performance or limit it to the evaluation of capacity and static voltage measurement. Ideally a measurement of other factors such as internal resistance would give a greater understanding of internal mechanical or electro-chemical changes. It would also provide data of how the primary performance attributes of the DUT have been impacted by vibration.

Table 3 summarises the recommendations for future vibration durability standards from this review.

Table 3: Recommendations for Future Battery Durability Vibration Test Standards to Improve Test Repeatability and Consistency

<table>
<tr><th>Test Parameter</th><th>Recommendation for Future Battery Vibration Test Standard</th></tr>
<tr><td>Profile type</td><td>Random PSD to be employed – closer representation of chassis mounted component environment. Must evaluate X, Y and Z axis of sample via three axis specific vibration profiles. Profiles must be generated from EV data and correlated to a specific design life – such as 100,000 miles or 10 years customer use.</td></tr>
<tr><td>Test profile control parameters</td><td>Random vibration tests must be conducted using the following control limits:
<table>
<tr><th>Control Parameter</th><th>Control Tolerance</th></tr>
<tr><td>Delta frequency</td><td>1.25 +/- 0.25 Hz</td></tr>
<tr><td>Inner range of tolerance</td><td>+/- 3 dB</td></tr>
<tr><td>Outer range of tolerance</td><td>+/- 6 dB</td></tr>
</table></td></tr>
<tr><td>Accelerometers</td><td>Minimum of two control accelerometers to be fitted to test fixture / sample</td></tr>
<tr><td>Accelerometer control strategy</td><td>Average, minimum or maximum must be employed. Must be consistent throughout test.</td></tr>
<tr><td>Orientation of sample during evaluation</td><td>Must be evaluated in “car line” – with respect to gravity to avoid unrealistic loading.</td></tr>
<tr><td>Test environment conditions</td><td>Tests should be conducted within a temperature tolerance (e.g. 21 °C ± 3 °C).</td></tr>
<tr><td>Test fixture requirements</td><td>Must replicate the “in vehicle” mounting condition and have a first natural frequency outside the test frequency range. Evaluate in accordance with the vibration fixture natural frequency requirements defined in BS60068. Recommended that the test fixture is fabricated from a material with a high Poisson’s ratio (greater than 0.3) such as aluminium to ensure high natural frequency performance.</td></tr>
<tr><td>Test sample electrical characterisation</td><td>Electrical characterisation which determines the capacity, impedance and OCV must be performed both pre and post testing, so that electrical degradation can be quantified.</td></tr>
<tr><td>Other</td><td>Future standards must provide scope for the assessment of the BMS and other RESS auxiliary systems (such as thermal management).</td></tr>
</table>

In summary, the critical review of the current EV vibration test standards has identified a significant need for the development of a durability focused vibration test

standard that is correlated to a given mileage or design life. This standard should be derived from actual lithium-ion EV battery measurements and should apply vibration using a random PSD methodology (as defined in Section 2.2.1.2). It is also recommended that the vibration profiles for both HEV and BEV applications are derived; however the focus within this thesis will be towards BEV systems. These test profiles must be optimised for time, but must also be evaluated for unrepresentative shock loading prior to use. All three major axis of the DUT must also be evaluated using three, axis specific, random profiles. Future standards and procedures must also employ the recommendations defined in Table 3.

2.2.3 Research Investigating the Vibration Environment of EV Batteries

[71] defines a methodology of comparing different vibration standard types against vibration measurements from a Volvo C30 Electric via assessing the shock response spectrum (SRS) and fatigue damage spectrum (FDS) (discussed further in Section 3.4.5) of the recorded vibration data against the SRS and FDS of current RESS vibration standards. Within [71] was an evaluation of the Z axis (vertical) vibration excitation for different locations of the vehicle. This was so that an understanding of FDS and SRS for different potential RESS mounting locations (of the centre of floor of the vehicle, the front of the floor area and in the trunk) could be determined. The lower suspension arm (spring leg) of the vehicle was also measured however the study does not clearly define this measurement location. Figure 8 illustrates the findings from this investigation.

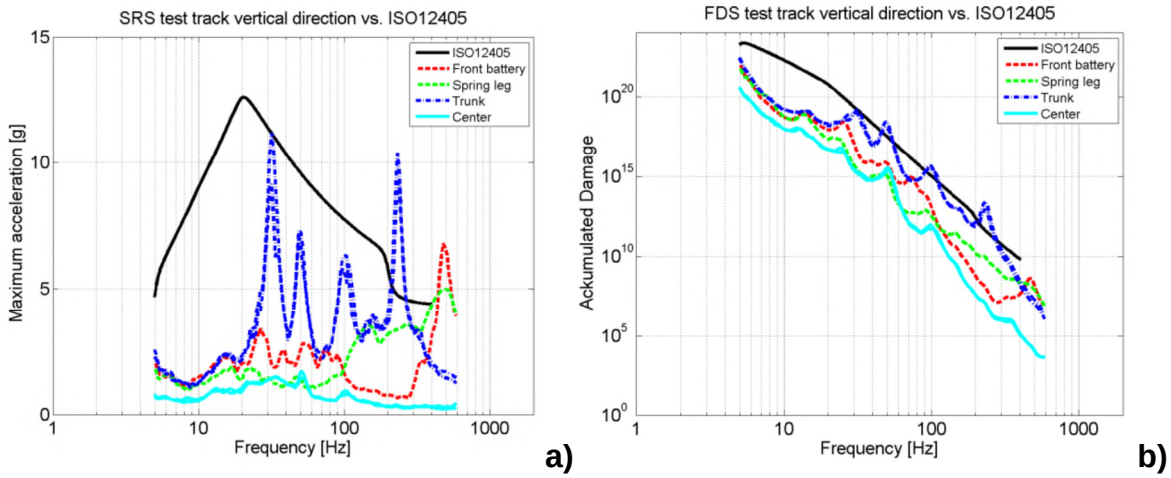

Figure 8 Response of Different Potential Battery Locations within a Volvo C30 Test Vehicle a) SRS of Locations b) FDS of Locations [71]

This study identified; that from 5 to 200 Hz, the shock loading of ISO12405 is far greater that of any of measurement locations on the vehicle. The fatigue damage resulting from the ISO12405 standard was noted to be significantly less from 0 to 400 Hz than the all measurement locations, with the exception of the trunk (boot). It is noteworthy that within this study, the trunk of the Volvo C30 experienced a greater level of fatigue damage and shock loading than underfloor measurement locations

typical of a traditional BEV RESS installation. This gives an indication that HEV batteries (which are often housed within the bulkhead between the trunk and passenger compartment) maybe subjected to a more aggressive vibration life than a BEV battery. The study also highlights that testing in all three directions is important and that test frequencies below 10 Hz must be performed [71]. In summary, the results presented within [71] illustrate that ISO12405 is unsuitable for durability evaluations.

The limitation of this study is that the vehicle was only ever driven over a rumble strip test track and not a variety of representative surfaces. A test profile from a single surface will only apply a limited magnitude of vibration energy for a particular set of frequencies which is unrepresentative of the multiple operational environments that a vehicle will see in service. It was also assumed by the study that 800 hours of driving on this single surface type was typical of 15 years customer operation.

In the study presented in [27] a vibration test profile (Figure 9) developed by BMW for the evaluation of EV battery assemblies is presented. However, the limitation of this study is that the profile was derived from conventional ICEV's rather than from an EV product. Since these measurement are not attributable to key locations on an EV (such as from the outer casing of a HV RESS) only generic conclusions with regard to the vibration environment can be made [26].

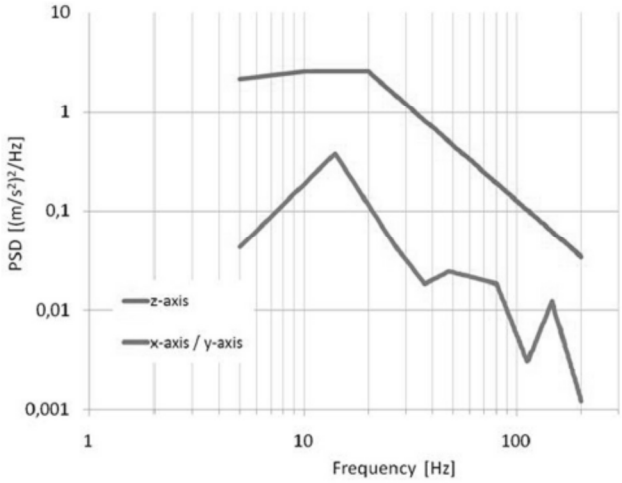

Figure 9: PSD's Derived by [27]

While [27] presents the PSD for the resultant vibration test profile for validating EV components, there is no discussion as to the derivation of the test profile. In particular, the relative exposure of the test vehicle to different road surfaces and how such measurements were sequenced to form a representative vehicle life from which an accelerated life durability assessment of the design could be made.

In addition, because the study discussed in [27] was conducted by BMW, critical details required to allow researchers and academics to replicate and utilise the

presented profile for research activities have been omitted. This information had been redacted to protect BMW's intellectual property.

In summary, whilst there have been a number of investigations which have had the objective of defining the vibration environment and loading experienced by EV RESS, each study has significant limitations. In summary, no one study has taken measured EV vibration data from multiple surface types, synthesised a test profile using surface sequencing representative of an EV durability life (discussed further in Chapter 3) and assessed the suitability of this profile to known vibration standards within a vehicle durability context, via suitable comparative techniques such as via SRS or FDS analysis. Furthermore, no study has presented in full a test profile which has been derived from vibration measurements from EV's with the necessary information to allow academics or engineers to replicate this profile on a shaker.

Subsequently, this review recommends that real world EV vibration measurements are utilised to define a new random vibration profile that is the equivalent of 100,000 miles of UK BEV usage. These profiles shall then be used to critique the current EV RESS vibration standards available to engineers via FDS and SRS analysis as defined within [71]. This profile could also be applied to support further battery durability studies as discussed within 2.4.

2.3 **Natural Vibration Characteristics of EV Batteries**

A review of current literature revealed that only one academic study has been published which investigates the natural vibration characteristics of battery cells. In this study [8], A suite of mechanical characterisation tests were performed on "used but serviceable" 10 Ah lithium-Ion battery cells which were approximately 120 mm by 65 mm in size, as shown in Figure 10 [8]. Within this study the natural vibration characteristics were examined by impact hammer excitation tests to support and to validate the development of a finite element model of a pouch cell [8]. This study observed three modes within the 0 to 1000 Hz test range, with the first mode occurring at approximately 267 Hz [8]. It also demonstrated that a basic two point hammer survey could be reliably conducted on lithium-ion pouch cells. However, this study had the following limitations; firstly it did not take the opportunity to define damping characteristics, mode shapes or stiffness behaviour of cells via experimental modal analysis techniques (which employ hammer excitation test methodology). This study also did not identify or characterise the effect of in-service factors such as SOC or temperature on the vibration characteristics of the test item. This study employed a limited sample size of four items and determines modes using a single excitation location and two measurement locations, one of which was likely to have been measured from a nodal position (a static position during modal excitation) resulting in limited accuracy of results [8]. Whilst the experiment was conducted up to 1000 Hz, the research does not outline the confidence of the measured natural frequencies via the use of coherence (discussed further in

4.3.4.2). Finally, this research did not take the opportunity to determine the effect of other external factors on the natural vibration behaviour of cells, such as SOC which has been known to result in external dimensional changes of pouch cells [75, 76]. This occurs though expansion and contraction of host materials due to lithium intercalation, electrode volume increase caused by irreversible reaction deposits, and volume and pressure changes within the cell case (depending on battery structure and construction) [75, 76].

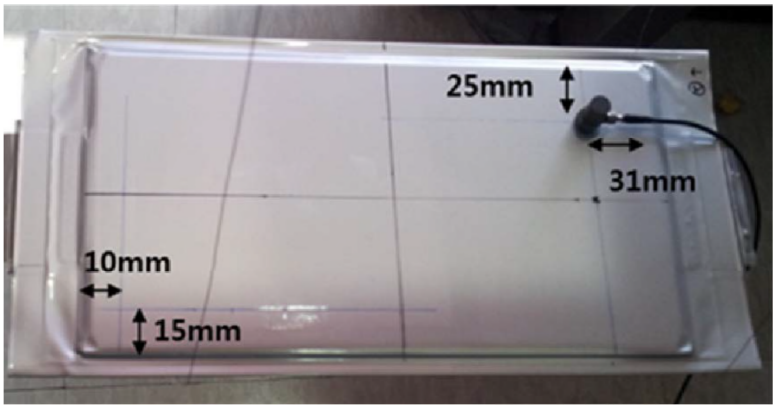

Figure 10: Lithium Polymer Pouch Cell Evaluated in Testing Conducted by Choi et al. [8]

In conclusion there is only one study which has investigated the natural vibration characteristics of battery components and cells. However, because this study was part of a wider investigation it did not detail mode shapes or damping characteristics of the cell. Therefore it is recommended that a future study is conducted to determine the natural vibration characteristics of battery cells and EV RESS components. It is proposed that this is conducted via the application of contemporary experimental modal analysis techniques to fully characterise the vibration response of these systems, including; natural frequencies, mode shapes and damping coefficients. It is also recommended that other in-service factors (such as cell SOC) are assessed to determine if these attributes can affect the vibration response behaviour of the test items.

2.4 Effect of Vibration on EV Battery Assemblies and Components

In an article by Pohl et al., it is suggested that “capacity-reducing effects caused by vibration” have been observed in Lithium-Ion Phosphate (LFP) battery assemblies [77]. However, the article presents no evidence to prove the capacity reduction or what vibration levels would cause this suggested aging effect on this particular battery chemistry [77]. It also does not indicate the percentage decrease in capacity or in what cell form this phenomenon has been observed in. Vibration has also been hypothesised as a possible cause of aging within battery cells by Suttman et al. [78].

Mechanical fatigue and performance degradation of battery cells has been observed via the application of just electrical cycling in the study presented in [79] with commercially available battery cell chemistries. This may indicate that vibration induced fatigue could occur within EV battery cells. It is hypothesised that

commercial battery cells durability could be affected by road induced or in-vehicle vibration.

In a study conducted by Chapin et al., the effect of vibration on different samples of 18650 cylindrical Lithium Cobalt Oxide (LCO), is presented. Within this study, the samples were initially electrically cycled prior to being subjected to vibration. This study was performed to determine if the batteries electrical behaviour change upon vibration after charging/discharging cycles. The start of test (SOT) and end of test (EOT) open circuit voltage (OCV) measurements, and cell mass are shown in Table 4 and Table 5 respectively. Pre and post-test computerised tomography (CT) scans of sample 7 are shown in Figure 11.

Table 4: Test Results – No Significant Issues Noted Post Vibration Testing [80, 81]

Sample No	1	2	3	4	5	6	7	8
No of Charge Discharge Cycles	Control Samples		100 cycles (at 25 °C)		100 cycles (at 45 °C)		200 cycles (at 45 °C)	
OCV at SOT	4.213	4.209	4.198	4.208	4.208	4.214	4.210	4.203
OCV at EOT	4.213	4.209	4.198	4.208	4.208	4.214	4.209	4.203
Change	0.000	0.000	0.000	0.000	0.000	0.000	0.001	0.000

Table 5: Test Results – No Significant Issues Noted Post Vibration Testing [80, 81]

Sample No	1	2	3	4	5	6	7	8
No of Charge Discharge Cycles	Control Samples		100 cycles (at 25 °C)		100 cycles (at 45 °C)		200 cycles (at 45 °C)	
Mass (g) at SOT	45.81	45.90	45.78	45.88	45.98	45.79	45.90	45.88
Mass (g) at EOT	45.81	45.90	45.78	45.88	45.98	45.79	45.90	45.88
Change	0.000	0.000	0.000	0.000	0.000	0.000	0.000	0.000

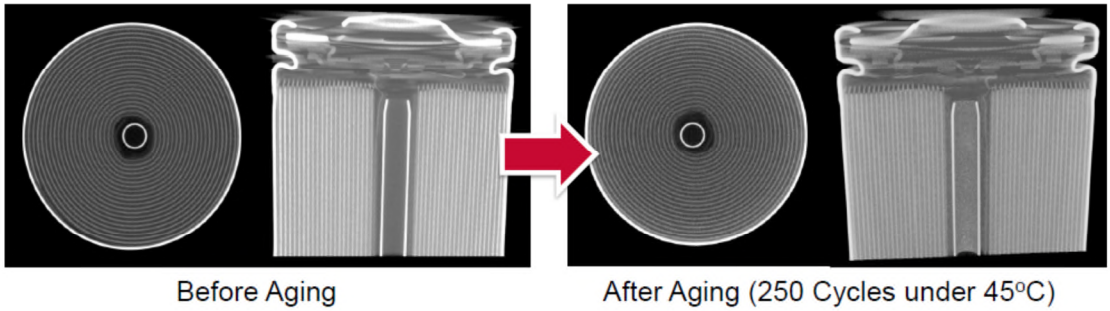

Figure 11: CT Scan Results from Chapin et al. Study into 18650 Cell Aging – No Significant Issues Noted Post Vibration Testing [80]

This study concluded that the 18650 cells evaluated were not effect by vibration as no difference was observed between OCV measurements between SOT and EOT.

It also concluded that no significant damage was observed in the post testing computed tomography (CT) imagining [80, 81]. However, the authors do not confirm the vibration test profile, cell orientation or duration of vibration energy applied to the cells post cell electrical cycling. Therefore, it cannot be concluded that these results are typical of an automotive EV application, nor is it possible to determine how representative the test conditions were. The authors do not confirm if any other cell characterisation, other than OCV measurement, were performed pre and post testing, indicating that important cell performance data (such as impedance and capacity) was omitted from this study.

In a paper published by Brand et al., the effects of vibrations and shock loading on 18650 cells and small lithium-ion pouch cells (of the size suitable for a consumer electronic application such as a mobile phone or small device) are evaluated [82]. The testing utilised the UN38.8 swept sine (test 3) robustness profile and performed additional shock testing in accordance with UN38.8 test 4. In addition to these evaluations, the study also undertook a long-term (186 day) vibration test using a swept sine profile from 4 to 20 Hz which had a Grms acceleration (discussed in Section 3.3) of 1.9 g_n via the use of a mechanical shaker table. In each of these experiments, the cells were evaluated in two different orientations with respect to the axis (Z and Y-axis) of the applied vibration. This axis orientation relationship and the cell forms tested are illustrated in Figure 12.

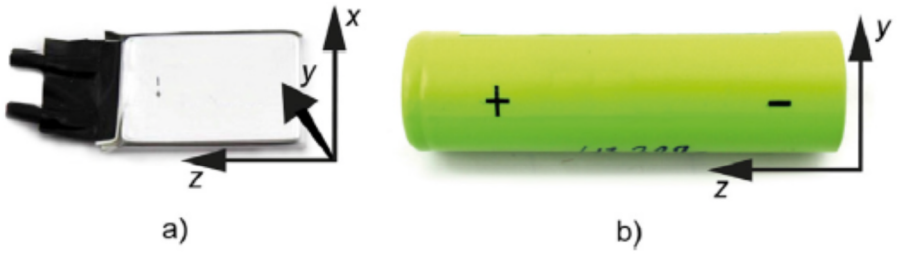

Figure 12:Photographs of Tested Cells from Brand et al. Study a) Pouch Cells b) Cylindrical Lithium-Ion Cells Including Direction of Mechanical Loads [82]

To determine the effects of the shock loading and vibration, the cells were characterised using electrochemical impedance spectroscopy (EIS) and pulse power measurements (to determine impedance) and capacity measurements [82]. Post testing the mechanical condition of the cells were assessed by scanning electron microscopy (SEM) to determine internal damage [82]. Polarised light microscopy (PLM) was also conducted to determine scorching of the separator materials prior to final disassembly of cells [82].

The swept sine evaluation in accordance with UN38.3 test 3 was applied to four cylindrical and four pouch cells. Two cells of every cell form were also kept as reference samples within the same room as the test cells; however no mechanical stress was applied to these reference cells. The 3 hour swept sine profile (swept from 7 to 200 Hz to a peak load of 8 g_n) was conducted 10 times. The electrical and

mechanical characterisation found that there was no significant or extraordinary degradation observed when these two cell forms was evaluated using this test profile. Observed changes in the internal resistance and capacity could be explained by variations in ambient temperatures [82]. The post mortem and SEM scanning of these cells identified no changes, except for a displacement of the mandrel within one 18650 cell sample [82].

The 186 hour, long term vibration test on four samples of each cell form, found that the pouch cells showed no degradation during or post testing. However, the 18650 cells which were vibrated in the cells Z axis during this assessment displayed a significant impedance increase during the evaluation. These samples also displayed a sudden drop in capacity when measured by a 1C discharge, which illustrates the link between impedance rise and voltage drop. These findings are illustrated in Figure 13.

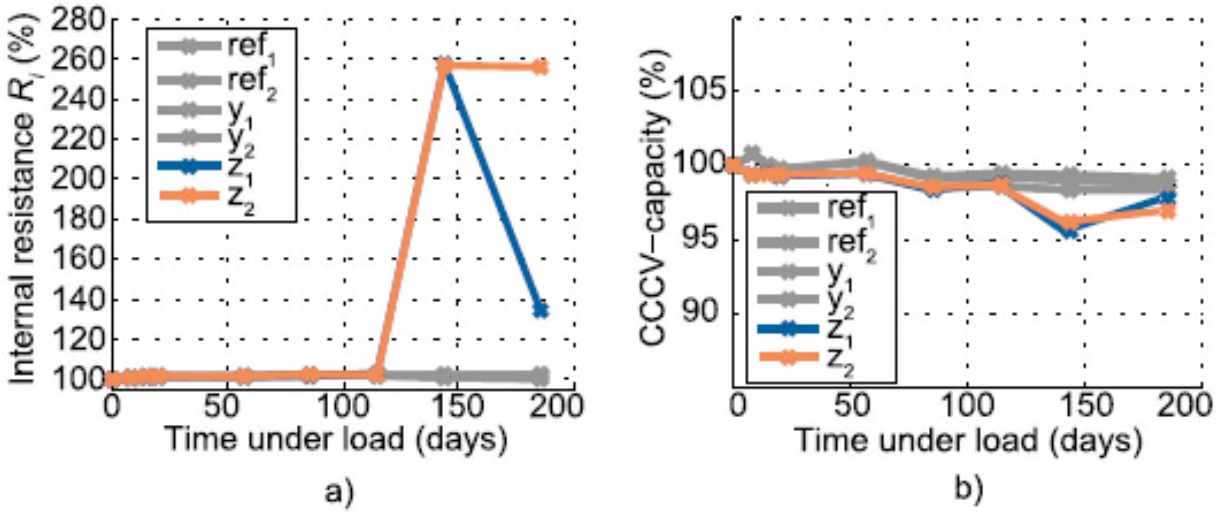

Figure 13: Development of a) Relative Internal Resistance (R_i) and b) Relative Constant Charge Constant Voltage (CC-CV) - Capacity for Long term Vibrational Testing of 18650 Cells [82]

It was found on disassembly that these changes in internal resistance and capacity (within the cells evaluated in the Z axis orientation) were a result of the mandrel becoming detached and striking the upper and lower components inside the cell such as the current collector and cell tabs. PLM assessments also identified scorching along the separator indicating internal shorting through the movement of the mandrel against these components [82].

Finally, the study conducted shock loading on the cells in accordance with UN38.3 test 4, where three hundred 150 g_n shocks were applied to four cells of each cell form. For both cell forms, changes in the cells capacity, as well as impedance were not noticeable [82]. However, upon post mortem of the 18650 cells the mandrels within these cells had become loose. The 18650 cells shocked in the Z axis also displayed deformation of the current interruption device (CID) and current collector as a result of the loose mandrel. This deformation is illustrated in Figure 14.

Interestingly this study indicates that this cell was still functioning despite this internal damage.

In summary, this study is a comprehensive assessment of the effect of vibration on lithium-ion cells. It employs multiple electrical and mechanical assessments of cell performance to define the degradation and failure modes. It has highlighted through multiple vibration and shock profiles that 18650 cells can be damaged significantly by vibration. Finally it has provided evidence that 18650 cells, when oriented in the cells vertical (Z axis) arrangement, are more susceptible to vibration ageing. Whilst these results are beneficial to engineers developing EV battery assemblies, the UN38.3 test profiles utilised within this assessment are not representative of a road vehicle durability application and are only suitable for evaluations of the cells robustness and air cargo safety [26].

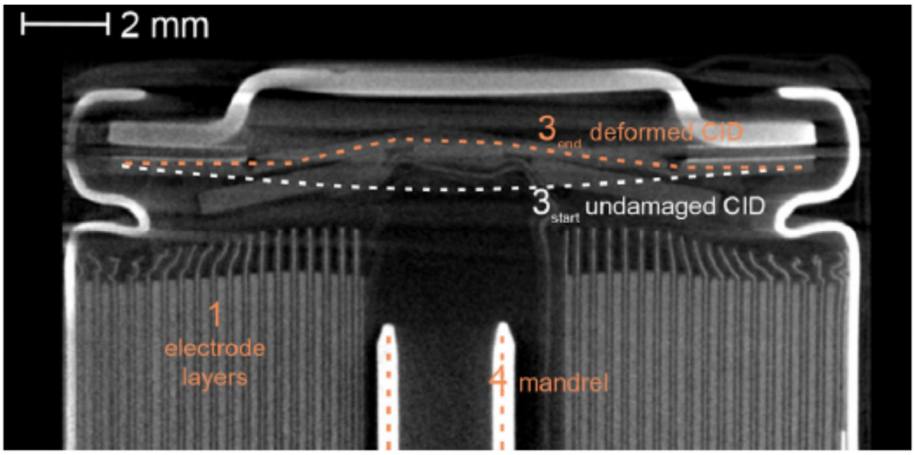

Figure 14: Positive Pole of 18650 Cell Shock Tested in Z Axis - Movement of Mandrel Visible [82]

The long term vibration testing utilises a swept sine profile which does not excite the cells within a road vehicle representative vibration spectra. It is also important to highlight that by their nature, swept sine profiles are regarded as an unrealistic representation of vibration phenomena that occurs within wheeled road vehicles [42] (discussed further in Chapter 3 and Submission 5). Finally, the vibration profiles used within this study have not been correlated to any given design or service life, and therefore conclusions with regard to warranty or susceptibility of in-service failure cannot be determined. Also, with regard to the long-term vibration testing, the experiments were conducted using a mechanical shaker table. These shaker systems have a limited vibration range and control accuracy. Subsequently they result in the generation of vibration spectra which is unrepresentative of an automotive application.

Another noteworthy finding when reviewing the test methodology for this study; is that the vibration was only applied to one axis of the cell during the whole testing program. In an automotive service environment, the cells would experience vibration in the X, Y and Z-axis simultaneously. As a result the findings are not representative of an automotive environment. Finally, the study does not define the test fixture, how

the cells were held to the excitation system or if the restraining condition was representative of a consumer electronic mounting condition. It is important to understand the test mounting condition as this could have an impact on the results due to the transmission of the vibration energy to the cells.

In the PhD thesis [83] two different lithium-ion chemistries (Lithium Manganese Oxide (LMO) and Lithium Cobalt Oxide (LCO) anode with a Lithium Titanate (LTO) cathode and LFP anode with graphite cathode) were evaluated for vibration durability. The pouch cells of these lithium-ion chemistries were of a commercial lithium-ion battery type and measured 130 mm x 200 mm, and were rated at 12 Ah. The motivation for this testing was in response to the study's findings of a lack of literature investigating the effect of vibration and temperature cycling on pouch cells for a heavy-duty vehicle application [83]. Three cells of each type were exposed to vibration and temperature cycling according to standard ISO16750-3, paragraph 4.1.2.7, "Test VII - Commercial vehicle, sprung masses". The cells were vibrated for 144 hours. The cells were exposed to random vibration levels of maximum 5.2 Grms within a frequency range of 8 Hz and 500 Hz. In addition, the temperature was ramped between -25 °C and +60 °C at a rate of 4 °C/minute [83]. The test fixture used within this study is shown in Figure 15.

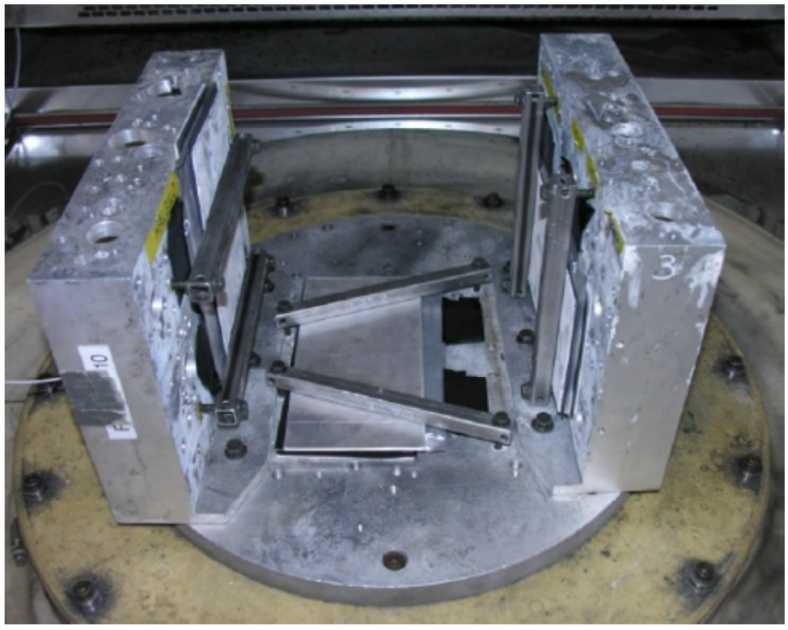

Figure 15: Test Fixture Utilised for the Evaluation of Pouch Cells [83]

Post testing capacity measurements (1C at 25 °C) were conducted on the vibrated and temperature cycled battery cells. These results showed no difference compared to the untested reference cells within the study. The measured variance in capacity between all tested cells was less than 0.5 %. This study concluded that the vibration and temperature cycling of the cells had no significant influence on electrochemical performance [83].

Whilst the cells capacity was measured and evaluated to reference samples post testing, the main objective of this investigation by Svens et al. was to determine the mechanical integrity of the thermal welds of the pouch cell packaging material (as illustrated in Figure 16).

Figure 16: Pouch Cell Packaging Prepared for Water Ingress Evaluation – Cell Welds Under Assessment High-lighted [83]

Interestingly this was conducted via water vapour transmission rate (WVTR) measurement which is more commonly used to assess the sealing capability of packaging materials [84]. WVTR measurements were performed according to the standard method for WVTR through plastic films and sheeting, American Society for Testing and Materials (ASTM) F 1249-06 [85].

This water ingress evaluation concluded that the applied forces on the welds caused by the vibration and temperature cycling were insufficient to induce defects in the cell packaging material with this make and type of pouch cells [83].

However, the papers and thesis reporting the results from this study do not define whether the testing was conducted in a single cell axis or if the cell was subjected to 48 hours in the X, Y and Z-axis (totalling the 144 hours vibration), separately. In some BEV battery assemblies, such as the Nissan Leaf, cells are installed in different axis orientations within the same RESS assembly [2, 86]. This means that the same cell type could be subjected to different axis vibration loadings within the same pack assembly. As a result, the axis orientation, in relationship to the road induced vibration excitation axis, may age or damage the cells differently. It could also be a factor in optimising the durability of cells when they are packaged in the RESS. This hypothesis is supported by studies into cell aging performance due to orientation by Ratnakumar, et al. in a static environment [87]. The argument to validate cells in multiple orientations is also supported by the findings of a CAE simulation presented in [88]. It was found that within an arrangement of 20 pouch cells within a hypothesised battery assembly, that varying stresses are observed depending on their location when the pack assembly is in a simulated resonance

condition [88]. Finally the fixture utilised in [83] (presented in Figure 15) is of a fork arrangement. Given that the evaluation was conducted from 0 to 500 Hz, it is possible that it had a flexible body mode within this test range, as the study does not confirm the bare fixture response. It is a possibility that the test item may have acted like a damper between the two vertical plates during the test [89], thus not replicating the in-service environment.

In [90] Kelty et al. defines the test methodology employed by Tesla Motors to select the supplier of the 18650 cells for the Tesla Roadster RESS. Within this document it is highlighted that Tesla subjected the 18650 cells to the SAE J2380 battery vibration standard, as this procedure corresponds to 100,000 miles of 90th percentile customer usage in North America [90]. The cells were also characterised at the SOT and EOT to determine the level of aging or damage that was caused by the application of vibration [90]. Due to the commercial nature of the testing, Tesla has not published the findings from their selection process. Whilst this presentation is evidence of their test methodology, it does not confirm if cells can be damaged or affected by vibration. It also fails to indicate if different suppliers or manufacturing methods employed in the assembly of the cell could result in discrete fatigue mechanisms within this cell type.

With regard to the testing presented in [90], reviewing the image of the battery vibration fixture (shown in Figure 17) it is likely that the cells were only validated in one possible orientation in the three X, Y and Z-axis (as stipulated in SAE J2380 [61]) as unlike the Nissan Leaf, cells within the RESS of the Tesla roadster are installed in a single orientation (horizontal across the vehicle's axis) [90]. As a result, the effect of potentially different cell orientations within the pack assembly was not investigated.

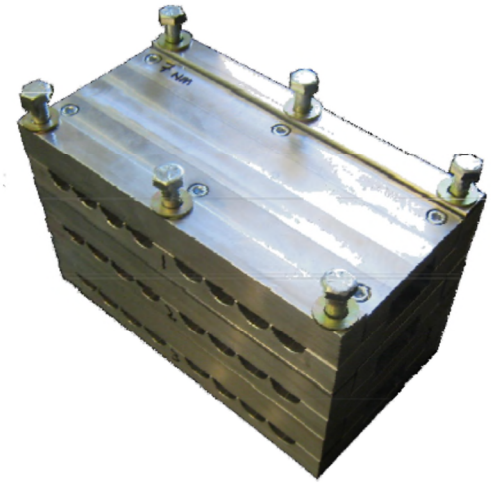

Figure 17: Tesla Roadster 18650 Battery Vibration Fixture [90]

The fixture utilised in the test is a layered block arrangement with semi-circular channels machined into billet of aluminium, with additional solid billets dropped on top which acts as a clamping surface onto the circular faces of the 18650 cells. This

simplified rig, does not represent the in-vehicle installation condition of the cells and is extremely reliant on the torque and torque sequencing of the clamping bolts. As a result, different cells within the stack could be subjected to different mechanical clamping forces. It is possible that this rig arrangement could cause mechanical degradation that is not representative of the in-service environment. However unlike the investigations performed in [80, 83], this study utilised a test standard that had been derived to represent 100,000 mile of durability and confirmed the results of the final chosen cell type using whole vehicle durability within a proving ground environment.

A study conducted by Preistley et al. in 1992 describes the test methodology and findings from combined climatic and vibration testing on prototype cylindrical Sodium Sulphur batteries at single cell, module and pack level [91]. Whilst not a contemporary lithium type battery study, this paper defines the test process undertaken to validate and the mechanical integrity of a battery assembly and its sub-assemblies. This study does confirm specific design issues, but indicates that at a cell level the cylindrical Sodium Sulphur batteries were subjected to vibration without any significant issues [91]. The study indicates that issues were experienced with RESS components when the cells were assessed at a module level and that the information gleaned from these tests were used to improve battery design [91].

Other investigations, performed on different non-lithium-ion cell chemistries have highlighted that simultaneous vibration with transient climatic loading can result in performance degradation of lead acid batteries. The application of temperature results in the electrodes flaking. The addition of vibration increases the rate at which these flakes break off [20]. These flakes then migrate to the separator and cause pore clogging thus reducing battery cell performance [20]. It is hypothesised by Sommerville et al. that this aging principle may be extrapolated to lithium-ion cells [20].

With regard to testing module and pack assemblies, [92] reports RESS casing fatigue cracking on a prototype battery assembly, at its mounting flanges, when it was evaluated in accordance with SAE J2380 (Figure 18). Cracking of RESS casings have also been observed in testing undertaken by Choi et al. when undertaking single axis vibration testing which represented 160,000 km. However Choi reports that multi axis shaker testing, does not replicate the single axis failure mode in the casing [93]. This highlights the variation between testing in a single axis versus multi-axis testing techniques. Stressing of the battery pack casings have also been identified by Lu et al. in CAE evaluations of the Chevrolet Volt assembly [94]. There is also evidence within academic literature that EV manufacturers, such as BMW have been conducting module and pack testing [27]. Whilst this study does not identify any specific design issues or observed aging mechanisms. It does however acknowledge that the prototype RESS assessed were done so in three axes and often installed in the design intent condition.

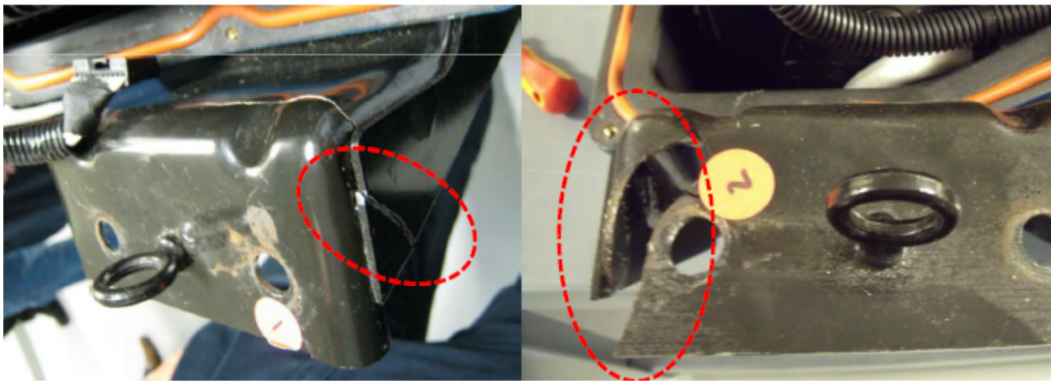

Figure 18: Cracking of RESS Casing Fatigue Cracks After Being Subjected to Vibration Testing in Accordance with SAE J2380 [92]

In summary there is limited published information available within both the academic and industrial communities which identify how battery cells and other associated EV assemblies are aged or affected by vibration. This finding is also echoed by [20, 83]. The literature review of previous experiments on battery cells has also highlighted the limited evidence that determines the effect of vibration. No single study defines specific electrical degradation data or ageing characteristics using a test method that has been correlated to a given automotive design life (such as 10 years or 100,000 miles). Many contemporary studies also fail to define what test specification has been used to validate the cells. This makes repeat experimentation to validate the findings impossible. There is also varying evidence to confirm that aging as a function of vibration is an observed phenomenon within standard or bespoke EV cell forms.

Another noteworthy observation is that the majority of studies do not confirm the cell test orientation. There is some evidence to suggest that cell orientation may have an effect on cell aging [82] and It is hypothesised that this aging could be exaggerated by dynamic excitation of the cell structure. It would be beneficial to determine if different cell orientations in relation to road excitation, age at different rates. Currently some RESS assemblies use multiple arrangements of cells within the same pack assembly (such as the Nissan Leaf [2]) for packaging purposes, which may not be ideal for cell longevity. The studies also do not indicate the cells SOC condition and if the mechanical stresses could vary given the change of electrochemical state of the cell.

Of the studies which did aim to determine the effect of vibration on cells via electrical performance, the tests applied to measure this performance are often limited in defining the cell degradation post vibration. In the majority of tests, OCV seems to have been the only measure used to judge the electrical health of cells. A more complete measurement of cell performance would be to conduct EIS, pulse power and capacity evaluations both pre and post-test so that any change in electrochemical performance could be quantified. There has been no evidence

within the previous studies of trying to determine the mechanical change of the cells under investigation by resonance characterisation at pre and post-test via swept sine or modal analysis techniques. This may be a useful measure in evaluating and quantifying the mechanical changes of a cell; and may correlate to electrical characterisation data.

Within the studies that supplied information on the test fixtures utilised for the vibration testing activity, there is little or no information supplied which confirm the fixtures vibration response prior to testing. Also there was some concern within the literature review about the accuracy of the test fixtures in replicating the in-vehicle mounting condition of the test item.

Finally, all but one of the studies identified within this critical review evaluated the test items using single axis excitation. Whilst it is industry practice to perform single axis vibration testing on automotive components due to factors such as equipment cost, equipment availability and test standardisation, it is recommended that the effect of multi-axis vibration is investigated, as this testing technique is more representative of the loading experienced in service by automotive components.

From this review of the literature it is recommended that studies should be conducted that determine if vibration profiles synthesised to represent 100,000 miles of automotive use can age battery cells. It should also investigate if cell SOC and orientation (in relationship to the vehicle axis) can affect the vibration durability life of EV battery cells and modules. It is recommended that full electrical characterisation of cells and modules are performed both pre and post testing via methods such as EIS, capacity discharge and pulse power so that changes in impedance and capacity can be determined.

Within any future experimentation, the fixtures designed and fabricated for vibration testing must be representative of a typical in-service mounting condition and must be validated and characterised prior to use.

3 Study 1 - Defining a Representative Vibration Profile for the Validation of BEV Batteries

3.1 Introduction

If future vibration durability tests are to be conducted with confidence, engineers require a set of vibration test profiles that are representative of a given warranty period. The review of existing standards and literature within Chapter 2 has identified a significant need for the development of a durability focused vibration test standard that is correlated to a given mileage or design life. This study aims to define a new random vibration profile that is the equivalent of 100,000 miles of UK BEV usage, to allow for accurate vibration durability testing of BEV batteries and assemblies. This study is a continuation of that discussed in [26] and utilises the same baseline vibration measurements. It defines the process taken to develop a vibration profile that could be applied by academic and industry researchers to determine the vibration durability behaviour of a RESS. It also assesses the severity of the measured vibration to all current vibration standards devised for evaluating EV RESS via the FDS and SRS comparison methodology (discussed in [71]).

This Chapter is structured as follows; Section 3.3 presents the experimental theory of defining a representative vibration profile from vehicle measurements. Section 3.4 discusses the vehicle measurement and raw data collection method. This section also defines the stages of deriving vibration test profiles that are representative of 100,000 miles of durability from this measured road load data. This section concludes by presenting the derived vibration test profiles. Section 3.5 compares the synthesised test profiles using the SRS and FDS method (discussed in Section 3.3.6) to the vibration standards identified within Section 2.2. Finally, discussion and conclusions are presented in Sections 3.6 and 3.7 respectively.

3.2 Objective and Aims of Study

3.2.1 Objective

To develop a set of random vibration profiles that are representative of 100,000 miles of UK customer usage of a chassis mounted battery within an BEV using actual BEV measurements. Use the derived vibration profile(s) to critically assess current random vibration test procedures via comparing the mechanical shock characteristic (SRS) and potential fatigue damage (FDS).

3.2.2 Aims

- To define methods of vibration profile derivation for shaker tables.
- To develop a set of vibration profiles based on measured BEV data.

- To critically review the defined EV RESS, module and cell vibration standards defined in Section 2.2.2 to measured data using SRS, FDS and PSD comparison methodology as defined in [71].

3.3 Theory of Defining a Representative Vibration Profile

According to Halfpenny et al.; a successful vibration durability test should satisfy the following criteria [95]. The test must be suitable for the item in question, be that a single component, sub-assembly or vehicle. The test should be accelerated where possible to improve development schedules and reduce cost. However, it should not incur unrealistically high loads that might alter the failure mechanism. Finally, the developed test specification should be suitable for laboratory based testing techniques.

A flow chart defining the key stages of the development process of random vibration durability tests is shown below in Figure 19.

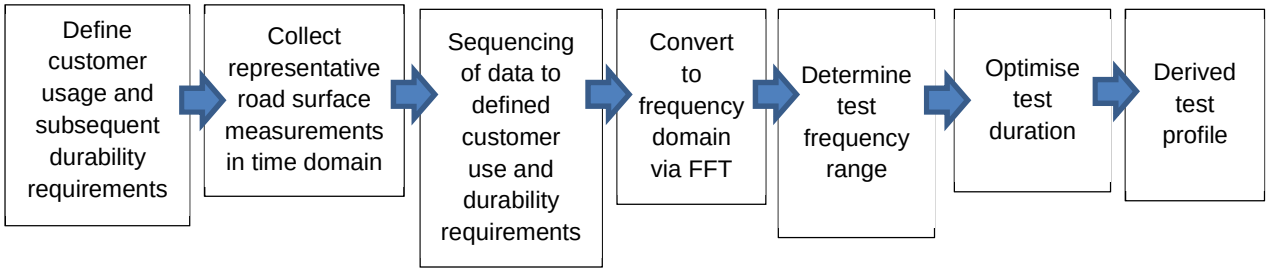

Figure 19: Vibration Durability Development Process

Each of the stages illustrated in Figure 19 are discussed in detail within this section. Whilst the majority of the steps outlined within this section are also applicable to the development of swept sine testing, random vibration profiles are the focus within this study. As discussed within [44], random profiles are a closer representation of the vibration environment witnessed by chassis mounted components, such as an BEV RESS.

3.3.1 Defining Customer Usage and Durability Requirements

Regardless of the vehicle propulsion system, the derived durability tests for components must be aligned with the intended 'in-service' use of the vehicle [96]. This alignment covers areas such as the intended market for the vehicle, what type of vehicle it is, the style of the vehicle, and the intended use [3]. It is therefore important for the accuracy of any rig based vibration durability test to understand and define the following requirements associated with the device to be tested [3]:

- What is the vehicle, who is the vehicle customer and what market will the vehicle be operated in?

- How long should the vehicle or vehicle component last?
- How will the customer use the product and what mix of road conditions will the customer drive upon?

This basic methodology of defining who the vehicle users are and their associated requirements, enables engineers to define the service load environment which corresponds to a predefined number of kilometres [3]. Engineers can then define a durability surface schedule or “mission profile” comprising of representative but repeatable road surfaces (such as those on a proving ground), which correspond to the defined design life and customer usage profile.

Defining the vehicle and its target customer is necessary to the development of any vehicle durability test. Different vehicles, customers and markets have specific and varied requirements associated with them. Taking the example of heavy commercial vehicles, a European commercial vehicle will be subjected to a completely different set of surfaces and driving situations to that of a vehicle sold into an Asian market. In some regions of the Asian market, the roads might be similar to that of a European off-road environment. Heavy commercial vehicles in some Asian markets could be operated at pay loads outside of the specification of the vehicle due to the less stringent vehicle laws governing vehicle operation. Vehicle type is also critical to mapping out user habits, for example a delivery vehicle may see a lot of kerb impacts during its life, have a greater number of ignition cycles, and spend time in urban areas covering short journeys, as well as covering a lot of ground on motorways [96], whilst a Sports Utility Vehicle (SUV), such as a Range Rover product is likely to spend a greater percentage of its life on off road surfaces than that of a typical family saloon.

According to Wynn et al., areas for consideration when testing BEVs and HEVs that differ from traditional ICEV tests include; driving style, average trip distance, speed profile and unique features of the vehicle (such as regenerative braking systems) [96]. While many of these appear to be the same as ICEV’s, there are differences which need to be accommodated, such as average trip distance. The current limited range of BEVs, means they may be designed and used primarily as urban vehicles, used for short stop-start motoring [96].

The next key stage in defining the test parameters is identifying the desired duration that a given component or vehicle should last for. If its durability life is too short, early component failure maybe witnessed, resulting in excessive warranty costs and subsequent damage to the company’s reputation via customer inconvenience.

Defining a vehicle and component life can be influenced by several factors. Firstly, if the item is safety critical, such as a component associated with the vehicles steering, suspension or braking, or could lead to customer injury or death a greater safety factor or durability life will be specified [3]. If the item is of a serviceable nature, its durability life may be reduced in accordance with the expected major service duration of the vehicle such as 60,000 miles or 4 years. A manufacturer may

also determine the desired durability life of a component or product via competitor benchmarking. It can be influenced further by customer expectation within the market [3] or by particular government incentives or legislation [97, 98]. However, automotive manufacturers typically aim for vehicles to have a minimum life of 10 years or 100,000 miles [99]. This will also be supported by a warranty period, which could range from 3 to 7 years (depending on the company's marketing and product strategy) where no significant failures are to be incurred.

The final step of this process is to determine the usage behaviour of the customer over the life of the product and how the vehicle will be used in the defined markets. The objective of defining the customer usage within the vibration durability test profile synthesis process is to generate a list of surfaces or events and a corresponding regularity of their incident during the vehicles desired lifetime. This is often referred to as either a "durability surface schedule" or a "mission profile" An example of such a schedule is shown below in Table 6.

Table 6: An Example of Surface Schedule for a Data Logging and Scheduling for a Mass Produced Truck [100]

Road type	% Weighting of Vehicle Operational Life
City Roads	25 %
Winding tarred roads	20 %
Country roads	35 %
Pothole and off road	20 %

85 % of vehicle life at gross vehicle weight (GVW)

A good mission profile should specifically define typical speeds of operation and the pay load condition of the vehicle. Some large vehicle manufacturers such as Ford, JLR and Volkswagen Audi Group (VAG) have pre-defined durability schedules or mission profiles which define a specific number of repeats of standardised proving ground surfaces that must be recorded to develop vibration tests. However, these industrial durability standards have a significant amount of embedded intellectual property (IP) and are subsequently unavailable for academic review or assessment.

Determining the surface types and specific surface events along with the vehicle payload condition and speed will vary considerably. It is affected by vehicle type, market of operation and the customer demographic. For example, if the component of interest is fitted to a Bus, the very nature of the product it is installed to means that it will be easy to define customer usage profiles [3] due to the regimented and fixed drive routes, constant and predictable passenger loading patterns throughout the day and low speed town operation. However, privately owned passenger cars are operated by individuals who are not restricted to specific routes around the town and country. As a result engineers have to employ a variety of different techniques to understand how a vehicle is or will be used by a variety of customers and what operational environments it will experience. These techniques include, the installation of global positioning sensors (GPS) and black box data logging

equipment to customer vehicles or an experimental vehicle fleet [27, 101], asking vehicle owners and operators to complete questionnaires on their driving habits [101] or employing data from government, academic and industrial studies [102].

The road surface classifications required to develop any durability surface schedule can be categorised into two distinct types of vehicle surface input. The first classification is events that involve continuous driving on a surface. These surfaces are typically classified by road type such as city, highway, A-road, rough road etc. With these surfaces, the road mix, vehicle pay loading and speed are important as they typically make up the bulk of any durability surface schedule [3]. The second classification is specific inputs. These are discreet inputs into the vehicle originating from driver manoeuvres or one-off inputs, such as the vehicle driving over potholes, speed bumps, railway crossings, kerb strikes and man hole covers. Specific inputs can also include panic braking, high speed cornering or driving over twist humps, all of which put strain into the vehicles chassis [3].

3.3.2 Collecting Representative Road Surface Measurements in Time Domain

A key step in the development of any vibration test is to record the vibration response from the component or vehicle of interest when it is subject to a variety of typical customer operating conditions or events as defined by the different methodologies discussed in Section 3.3.1. With respect to vibration tests with a durability focus, the objective is to define the loading characteristics of a given component, assembly or vehicle via accelerometer measurements.

Accelerometers measure the acceleration of the mounted location. They work on the principle of a single degree of freedom (SDOF) mass-spring system installed in a case, in which the acceleration response of the mass is proportional to the case excitation at frequencies well below the natural frequency of the transducer [3]. For vehicle structural studies, accelerometers with a response to DC or zero frequency are typically used for measurement accuracy [3].

Accelerometers are connected to a data logger which contain signal conditioning equipment and will amplify and filter the signal for recording. Contemporary digital data recorders are capable of sample rates greater than 2,000 Hz. The sampling rate capabilities and filter settings of the chosen data recorder are important to ensure that the relevant information can be extracted from the data and that it is meaningful [3]. As the data within the context of developing vibration profiles will be used to compare acceleration loading, potential for fatigue and also shock it is the resolution of the peaks in the data that will be critical. Good peak resolution can be obtained at sample rates 10 times the highest frequency of interest in the data [3]. This should not be confused with “Nyquist rate” theory wherein sampling at 2.5 times the highest frequency of the data defines the frequency composition [3]. Therefore if the data is sampled at 1,000 Hz, then the analysis frequency bandwidth will be up to 500 Hz and the peaks can be resolved up to 100 Hz [3].

Prior to installing accelerometers to the vehicle or component of interest, it is necessary to ensure that they are calibrated and produce the correct measurement response. This is discussed further in Submission 5 and [3], however in practice, a calibration curve with the transducer sensitivity in mV/g_n is supplied with the accelerometer. This parameter can be used to convert the output voltage to acceleration [3].

When installing the accelerometers for data collection, the choice of measurement location and installation method is critical. When recording the response of a specific item or component, accelerometers are typically installed to the mounting(s) of the item of interest or a solid part of the component itself. However, this location must be significantly ridged enough to allow for successful measurement and free of any unrealistic localised resonances.

Another consideration for accelerometer mountings on vehicles is that they should also be away from significant sources of heat (such as powertrain thermal management systems) which may result in measurement drift. Like any transducer measurement, the method of accelerometer mounting can influence the accuracy of the measured vibration response [103] as the mounting methods natural frequency (and subsequently its suitability for measurement) is directly dependant on its stiffness [104]. This is illustrated in Figure 20.

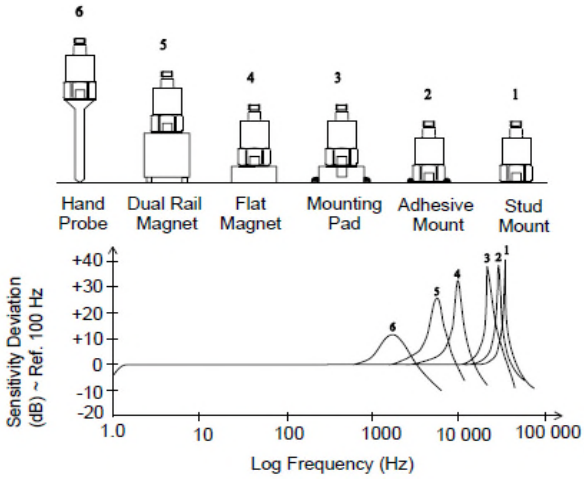

Figure 20: Accelerometer Mounting Methods Sensitivity vs Frequency [104]

There are multiple mechanical attachment methods available but for road load data collection at frequencies greater than 2,000 Hz, it is necessary to attach accelerometers via stud, adhesive or bonded mounting pad. These mounting methods, typically have natural frequencies greater than 10 kHz [104]. Further information on the advantages and disadvantages of different accelerometer mounting methodology are discussed in [105].

Prior to recording data for the test synthesis, it is recommended to conduct pre-test measurements to ensure that the recording equipment and accelerometer mounting locations are suitable. There are several common issues that can impact the quality

of the measured response. Firstly there are issues which can be a function of the transducers characteristics or sensitivity [3] such as an offset voltage originating from the transducer.

Another issue is aliasing. If the sampling frequency in relation to the frequency content of the signal is too small, the presence of high frequencies in the original signal could be misinterpreted in the discretisation process [106]. As a result, high frequencies can be interpreted or indistinguishable from low frequencies. This “aliasing” phenomenon is illustrated in Figure 21 by the red trace.

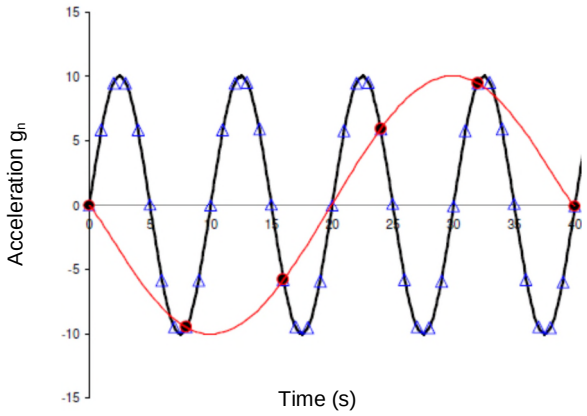

Figure 21: Aliasing - High Frequency Manifested as Low Frequency [107]

Additional information on aliasing is discussed within Submission 5; however it can be solved by suitable filtering.

Noise is another common issue that can occur within vehicle acceleration measurements. It is often the result of a loose attachment of the transducer, a faulty accelerometer or accelerometer cable or poor or loose connection between the accelerometer and data recorder [3].

Spikes are a data measurement issue which may not be avoidable. Whilst they can be caused electrically through a poor or faulty connection or a degrading accelerometer cable, they can be the result of a mechanical excitation such as road debris hitting an accelerometer [3]. Spikes however can be removed from the data prior to any data analysis via a range of different software packages.

Drift is usually due to a fault in the signal conditioning equipment. The mean value of the signal at the start of the recording is not the same as the value at the end on the recording [3]. If drift is observed in any of the data channels then the cause must be identified and fixed, prior to subsequent data analysis [3].

Once the data logging system has been proven to be functioning correctly via preliminary measurements, it is important to document clearly all the parameters of the test set up and also the test conditions.

3.3.3 Sequencing of Data to Defined Customer Use and Durability Requirements

Once the vibration response measurements have been made from the vehicle or component of interest when subjected to a defined mission profile (as defined from the investigations discussed in Section 3.3.1), the measured data has to be sequenced in a manner that correlates with this user behaviour. As discussed in Section 3.3.1, one of the outputs from this investigation should be a table of surfaces and "weightings" of how often these surfaces are predicted to occur within the vehicles life. The measured events can then be sequenced (typically within a software package such as nCode™) to form a single time series which is representative of the vibration life of the vehicle.

3.3.4 Converting Time Domain Measurements to Frequency Domain

Once the time domain data has been sequenced to represent the desired customer usage, the measured excitation is transferred from the time domain to the frequency domain so that a PSD profile suitable for a shaker system application can be generated. This is achieved via the use of a Fourier transform (FT). More specifically, a version known as the discrete Fourier transform (DFT) as this can very readily be implemented by using an efficient set of algorithms on computers, known as the FFT [108], which is illustrated in Equation 2.

$$x_k = \sum_{n=0}^{N-1} x_n \; e^{-\frac{2\pi i}{N} kn}$$

Equation 2

Where x_n represents a complex time-domain data set, x_k - a complex frequency-domain data set and N, the size of the data sets (which are assumed to be equal). The notation used in the DFT one sees two indices: n and k [108, 109]. Within the application of Fourier methods to time domain data, is that the frequency representation of a periodic waveform may represent a much smaller amount of information than the time representation [108, 109]. Fourier methods also have the advantage that they can distinguish frequency information within recorded data that is hidden within signal noise [108, 109].

3.3.5 Determine Test Frequency Range

A significant component of a vibration test profile is the chosen frequency range under assessment. The frequency range is typically defined by the capabilities of the shaker facilities and the frequency band where the peak energy occurs within the measured data. Ideally some consideration towards the desired test frequency bandwidth will have been performed prior to recording data as factors such as equipment specifications can be determined before measurement. Table 7 gives examples of the specification of two different types of shaker table system which could be used to guide the frequency bandwidth for testing

Table 7: Example Specifications of Vibration Shaker Tables [104, 110-112]

Type	Typical Force Range	Frequency Range	Application	Nature of Vibration Signal	Maximum Acceleration (Sine Peak) (g_n)
Single Axis Shaker Table					
Hydraulic Shaker	250 kN	< 0.1Hz to < 100 Hz	Durability testing, robustness testing, fatigue testing, modal testing.	Swept sine, random, sine on random. Real time replication.	5
Electromagnetic Shaker (LDS V8)	57.8 kN – peak sine 55.6 kN rms – peak random	5 Hz to 2000 Hz	Durability testing, robustness testing resonance search, fatigue testing, modal testing.	Swept sine, random, sine on random. Real time replication.	40

3.3.6 Optimise Test Duration

To replicate a vibration test that is representative of 100,000 miles could take somewhere in the region of 2500 hours per axis (on a single axis test) to replicate in a laboratory. Therefore it is necessary with any vibration test to optimise it for time [3] so that the test costs are reduced and that the test programme duration is minimised to enable faster delivery to market.

It is theoretically possible to compress a synthesised random PSD to any duration while maintaining the same energy content in the signal. This can be performed via mechanisms such as increasing the Grms level of the synthesised PSD so that the same FDS is achieved in less time through an increase in the SRS. However a high time-forcing factor can result in other damage mechanisms occurring during the test [71]. As discussed in [26, 71] the shorter the duration of the test profile, the greater the severity of the shock loads applied to the system to achieve the desired fatigue damage spectrum. Because the application of a compression factor to achieve the desired test duration is linked to the SRS and FDS, these two concepts are presented.

The SRS is used to determine the peak amplitude of loading seen during a series of road surface events (such as discreet impacts like kerb strikes, pot holes, high speed negotiation of speed humps etc.) impacts or a vibration test [71, 113, 114]. It represents a plot of the peak amplitude vs. frequency [113]. It can also be used to determine the safety margin of the test by comparing the test SRS with the SRS from measured vehicle data.

It is necessary to consider SRS during both the development and evaluation of vibration tests as it is insufficient to simply record and compare the highest static acceleration levels observed [113]. A comparison of acceleration does not account for the frequency of the vibration [113]. It is important to consider both acceleration amplitude and frequency of a vibration assessment as dynamic systems are more sensitive to certain frequencies than others, such as at the natural frequency of the system [35, 113]. Structural failure is also attributable to excessive strain energy.

Strain energy in a vibrating component is proportional to displacement rather than acceleration [113]. Subsequently the damaging effect of acceleration is seen to reduce with the square of the frequency, resulting in higher frequencies being less damaging than lower frequencies [113].

The mathematical theory behind SRS is discussed in Submission 5. However an example of calculating SRS for a typical automotive component is presented in Appendix A.

The FDS is directly related to damage (if the damage mechanism is fatigue) and it can be calculated for all types of signals [71]. The fatigue damage dosage applied to a vehicle or component by a particular vibration environment is calculated using a FDS which effectively plots damage vs. frequency [114]. It is used within the analysis and development of vibration profiles to determine the accumulated damage caused by long term exposure to fatigue damaging vibrations which, whilst can be modest in amplitude, often give rise to microscopic cracks that steadily propagate over time and lead to eventual fatigue failure [114].

FDS can also be used as a tool to compare damage generated by test profiles. However it must be noted that damage in real life is more complicated and therefore ‘engineering judgment’ must be used when using the FDS to assess the potential wearing nature of a given vibration signal or test profile [71]. It is therefore used as a measure of comparison, rather than an absolute calculation of fatigue damage. The mathematical theory behind FDS is discussed in Submission 5 and is presented in Appendix B.

As discussed within the introduction to this section, whilst it is theoretically possible to compress a synthesised PSD to any duration to replicate the same FDS content in the signal, a high time-forcing factor can cause other damage mechanisms during a test than during real service life [71].

To determine if the time compressed test profile is suitable and not too severe the calculated SRS of the compressed test profile needs to be compared to that of the SRS for the data that the test was generated from to ensure that it is not exceeded. An example of this analysis is shown in Figure 22.

Within this example the original data that the profile was generated from is referred to as the “target SRS”. In the example shown in Figure 22, both the 50 hour and 100 hour test durations would be suitable to test with, whilst the 10 hour test is above the target shock response and therefore indicates that the 10 hour PSD profile would be unsuitable for testing.

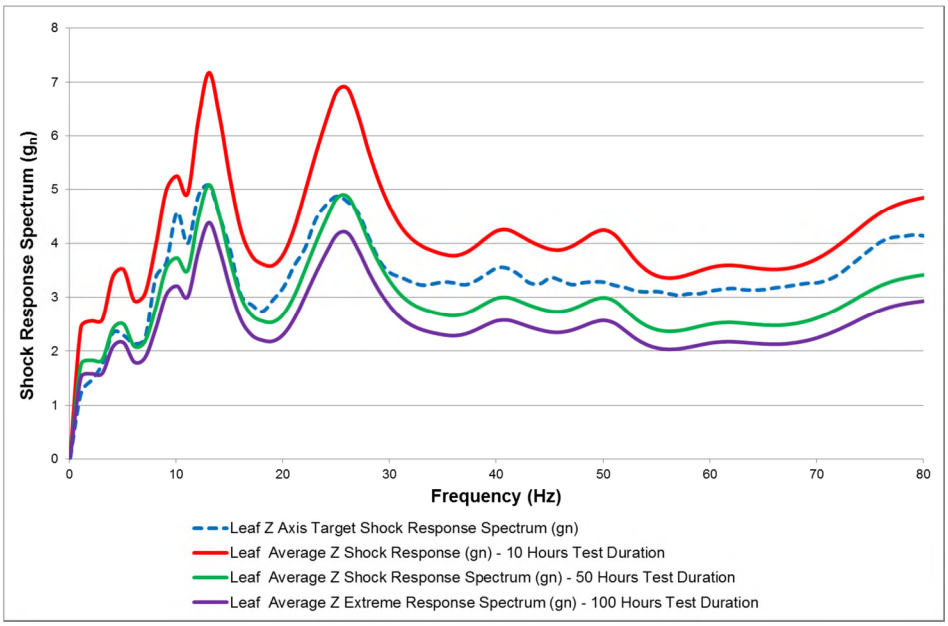

Figure 22 Effect of Test Duration of Derived PSD's SRS in Relationship to the Target Shock Response [26]

3.3.7 Derived Test Profile

Once the test profile has been optimised for time and frequency bandwidth, the subsequent PSD has to be adapted to allow it to be replicated on a shaker system. Practically it may not be possible to transfer all PSD spectra points into a shaker control system. It is therefore necessary to choose the key points of the PSD so that the spectra can be reproduced by the control system. Figure 23 illustrates this process.

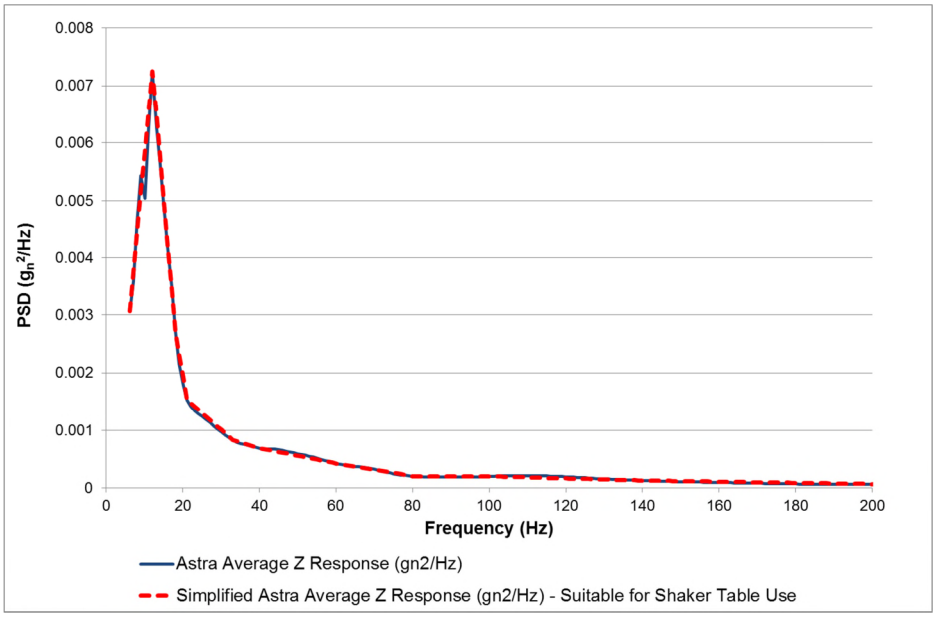

Figure 23: Example Z Axis Test Profile Suitable for Shaker Table, Derived from PSD for Test Vehicle

Within this example the simplified PSD is defined by 12 breakpoints from 6 Hz to 200 Hz. It is necessary to check the SRS of the simplified profile with that of the original data to ensure that the original data is not exceeded significantly by the simplified profile. Finally the derived test profile can be used for durability evaluations of the target component or assembly.

3.4 Synthesis of Vibration Profile Representative of 100,000 Miles of UK BEV Usage

The following chapter summarises the experimental method employed to measure the vibration experienced by the RESS within contemporary BEV products when subjected to road surfaces typically of normal customer usage. It defines the stages associated with converting these vehicle measurements into a random vibration profile that could be replicated on either a hydraulic or electromagnetic shaker system. A summary of this process is presented graphically in Figure 24. The commercially available nCode 11.1 software was employed within this study to process the desired PSD plots for each of the X, Y and Z axes, and the associated FDS and SRS data.

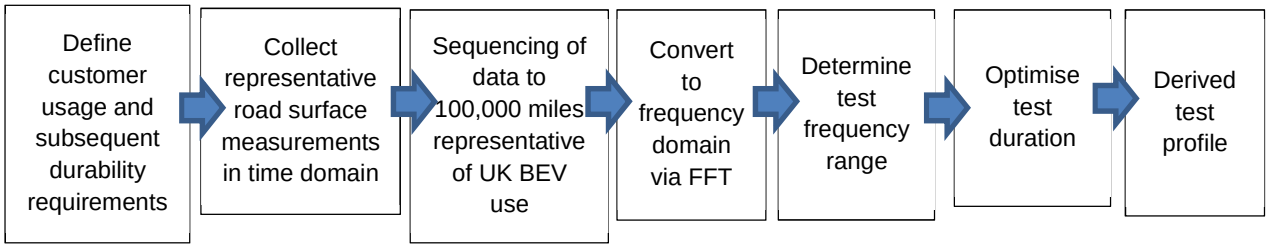

Figure 24: Process of Generating a Random PSD from Road Load Data

3.4.1 Defining Customer Usage and Durability Requirements

Within this study a known whole vehicle durability schedule was employed as a framework to define the number of repeated road surfaces that would be sequenced together to form 100,000 miles of proving ground durability. This procedure was the Millbrook structural durability schedule [115]. While this procedure represents an internal organisational standard, it has evolved over 20 years of experience and is currently employed by a number of leading vehicle manufacturers to assess the service life of their products [32]. It defines a number of repeats for each measured surface to replicate a representative vehicle life within a European market. As discussed within [26, 32] the weighting of surface classification (urban, rural or motorway surfaces) within the Millbrook durability schedule is based on ICEV usage. The original surface weighting for each surface classification is illustrated in Table 8.

Table 8: Surface Classification Weightings [115, 116]

Surface Classification	Original Millbrook Structural Durability Surface Classification Weighting (%) [115]	Revised Surface Classification Weighting - based on 2014 University of Warwick Study of BEV Journeys (%) [116]
Urban	45	37.3
Rural	31	39.1
Motorway	24	23.5

3.4.2 Collecting Representative Road Surface Data

The road surface data was collected initially for an MSc project presented in [26] and was utilised for this study. The vibration data was measured from the RESS of three different commercially available BEVs when driven over the specialised durability surfaces available at Millbrook Proving Ground (MPG). The three BEV's evaluated were the Smart ED, Nissan Leaf and Mitsubishi iMiEV. Additional information on the vehicle specifications are presented in [26, 32]. Each BEV was instrumented with two tri-axial accelerometers mounted directly mounted on the battery system.

The collection of the road load data was conducted using LMS V8 SCADAS mobile input cards installed into a single LMS SCM05 mainframe which logged the vibration response of each accelerometer via LMS "Test.Xpress" Time Data Acquisition. The accelerometers used were Piezoelectric Tri-axial ICP accelerometers (PCB 356B08), which were mounted to the desired location of the vehicle via a mounting base and Hottinger Baldwin Messtechnik GmbH (HBM) X60 adhesive. Data was collected at a sample rate of 2000 Hz, which was the maximum sample rate of measurement equipment. This resulted in a maximum post processed frequency of 800 Hz in accordance with "Nyquist rate" guidelines. This sample rate also allowed for peaks within the data to be resolved up-to a frequency of 200 Hz. The data was recorded using the SAE J670e vehicle axis convention shown in Figure 4.

The vibration response at each of the measurement locations was recorded by driving the vehicles over the durability surfaces at MPG. A short description of the different road surfaces utilised for vehicle measurement is provided in Appendix C.

Unlike previous studies discussed in [71], measurements of multiple surface types and conditions commensurate with those witnessed during a vehicle's life time were recorded. These surfaces were selected in accordance with the Millbrook structural durability procedure [115] which defines surfaces and a driving framework typical of European customer operation.

All vehicles were assessed with the same driver and passenger who both weighed approximately 74 Kg (+/- 2 Kg) to ensure consistency in vehicle payload and repeatability of measurement methodology. Each vehicle battery was charged to 100% state of charge (SOC) prior to the start of vehicle measurement and tyres were inflated to the manufacturers recommended "normal operation" pressure. A

summary of the test vehicle dimensions and specifications are shown in Appendix D.

3.4.3 Sequencing of Surfaces to Represent an BEV Service Life

To generate a representative vibration profile, a random PSD was generated from a variety of different surfaces and operational environments. These surfaces were sequenced and repeated in a manner that was consummate with the typical usage behaviour of the target vehicle type. Within this study, a new surface weighting factor based on the road surface classification by drivers of BEV (shown in Table 8) undertaken by a separate study at the University of Warwick [116] was applied to the surface repeats defined in [115]. The revised repeats of each test surface with this BEV weighting applied for a cumulative mileage of 100,000 miles is defined in Table 9.

Each measured surface from each of the three test vehicle were sequenced within "nCode 11.1 glyphworks" using the test schedule create function.

Table 9: Number of Repeats of Each Measured Surface to Replicate 100,000 miles of BEV Customer Usage

BEV Study Surface Relating to Module	Surface in km	Classification of Surface	Repeats of Surface Required to Simulate 100,000 Miles (160,934 km) of BEV weightings	Total Distance in km
Belgian Pave	1.45	Urban	3395	4923
Cats Eyes 30mph	0.16	Rural	5295	847
Cats Eyes 50mph	0.16	Rural	5295	847
City Course	1.29	Urban	37177	47958
Handling Circuit	4.51	Rural	1933	8719
Hill route (Loop 1)	1.77	Rural	29695	52560
HSC	5.95	Motorway	2851	16961
Mile Straight (PT)	1.29	Motorway	8141	10502
Mile Straight (WOT)	1.29	Motorway	8141	10502
Pot Holes	0.16	Urban	306	49
Random Waves	0.64	Urban	6791	4346
Sine Wave	0.16	Urban	6813	1090
Twist Humps	0.16	Urban	10186	1630
TOTAL (km)				**160934**

3.4.4 Convert to Frequency Domain and Determination of Test Frequency Range

Within this study, the measured and sequenced data was converted to the frequency domain within "nCode 11.1 glyphworks" using the FFT function. 5 to 200 Hz was chosen for the BEV RESS test profiles within this study and is illustrated in Figure 25.

A peak frequency of 200 Hz was chosen to ensure that it could be replicated on hydraulic shakers (which typically display performance run off above 250 to 300 Hz [45, 117]), whilst a 5 Hz starting point was chosen so that the profile could be conducted on electromagnetic shaker facilities which typically cannot replicate frequencies below 5 Hz (due to the lower displacement associated with these

facilities). Reviewing PSD's of the test data highlighted that the majority of vibration energy occurred between 0 to 120 Hz.

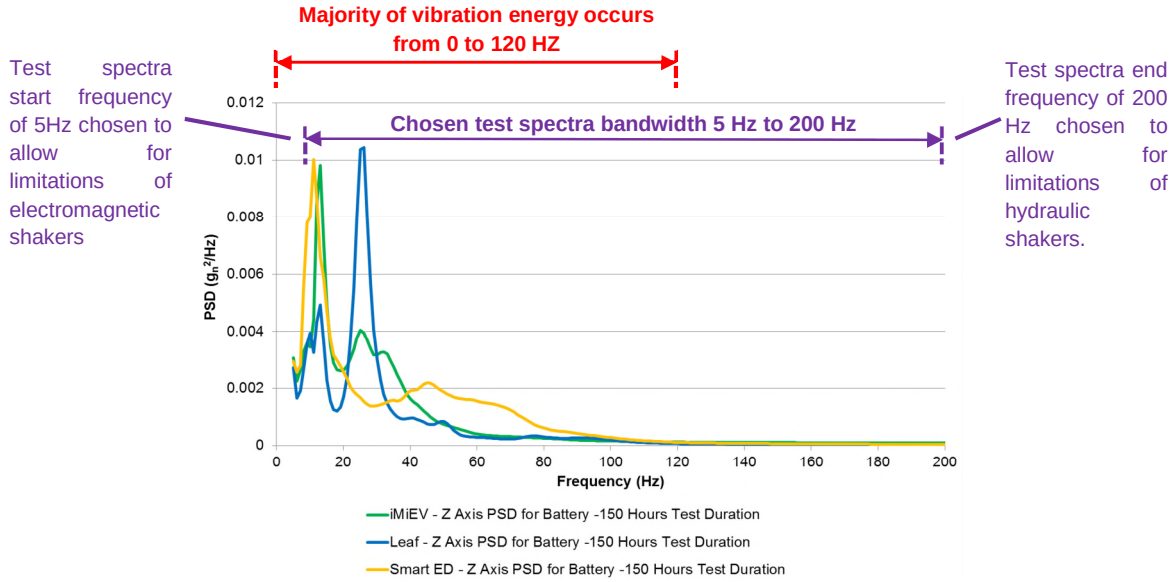

Figure 25: Illustration of Selected Frequency Bandwidth for Synthesised Test Profile

3.4.5 Optimise Test Duration

Within this study, the test was optimised with respect to time for two different test durations of 50 hours and 150 hour per axis. 50 hours was chosen so that 1 hour was representative to 2000 miles of durability loading in the desired test axis. 150 hours per axis was chosen as a conservative test duration that would result in lower shock loading and subsequently a higher degree of correlation with the in-service environment. Figure 26 shows a SRS of each of the two test durations compared to the SRS analysis of the pre sequenced data in g_n (as shown by the red dashed line in Figure 26).

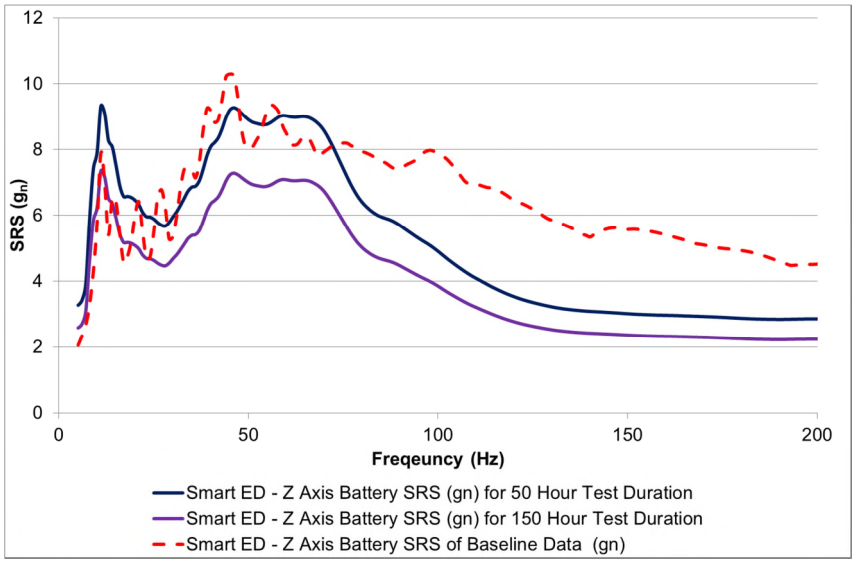

Figure 26: Effect of Test Duration of Derived PSD's SRS in Relationship to the SRS of Un-sequenced Surface Data

It can been seen that the 150 hour test duration is well within the SRS of the baseline SRS, whilst the 50 hour test has a greater shock loading than the pre sequenced data from 5 to 20 Hz and 55 to 70 Hz which indicates that this test is over accelerated with respect to its time compression within these frequencies. Subsequently the 50 hour test duration is not considered to be representative of the in service condition.

3.4.6 Derived Test Profile

To define a generic test profile that would be suitable for a wide range of passenger BEV's the generated PSD for each axis from each vehicle were overlaid. The peak values were selected. These peak values were then used to derive a simplified PSD that enveloped the greatest vibration witnessed by the RESS within A and C segment BEV's within this study. This peak enveloping process is illustrated in Figure 27.

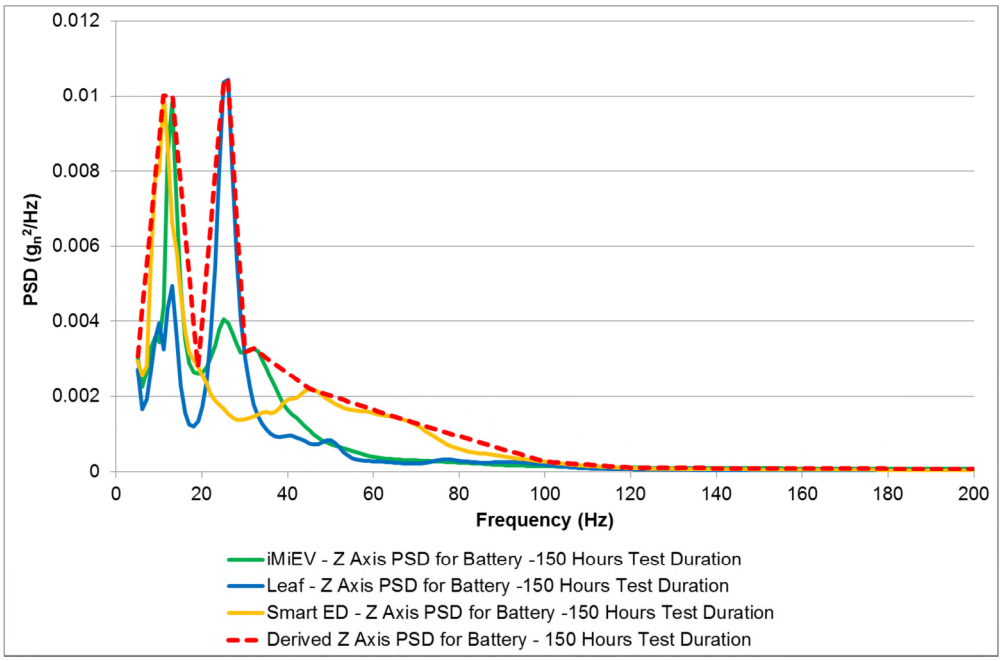

Figure 27: Example Z-Axis Test Profile Derived by Peak Enveloping of Derived PSD for Each Test Vehicle

The derived profiles were defined via no more than 15 break points of variable frequency spacing. This was to ensure that they could be uploaded into a wide range of shaker system controllers whilst maintaining suitable PSD resolution to define the desired vibration loading.

The subsequent synthesised vibration test profiles, representative of 100,000 miles of durability for the X, Y and Z axis of a RESS are illustrated in Figure 28, whilst the break points of the synthesised profile are defined in Table 10.

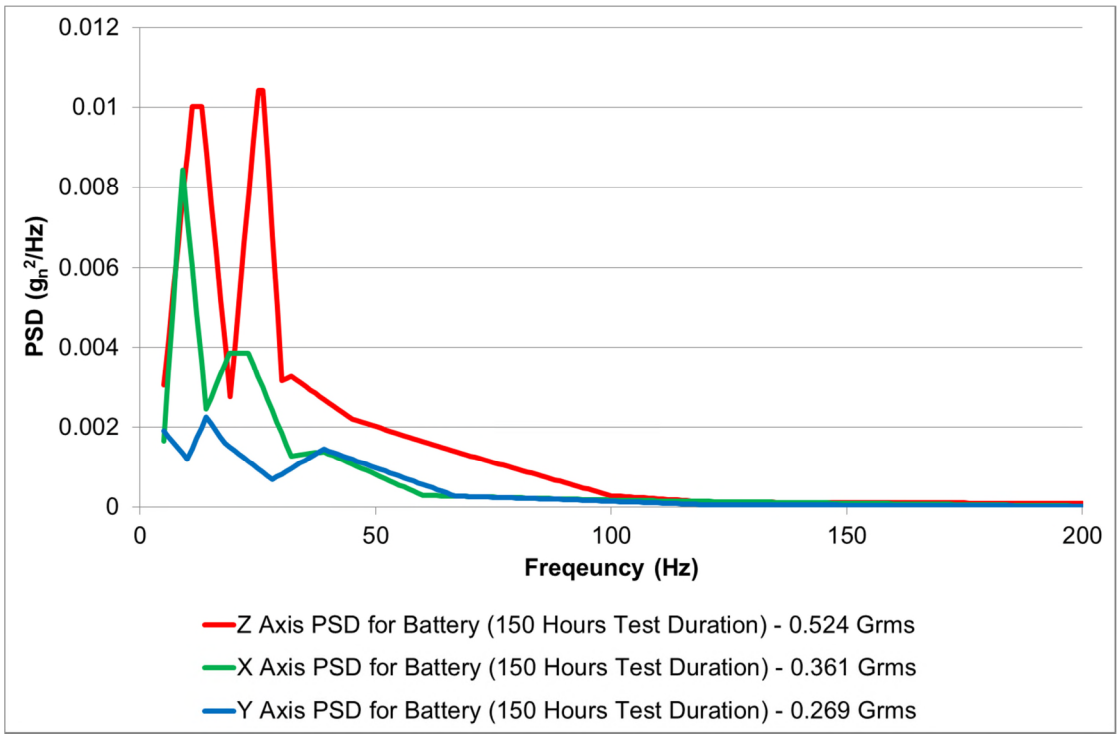

Figure 28: Synthesised Test PSD's for 150 Hours Test Duration per Axis

Table 10: Break Points for Derived BEV Random Vibration Profile Representative of 100,000 Miles of Customer Usage in UK for 150 Hours Test Duration

Frequency (Hz)	X Axis PSD for Battery (150 Hours Test Duration) g_n^2/Hz Grms = 0.361	Frequency (Hz)	Y Axis PSD for Battery (150 Hours Test Duration) g_n^2/Hz Grms = 0.269	Frequency (Hz)	Z Axis PSD for Battery (150 Hours Test Duration) g_n^2/Hz Grms = 0.524
5	0.0016585	**5**	0.0019155	**5**	0.003062
9	0.0084295	**10**	0.0011905	**9**	0.0078005
14	0.0024565	**14**	0.002253	**11**	0.010018
19	0.0038555	**18**	0.0015989	**13**	0.010018
23	0.0038555	**28**	0.00068665	**19**	0.002771
32	0.001272	**39**	0.001444	**25**	0.010439
39	0.0013865	**67**	0.00026895	**26**	0.010439
60	0.0002894	**85**	0.0002043	**30**	0.003168
100	0.0001643	**120**	0.00005535	**32**	0.0032675
200	0.000019045	**200**	0.000016065	**45**	0.0021935
				68	0.00134415
				100	0.00027795
				120	0.0001233
				150	0.0001044
				200	0.000088275

3.5 **Comparison of Test Standards to Measured Data**

Within this Chapter the FDS and SRS of the synthesised profiles (presented in Figure 28 and Table 10) are compared to the FDS and SRS of the RESS tests standards presented in Chapter 2. The purpose of this is to understand the suitability of contemporary standards for vibration durability assessments via comparisons to test profiles that have been derived from real world BEV RESS measurements to replicate 100,000 miles of UK customer usage.

Within this study, the FDS and SRS were calculated using an assumed damping of 5 % (Q = 10). This value of damping was chosen based on the work discussed within [71]. All FDS within this study are calculated for a comparative dimensionless analysis; they use a default system stiffness (K) of 1 N/m^3 as the proportional constant between displacement and stress for a single degree-of-freedom, and a Basquin coefficient C of 1. In the calculations the value of the Basquin exponent material parameter b, was set to 4. 4 was chosen as the value for the material parameter of b based on the study discussed in [71] and the analysis of empirical data discussed in [113, 118]. A summary of the parameters utilised within this study are shown in Appendix E to allow for the replication of the results from this investigation in future studies.

For the analysis of ISO12405, the 21 hour test duration was chosen within this comparison as this is the longest test duration provided and therefore assumed to be the most damaging. For USABC Procedure 10, the long and short test durations for the random profile procedures are both presented. Within the swept sine tests for USABC procedure 10, the additional 6000 sine cycles for the X, Y and Z axis were performed at 13 Hz (for the Z axis) and 19 Hz (for the X and Y Axis). These frequencies were selected by reviewing where natural frequencies were witnessed within the measured vehicle data discussed in [26] and within the PSD profiles shown in Figure 28 and Table 10.

As discussed in Section 3.3.6, FDS is presented as a comparative measure within this study of fatigue potential of different test profiles and is not presented as an absolute measure of fatigue damage. The FDS and SRS functions with nCode V11.1 were utilised to develop the data presented within this Chapter. Whilst nCode V11.1 contains specific IP which produces refined SRS and FDS data it utilises the theory defined within Appendix A and B within the calculation of these spectra.

3.5.1 Comparison of FDS – Random Test Procedures

Figure 29 shows a comparison of the FDS of the derived BEV profiles to current test standards. Reviewing the potential fatigue damage for the Z-axis (as shown in Figure 29a), it is noticeable the derived profiles have a comparable fatigue damage from 30 to 70 Hz as the USABC Procedure 10 standard. However, the synthesized profiles typically have a greater fatigue loading from 5 to 15 Hz. Both the ISO12405 and BS62660 Z-axis profiles have a greater fatigue loading than the profiles

generated from BEV battery measurements, indicating they are too aggressive for durability assessments.

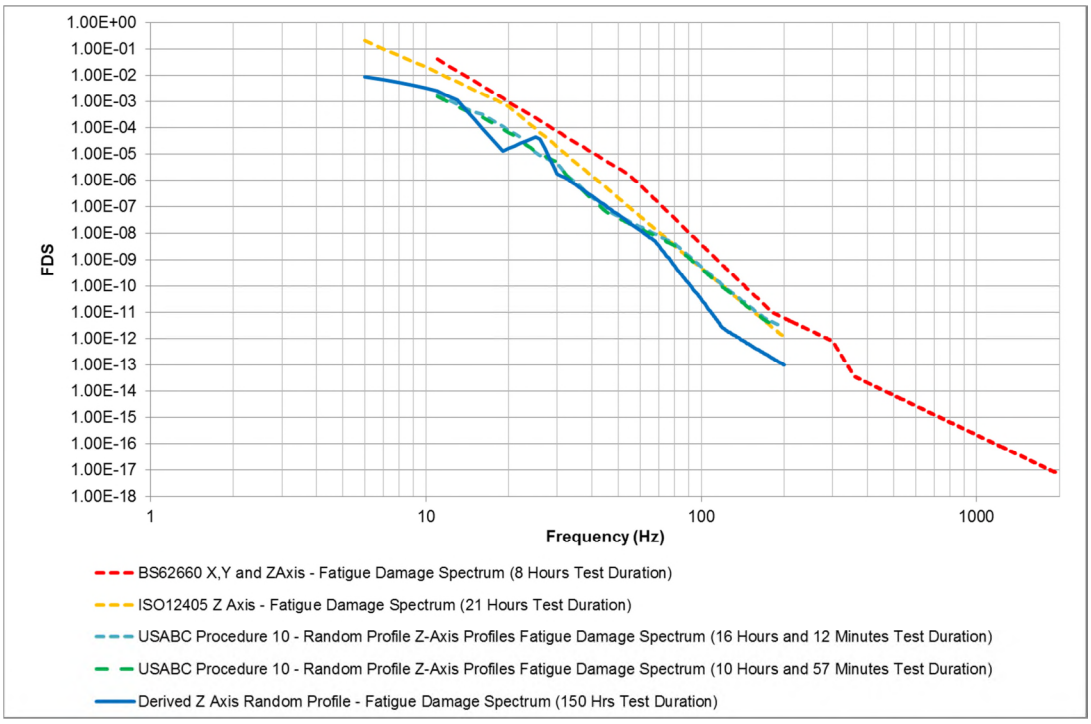

a)

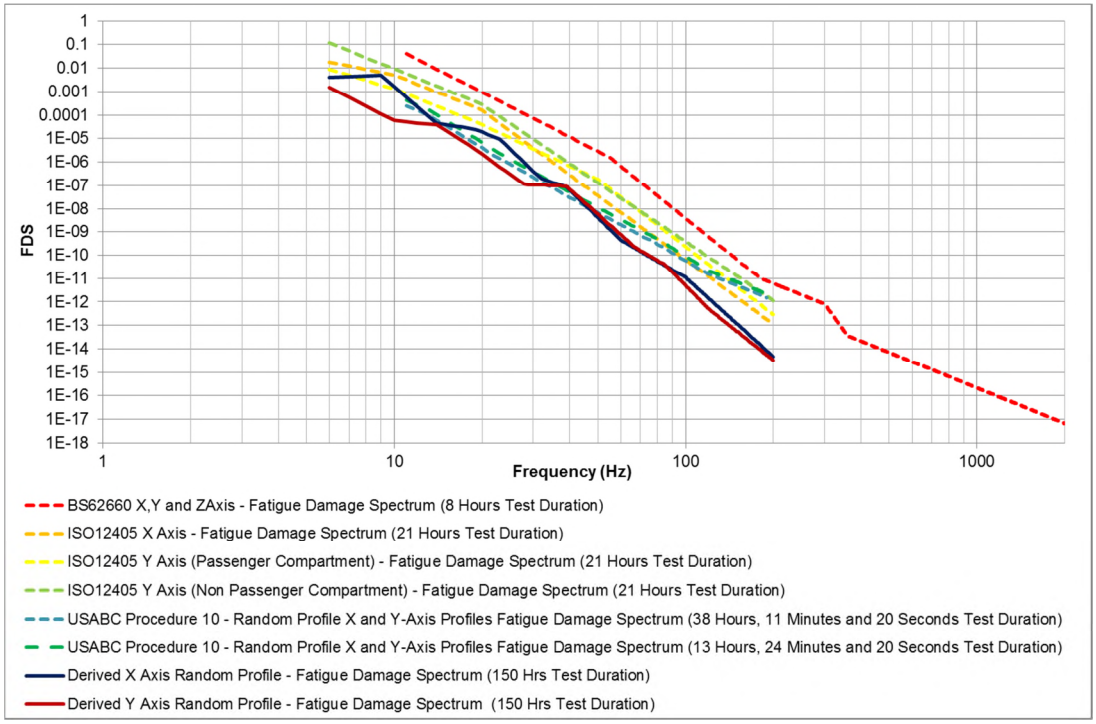

b)

Figure 29: FDS of Standards Utilising Random Profiles vs FDS from Derived Test Profiles a) Z -axis, b) X and Y-axis

Assessing the X and Y-axis FDS (as shown in Figure 29b), it is noticeable that the potential fatigue damage of the USABC Procedure 10 standard is lower than that generated by the synthesised test data from 15 to 30 Hz for the X-axis. This

demonstrates the importance of having two separate test profiles for the X and Y-axis of the vehicle and not relying on a simplified profile for the horizontal and longitudinal axis. However, it must also be noted that the USABC Procedure 10 also has been developed from North American market data, wherein the profiles developed in this study have been generated from European surfaces weighted to a UK customer usage. Also two “A segment vehicles” (Smart ED and Mitsubishi iMiEV) were measured within this study, both of which are likely to have greater roll and pitch moments due to their compact dimensions that the vehicles used within the development of the USABC manual such as the General Motors (GM) EV1 [119].

Like the Z-axis both BS62660 and ISO12405 show a significantly higher fatigue damage potential than profiles derived from 100,000 miles of durability suggesting that they are too aggressive to determine the degradation of battery assemblies, with normal customer use and are only suitable for robustness studies. It is also notable that the fatigue potential of all the random profiles currently available is significantly higher in all three axis at frequencies above 70 Hz than the profiles derived from BEV measurements.

3.5.2 Comparison of FDS - Swept Sine Test Procedures

Figure 30 shows the comparison of the FDS of the synthesised X, Y and Z-axis vibration profiles for 150 hours duration and the FDS for test procedures that apply vibration via a swept sine profile. It is noteworthy that at lower frequencies of 5 to 20 Hz, the FDS of the majority of swept sine test procedures are less than that of the profiles generated from actual BEV measurements within this study. Subsequently they are not severe enough within the 5 to 20 Hz bandwidth.

UL2271, has a fatigue damage potential which is significantly lower than the measured vehicle data (and other swept sine test standards) up to 100 Hz, which indicates that this procedure is unsuitable for even robustness assessments of BEV battery assemblies. UL1641 also has limited FDS correlation with the profiles generated from measured BEV data and other swept sine profiles. This standard also has a limited bandwidth of evaluation and subsequently is unsuitable for durability assessments or even robustness quantification of BEV RESS.

Like UL2271 and UL1642, AIS-048 has a FDS which has no comparable trend to that of the measured vehicle data. It has a far lower fatigue damage potential at low frequencies and excessive fatigue damage at frequencies greater than 30 Hz.

GB/T31486-2015 has greater fatigue loading than the profiles derived from measured vehicle data and a FDS loading trend that is comparable, making it a suitable homologation robustness test for the Z-axis of a given battery system. However whilst it does apply significantly more fatigue damage at frequencies above 25 Hz, it does have a limited frequency excitation range.

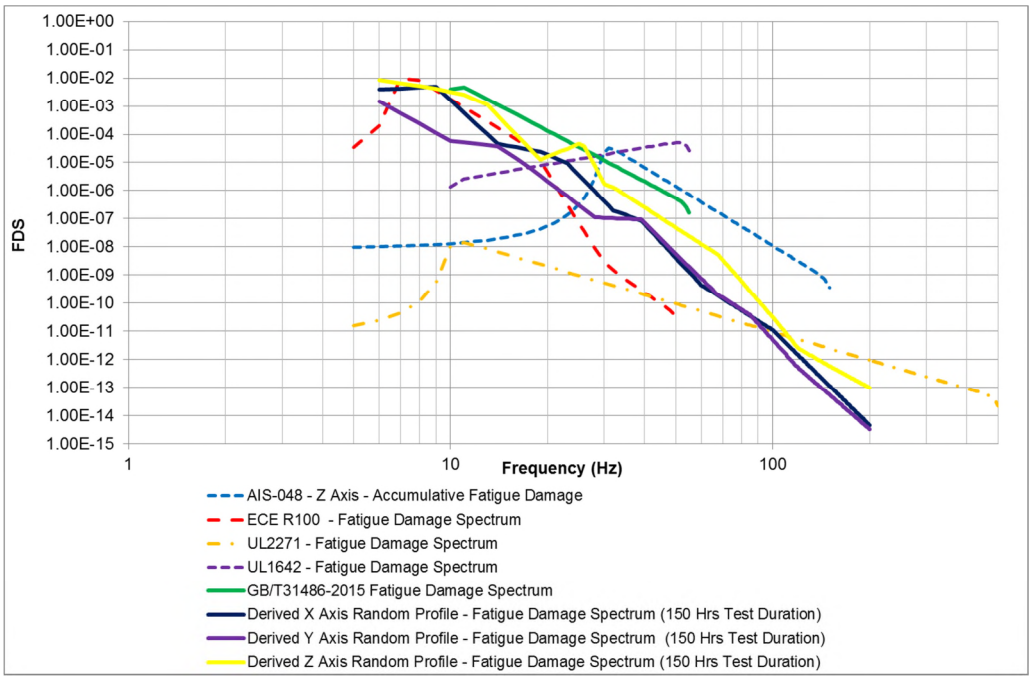

a)

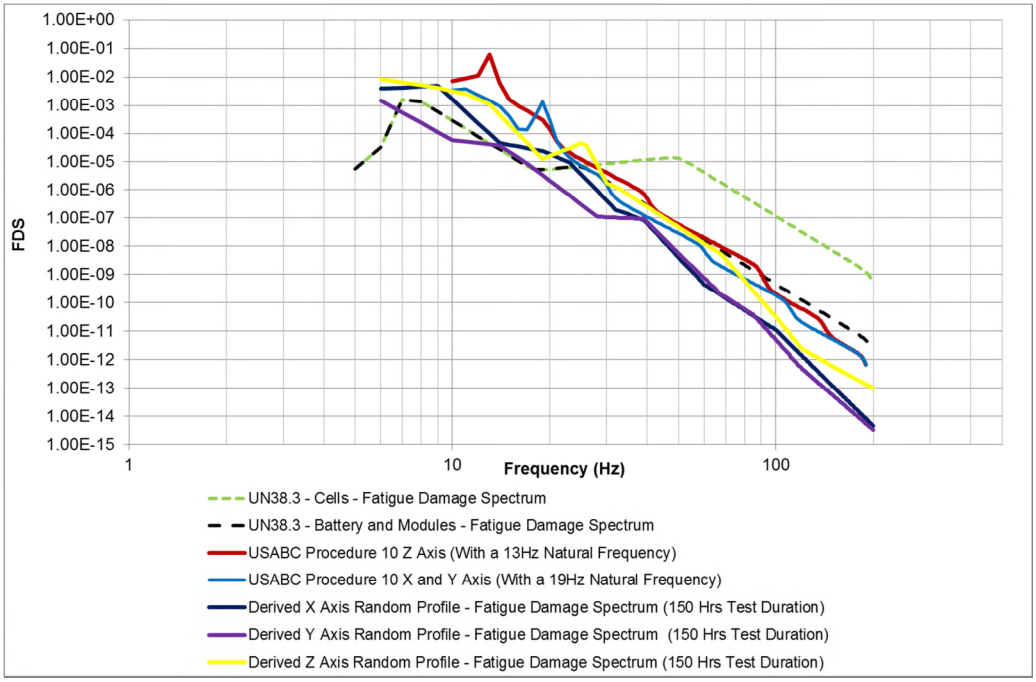

b)

Figure 30: FDS of Standards Utilising Swept Sine Profile vs FDS from Derived Test Profiles for 150 Hours Duration a) Shows the Comparison to AIS-048, ECE R100, UL1642, UL2771 and GB/T31486-2015 b) Shows the Comparison to UN38.3 and USABC Procedure 10

Interestingly the FDS of the UN38.3 “battery and module” test is comparable to the derived Z axis profile between 30 to 70 Hz. However both UN38.3 test methods, typically apply lower fatigue damage than the derived Z and X-axis profiles at frequencies below 20 Hz. Given that this standard has been developed to evaluate the airworthiness of a RESS when in a cargo condition it is understandable that there is this difference between real vehicle data and UN38.3.

ECE R100 has some low frequency fatigue damage correlation with the measured Z axis data, however after 20 Hz, the correlation declines. Given that ECE R100 is a robustness test for European homologation it should ideally be reworked so that the, the fatigue loading at frequencies above 20 Hz are greater than the profiles from measured data which have a durability focus.

The swept sine profiles within USABC Procedure 10 have much higher fatigue damage than measured data that has also been sequenced to 100,000 miles durability. The X and Y-axis FDS within the sine profiles for USABC procedure 10 are very severe by comparison to the derived X and Y profiles FDS. This indicates that there is a high time compression factor being applied to the swept sine profiles. However it is noteworthy that there is some correlation between the derived Z axis profiles and the Z axis profile for USABC Procedure 10 between 40 to 70 Hz.

As highlighted within [71], this comparison of FDS shows that it is necessary to evaluate each axis of the vehicle with a different vibration profile as the potential for fatigue differs from axis to axis. This is a key limitation of the current suite of swept sine profiles available to engineers for validating RESS, in that they only apply vibration in the vertical axis, or rely on the same vibration profile for all three axis of the vehicle.

3.5.3 Comparison of SRS – Random Test Procedures

Figure 31 shows the SRS spectrum of the developed vibration profiles compared to that generated from ISO12405, USABC Procedure 10 and BS62660 for the X, Y and Z-axis. BS62660 (which uses the same profile for all axis of the DUT) displays shock levels which are typically 2 to 4 times greater than that witnessed in profiles generated from BEV battery data indicating that this test is unsuitable for durability assessment of BEV RESS and their associated components. Like BS62660, USABC Procedure 10 and ISO12405 profiles apply a significantly higher shock load than that applied by durability profiles sequenced to replicate 100,000 miles of durability. For the X and Y-axis data (presented in Figure 31b) the trends in SRS differ from standard to standard, with the poorest correlation in SRS being witnessed with USABC Procedure 10.

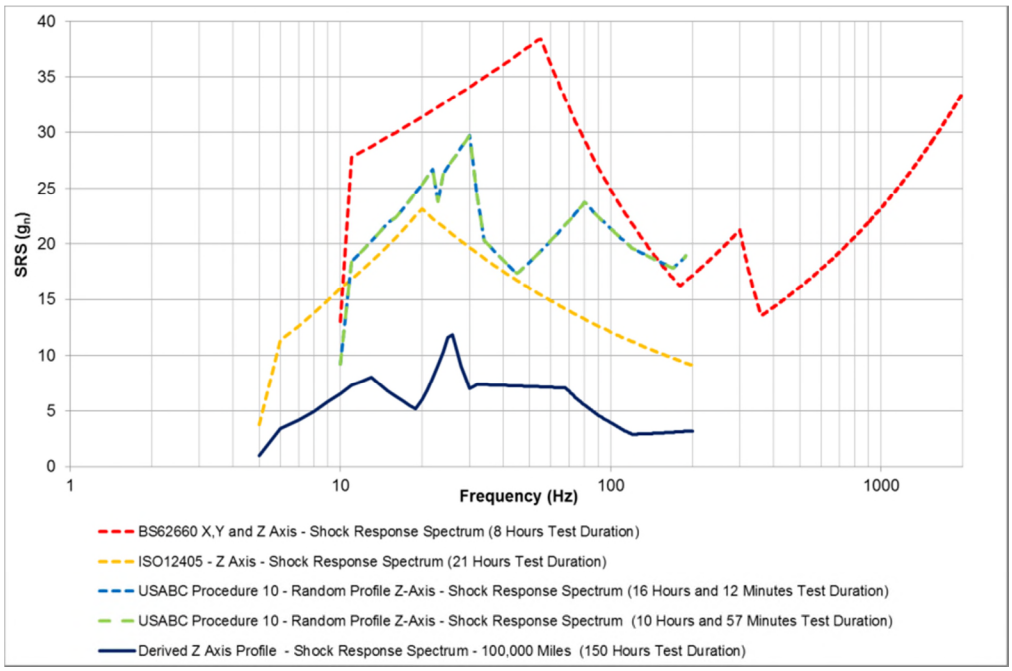

a)

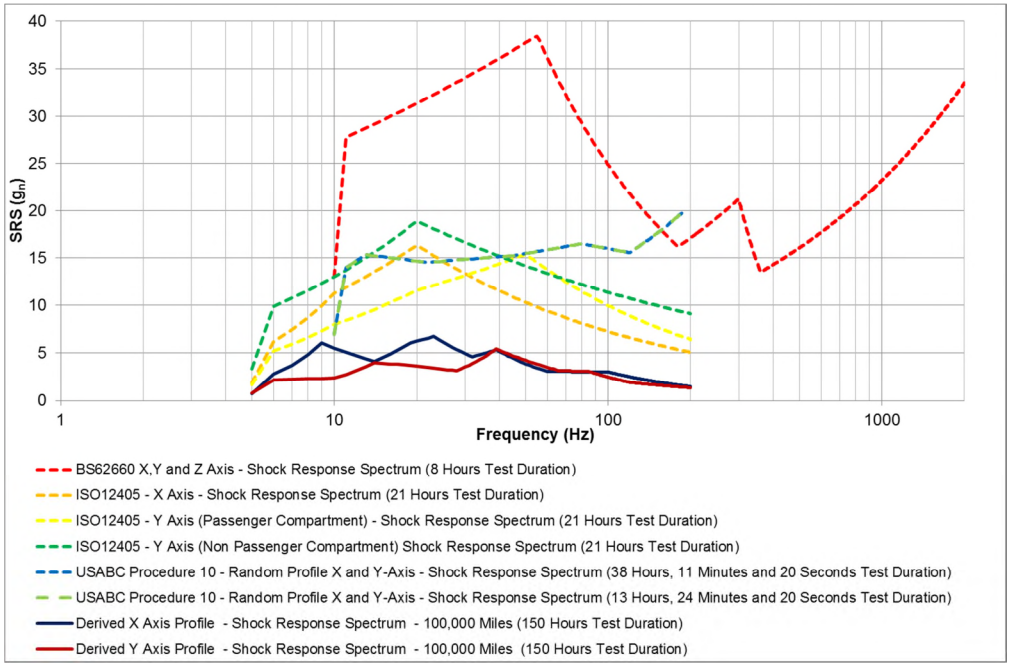

b)

Figure 31: SRS of Standards Utilising Random Profiles vs SRS from Derived Test Profiles a) Z-axis, b) X and Y-axis

3.5.4 Comparison of SRS - Swept Sine Test Procedures

Figure 32 illustrates a comparison of the SRS of test procedures that apply vibration via a swept sine profile with the SRS from the derived vibration profiles for the X, Y and Z-axis from BEV measurements for 150 hours test duration. What is noticeable from this comparison is that all the current swept sine profiles have little correlation with respect to SRS. At frequencies between 5 and 30 Hz, UL1642 and UL2271 have a lower SRS loading than profiles derived from vehicle data. Similarly AIS048

has significantly lower shock loading at frequencies between 5 and 20Hz. From this evidence it would be undesirable to use these standards to validate the robustness or durability of the BEV RESS. GB/T31486-2015 has a constant SRS over its test frequency range and shows little relationship to the SRS from BEV data. Like UL1642 and UL2271, this standard is overly simplified and subsequently unsuitable for robustness or durability evaluation of RESS. However it is noteworthy that both UL1642 and UL2271 have some correlations with the derived X and Y axis profiles from 30 to 40 Hz.

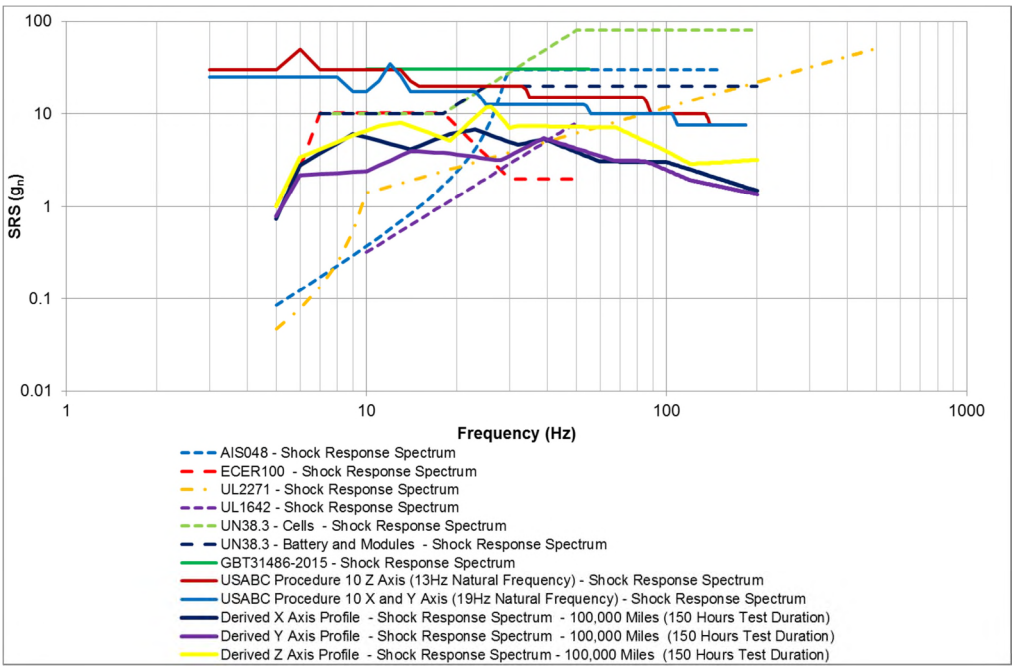

Figure 32: SRS of Standards Utilising Swept Sine Profile vs SRS from Derived Test Profiles for 150 Hours Duration

Looking at the SRS for UN38.3 and ECE R100, it could be argued that the shock loading envelopes the Z axis SRS from the derived vibration profiles from 5 to 20 Hz. Beyond this bandwidth, the correlation between these standards and the derived profiles declines. It is possible that the UN38.3 profile for battery and modules could be adjusted with respect to duration (increased in time) so that the SRS was reduced and thus produced a more representative shock load beyond 25 Hz. This maybe achived through a reduction in the time compression factor applied to this standard.

The SRS of the USABC Procedure 10 swept sine profiles is greater than the measured SRS and like the random PSD profiles within the standard indicate a high time compression factor resulting in an overly aggressive test.

What is clear from this comparison is that the SRS is significantly different for each of the vehicle axis. Validating with a single vibration spectrum for X, Y and Z of the DUT or just validating a RESS in its Z axis only, is undesirable for determining its durability or robustness with respect to vibration.

3.5.5 PSD Comparison - Random Profile Based Tests Only

A comparison of the PSD's of derived vibration profiles to that of the PSDs for the test specifications that apply vibration spectra via random vibration profiles has also been conducted within this study (illustrated in Figure 33).

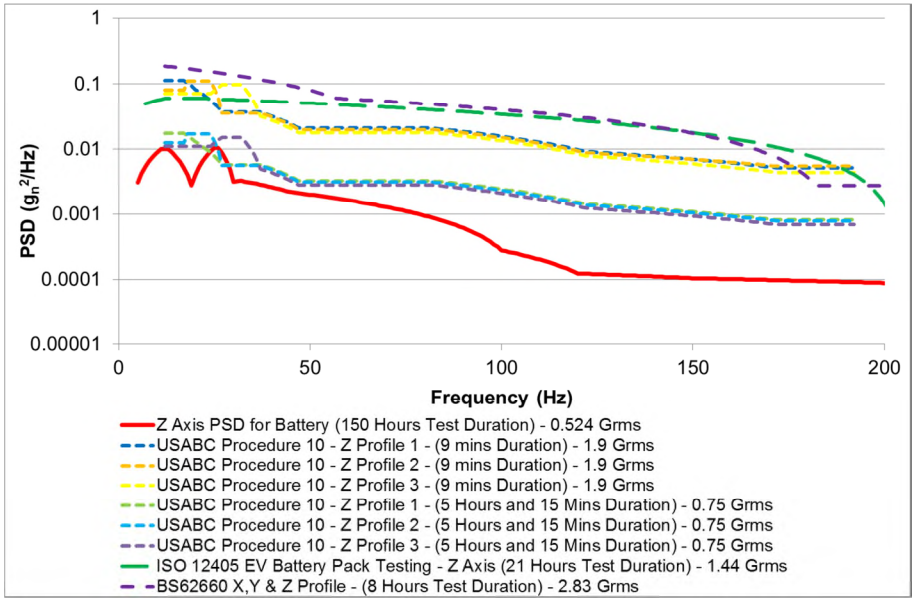

a)

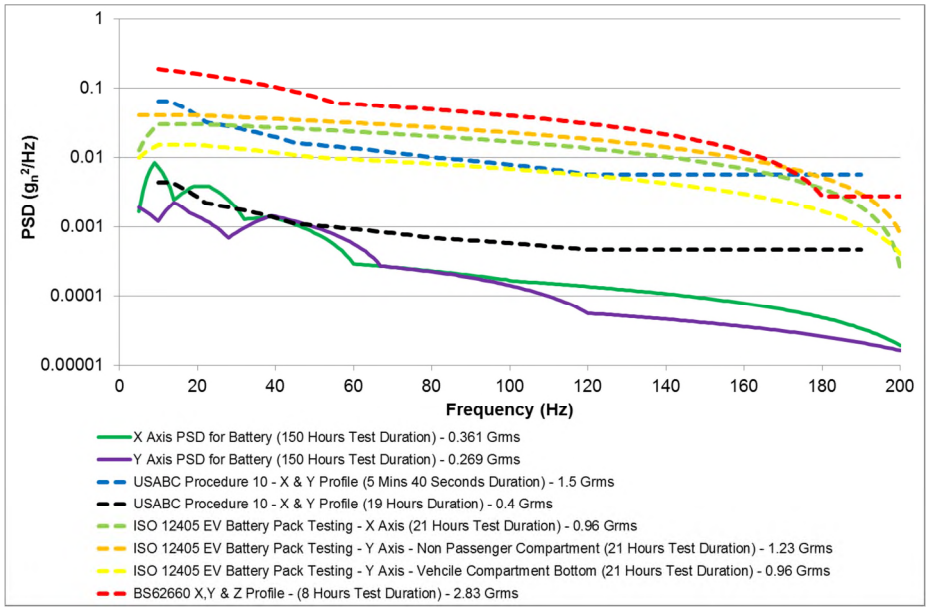

b)

Figure 33: Comparison of PSD for Current Vibration Tests that Apply Vibration via a Random Test Methodology and Synthesised Vibration Profiles a) Z Axis Comparison b) X and Y Axis Comparison

The PSD profiles presented have been adjusted to take into account the specified Grms level within the given standards. Whilst the author recognises that a comparison of the PSD content does not take into account the effect of time compression (hence the comparisons via SRS and FDS), it has been included within this assessment to look at notable trends within the PSD spectra shapes.

What is noticeable from Figure 33 is that the acceleration levels of USABC Procedure 10 profile for the lower Grms levels (0.75 Grms for Z axis and 0.4 Grms for X and Y axis) show close correlation to the synthesised profiles for 10 to 60 Hz. The acceleration content declines significantly, beyond this bandwidth for the lower Grms levels for USABC Procedure 10. It is noteworthy that both USABC Procedure 10 and the generated profiles are for 100,000 miles durability.

The acceleration content for both BS62660 and ISO12405 is significantly higher than that within the synthesised vibration profiles are not suitable for durability studies.

3.6 **Discussion**

The findings discussed within Section 3.5 are summarised in Table 11 and Table 12. Table 11 summarises the results for random PSD standards whilst Table 12 summarises the comparison for swept sine profiles. For simplicity, these tables are colour coded to indicate the degree of visual correlation between the profiles synthesised from BEV measurements and the test standard of interest. Red indicates no correlation; amber indicates partial correlation within a defined frequency band, whilst green indicates correlation.

Table 11: Summary of Comparison of FDS and SRS for Current EV Vibration Test Standards which Apply Vibration via a Random PSD when Compared to 100,000 Miles of UK BEV Durability

		Frequency Range for Comparison to Measured Vehicle Data					
Procedure	**FDS / SRS**	**5 Hz to 10 Hz**	**10 to 30 Hz**	**30 Hz to 55 Hz**	**55 Hz to 70 Hz**	**70 Hz to 100 Hz**	**100 Hz to 200 Hz**
Random Profiles							
USABC Procedure 10 X and Y Axis	**FDS**		No correlation with X and Y Axis. Lower SRS for X Axis, greater SRS for Y Axis	Correlation from 30 Hz to 50 Hz to measured X axis data	No correlation – greater FDS	No correlation – greater FDS	No correlation – greater FDS
	SRS		No correlation – greater SRS	No correlation – greater SRS	No correlation – greater SRS	No correlation – greater SRS	No correlation – greater SRS
USABC Procedure 10 Z Axis	**FDS**		Partial correlation from 10 to 15 Hz with measured Z axis data	Correlation with measured Z axis data	Correlation with measured Z axis data	No correlation – greater FDS	No correlation – greater FDS
	SRS		No correlation – greater SRS	No correlation – greater SRS	No correlation – greater SRS	No correlation – greater SRS	No correlation – greater SRS
ISO12405 X Axis	**FDS**	No correlation – greater FDS	No correlation – greater FDS	No correlation – greater FDS	No correlation – greater FDS	No correlation – greater FDS	No correlation – greater FDS
	SRS	No correlation – greater SRS	No correlation – greater SRS	No correlation – greater SRS	No correlation – greater SRS	No correlation – greater SRS	No correlation – greater SRS
ISO12405 Y Axis	**FDS**	No correlation – greater FDS	No correlation – greater FDS	No correlation – greater FDS	No correlation – greater FDS	No correlation – greater FDS	No correlation – greater FDS
	SRS	No correlation – greater SRS	No correlation – greater SRS	No correlation – greater SRS	No correlation – greater SRS	No correlation – greater SRS	No correlation – greater SRS
ISO12405 Y Axis	**FDS**	No correlation – greater FDS	No correlation – greater FDS	No correlation – greater FDS	No correlation – greater FDS	No correlation – greater FDS	No correlation – greater FDS
	SRS	No correlation – greater SRS	No correlation – greater SRS	No correlation – greater SRS	No correlation – greater SRS	No correlation – greater SRS	No correlation – greater SRS
ISO12405 Z Axis	**FDS**	No correlation – greater FDS	No correlation – greater FDS	No correlation – greater FDS	No correlation – greater FDS	No correlation – greater FDS	No correlation – greater FDS
	SRS	No correlation – greater SRS	No correlation – greater SRS	No correlation – greater SRS	No correlation – greater SRS	No correlation – greater SRS	No correlation – greater SRS
BS62660 X, Y and Z Axis	**FDS**		No correlation – greater FDS	No correlation – greater FDS	No correlation – greater FDS	No correlation – greater FDS	No correlation – greater FDS
	SRS		No correlation – greater SRS	No correlation – greater SRS	No correlation – greater SRS	No correlation – greater SRS	No correlation – greater SRS

Table 12: Summary of Comparison of FDS and SRS for Current EV Vibration Test Standards which Apply Vibration via a Swept Sine Profile when Compared to 100,000 Miles of UK BEV Durability

		Frequency Range for Comparison to Measured Vehicle Data					
Procedure	**FDS / SRS**	**5 Hz to 10 Hz**	**10 to 30 Hz**	**30 Hz to 55 Hz**	**55 Hz to 70 Hz**	**70 Hz to 100 Hz**	**100 Hz to 200 Hz**
Swept Sine Profiles							
USABC Procedure 10 X and Y Axis	**FDS**		No correlation – greater FDS	No correlation – greater FDS	No correlation – greater FDS	No correlation – greater FDS	No correlation – greater FDS
	SRS		No correlation – greater SRS	No correlation – greater SRS	No correlation – greater SRS	No correlation – greater SRS	No correlation – greater SRS
USABC Procedure 10 Z Axis	**FDS**		No correlation – greater FDS	Correlation with measured Z axis data from 40 Hz	Correlation with measured Z axis data	No correlation – greater FDS	No correlation – greater FDS
	SRS		No correlation – greater SRS	No correlation – greater SRS	No correlation – greater SRS	No correlation – greater SRS	No correlation – greater SRS
UN38.3 Cell	**FDS**	No correlation – lower FDS	No correlation – lower FDS	No correlation – greater FDS	No correlation – greater FDS	No correlation – greater FDS	No correlation – greater FDS
	SRS	Partial correlation	Partial correlation	No correlation – greater SRS	No correlation – greater SRS	No correlation – greater SRS	No correlation – greater SRS
UN38.3 Battery	**FDS**	No correlation – lower FDS	No correlation – lower FDS	Partial correlation with measured Z and X axis data	Partial correlation with measured Z and X axis data	No correlation – greater FDS	No correlation – greater FDS
	SRS	Partial correlation	Partial correlation	No correlation – greater SRS	No correlation – greater SRS	No correlation – greater SRS	No correlation – greater SRS
UL2771	**FDS**		No correlation – lower FDS	No correlation – lower FDS	No correlation – lower FDS	No correlation – lower FDS	No correlation – lower FDS
	SRS		No correlation – lower FDS	Partial correlation from 30 to 40 Hz with measured X and Y axis data	No correlation – greater SRS	No correlation – greater SRS	No correlation – greater SRS
UL1642	**FDS**		No correlation – lower FDS	No correlation – greater FDS			
	SRS		No correlation – lower SRS	Partial correlation from 30 to 40 Hz with measured X and Y axis data			
ECE R100	**FDS**	Correlation	Partial correlation with Z axis data up to 20 Hz. Beyond this frequency the FDS is lower.	No correlation – lower FDS			
	SRS	Partial correlation	Partial correlation	No correlation – lower SRS			
AIS-048	**FDS**	No correlation – lower FDS	No correlation – lower FDS	No correlation – greater FDS	No correlation – greater FDS	No correlation – greater FDS	No correlation – greater FDS
	SRS	No correlation – lower SRS	No correlation – lower SRS	No correlation – greater SRS	No correlation – greater SRS	No correlation – greater SRS	No correlation – greater SRS
GB/T31486-2015	**FDS**		Partial correlation from 10 to 25 Hz	No correlation – greater FDS			
	SRS		No correlation – greater SRS	No correlation – greater SRS			

The comparison shown has a durability focus, so whilst typically these standards display poor correlation with the profiles derived from BEV RESS measurements, specifications such as UN38.3, ECE R100 and GB/T31486-2015 are still desirable robustness testing methods as these apply a greater SRS and FDS. What is noticeable from this summary of the FDS and SRS comparison is that there is a greater occurrence of correlation between the FDS of the synthesised profiles and the test standards at lower frequencies. This also highlights that these tests are overly simplified and have a high time compression factor. Overall the current standards are undesirable for durability assessments of BEV RESS, which are to be integrated into A and C segment vehicles.

3.7 Conclusions

This study has devised vibration profiles for testing the X, Y and Z-axis of a RESS (and its sub components) for a 150 hours per axis that is representative of 100,000 miles UK BEV road usage, for A and C segment vehicles. The devised test profiles apply vibration from 5 to 200 Hz. This ensures that they can be replicated on a wide range of shaker systems whilst exciting the DUT within a suitable frequency range.

USABC Procedure 10, BS62660 and ISO12405 both have a significantly greater fatigue damage potential and shock loading when compared to vibration profiles developed from BEV vibration measurements representative of 100,000 miles UK A and C segment vehicle durability. This indicates that they are suitable for robustness testing as they replicate vibration loading that is excessive of normal customer operation.

UL1642, UL2271 and AIS-048 have limited SRS and FDS correlation to vibration profiles synthesised from BEV measurements for 100,000 miles durability and subsequently unsuitable for durability or robustness assessments of battery modules or RESS assemblies.

UN38.3 and ECE R100 have some partial correlation with the FDS and SRS of the profiles generated from BEV data for 100,000 miles durability however these standards are only suitable for robustness assessments due to their swept sine methodology.

Whilst GB/T31486-2015 has a suitable FDS strategy for a robustness test, its SRS spectra shows little comparison to that observed within measured vehicle data. It is therefore unrepresentative of the vibration environment witnessed by a BEV RESS.

A significant limitation with all test procedures (except ISO12405) is that they do not discriminate between the X, Y and Z axis vibration for the DUT. Some standards (such as ECE R100, GB/T31486-2015 and AIS-048) choose to completely or partially ignore the horizontal axis all together. Subsequently this simplified testing methodology either results in significant under or over testing of the DUT which is undesirable from both a robustness and durability perspective.

4 Study 2 – Modal Characterisation of EV Batteries

4.1 Introduction

As discussed in Chapter 2, one of the key factors in characterising the effect of vibration on EV battery components is defining their natural vibration characteristics. However, a critical review of the current literature has concluded that no studies exist which have fully characterised the inherent mechanical properties of EV cells to vibration stimuli. If future BEV and HEV batteries are to be designed such that the impact of vibration induced resonance is minimised, engineers tasked with the design of the vehicle's energy storage system must have a rigorous understanding of key system attributes such as the natural frequencies of the cell, the level of damping present and the mode shapes induced within the battery under mechanical load.

This study describes the underpinning theory and experimental method employed when using the impulse excitation technique to quantify the natural frequencies and mode shapes of a commercially available 25 Ah Nickel Manganese Cobalt Oxide (NMC) laminate pouch cell. Experimental results are presented for fifteen cells at five different values of SOC. The results indicate that irrespective of the energy content within the cell, the same four modes of vibration (torsion and bending) exist within a frequency range of 191 Hz to 360 Hz. This is above the frequency range (0 to 150 Hz) typically associated with road-induced vibration. The results also indicate that the cell's natural frequencies of vibration and damping do not vary with changing values of SOC.

This Chapter is structured as follows; Section 4.3 presents the experimental theory whilst Section 4.4 defines the test employed within this study to determine the natural vibration characteristics of NMC laminate pouch cells. The results and analysis are discussed in Section 4.5, whilst the discussion and conclusions are defined in Section 4.6 and 4.7 respectively.

4.2 Study Aim and Objectives

4.2.1 Objective

To determine the natural vibration characteristics of 25 Ah lithium-ion laminate pouch cells via the application of hammer survey experimental modal analysis testing and to understand if SOC has an effect on the observed vibration response behaviour.

4.2.2 Aims

- To measure and determine the natural frequencies, mode shapes, damping coefficients via experimental modal analysis of 25 Ah lithium-ion laminate pouch cells.

- To measure and assess if cell SOC effects the observed vibration response behaviour of the test items.

4.3 **Experimental Theory**

The aim of this section is to describe the theory associated with modal analysis using impulse excitation. Particular consideration is given to the method employed to secure and mount the pouch cell during testing, the excitation technique and the interpretation of the results obtained.

4.3.1 Cell Mounting and Support

When conducting experimental modal analysis, it is necessary to ensure that the correct method of support is selected. There are typically two options available, either unrestrained (free - free) or clamped (grounded). This discussion will primarily address the unrestrained support, since this was the method employed within the experimental activity. The use of an unrestrained support medium is preferred since the results obtained reflect only the mechanical properties of the component. Rigidly clamping the component to the test fixture is only used to emulate the in-service mounting conditions of the device and therefore includes the dynamics of the component and its support structure. A further detailed discussion of each support method is provided in Submission 2 and [106].

The definition of an unrestrained support is where the component is freely suspended in space [106, 120]. Within this ideal, the component exhibits six rigid body modes; three displacements (in the X, Y, Z co-ordinate axis) and three rotations around each of the three axes [106, 120]. Because this ideal condition assumes that no boundary condition exists, reactions between the support and the component have a natural frequency equal to zero. In practice, components are suspended on soft springs or foam pads. As a result, a true free-free support condition can never be realized. The use of low-density foam pads results in the six ridged body modes occurring at very low natural frequencies. In practice a support method and component is regarded as being within the free-free condition if the highest natural frequency of the support medium is less than 10 % of the value of the lowest natural frequency of the component under test or if there is at least a 100 Hz separation between them. The experimental results presented in Section 4.5, highlight a frequency separation of approximately 150 Hz between the foam pads employed to support the lithium-ion pouch cells and the first natural frequency of the cell itself (irrespective of the cell's SOC).

4.3.2 Cell Excitation and Response Measurement

There are three methods of excitation commonly employed when measuring the modal response of a component or system; impulse excitation (often referred to as either hammer surveying, impact testing or impact excitation), dynamic excitation and operational excitation.

Operational excitation requires the system to be subject to the actual loading profile that it will experience within the real world. This method is typically only employed when the system will be subject to a predefined loading or performed in conjunction with the impulse or dynamic excitation as a final verification test. Given the diverse nature of the different terrain profiles experienced by vehicles within either urban or highway environments in different parts of the world, the use of operational excitation would not be appropriate to assess the natural frequency of a BEV or HEV battery system. Dynamic excitation is often employed for components that may be damaged through impulse excitation [106]. Dynamic excitation typically employs a small electro-magnetic shaker (EMS) or hydraulic shaker to apply a known input (force and frequency) to the device or structure. The advantages of dynamic excitation are often cited to include a more repeatable test profile [106, 120, 121], with the ability to apply a broader range of test signals (force and frequency range). However, the resources required to implement a test program using this method are equally more demanding than impact excitation. The financial cost of the EMS or hydraulic shaker may well be prohibitive for a number of end-users [106, 121] . Similarly, the effort required to emulate the desired free-free test condition will require the design of a bespoke test assembly in which the cell is suspended onto the shaker. For these reasons, impulse excitation was defined as the desirable test method. For completeness, further information on both operational and dynamic excitations methods can be found in Submission 2 and [106, 122].

In addition to those reasons highlighted above, the reasons often cited for the use of impulse excitation include; reduced test preparation time, no specific requirements for test infrastructure (particularly when employed to undertake unrestrained testing) and the cost of the test equipment is not prohibitive [106, 120-122]. Impulse excitation is performed using an impact device such as an instrumented hammer of calibrated mass. A typical instrument is shown in Figure 34.

Figure 34: Example Instrumented Impact Hammer for Impulse Excitation [123]

The device consists of a head which can allow for the inclusion of additional masses, a calibrated force transducer, an interchangeable impact tip and handle

[106, 121]. A collection of tips are often supplied, each of different stiffness to allow the user to vary the characteristics of the impulse applied. The force transducer detects the magnitude of the impact force that is assumed to be equal and opposite to that experienced by the structure. As discussed within [106, 122], through careful selection of the hammer mass (H_m) tip stiffness (k_p), the upper frequency (f_{max}) in Hz, that the input excitation will excite can be approximated using Equation 3.

$$f_{max} = \frac{1}{2\pi}\sqrt{\left(\frac{k_p}{H_m}\right)}$$

Equation 3

f in Hz is defined by Equation 4 where ω is the frequency in Rad/s.

$$f = \frac{\omega}{2\pi}$$

Equation 4

The frequency (f_{max}) defines the cut-off frequency above which the energy supplied by the hammer reduces at a rate of 40 dB per decade. Section 4.4 discusses further the actual instrumentation employed within the experimental work, including the selection of hammer mass and tip stiffness to evaluate the frequency response of the NMC lithium-ion pouch cell.

Publications [106, 121, 122] state that the disadvantages associated with the use of impulse excitation include: the limited control of the experimental frequency range and a relatively high potential for operator error and measurement inaccuracy. Section 4.4 discusses further the steps employed to post-process the experimental results to reduce potential inaccuracy through spectrum averaging.

4.3.3 Mounting of Accelerometers

A key requirement for any modal analysis is the accurate measurement of the applied force and the response of the component. For impulse excitation, the input force is measured via a load cell installed within the impact hammer. Conversely, the vibration response of the component is measured using either single or multiple accelerometers mounted to the surface of the component. When mounting the accelerometers, the combined weight of the sensor including any mounting interface or adhesive must be less than 1% of the mass of the component [106]. As discussed within [106], above this threshold there is the potential to significantly change the natural frequency of the component and its frequency response. When selecting an accelerometer, there is typically a comprise between component weight and sensitivity; reducing the mass of the sensor will reduce its sensitivity, but will increase the frequency range of measurement [106].

As discussed in Section 3.3.2, there are multiple methods of bonding the accelerometers to the component. These include stud mounting, magnetic mounting

or pad mounting. For the experimentation discussed in Sections 4.4 and 4.5, an adhesive was employed to bond the accelerometer to the surface of the cell. Compliant materials, such as mounting waxes or interface mounts, can create a mechanical filtering effect by isolating and damping high-frequency transmissibility [124]. As discussed within [125], Petro-wax is often employed as it requires minimal surface preparation and does not significantly reduce the effective frequency range of the transducer [125]. Petro-wax is known to be a durable adhesive at lower temperatures, has a quick application time and no cure time. However, its transmissibility properties at high levels of force are limited and as such, it is only suitable for frequencies below 10 kHz [124]. It is also significantly affected by temperature elevation above a threshold of 30 °C.

4.3.4 Signal Analysis and Interpretation

4.3.4.1 System Dynamics

Impulse excitation is based on the assumption that the component under evaluation is a linear time invariant (LTI) system. Linearity means that the relationship between the input and the output of the system follows the law of superposition. Namely, if $x_1(t)$ produces a response $y_1(t)$ and $x_2(t)$ produces a response $y_2(t)$, then a scaled and summed input of $ax_1(t) + bx_2(t)$ will produce an output: $ay_1(t) + by_2(t)$. Time invariance means that for the input $x_1(t)$ the output is $y_1(t)$, the input $x_1(t - T)$ will produce the same output delayed in time by a value of T: $y_1(t - T)$.

The Impulse function, $\delta(t)$, is defined as a signal in which the amplitude (*A*): $A \to \infty$, while the time duration of the signal (*t*): $t \to 0$. The value (area) of $\delta(t)$ is unity. For a LTI system:

$$Y(s) = H(s)X(s)$$

Equation 5

Where $Y(s)$ is the output, $X(s)$ is the input and $H(s)$ is the transfer function that defines the dynamics of the system and *s* is the Laplace operator. When $X(s)$ equals unity, the output $Y(s) = H(s)$. Given that:

$$H(j\omega) = H(s)_{s=j\omega}$$

Equation 6

means that the resulting frequency response function (FRF) characterises completely the dynamics of the system in terms of both gain and phase:

$$Gain \ = |H(j\omega)|$$

Equation 7

$$Phase = \angle H(j\omega)$$

Equation 8

When quantifying the damping ratio and stiffness of the cell, the assumption is made that the system is dominated by second-order dynamics. As a result, the system transfer function can be approximated by:

$$H(j\omega) = \frac{{\omega_n}^2}{({\omega_n}^2 - \omega^2) - j2\varsigma\omega_n\omega}$$

Equation 9

Where ω_n defines the natural frequency in Rad/s and ς the damping ratio. Assuming the cell can be represented by a 2nd order mechanical (mass-spring-damper) system and with reference to Equation 9, the bulk stiffness within the cell can be approximated from:

$$k_c = \omega_n^2 m_c$$

Equation 10

where k_c and m_c define the cell stiffness (Nm^{-1}) and mass respectively (kg). From the FRF measured, the level of damping for each natural frequency observed can be approximated from:

$$\varsigma = \frac{1}{2Q}$$

Equation 11

where Q is defined as the Quality-Factor and equal to:

$$Q = \frac{\omega_n}{\Delta\omega}$$

Equation 12

where $\Delta\omega$ defines the width of the range of frequencies for which the energy within the system output is at least half of its peak value.

4.3.4.2 Coherence

The coherence function, $C_{xy}(\omega)$, given by Equation 13, indicates the portion of the output energy correlated to the input energy [106].

$$C_{xy}(\omega) = \frac{|G_{xy}(\omega)|^2}{G_{xx}(\omega)G_{yy}(\omega)}$$

Equation 13

Where $G_{xy}(\omega)$ defines the cross-spectral density between the input x and the output y, and $G_{xx}(\omega)$ and $G_{yy}(\omega)$ define the auto-spectral density of the signals x and y respectively. $C_{xy}(\omega)$ is used in experimental modal analysis to identify excess noise or uncertainty between the input and the output [106, 126, 127]. Equation 13 yields a value between zero and unity. A value of one at a given frequency indicates that all of the response energy is due to the stimulus or input signal. Conversely, a value of zero indicates that there is no correlation between the input and output signals [106]. When reviewing results, a value of $C_{xy}(\omega)$ greater than 0.9 is deemed to represent a valid measurement point.

4.3.4.3 Mode shape Definition

To identify the mode shapes generated within a given structure multiple FRFs must be recorded from multiple locations and a response matrix generated in which each FRF is mapped to a location and excitation. Mode shapes cannot be determined from a single FRF and/or from a single test position. Figure 35 presents an illustrative example that explains the source of the mode shapes [122, 128].

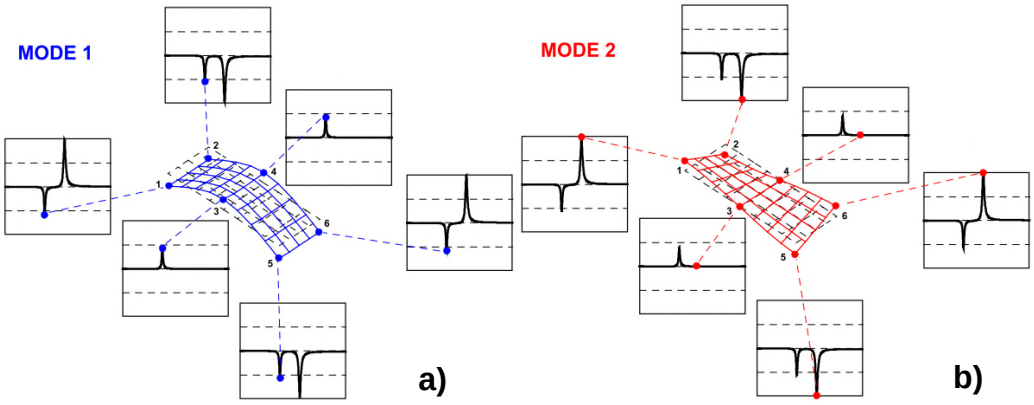

Figure 35: Determination of Mode Shapes of First Two Modes of a Simple Plate via Assessment of Six FRF's from Six Measurement Locations [122]

Within this example there are six locations on a rectangular structure where the input excitation is applied. Figure 35a show that the first mode shape for the structure, correlating to the first natural frequency, is a bending moment. The bending moment is produced since the FRF at positions 1, 2, 5 and 6 are in anti-resonance, while the response in positions in 3 and 4 are in resonance. Correlating the FRFs to a simple mesh model of the structure facilitates the definition of the mode shape. Similarly, Figure 35b shows the mode shape for the second natural frequency, in which the FRF at positions 1 and 6 are positive whereas at positions 2 and 5 they are in anti-resonance. As a consequence, the mode shape corresponding to the second natural frequency is torsion. The experimental method

and results presented in Sections 4.4 and 4.5 describe the use of MATLAB and IDEAS to generate the respective FRFs and mode shapes for the lithium-ion cells.

4.4 **Experimental Setup**

4.4.1 Cell Conditioning

The frequency response of fifteen commercially available 25 Ah pouch cells was evaluated. In order to study the impact of cell-to-cell variations and the differences in the cell's FRF that may arise due to changes in SOC, three cells were charged to the SOC values: 10 %, 25 %, 50 %, 75 % and 90 %. Table 13 defines the SOC value for each of the fifteen cells under test.

Table 13: Experimental Modal Analysis Test Matrix

SOC (%)	Quantity	Sample Serial Numbers Prepared to this SOC
10	3	259, 267 and 268
25	3	260, 261 and 266
50	3	262, 264 and 265
75	3	263, 269 and 270
90	3	273, 275 and 276
Total	**15**	

The SOC range was primary selected, since as reported within [8, 129] to mitigate against the effects of cell degradation the BMS will often seek to constrain the SOC and limit excursions to values greater than 90 % or less than 10 %. Furthermore, while the theory of modal analysis could be applied to a damaged cell, all of the cells employed within this study were deemed to be within the manufacturer's specification. Overcoming the health and safety implications of testing a damaged cell was deemed to be outside of the scope of this study. In addition, even when performing such experimental it would be desirable to have the FRF for an undamaged cell to facilitate a comparison between the two datasets (for example to identify any changes in the natural frequency, phase-shift, stiffness or damping within the battery).

The constant current constant voltage (CC-CV) charging/discharging procedure employed to pre-condition the cells is summarized below:

1. Cell discharged at 1C (CC-CV) to manufacturer's defined lower voltage threshold at which point the cell voltage was allowed to stabilize for three hours.
2. Cell charged at 1C (CC-CV) to manufacturer's defined upper voltage threshold at which point the cell voltage was allowed to stabilize for three hours.
3. Cell discharged at 1C (CC-CV) to a voltage threshold commensurate with the target SOC value and allowed to stabilize for three hours.

During the pre-conditioning phase, the storage and cycling of each cell was undertaken within a temperature-regulated environment (21 °C ± 0.5 °C).

4.4.2 Modal Analysis

As discussed in 4.3.2, the method of experimental modal analysis chosen was to conduct a hammer survey via a single input single output (SISO) method. Figure 36 displays the grid layout marked onto each cell. Each intersection (locations 1-25) defines a unique impact point. Each cell location was impacted five times and the results of each measurement averaged to generate a SISO response for that test location.

The testing of each cell was conducted within an air-conditioned laboratory, with a regulated temperature of 21 °C ± 3 °C. Testing was conducted using an impulse hammer (type: PCB 086C08). The mass of the hammer was 0.32 kg and the tip stiffness was approximately equal to 3,158 kNm^{-1}. From Equation 3 this provided a measurement frequency range of approximately 0-500 Hz and encompasses the region of typical road induced vibration [32]. A single axis accelerometer (type: PCB 352C65) was employed to measure the output vibration from each cell. Figure 36 shows the location on the cell where the accelerometer was bonded.

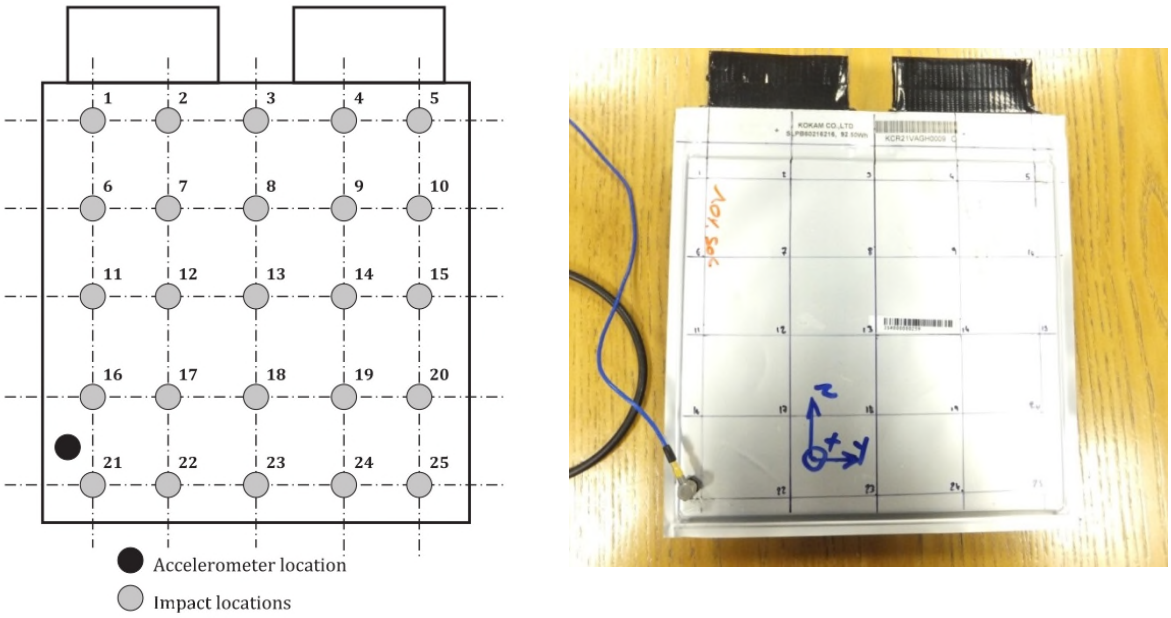

a) **b)**

Figure 36: a) Grid Layout Employed for SISO Impulse Excitation Tests b) Test Item with Grid Layout

The weight of the accelerometer was 2 grams (less than 0.4 % of total cell mass); minimising the possibility of experimental error through increasing the mass of the cell. Due to the irregular surface of the cell and the desire not to change the structure or to damage the cell (that may result through the use of permanent adhesives), the accelerometer was bonded to the cell surface using petro-wax. The data logger and frequency analyser employed was a Brüel and Kjær 7539A Controller and a Brüel and Kjær 3038 type Input Module. During the modal analysis,

each cell was placed on four blocks of polyurethane foam that were approximately 40 mm x 40 mm by 20 mm deep. The blocks were positioned under the four corners of the cell. Figure 37 shows an example frequency response (magnitude plot) for one pouch cell mounted on the foam pads.

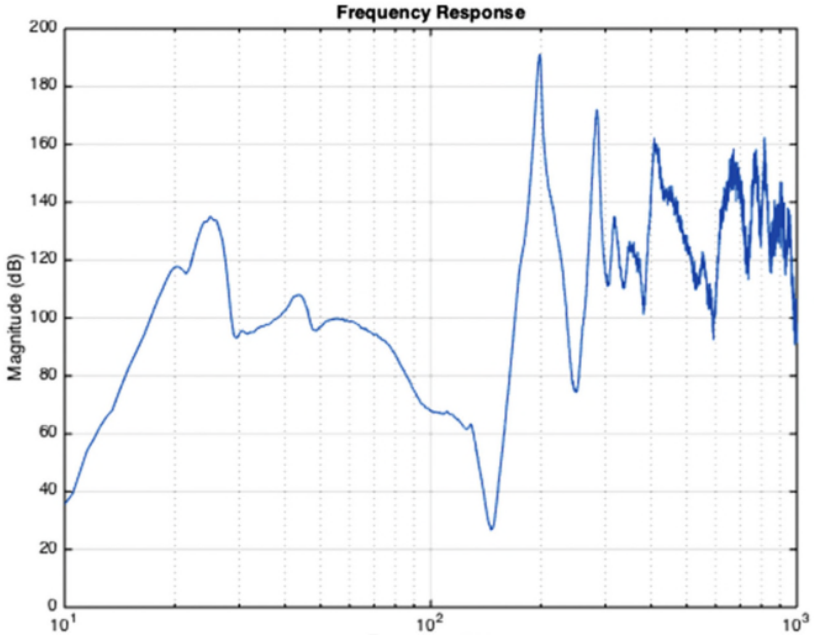

Figure 37: Example Frequency Response Showing the Free-Free test Condition for the Cells

It can be seen that lowest natural frequency of the cell is approximately 200 Hz, whereas the highest resonance of the foam pad occurs at approximately 36.5 Hz. As discussed in Section 4.3.1, this level of frequency separation between the mounting medium and the cell, confirms the required free-free test condition.

4.4.3 Data Analysis and Post-Processing

For each cell defined in Table 13, the following method was employed to post-process the measured data and to quantify the cell's frequency response function (FRF). From Equation 7 and Equation 8 it is possible to calculate the FRF for each of the cell's 25 impact locations. Given the geometry of each cell and the dimensions of the measurement grid shown in Figure 36, the Brüel and Kjær software (that include elements of IDEAS functionality) is able to quantify the mode shapes for each natural frequency within the cell. The mathematical software MATLAB was also employed to average each of the 25 frequency responses for each cell into a single FRF for the cell. As discussed in Section 4.3, based on the average frequency response and through Equation 10 and Equation 11, it is possible to estimate the damping for each natural frequency and the bulk stiffness of the cell.

4.5 **Results**

4.5.1 Cell Natural Frequencies and Modal Shapes

Figure 38 presents an example of twenty-five frequency response (magnitude) plots for Cell 262 that corresponds to each impact location defined in Figure 36.

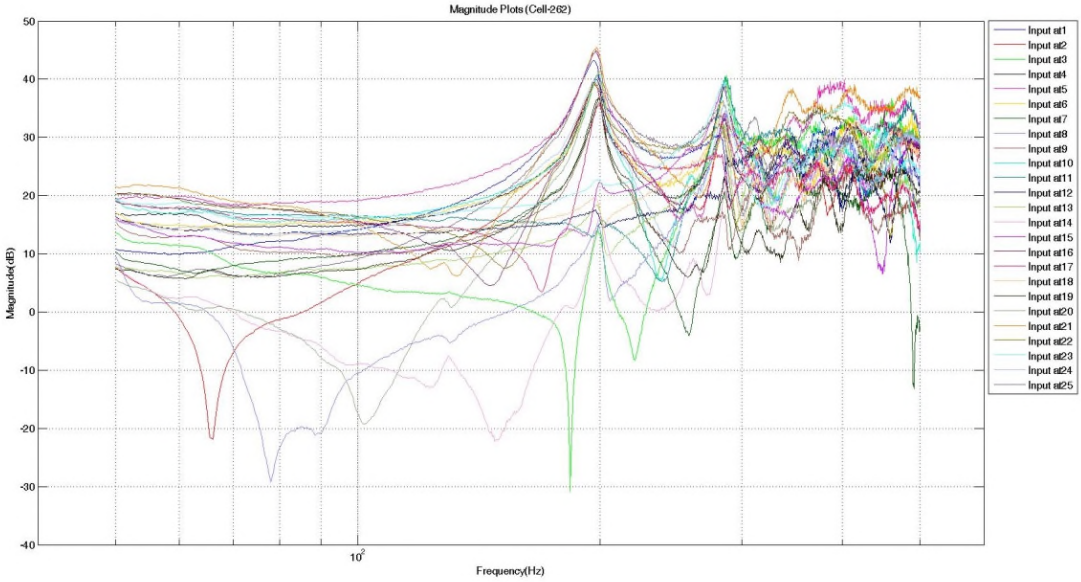

Figure 38: Cell 262 - Frequency Response (Magnitude Plots) for Each Impact Location

Using MATLAB, an averaged FRF was calculated for the cell. Figure 39 and Figure 40 present the gain and phase components of the averaged FRF respectively.

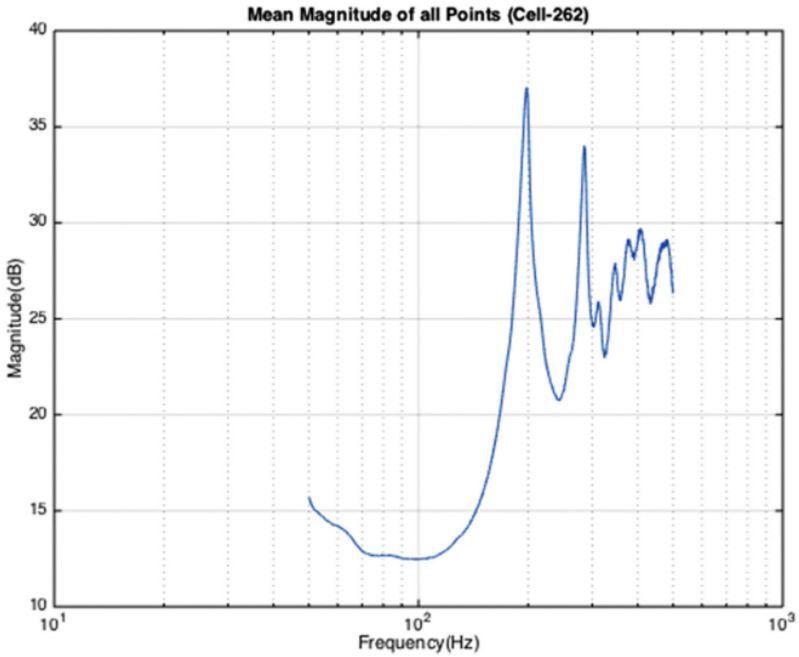

Figure 39: Example of Averaged Frequency Response (Magnitude Plot) of Cell 262

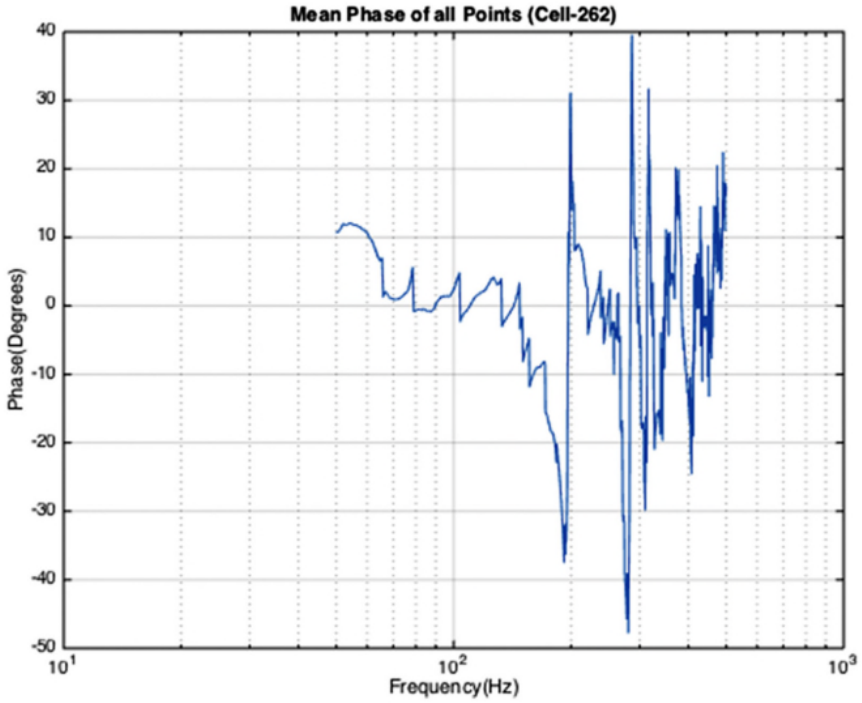

Figure 40: Example of Averaged Frequency Response (Phase Plot) of Cell 262

As it can be seen, the cell exhibits seven natural frequencies (represented by the peaks in the magnitude plot and a corresponding transition in the phase plot). The coherence plot presented in Figure 41 demonstrates a high degree of correlation between the input and output energy levels (greater than 92 %) for frequencies up to 400 Hz.

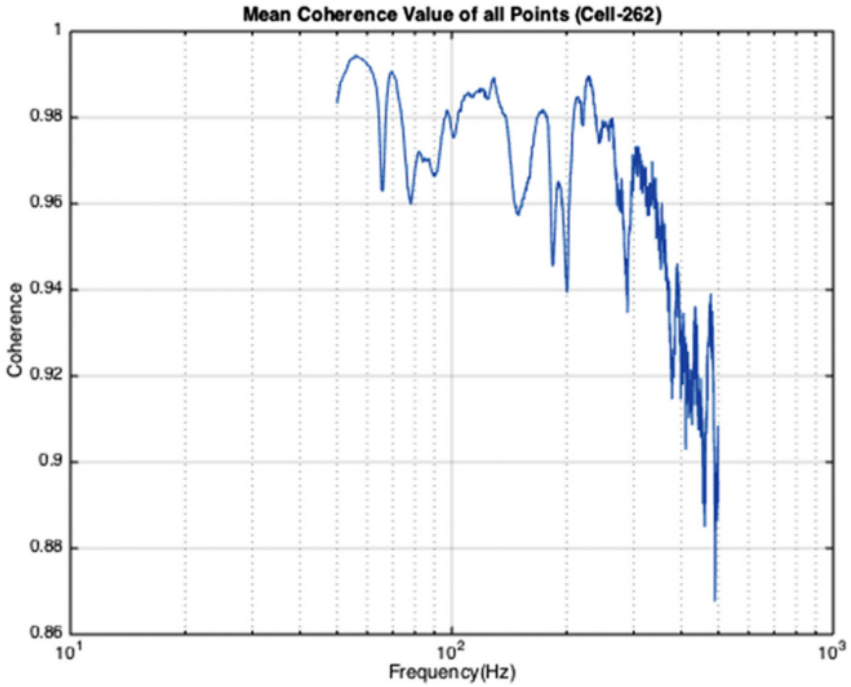

Figure 41: Example of Coherence Plot of Cell 262

Above this threshold, the coherence value reduces as external disturbances and non-linearity dominate the cell's response. As discussed in Section 4.4.3, taking the geometry of the cell into consideration it is possible to identify the mode shapes for the cell. Figure 42 presents the seven mode shapes calculated through the IDEAS software.

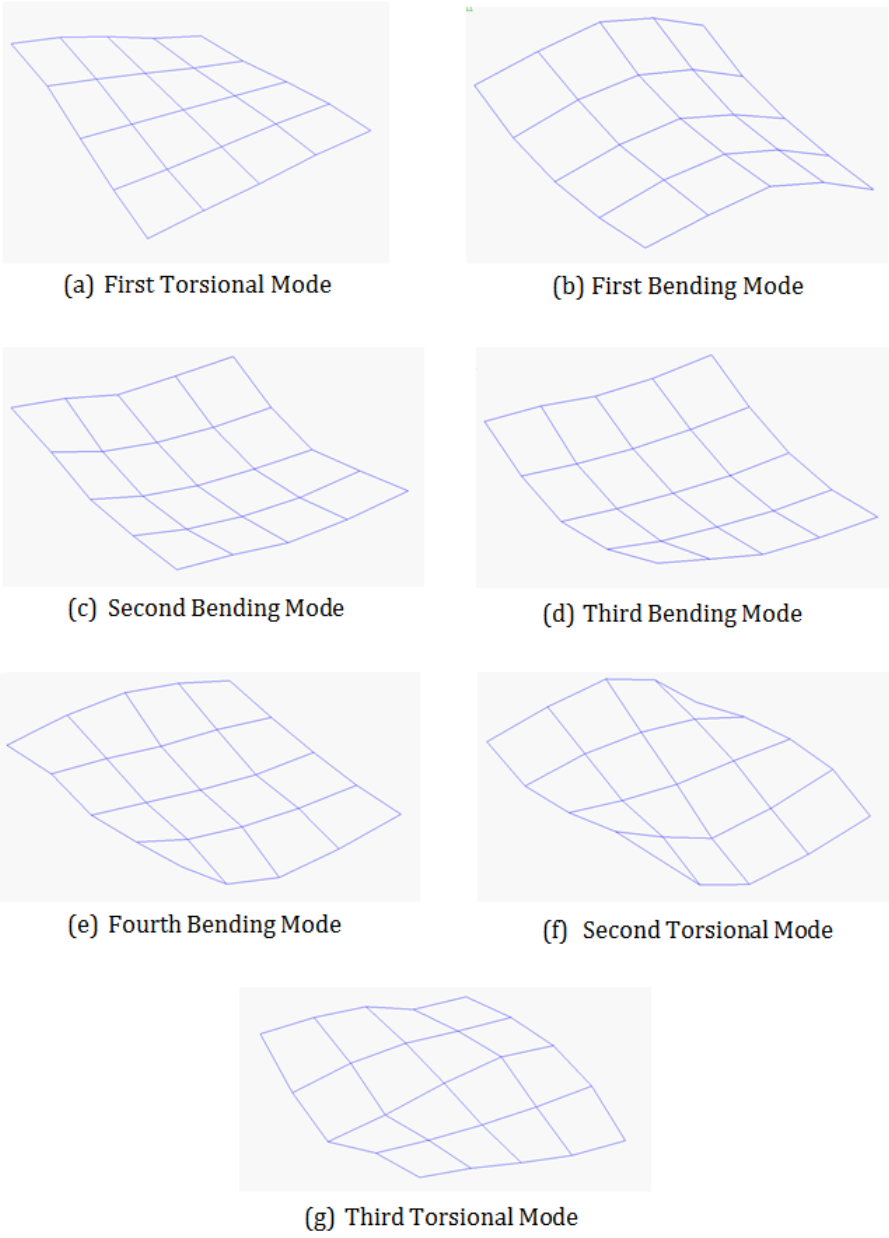

Figure 42: Example of the Seven Modal Shapes Corresponding to Each Natural Frequency of Cell 262

Table 14 presents the complete results from the modal analysis. The table defines the natural frequencies measured for each cell. As it can be seen, irrespective of the SOC value, the same initial four modes (torsion, bending, bending and bending) are present in each cell at frequencies in the order of: 191 – 205 Hz; 262 – 296 Hz; 288 – 334 Hz and 337 – 360 Hz respectively.

Table 14: Estimated Natural Frequencies for Each Cell Corresponding to the Seven Mode Shapes Identified

Cell ID	SOC (%)	First Torsional Mode (Hz)	First Bending Mode (Hz)	Second Bending Mode (Hz)	Third Bending Mode (Hz)	Fourth Bending Mode (Hz)	Second Torsional Mode (Hz)	Third Torsional Mode (Hz)
259	10	191.5	271.5	293	351		408	468
267	10	203.5	291	316	337.5	380	442	489.5
268	10	202	296	307	357		403.5	474
260	25	195	278.5	293.5	347	370	414	475
261	25	186	267.5	316	336			
266	25	193	289.5	334.5	360	378.5	401.5	453.5
262	50	197.5	285.5	313	346.5	377.5	407	478.5
264	50	200.5	286	313	367.5	389		446.5
265	50	197.5	262.5	288	339.5	380	410	461
263	75	201	283.5	298.5	357.5	386	412.5	471
269	75	199	282.5	297.5	340.5	378	395.5	456.5
270	75	201.5	294.5	323	342.5	389.5	423	472.5
273	90	200.5	282.5	305	353	397.5	417.5	491
275	90	205.5	287.5	306	356	396	416	478
276	90	204	285	306	343.5	389.5	434	480

However, above approximately 350 Hz some of the cells exhibit different dynamic behaviour. For example, the fourth bending mode is only present in a subset of the cells charged to 10 % and 25 % SOC. Similarly, from the frequency response data measured for Cell 264 there was no discernible resonance at: 400 Hz (corresponding to the second torsional mode) and for cell 261, it was not possible to identify any resonances above 336 Hz. One reason for this can be seen from the corresponding coherence plot for cell 261 that clearly shows a reduction in coherence to nearly 40 %. The most likely reason for this is operator error during the experiment.

Acknowledging the sample size for this experiment is relatively small; the results presented in Table 14 imply that the natural frequencies for the lithium-ion cell are not dependent on the cells SOC. Differences in resonance, between cells, for a given SOC are most likely attributable to cell-to-cell variations resulting from the manufacturing processes employed. As part of the study, the mass and dimensions

(width, length and thickness) of each cell were recorded and differences in the order of 1 mm were noted between the thinnest and thickest cell. It is noteworthy that 80% of cells tested were outside of the specified manufacturing tolerance for thickness, at one or more measurement location.

4.5.2 Cell Damping

Table 15 presents the damping coefficient (ς) calculated from Equation 11 for each of the seven mode shapes and for each cell.

Table 15: Calculated Damping Coefficient for Each Cell and Natural Frequency

Cell ID	SOC (%)	First Torsional Mode (Damping Coefficient)	First Bending Mode (Damping Coefficient)	Second Bending Mode (Damping Coefficient)	Third Bending Mode (Damping Coefficient)	Fourth Bending Mode (Damping Coefficient)	Second Torsional Mode (Damping Coefficient)	Third Torsional Mode (Damping Coefficient)
259	10	0.0196	0.0133	0.0198	0.0147		0.0109	0.0155
267	10	0.0052	0.0074	0.0204	0.0266	0.0151	0.0152	0.0096
268	10	0.0038	0.0119	0.0133	0.0191		0.0105	0.0053
260	25	0.0075	0.0132	0.0207	0.0129	0.0214	0.0205	0.0197
261	25	0.0160	0.0289	0.0249	0.0262			
266	25	0.0128	0.0096	0.0225	0.0162	0.0149	0.0136	0.0124
262	50	0.0071	0.0100	0.0256	0.0203	0.0174	0.0163	0.0176
264	50	0.0050	0.0093	0.0174	0.0231	0.0141		0.0084
265	50	0.0080	0.0321	0.0106	0.0202	0.0149	0.0182	0.0156
263	75	0.0067	0.0204	0.0139	0.0247	0.0168	0.0199	0.0158
269	75	0.0106	0.0140	0.0175	0.0225	0.0149	0.0189	0.0191
270	75	0.0063	0.0077	0.0217	0.0287	0.0112	0.0173	0.0142
273	90	0.0105	0.0102	0.0254	0.0075	0.0268	0.0118	0.0155
275	90	0.0080	0.0160	0.0121	0.0231	0.0130	0.0185	0.012
276	90	0.0058	0.0170	0.0114	0.0237	0.0131	0.0156	0.011

Table 16 presents the averaged values of ς for each SOC threshold. MATLAB was further employed to generate a linear best-fit function defining the relationship between cell damping and SOC.

Table 16: Average Damping Coefficients for Each SOC Threshold

SOC (%)	First Torsional Mode (Average Damping Coefficient)	First Bending Mode (Average Damping Coefficient)	Second Bending Mode (Average Damping Coefficient)	Third Bending Mode (Average Damping Coefficient)	Fourth Bending Mode (Average Damping Coefficient)	Second Torsional Mode (Average Damping Coefficient)	Third Torsional Mode (Average Damping Coefficient)
10	0.0095	0.0109	0.0178	0.0201	0.0151	0.0122	0.0101
25	0.0121	0.0172	0.0227	0.0184	0.0182	0.0171	0.0161
50	0.0067	0.0171	0.0179	0.0212	0.0155	0.0173	0.0139
75	0.0079	0.0140	0.0177	0.0253	0.0143	0.0187	0.0164
90	0.0081	0.0144	0.0163	0.0181	0.0176	0.0153	0.0128

The results presented in Figure 43 highlight that, given the sample-size and cell technology tested, there does not appear to be a discernible relationship between the damping for each natural frequency and cell's SOC. Within Submission 2, additional statistical analysis is presented which can be determined with 99 % confidence that the no significant relationship between cell SOC and the percentage damping within this data set.

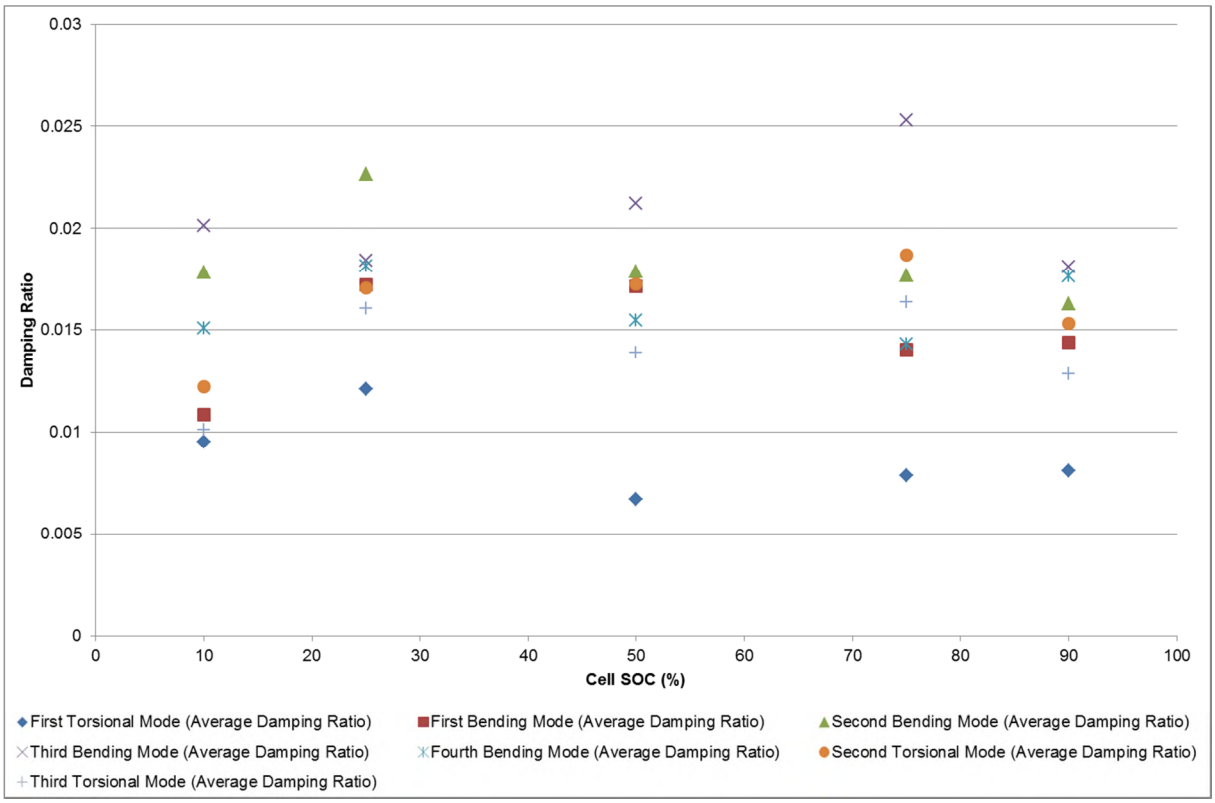

Figure 43: Averaged Damping of Each Mode for Each SOC

4.5.3 Cell Stiffness

Table 17 presents the calculated stiffness (k_c) for each cell based on the 1st natural frequency (measured between 191-205 Hz).

Table 17: Calculated Cell Stiffness

Cell ID	SOC (%)	Cell Weight (g)	Stiffness constant (Nm^{-1})
259	**10**	577	835358.90
267	**10**	577	866173.26
268	**10**	577	789429.70
260	**25**	577	890065.11
261	**25**	578	921891.24
266	**25**	576	917310.42
262	**50**	578	886985.30
264	**50**	578	847026.19
265	**50**	576	943331.59
263	**75**	578	929476.23
269	**75**	577	902073.04
270	**75**	578	926483.47
273	**90**	573	909375.21
275	**90**	576	960297.66
276	**90**	575	944686.95

Table 18: Averaged Cell Stiffness for Each SOC Threshold

SOC (%)	Mean Stiffness at Cell Weight (Nm^{-1})
10	830320.62
25	909755.59
50	892447.69
75	919344.25
90	938119.94

Equation 10 was employed to calculate k_c. For completeness, the measured value of cell mass (m_c) was used in the calculations and is provided for reference. As

discussed in Section 4.5.1, variations in cell mass were found to be in the order of 1 mm. Table 18 presents the mean stiffness value corresponding to each SOC threshold. Figure 44 presents a graphical representation of and clearly indicates a trend of increasing k_c for higher values of SOC.

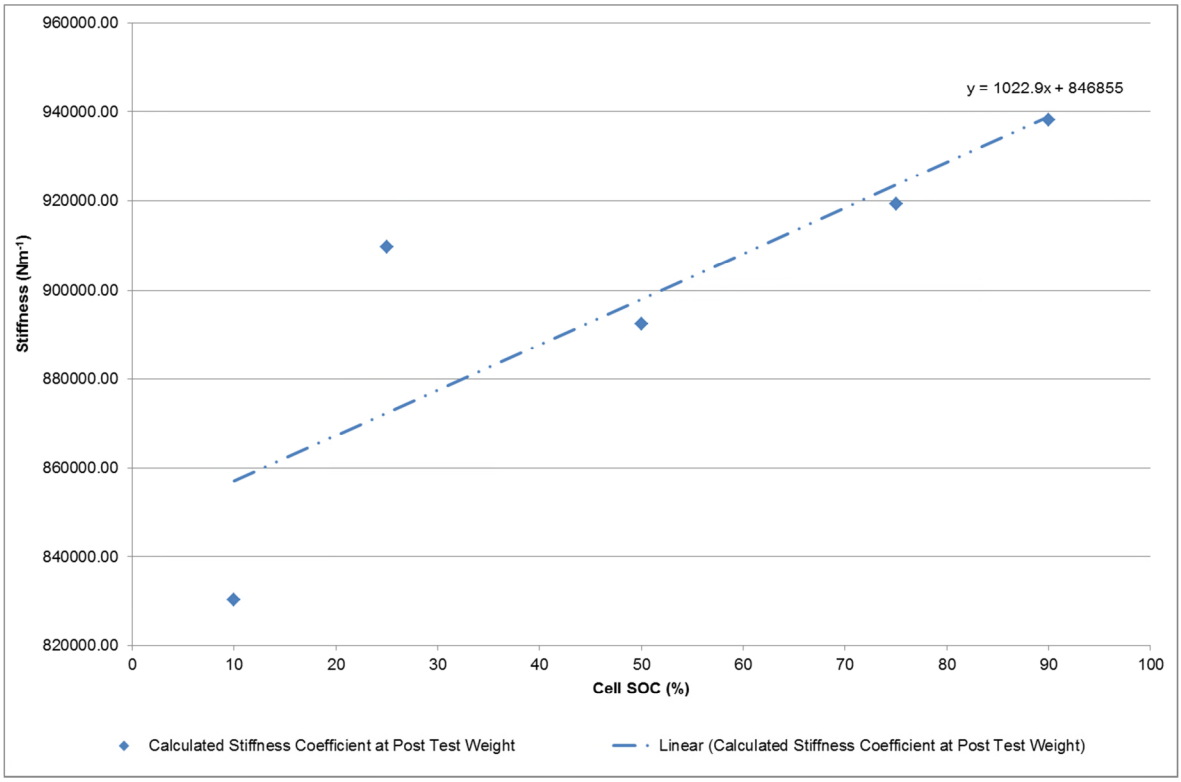

Figure 44: Average Cell Stiffness vs. Cell SOC

It is hypothesised that the two outliers for 10 % and 25 % SOC maybe a result of the transition of lithium between the anode and cathode at these lower charge states. However it is also likely that these outliers are function of the limited sample size per SOC. Because only three samples were evaluated for each SOC, a specific characteristic or inhomogeneity within a single sample would impact the averaged result for a particular charge state. Therefore it is recommended that this experiment is repeated in future a future study to determine the robustness of this trend.

This result contradicts that observed in Section 4.5.1 that shows insensitivity between the cells natural frequency and SOC. For a simple mechanical structure, in accordance with Equation 10, one would expect to see an increase in natural frequency as the stiffness of the specimen is increased (with mass held constant). At present, only the experimental data and observations are noted.

4.6 **Discussion**

The results presented highlight that the first natural frequency of the cells tested (irrespective of SOC) occurs at a frequency in excess of 180 Hz. The study presented in Chapter 3 found that the majority of road-induced vibration occurs within the frequency range of 0 to 150 Hz. This is illustrated in Figure 45 that

highlights the vibration energy measured in the Z-axis within the Nissan Leaf, the Smart EV and the Mitsubishi i-MiEV that has been sequenced to a 100,000 miles of vehicle durability as defined in Chapter 3. Comparing the isolated cell data from Section 4.5 with the in-vehicle data presented in Figure 45 indicates that it is unlikely that these NMC pouch cells would be excited by road surface vibration. However, it is noteworthy that Figure 45 corresponds to the vibration energy measured on the surface of the battery pack and this may differ to that experienced within the battery enclosure. Additional higher frequency vibrations may be induced from the thermal management systems, the power electronics and the use of cell-level restraints.

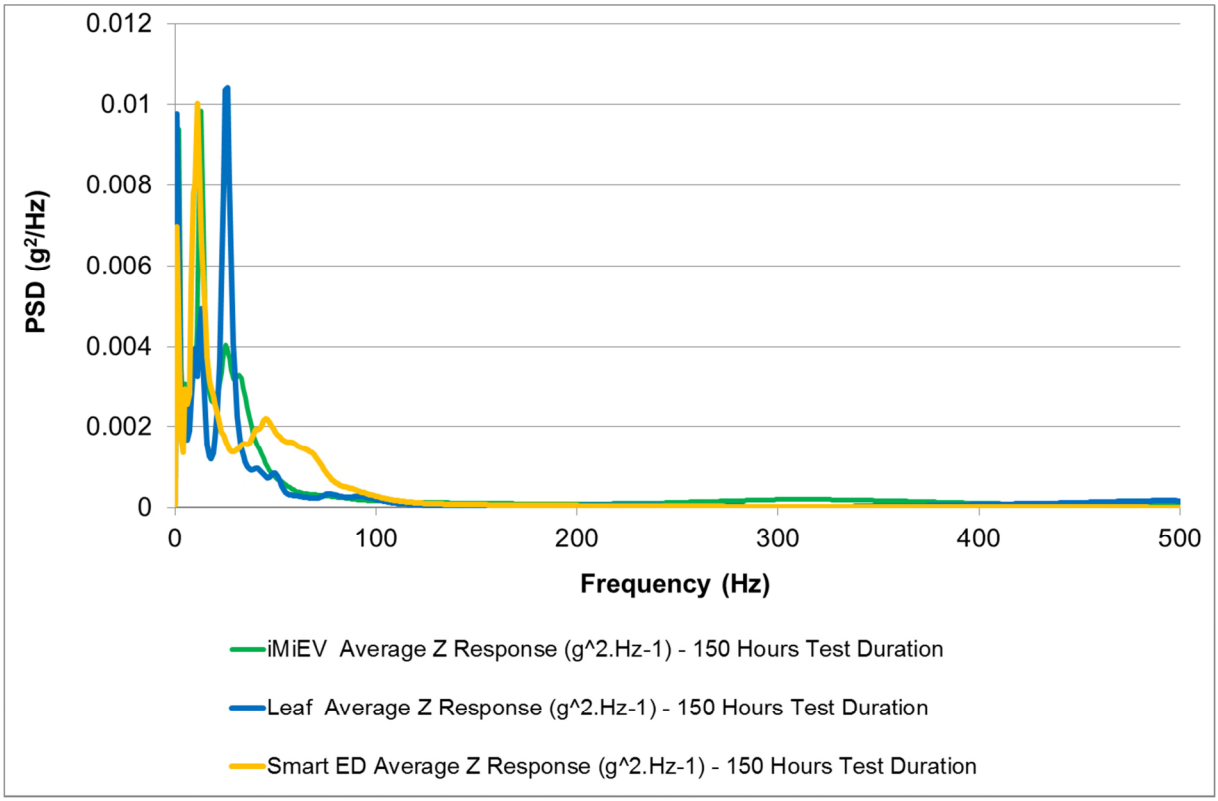

Figure 45: PSD Plot (Z-axis) Vibration of a Nissan Leaf, Smart ED and Mitsubishi i-MiEV Subject to Durability Surfaces

4.7 **Conclusions**

This study has addressed the gap in knowledge identified in Chapter 2, relating to the limited number of publications which have identified the natural vibration characteristics of battery cells and components. Quantification of this new data has been achieved through the application of contemporary impact survey modal analysis techniques to lithium-ion laminate pouch cells. The test methodology developed during this study and the associated results have been published in [35].

This study has presented the underpinning theory and experimental method employed to ascertain the FRF and mode shapes for a range of commercially

available 25 Ah NMC Laminate Pouch Cells. Each cell was pre-conditioned to a different value of SOC. The primary conclusions that can be drawn from the results presented are firstly, irrespective of cell SOC; the same initial four modes (torsion, bending, bending and bending) are present in each cell and occur within a frequency range of 191 Hz - 360 Hz. Further, the results imply that the natural frequencies are not dependent on the cell's SOC and are most likely attributable to subtle cell-to-cell variations resulting from the manufacturing processes employed. Secondly, the approximated damping calculated for each natural frequency within each cell suggests that there is no discernible relationship between the value of damping present and cell's SOC. Finally, the lowest natural frequency recorded within the cells is above the frequency range (0 - 150 Hz) typically associated with road-induced vibration. As a result, it is unlikely that these NMC pouch cells will be excited by road induced vibration.

5 Study 3- Vibration Durability Behaviour of EV Batteries via Single Axis Testing Techniques

5.1 Introduction

As presented in Chapter 2, the current academic literature studying the effect of vibration on the electromechanical aging of lithium-ion cells presents conflicting evidence with regard to the susceptibility of lithium-ion cells to mechanical excitation. In addition, contemporary research has not been scoped towards determining the effect of vibration during a typical automotive life and has often applied vibration profiles which are unrepresentative of an EV application.

This Chapter presents the results from two investigations which examined the effect of mechanical induced vibration, on a commercially available NMC 2.2 Ah and nickel cobalt aluminium oxide (NCA) 3.1 Ah 18650 cylindrical cells. Within these studies USABC Procedure 10 and the profile developed within Chapter 3 (which is referred to as the Warwick Manufacturing Group Millbrook (WMG-MPG) PSD) were employed. These profiles are presented in Figure 33 and Figure 28 respectively. Both vibration test profiles were developed to underpin durability evaluation and to replicate a 100,000 miles of BEV use. Both these specifications apply vibration loading through random excitation which is more representative of road-induced structural vibration [42]. Also unlike the previous studies discussed in Chapters 2, each cell evaluated experience vibration excitation in the X, Y and Z axis, as opposed to experiencing vibration in a single axis for the duration of the test, which is more representative of the vibration observed by cells within an EV battery assembly.

This study comprises of two separate, but inter-related investigations. Within the first investigation, a sample of 27 NMC 18650 2.2 Ah cells are evaluated via either USABC Procedure 10 or the WMG-MPG profiles. Within this investigation, the effects of three different SOC and different in-pack orientations on the susceptibility of cell degradation to vibration were investigated.

Within the second study a sample of 12 NCA 18650 3.1 Ah cells were evaluated using just USABC Procedure 10. The study was further rationalised in comparison to the initial investigation on NMC cells as a single charge state of 75 % SOC was employed. However, the effect of three different in-pack orientations on the susceptibility of cell degradation was examined further. The second study was an evolution of the first and the selection of cell chemistry and cell type was at the request of the sponsoring organisation (JLR) for commercial benchmarking.

This Chapter is structured as follows: Section 5.3 of this Chapter provides a detailed overview of the experimental method employed within both investigations, including the design of the test equipment and fixtures. Other factors that are central to ensuring measurement accuracy are also defined. Results from both investigations are presented in Section 5.4. This section includes assessments of the mechanical

degradation (visual inspection and natural frequency) as well as an assessment of changes in the electrochemical performance (capacity, impedance etc.) of the cells. Discussion and conclusions are presented in Sections 5.6 and 5.7, respectively.

5.2 **Objective and Aims of Study**

5.2.1 Objective

To determine if 18650 battery cells can be electrochemically and mechanically aged by mechanical induced vibration of the cell assembly via the use of a single axis electromagnetic shaker table and vibration profiles that are representative of a given durability life. The study shall investigate if cell SOC and orientation influences the observed degradation resulting from vibration.

5.2.2 Aims

- To determine if vibration profiles synthesised to represent 100,000 miles of automotive use can age 18650 battery cells.
- To measure if cell SOC can affect the vibration durability life of 18650 battery cells.
- To measure if cell orientation in relationship to the input axis can affect the vibration durability life of 18650 battery cells.

5.3 **Experimental Method**

The following section outlines the experimental method, including the test process, fixture design, rig assembly and cell characterisation employed within the investigations on the NMC and NCA 18650 cells. A summary of the experimental procedure for both investigations is presented in Figure 46.

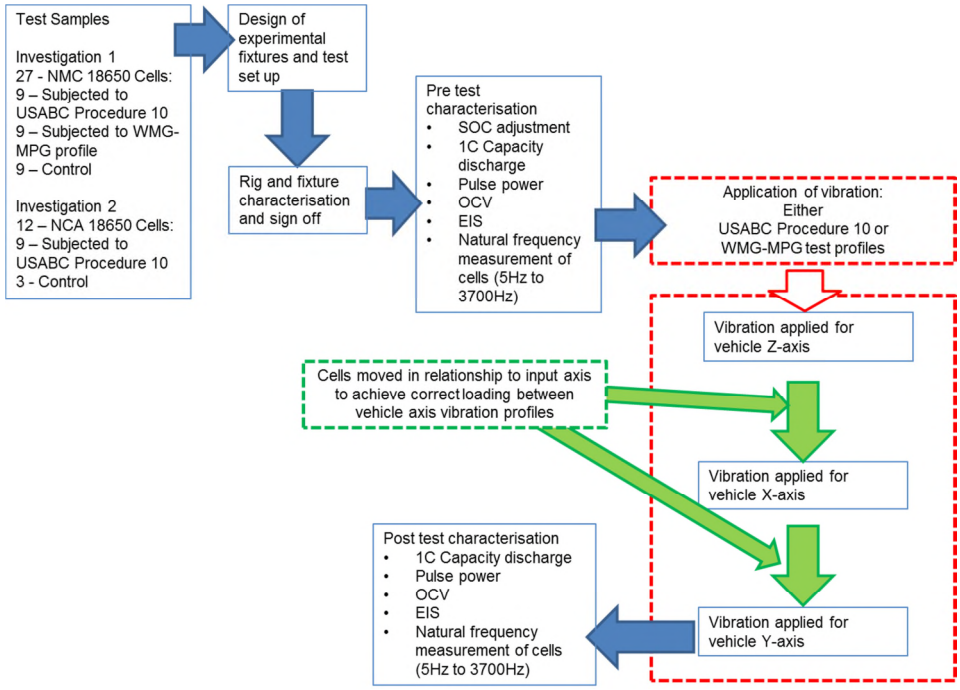

Figure 46: Schematic of Test Process

5.3.1 Test Samples

The details of sample preparation, cell SOC and cell orientation for each of the two investigations are defined in Table 19.

Table 19: Test Sample Information

Sample No	Test Profile	SOC (%)	Cell Orientation (Vehicle Axis : Cell Axis)
Investigation 1 – NMC			
1	In permanent storage	25 %	Control
2	Followed USABC Procedure 10 samples	25 %	Control
3	Followed WMG-MPG samples	25 %	Control
4	In permanent storage	50 %	Control
5	Followed USABC Procedure 10 samples	50 %	Control
6	Followed WMG-MPG samples	50 %	Control
7	In permanent storage	75 %	Control
8	Followed USABC Procedure 10 samples	75 %	Control
9	Followed WMG-MPG samples	75 %	Control
10	USABC Procedure 10	25 %	Z:Z
11		25 %	Z:X
12		25 %	Z:Y
13		50 %	Z:Z
14		50 %	Z:X
15		50 %	Z:Y
16		75 %	Z:Z
17		75 %	Z:X
18		75 %	Z:Y
19	WMG-MPG	25 %	Z:Z
20		25 %	Z:X
21		25 %	Z:Y
22		50 %	Z:Z
23		50 %	Z:X
24		50 %	Z:Y
25		75 %	Z:Z
26		75 %	Z:X
27		75 %	Z:Y
Investigation 2- NCA			
1	USABC Procedure 10	75 %	Z:Z
2		75 %	Z:Z
3		75 %	Z:Z
4		75 %	Z:X
5		75 %	Z:X
6		75 %	Z:X
7		75 %	Z:Y
8		75 %	Z:Y
9		75 %	Z:Y
10	Followed USABC Procedure 10 samples	75 %	Control
11		75 %	Control
12		75 %	Control

Twenty seven 2.2 Ah 18650 NMC cells were evaluated in investigation 1 and twelve 3.1 Ah 18650 NCA cells were evaluated in investigation 2. Each cell was pre-conditioned to a defined SOC prior to durability testing and allocated a test

orientation with respect to the vehicle Z-axis. An explanation of the two test profiles and the sample orientation as defined in Table 19 are discussed in Section 5.3.5.

5.3.2 Design of Experimental Fixtures and Test Set Up

Detailed designs and specifications of the test fixtures developed to undertake these studies are defined in Submission 3; however a summary of the rigs employed are presented here for completeness.

Figure 47a presents the cell-mounting fixture that was designed and fabricated to support the investigations into the effect of single axis vibration on 18650 cells. Each fixture holds up to three cells and is intended to recreate a generic but representative 18650 EV RESS mounting condition. 5 mm of each end of the cell are clamped within the cell test fixture. Because a single axis EMS table was used, 3 cell-mounting fixtures were made, all based on the same design to allow the concurrent evaluation of multiple cells in different orientations during a single vibration test (presented in Figure 47b). The different cell orientations (X, Y and Z) were achieved by mounting the 3 fixtures onto different surfaces of the durability fixture. During the test programme, the cells were subject to different axis of vibration by relocating the cell fixture onto different surfaces of the durability fixture. Installation of the durability fixture and the cell-mounting fixture onto the EMS table, complete with instrumentation, is presented in Figure 47b.

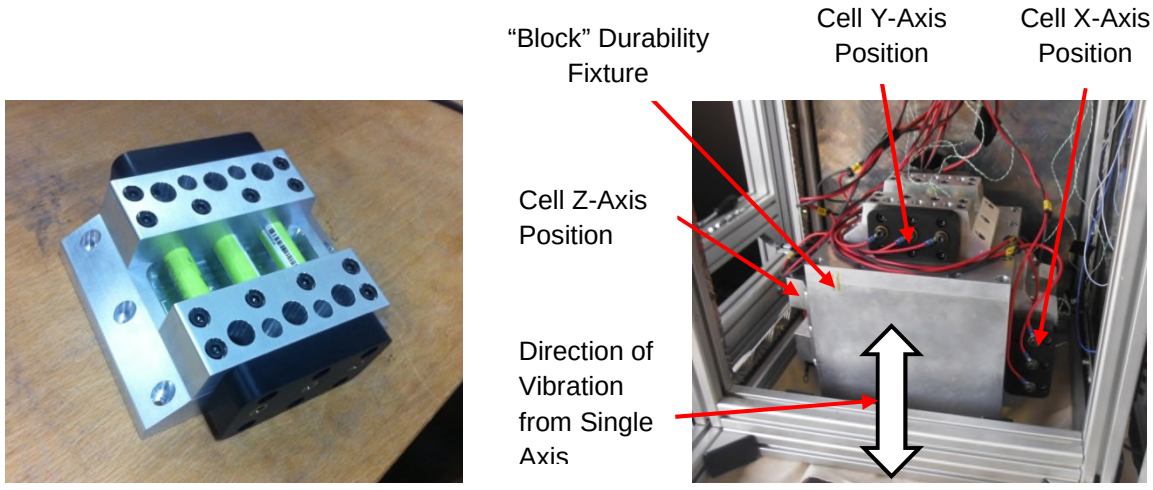

Figure 47: a) Single Test Fixture b) Assembled Test Fixture on Shaker Table with Test Positions

All vibration durability and assessment fixtures employed were constructed from 6082-T6 grade aluminium. This is due to the high Poisson's ratio associated with this material (circa: 0.33) [130] . The Poisson's Ratio is defined in Equation 14 where the materials Young's modulus is defined as E (in GPa) and density as ρ (in g/cm^3) [89, 130, 131]. A high materials ratio (e.g. greater than 0.3) indicates a high material natural frequency [89, 131] and results in a lower risk of undesirable fixture

resonances impacting the control and measurement accuracy of the experimentation.

$$Poisson's\ Ratio\ = \frac{E}{\rho}$$

Equation 14

The test environment used to mechanically induce vibration to the Lithium-ion cells is presented in Figure 48.

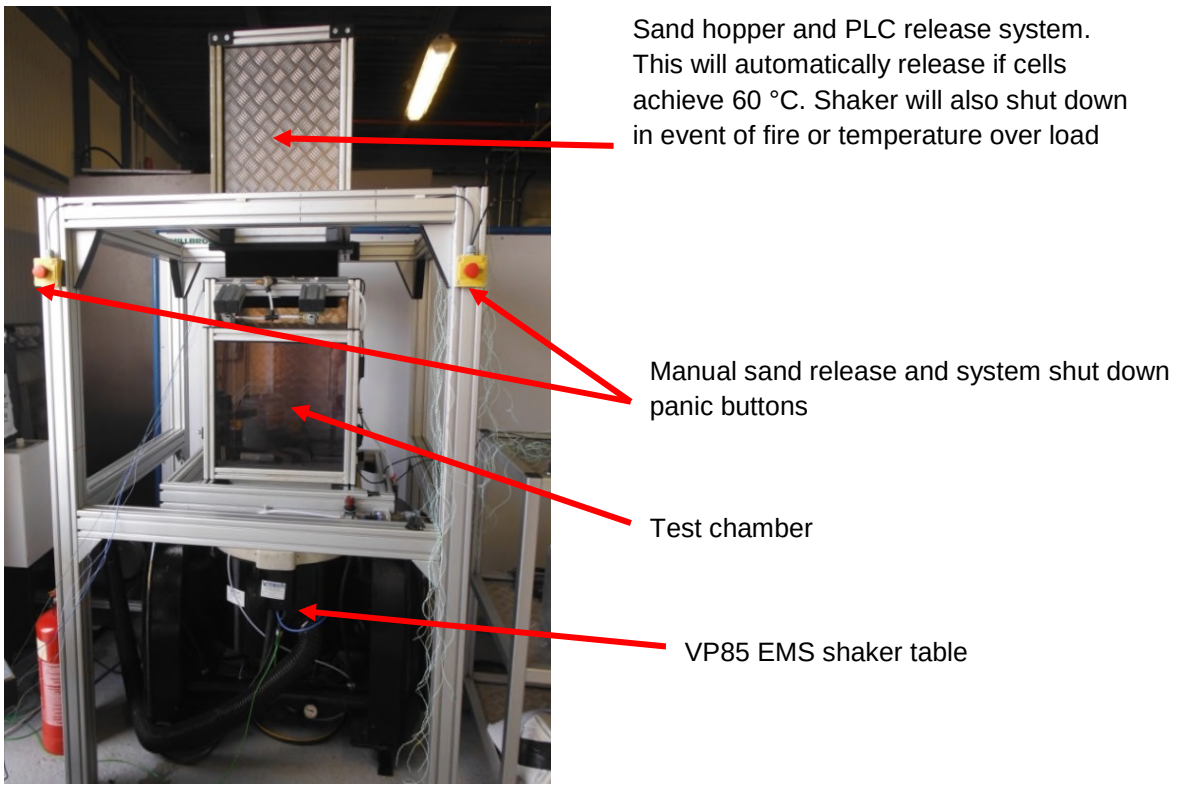

Figure 48: Test Set Up for the Single Axis Testing of 18650 Cells

The test rig employs a 700 kg force, single axis, EMS table manufactured by Derritron (model number: VP85, serial number: 74). A LMS Scadas III (serial number: 23-4709-58) digital vibration controller was programmed with both the USABC Procedure 10 and WMG-MPG vibration profiles. To facilitate closed-loop vibration control, two single axis accelerometers (PCB 352C65) were mounted at opposite sides of the durability fixture via HBM X60 adhesive. A LabVIEW PXie-1075 chassis was used with an integrated Ni-PXIe-8133 controller and input modules for 32 thermocouple sensors (NI PXIe-4353), 4 channels for accelerometer measurements (NI PXI-4462) and a multifunctional data module (Ni PXIe-6363) was used for data acquisition. To mitigate against any potential risk of catastrophic cell failure during vibration testing, the EMS shaker table was installed within a blast proof enclosure. Integrated with the enclosure was a programmable logic controlled (PLC) fire extinguishing mechanism that would automatically activate if either a cell

surface temperature greater than 60 °C or an increase in cell temperature of greater than 4 °C/s was observed. Within the test environment, K-type thermocouples and accelerometers were employed to provide suitable test accuracy and safety.

5.3.3 Rig and Fixture Pre-testing Characterisation

5.3.3.1 Response of EMS

As discussed within [132-134] prior to commencing any vibration study, a key requirement is to fully understand the frequency response of the EMS to ensure that the armature assembly does not exhibit a resonance within the frequency range of interest. The vibration response of the EMS was measured using a swept sine wave of amplitude 1 g_n over a frequency range of 5 – 3700 Hz at 1 octave/minute prior to testing. Upon analysing the response of the EMS shaker used in this study, no significant resonances were identified that would detrimentally impact the accuracy or reliability of the durability test programme. The results of the EMS response are presented in Figure 49.

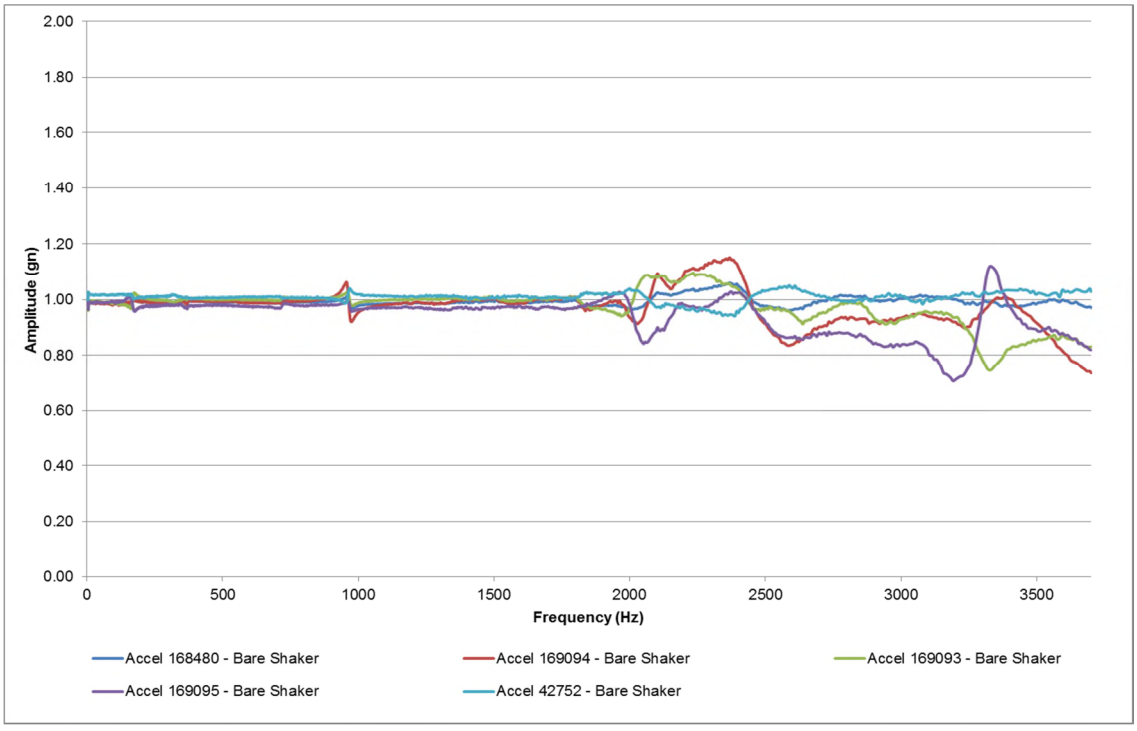

Figure 49: Multiple Accelerometer Resonance Evaluation of Bare VP85 EMS Armature

5.3.3.2 Transmissibility and Response of Fixtures

The primary requirement for durability testing is to ensure that the vibration profile demanded by the electronic controller is faithfully applied to the samples under test. This is achieved by designing the experimental fixture to maximize the transmissibility of the vibration energy from the EMS table to the sample and to concurrently minimise the cross-axis behaviour of the durability fixture. Transmissibility is a comparison of the output signal to the input signal [135] and is

determined by pre-test experimental evaluations of the fixture. At a transmissibility of unity, the output faithfully follows input [135]. To ensure a uniform transmission of acceleration from the vibration exciter, the fixture must carry the force to the test object with a minimum of loss and distortion. This is accomplished by ensuring the rigidity of the fixture so that the force is not deflected by the specimen load and that the fixture transfers motion with high fidelity [89, 135, 136]. Ideally, a dynamic test fixture couples the motion from the vibration shaker table to the specimen with zero distortion at all amplitudes and frequencies specified by the test procedure [135, 137]. Practically, an ideal value of 1.0 over a wide test frequency cannot be met; therefore fixtures are characterised via swept sine resonance search evaluations prior to testing to ensure that no significant resonances occur in the three axis of the vibration fixture. The cross-axis behaviour of the experimental set-up, (Figure 47b) was evaluated in accordance with BS EN 60068 to ensure that "the maximum vibration amplitude in any axis perpendicular to the specified axis shall not exceed 50 % of the specified amplitude up to 500 Hz or 100 % for frequencies in excess of 500 Hz [134]".

To measure the vibration characteristics of the test fixture, accelerometers were placed in the X, Y and Z-axis of the assembled fixture, within or close to every cell mounting position. The fixture was excited in the Z-axis. The test samples were not installed into the fixture during the transmissibility investigation. Prior to conducting the transmissibility measurement activity several vibration test standards were consulted. It was noted that there is ambiguity within the regulatory and industrial guidelines with respect to assessing the suitability of fixtures for durability assessments. For example, standards such as the NASA GSFC-STD-7000A [138] and MIL-STD-810F [139] request that fixture transmissibility is assessed on the fixture in isolation. However BS60068 and DEF STAN 0035 (Part 3) [140] suggest testing both with and without the DUT installed.

Figure 50 shows the measured response of the fixture in the X, Y and Z-axis when excited in the Z-axis via a swept sine wave, of amplitude 1 g_n over a frequency range from 5-800 Hz (800 Hz is peak frequency of durability profiles utilized within this study) at a rate of 1 octave per minute.

The results show that the vibration responses measured, in all three axes, are within the limits specified by BS EN 60068. The data presented in Figure 50 is a sample of the total data recorded for illustrative purposes. A full data set is presented within Submission 3.

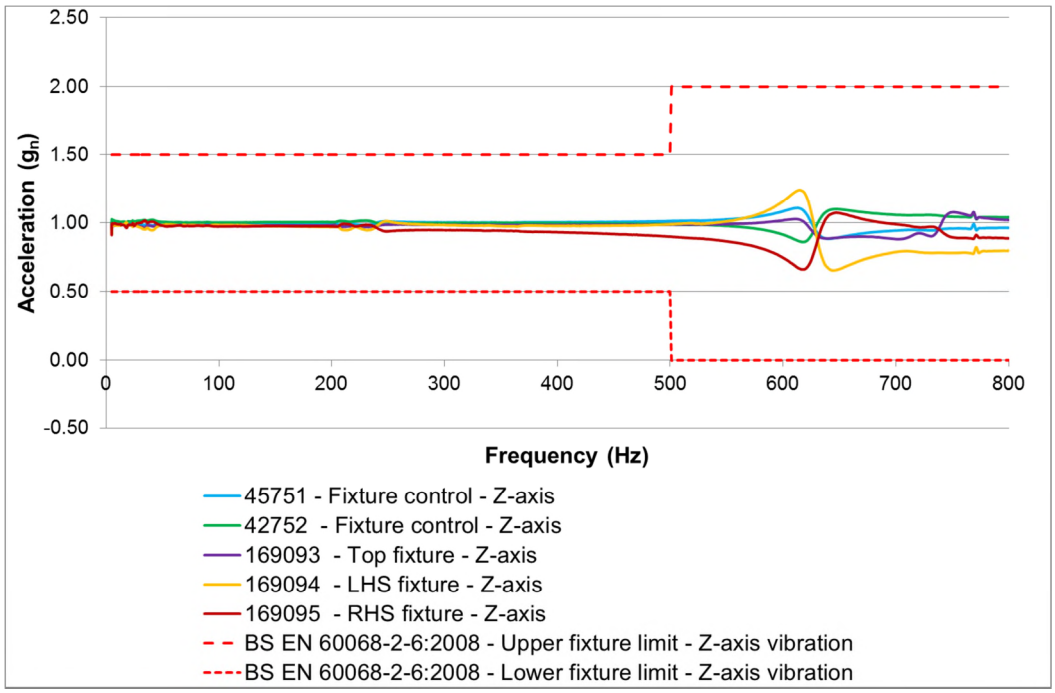

a)

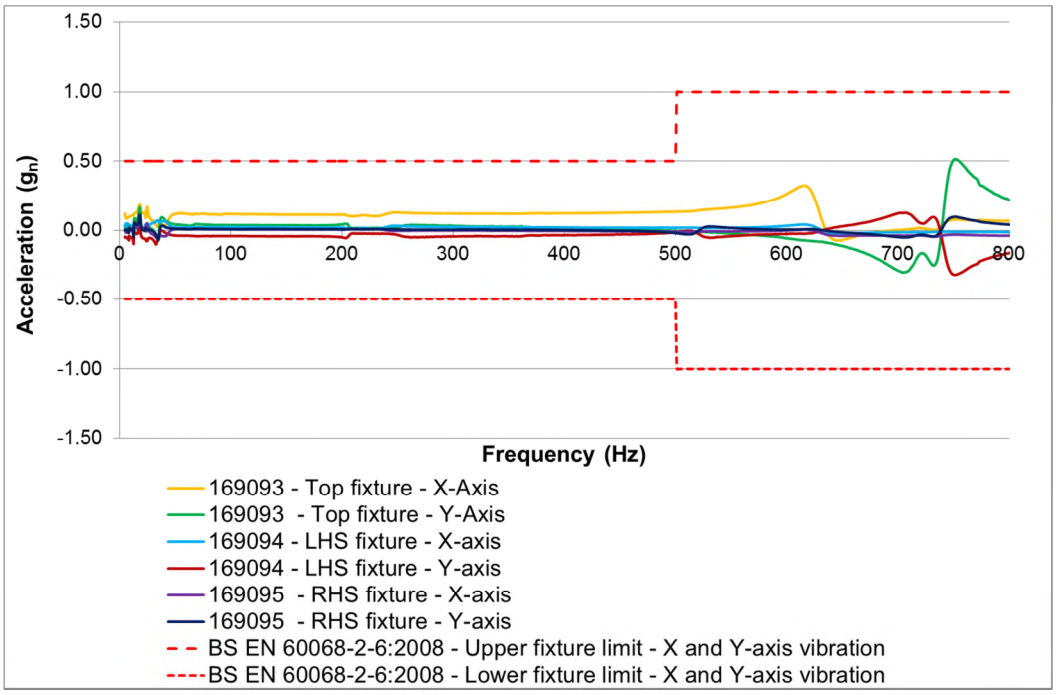

b)

Figure 50: BS EN 60068 Resonance Evaluation of 18650 Durability Fixture: a) Z-Axis of Fixture b) X and Y-Axis of Fixture

To mechanically characterise the cells at the start and end of test (discussed in 5.3.4.6), an additional “cell resonance search plate” fixture was fabricated to allow for accurate natural frequency measurements outside the frequency range (> 800 Hz) of the durability fixture assembly. The cell resonance search plate which

was designed to accept a three cell test fixture (shown in Figure 47a). The assembled resonance search plate and three cell test fixture is shown in Figure 51b.

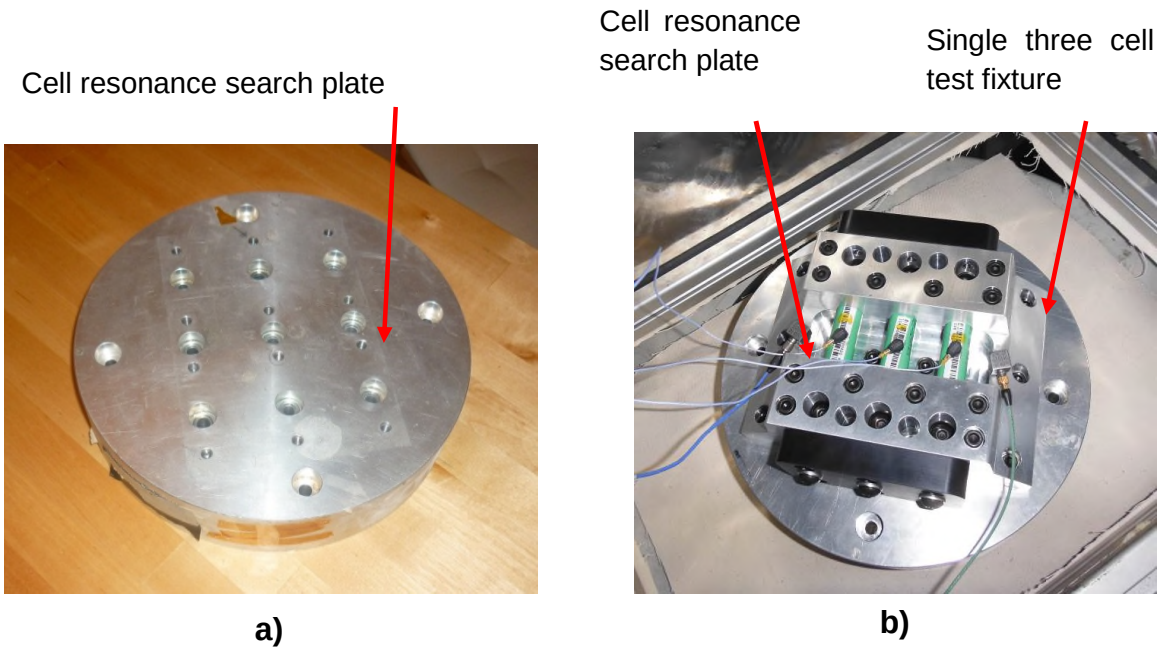

Figure 51: a) Cell Resonance Search Plate b) Cell Resonance Search Plate with Single 18650 Three Cell Fixture Installed on VP85 EMS

The resonance search plate fixture assembly shown in Figure 51b was evaluated in accordance with BS EN 60068 (without test samples installed) and was excited in the Z axis via a 1 g_n swept sine from 5 to 3700 Hz at a sweep rate of 1 octave/minute. To measure the vibration characteristics of the test fixture, accelerometers were placed in the X, Y and Z-axis of the assembled fixture, within or close to every cell mounting position. The resonance search plate with a single 18650 three cell fixture installed met the requirements of BS EN 60068 from 5 to 3700 Hz, however a 0.5 g_n resonance (which is within the limits of BS EN 60068) was noted at 1500 Hz. The results from this assessment are shown in Figure 52.

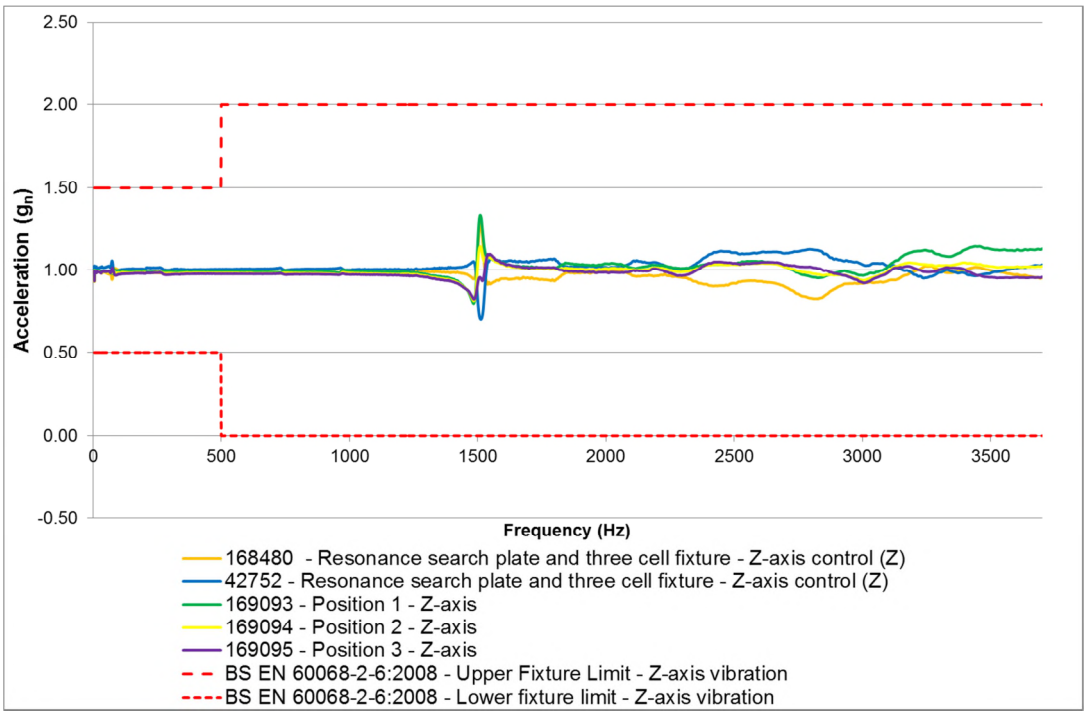

a)

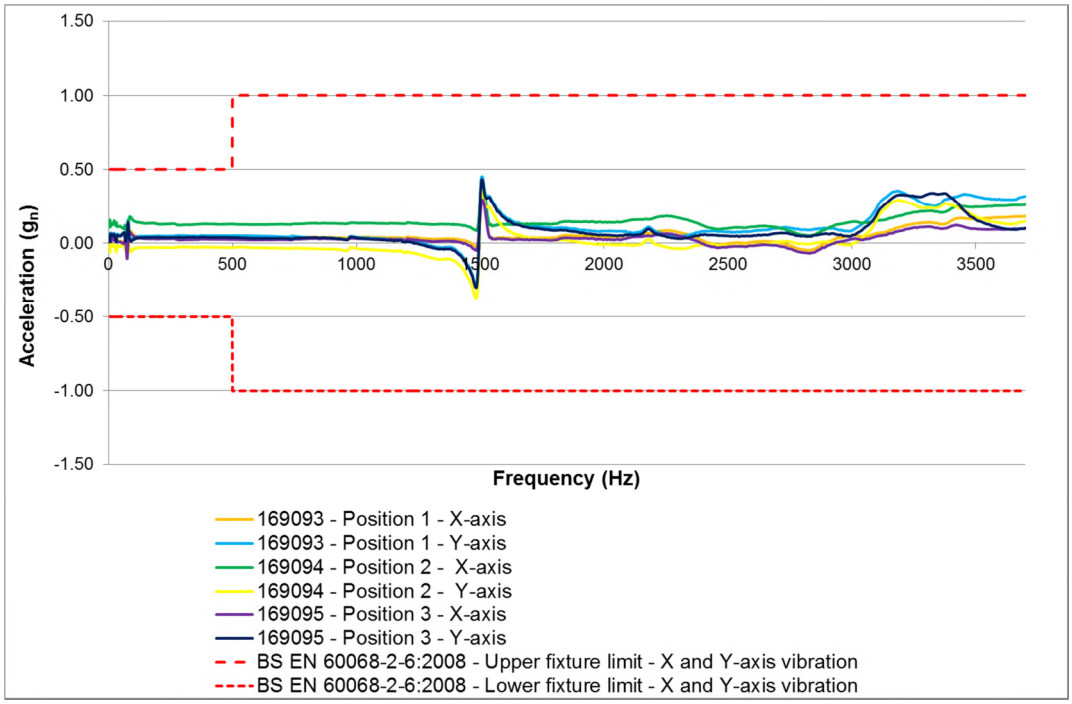

b)

Figure 52: BS EN 60068 Resonance Evaluation of Resonance Search Plate a) Z-Axis of Search Plate b) X and Y-Axis of Search Plate

5.3.4 Pre-Test Electrical and Mechanical Characterisation

The following tests were performed on each cell at the SOT for the investigations on both the NMC and NCA samples. All electrical characterisation tests were performed in a climate controlled chamber at 21 ± 0.5 °C, whilst mechanical characterisation were conducted in the EMS laboratory at 21 ± 5 °C. The presented

electrical characterisation techniques were conducted in accordance with agreed JLR and WMG working practices and are defined in the WMG Catapult procedure CAT-C-140 [102] and CAT-C-183 [141]. These electrical measurement procedures are based on standards [66, 142] and embody additional research and revised methodology, such as those published within [143-145]. The mechanical characterisation testing of the cells was undertaken by the author. The electrical characterisation was performed by JLR engineers, with support from the author.

5.3.4.1 SOC Adjustment

The cell SOC was adjusted by fully charging the cells via a CC-CV method. A constant current of 1.1 A (C/3) to 4.2 V followed by a constant voltage phase at 4.2 V until the current reduced to 0.05 A (C/65). At the end of charge, the cells were allowed to rest for 4 hours prior to being discharged at 1C for 45, 30 and 15 min, to achieve a cell SOC of 25 %, 50 % or 75 %, respectively. The cells were allowed to reach equilibrium for 4 hours before the application of vibration energy.

5.3.4.2 1C capacity

The cells were fully charged using a constant current phase of 1.1 A (C/3) to 4.2 V followed by a constant voltage phase at 4.2 V until the current reduced to 0.05 A (C/65). The cells were allowed to rest for 4 hours prior to being fully discharged at 1C to 2.75 V that represents the lower voltage threshold defined by the manufacturer. The energy extracted from the cells during the discharge was recorded as a measure of the 1C capacity.

5.3.4.3 Pulse power

To determine the DC resistance (R_{DC}) of the cells, a series of pulses were applied to the cells after they were set to 50 % SOC. Each current pulse was 10 seconds in length and the pulse current magnitude was 20 %, 40 %, 60 %, 80 % and 100 % of the cell's rated maximum pulse discharge current (of 4.4 A for both sample types). Each discharge pulse at a current level was followed by a 30 minute rest period prior to performing the charge pulse at the same current level. The DC resistance of the cell was calculated as described in Equation 15 and Equation 16 for each excitation pulse. V_{OCV} is the voltage prior the application of the maximum applied current pulse (I_{max}), V_{10s} is the cell voltage at the end of the 10 s current pulse at I_{max}. An average value of R_{DC} was computed as the mean value of resistance from each of the five pulses as per Equation 16.

$$R_{DC} = \frac{(V_{OCV} - V_{10\,s})}{I_{max}}$$

Equation 15

$$R_{DC} = \sum_{n=1}^{n=5} \frac{R_{DC}}{n}$$

Equation 16

5.3.4.4 Open circuit voltage (OCV)

The OCV of the cells under evaluation was measured with the cell isolated from any electrical load using a standard laboratory voltmeter. The OCV was recorded at the start and end of test. It was also recorded prior to moving the samples on the durability fixture.

5.3.4.5 Electrochemical impedance spectroscopy (EIS)

EIS data was recorded 4 hours after the last pulse of the pulse power tests, as suggested by Barai et al. [143] and was performed at 50 % SOC. The EIS measurement was carried out in a galvanostatic mode using a ModuLab® (Solartron) electrochemical system model 2100A fitted with a 2 A booster and driven by Modulab® ECS software. The EIS spectra were collected within the frequency range of 10 mHz to 10 kHz using 10 frequency points per decade. The amplitude of the applied current was 200 mA (RMS). No DC current was superimposed on the RMS value. The commercially available Z view® software was employed to fit the EIS spectra to an equivalent circuit model (ECM) of the cell, thereby facilitating the quantification of key cell parameters such as: ohmic resistance (R_O) and charge transfer resistance (R_{CT}).

5.3.4.6 Natural frequency

The cells' natural frequency was recorded at SOT and EOT to quantify the mechanical characteristics of each cell. Changes in natural frequency can indicate a change in material properties (such as stiffness) through mechanisms such as cracking or work hardening. The natural frequency of each cell was measured by fastening the respective cell to the EMS table (as illustrated in Figure 53) and applying a swept sine wave from 5 to 3700 Hz, of amplitude 1 g_n at a rate of 1 octave/minute.

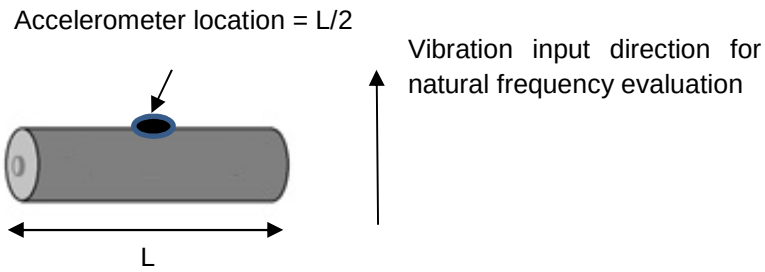

Figure 53: Location of Cell Accelerometer for Natural Frequency Measurement via Swept Sine Frequency Sweep

The response of the cell in relation to this 1 g_n excitation, was recoded via a lightweight, single axis, accelerometer (PCB 352A24) mounted as shown in Figure

53. These were secured to the centre of the cell using a petro wax adhesive. With a weight of only 0.8 g (1.9 % additional mass for each cell), their inclusion within the experimental set-up was not deemed to have any significant impact on test accuracy through the addition of extra mass.

Two control accelerometers were secured at opposite ends at the top of the test fixture. Each control accelerometer was mounted close to the specimens. An averaging control strategy was employed during the natural frequency measurement. Data was recorded at 2.5 times the desired peak frequency in accordance with Nyquist rate guidelines [107]. With this test program, the peak desired frequency was the maximum achievable frequency of the VP85 EMS, defined by the manufacturer as 3.7 kHz. Therefore, accelerometer data was measured at a frequency greater than 9.25 kHz.

Post natural frequency measurement, each cell was allowed to rest for a minimum of 3 hours before commencing the vibration durability test profiles to allow them to stabilise, prior to the application of mechanical excitation. The control samples were not measured during the natural frequency assessment; this was to ensure that they were not subject to any mechanical loading which could potentially affect the electrical characterisation results.

5.3.5 Application of Vibration

Once the cells presented in Table 19 were characterised as described in Section 5.3.4 they were prepared for their respective vibration test. Within investigation 1 the 27 NMC 18650 cells were then divided into three equal batches, comprising nine cells each. The first batch was subjected to the random vibration profiles defined in the USABC Procedure 10 standard whilst the second batch was subjected to the WMG-MPG vibration profiles presented in Chapter 3. The remaining cells were defined as control samples. Control samples were either co-located within the same environmental conditions (within the manufacturer supplied shipping carton), but not subject to any vibration loading as the test cells or remained in climatically controlled storage at the university.

Within investigation 2 the twelve NCA 18650 cells were divided into two groups. The first group of nine cells were subjected to the USABC Procedure 10 vibration profiles, whilst the second group of three cells were control samples. The control samples were placed in the manufacturer supplied shipping carton in the test facility but were not subjected to vibration.

Depending on the vehicle packaging constraints and application, 18650 cells are packaged in different orientations within different automotive battery packs [2, 90, 146, 147]. Therefore, one of the objectives of this study is to evaluate the effect of the X, Y and Z “vehicle axis” vibration profiles, to the three possible X, Y and Z-axis cell orientations. The vehicle and cell axis conventions are defined in Figure 54.

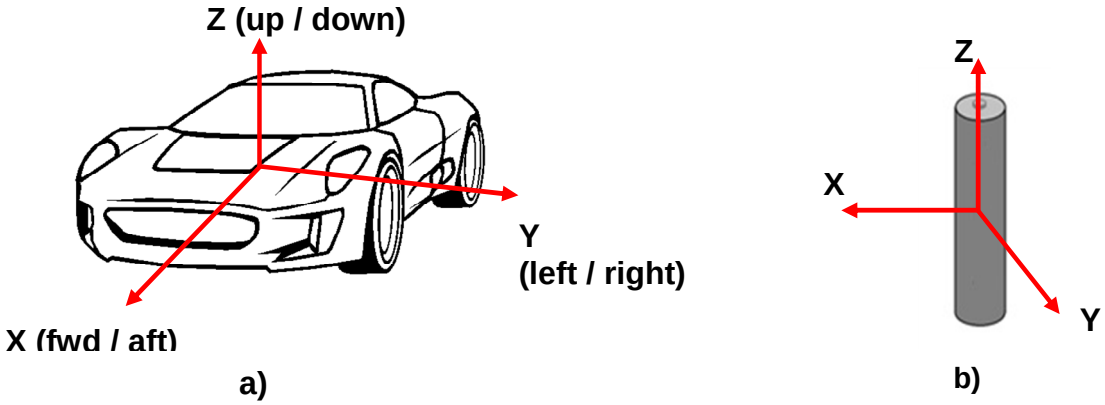

Figure 54: a) Axis Convention of Vehicle Vibration Durability Profiles (SAE J670e) [41], b) Axis Convention of Cells

Both vibration tests comprise a vertical (Z-axis) profile in addition to vibration profiles defined for the horizontal plane (X-axis and Y-axis). As part of the experimental procedure, each profile is sequentially applied to the cells to achieve the desired 100,000 miles of representative EV life. The three different combinations of vibration load with respect to each cell orientation are defined below:

- Z:Z to X:X to Y:Y
- Z:X to X:Y to Y:Z
- Z:Y to X:Z to Y:X

Using the above notation, for each pair of letters, the first letter refers to the vehicle axis, whilst the second refers to cell orientation. For simplicity, this report identifies the cell orientation in relationship to the vertical (Z axis) of the vehicle. For example a cell that was subjected to the vibration sequence of Z:X to X:Y to Y:Z, is referred to as being evaluated in the Z:X orientation. Figure 55 presents the orientation of the 9 cells mounted onto the durability fixture for the three orientations associated with the test programme.

Due to limited equipment availability, a single axis shaker was employed for durability testing. Because the orientation of the EMS could not be changed, the cells had to be rotated on the durability fixture between the X, Y and Z axis to achieve the correct loading. This test methodology is termed as not testing “with respect to gravity” and does not take into account changes in cell mass during the re-orientation of cells with respect to the input axis of vibration. Within these experiments, it is assumed that this limitation will not significantly impact the results. However, this is discussed further in Section 5.6.

Durability testing was conducted within an air-conditioned laboratory at a temperature of 21 ± 5 °C. The closed loop application of the vibration profile was achieved by using an averaging control strategy, as defined within [148] that includes a ± 3 dB alarm limits, ± 6 dB abort limits and 3 sigma limit control to ensure the safe execution of the test.

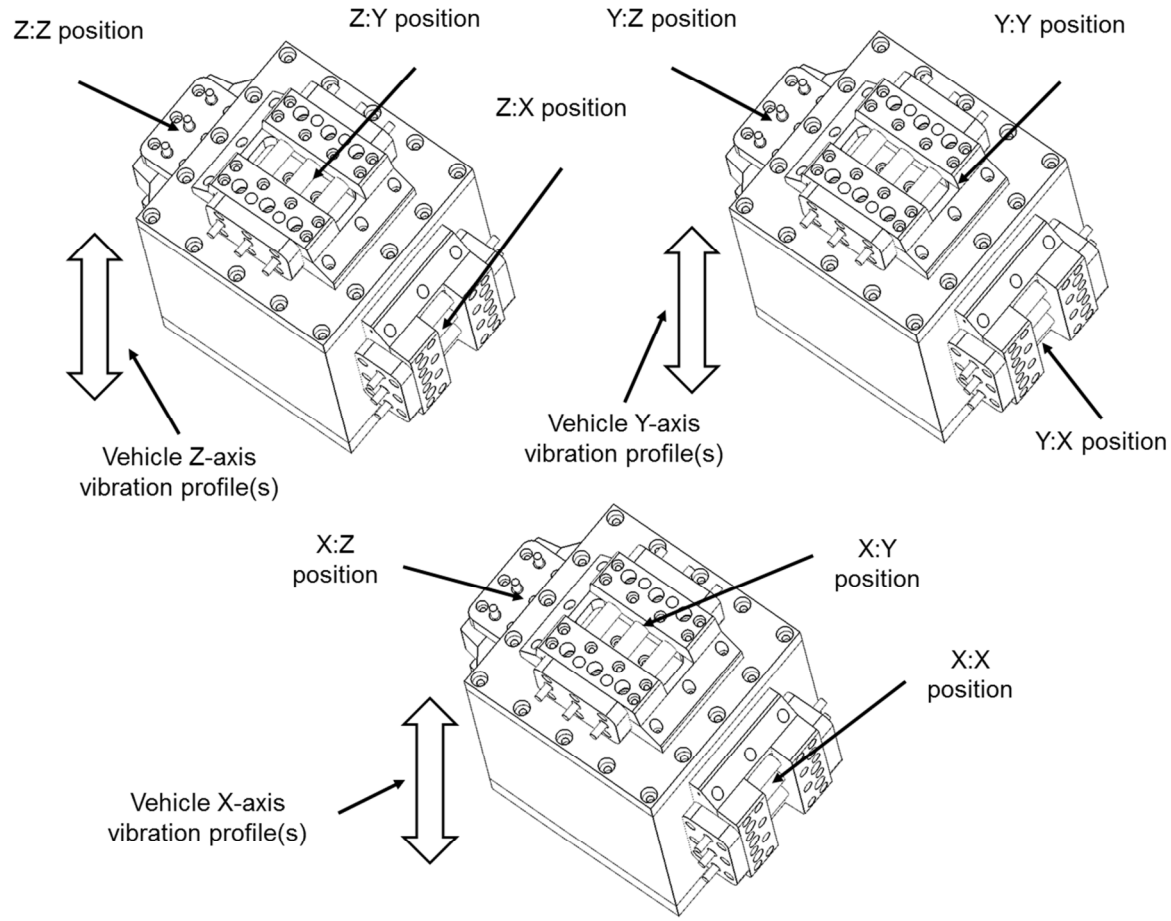

Figure 55: Experimental Orientations and Test Positions on Durability Fixture

Once the cells were installed to the durability fixture and mounted onto the EMS table, the Z-axis vibration profile of either USABC Procedure 10 or WMG-MPG was applied first (Table 20). On completion, the cells were left to stabilize for a minimum of 4 hours. The cells were then moved on the durability fixture to the corresponding vehicle X-axis and subjected to the X-axis vibration profile (Table 21). Finally, the cells were repositioned on the durability fixture to facilitate the application of the vehicle Y-axis vibration profile (Table 22). At the end of the vibration profile, the cells were left to stabilize for 4 hours prior to visual inspection.

Table 20: Z-Axis Vibration Profiles Schedule

USABC Procedure 10		WMG-MPG	
Profile Description	**Duration (HH:MM)**	**Profile Description**	**Duration (HH:MM)**
Subject cells to 9 minutes of Vertical Profile 1 at 1.9 Grms in the Z-axis orientation of the cells under assessment.	00:09	Subject cells to 150 hours of vertical Frequency in the Z-axis orientation of the cells under assessment.	150:00
Subject cells to 5 hours and 15 minutes of Vertical Profile 1 at 0.75 Grms in the Z-axis orientation of the cells under assessment.	05:15		
Subject cells to 9 minutes of Vertical Profile 2 at 1.9 Grms in the Z-axis orientation of the cells under assessment.	00:09		
Subject cells to 5 hours and 15 minutes of vertical Frequency Spectrum 2 at 0.75 Grms in the Z-axis orientation of the cells under assessment.	05:15		
Subject cells to 9 minutes of Vertical Profile 3 at 1.9 Grms in the Z-axis orientation of the cells under assessment.	00:09		
Subject cells to 5 hours and 15 minutes of Vertical Profile 3 at 0.75 Grms in the Z-axis orientation of the cells under assessment.	05:15		
Total	**16:12**	**Total**	**150:00**

Table 21: X-Axis Vibration Profiles Schedule

USABC Procedure 10		WMG-MPG	
Profile Description	**Duration (HH:MM)**	**Profile Description**	**Duration (HH:MM)**
Subject cells to 5 minutes of Longitudinal Profile at 1.5 Grms in the X-axis orientation of the cells under assessment.	00:05	Subject cells to 150 hours of horizontal Frequency in the X-axis orientation of the cells under assessment.	150:00
Subject cells to 19 hours of Longitudinal Profile at 0.4 Grms in the X-axis orientation of the cells under assessment.	19:00		
Subject cells to 5 minutes of Longitudinal Profile at 1.5 Grms in the X-axis orientation of the cells under assessment.	00:05		
Subject cells to 19 hours of Longitudinal Profile at 0.4 Grms in the X-axis orientation of the cells under assessment.	19:00		
Total	**38:10**	**Total**	**150:00**

Table 22: Y-Axis Vibration Profiles Schedule

USABC Procedure 10		WMG-MPG	
Profile Description	**Duration (HH:MM)**	**Profile Description**	**Duration (HH:MM)**
Subject cells to 5 minutes of Longitudinal Profile at 1.5 Grms in the Y-axis orientation of the cells under assessment.	00:05	Subject cells to 150 hours of horizontal Frequency in the Y-axis orientation of the cells under assessment.	150:00
Subject cells to 19 hours of Longitudinal Profile at 0.4 Grms in the Y-axis orientation of the cells under assessment.	19:00		
Subject cells to 5 minutes of Longitudinal Profile at 1.5 Grms in the Y-axis orientation of the cells under assessment.	00:05		
Subject cells to 19 hours of Longitudinal Profile at 0.4 Grms in the Y-axis orientation of the cells under assessment.	19:00		
Total	**38:10**	**Total**	**150:00**

5.3.6 Post-Test Electrical and Mechanical Characterisation

Post the application of the desired vibration profiles, the cells were left to stabilise for 4 hours prior to visual inspection. EOT characterisation of the cells, both in terms of the electrical performance and mechanical attributes were conducted by repeating the tests defined in Section 5.3.4.

5.4 **Results – Investigation 1 – NMC 18650 Samples**

The key findings are presented within this section; however, a full set of tabulated results are presented in Appendix F to L. Additional analysis is also presented in Submissions 3 and 4 of the portfolio. Equation 17 was used to calculate the averages within this section, where $\sum_x$ is the sum of all the data values, and n is the number of values.

$$Average = \frac{\sum_x}{n}$$

Equation 17

5.4.1 Post-Test External (Visual) Condition of Cells

No significant external degradation was observed on any of the samples post application of either vibration test with the exception of sample 16 which had a surface irregularity post testing. Regardless of this observation, no electrolyte leakage or external cracking of the cell casing was observed in any of the test samples. There was a consistent observation of witness marking resulting from the clamping of external surface of the cell within the test fixtures.

5.4.2 1C Discharge Capacity Results

Table 23 to Table 25 present the 1C discharge capacity for each cell at SOT and EOT. Reviewing the two data sets together, it is noticeable that there is a tendency for the 75 % charge condition to be more susceptible to a reduction in capacity regardless of vibration profile applied to them. Both test profiles have a tendency for 50 % SOC being the charge state with the least degradation with respect to capacity fade, with a significant improvement in capacity being observed in some samples at this SOC. This could be due to an increased electrode wetting resulting from the application of vibration.

Table 23: Percentage Change in 1C Capacity Discharge Performance of Cells Evaluated to USABC Procedure 10 by SOC and Orientation

		SOC			
		25 %	**50 %**	**75 %**	**Average % Change**
Orientation	**Z:X**	−2.33	0.93	−0.93	**-0.78**
	Z:Y	0.46	−1.83	−6.79	**-2.71**
	Z:Z	0	−1.79	−12.22	**-4.67**
	Average % Change	**-0.62**	**-0.89**	**-6.64**	

Table 24: Percentage Change in 1C Capacity Discharge Performance of Cells Evaluated to WMG-MPG Profile by SOC and Orientation

		SOC			
		25 %	**50 %**	**75 %**	**Average % Change**
Orientation	**Z:X**	0.00	3.90	−1.43	**0.82**
	Z:Y	0.00	10.42	0.00	**3.47**
	Z:Z	0.00	−4.59	1.45	**-4.10**
	Average % Change	**0.00**	**3.24**	**0.01**	

Table 25: Percentage Change in 1C Capacity Discharge Performance of Control Samples

SOC	Procedure	% Change
25 %	USABC Procedure 10	−3.18
50 %	USABC Procedure 10	0.46
75 %	USABC Procedure 10	−4.63
25 %	WMG-MPG	0.00
50 %	WMG-MPG	8.85
75 %	WMG-MPG	−0.47

With regard to cell orientation, results indicate that cells oriented in the Z:Z position and subjected to either test profiles, have a greater susceptibility to capacity degradation.

5.4.3 Pulse Power Results

Table 26 to Table 28 presents the R_{DC} resistance of the cells at SOT and EOT. It can be seen that irrespective of the vibration profile employed (including variations in cell SOC and orientation) each cell exhibits an increase in internal resistance. As discussed within [82], this potentially indicates a reduction in contact area within the current collectors or possible internal fatigue of components within the cell due to the mechanical load.

Table 26: Percentage Change in DC Resistance of Cells Evaluated to USABC Procedure 10 by SOC and Orientation

		SOC			
		25 %	**50 %**	**75 %**	**Average % Change**
Orientation	**Z:X**	82.4	60.0	121.4	**87.9**
	Z:Y	108.4	92.4	79.5	**93.4**
	Z:Z	64.5	45.2	128.1	**79.3**
	Average % Change	**85.1**	**65.9**	**109.7**	

Table 27: Percentage Change in DC Resistance of Cells Evaluated to WMG-MPG Profile by SOC and Orientation

		SOC			
		25 %	**50 %**	**75 %**	**Average % Change**
Orientation	**Z:X**	97.8	30.4	22.2	**50.1**
	Z:Y	68.5	51.7	17.4	**45.9**
	Z:Z	75.2	58.1	95.2	**76.2**
	Average % Change	**80.5**	**46.7**	**44.9**	

Table 28: Percentage Change in R_{DC} Performance of Control Samples

SOC	Procedure	% Change in R_{DC}
25 %	USABC Procedure 10	1.9
50 %	USABC Procedure 10	14.5
75 %	USABC Procedure 10	-0.9
25 %	WMG-MPG	1
50 %	WMG-MPG	0
75 %	WMG-MPG	-0.6

The sample oriented in Z:Z, conditioned to 75% SOC and subjected to USABC Procedure 10 (Sample 16) displays the greatest variation in resistance with a

128.1 % increase from SOT to EOT. Conversely, the sample oriented in Z:Y, conditioned to 75 % SOC and subjected to WMG-MPG profiles (Sample 27) shows the least amount of increase (17.4 %). Interestingly, both cells were pre-conditioned to 75 % SOC. However; the vibration profiles employed were different, as was their respective orientation when mechanically loaded. Similarly, 9 out of 10 of the cells that exhibit the greatest rise in resistance were pre-conditioned to either 25 % or 75 % SOC.

For the cells that underwent the USABC Procedure 10 vibration profiles, the cell orientated along the Z:Z axis and pre-conditioned at 75 % SOC exhibited the greatest change in DC resistance, 128.1 %. Likewise, the cell orientated along the Z:Z axis and pre-conditioned at 50 % SOC exhibited the least change in $R_{DC,}$ of 17.4 %. Moreover, for the cells which underwent the WMG-MPG vibration profiles, the cell placed along the Z:X axis and pre-conditioned at 25 % SOC exhibited the greatest change in DC resistance, 97.8 %. Similarly, the cell orientated along the Z:Y axis and pre-conditioned at 75 % SOC exhibited the least change in DC resistance, 45.2 %.

5.4.4 OCV Results

Appendix H presents the measured OCV for each cell both at SOT and EOT. None of the tested cells displayed any significant change in OCV, irrespective of the vibration profile, the cell SOC or cell orientation employed. The voltage difference recorded is within the tolerance of error of the measurement equipment. This supports the results presented in [80, 81] that also noted that OCV is not adversely affected by vibration loading.

5.4.5 EIS Results

As well as pulse power, impedance was measured via EIS testing. EIS is used to determine the frequency-dependent impedances of a cell [82]. From EIS traces it is possible to determine changes in the properties of the cell. The two key attributes of the EIS niquist graph utilised within this study to assess the degradation and change in cell electrical performance are the R_O and R_{CT}. R_O is related to the internal connectivity performance of the cell [149]. A change in this resistance can be related to mechanical alterations of internal cell components such as anode and the cathode and their associated active material, the current collectors and the electrolyte [150]. The internal resistance is further influenced by material contacts (e.g., between active material and the current collector), geometrical electrode (thickness, dimensions) and internal construction aspects [150]. R_{CT} is defined as the electron transfer from one phase (e.g. electrode) to another (e.g. electrolyte) and is related to the kinetics of the electrochemical reactions [149]. A complete explanation of EIS is beyond the scope of this report, however it is well documented in a number of academic and educational texts [149, 151].

Like the pulse power results, further evaluation of the electrical performance of the cells via EIS testing indicate a significant change in cell performance post testing on all cells subjected to vibration. This typical change in performance is illustrated in Figure 56. It must be noted that despite numerous attempts, that sample 16 could not be measured for EIS post vibration testing due to an undiagnosed internal failure. This is assumed to relate to internal fatigue damage within the cell. Further investigation into the exact nature of the failure mode, is beyond the scope of this study, but is discussed further in [40]. As a result, this study is concluding that this cell would have the greatest change in EIS performance between SOT and EOT.

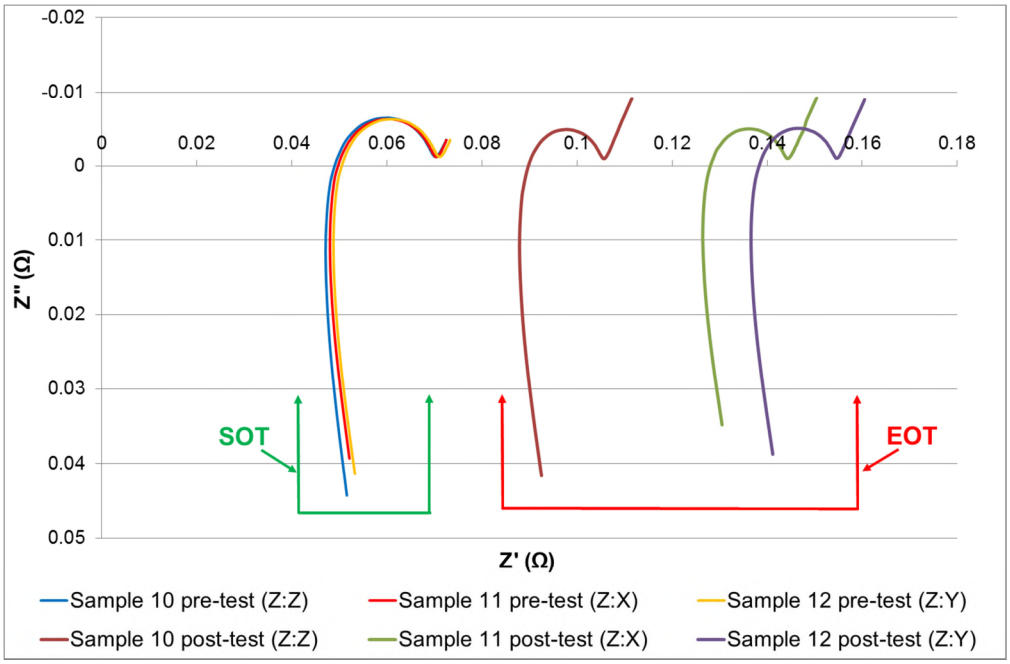

Figure 56: Typical EIS Pre and Post Test Results (Note Samples Presented Subjected to USABC Procedure 10)

Table 29 to Table 33 show the change in R_O and R_{CT}, between the SOT and EOT. Comparing Table 26 and Table 27, it can be seen that the increase in R_{DC} of the cell is accompanied by an increase in R_O. Though the magnitude may differ from one technique to another, this concurs with the origin of these parameters.

Table 29: Percentage Change in R_O of Cells Evaluated to USABC Procedure 10 Profiles by SOC and Orientation

		SOC			
		25 %	**50 %**	**75 %**	**Average % Change**
Orientation	**Z:X**	168.66	141.44	209.74	**173.28**
	Z:Y	184.07	254.53	203.66	**214.09**
	Z:Z	89.00	82.61	*	**85.81**
	Average % Change	**147.24**	**159.53**	**206.70**	

*= No data available due to cell issue

Table 30: Percentage Change in R_O of Cells Evaluated to WMG-MPG Profile by SOC and Orientation

		SOC			
		25 %	**50 %**	**75 %**	**Average % Change**
Orientation	**Z:X**	227.29	93.97	143.19	**154.82**
	Z:Y	121.69	42.74	38.09	**67.51**
	Z:Z	257.82	69.80	231.20	**186.27**
	Average % Change	**202.27**	**68.84**	**137.49**	

Table 31: Percentage Change in R_{CT} of Cells Evaluated to USABC Procedure 10 Profile by SOC and Orientation

		SOC			
		25 %	**50 %**	**75 %**	**Average % Change**
Orientation	**Z:X**	-20.74	-26.32	-28.57	**-25.21**
	Z:Y	-16.23	-24.05	-35.15	**-25.14**
	Z:Z	-21.16	-24.68	*	**-22.92**
	Average % Change	**-19.38**	**-25.02**	**-31.86**	

*= No data available due to cell issue

Table 32: Percentage Change in R_{CT} of Cells Evaluated to WMG-MPG Profile by SOC and Orientation

		SOC			
		25 %	**50 %**	**75 %**	**Average % Change**
Orientation	**Z:X**	-28.51	-33.71	-28.25	**-30.16**
	Z:Y	-34.59	-32.80	-28.19	**-31.86**
	Z:Z	-30.14	-34.29	-23.21	**-29.21**
	Average % Change	**-31.08**	**-33.60**	**-26.55**	

Table 33: Percentage Change in R_O and R_{CT} of Control Samples

SOC	Procedure	% Change R_O	% Change R_{CT}
25 %	USABC Procedure 10	6.71	-42.01
50 %	USABC Procedure 10	22.58	-28.28
75 %	USABC Procedure 10	0.00	-36.18
25 %	WMG-MPG	1.40	-32.25
50 %	WMG-MPG	1.30	-38.17
75 %	WMG-MPG	2.60	-43.30

Table 29 and Table 30 highlight that irrespective of the vibration profile, SOC or cell orientation; all the cells exhibit a significant increase in R_O at EOT. For the cells that underwent the USABC Procedure 10 vibration profiles, the cell orientated along the Z:Y axis and pre-conditioned at 50 % SOC exhibited the greatest change in R_O, 254.53 %. Moreover, the cell orientated along the Z:Z axis and pre-conditioned at 50 % SOC exhibited the least change in R_O, 82.61 %. Similarly, for the cells that underwent the MBK-MPG vibration profile, the cell positioned along the Z:Z axis and pre-conditioned at 25 % SOC exhibited the greatest change in R_O, 257.82 %. Likewise, the cell placed along the Z:Y axis and pre-conditioned at 75 % SOC exhibited the least change in R_O, 38.09 %.

Table 31 to Table 33 illustrate that all cells that underwent vibration testing show a similar decrease in R_{CT} as the control samples. Consequently, it suggests that this parameter is unaffected by vibration.

5.4.6 Mechanical Characterisation Results

Table 34 to Table 37 present the natural frequency and amplitude of the first resonant mode of each cell, respectively. The results show that every cell subject to a vibration ageing profile, irrespective of the type of profile used, exhibited a reduction in its natural frequency. Similarly, the amplitude of the first resonant mode is also affected by the vibration ageing cycle. The change in natural frequency was previously attributed to a change in the material properties caused for example by internal cracking, delamination or fracture. The change in the amplitude of the acceleration at the natural frequency was found to indicate a change in the level of component damping [35]. As none of the cells experienced any reduction in mass after either of the vibration ageing cycles, these results may indicate a reduction or increase in the internal stiffness of the cell assembly.

Table 34: Percentage Change in Frequency of First Natural Frequency of Test Cells Evaluated to USABC Procedure 10 Profiles by SOC and Orientation

		SOC			
		25 %	**50 %**	**75 %**	**Average % Change**
Axis	**Z:X**	-12.68	-8.62	-6.39	**-9.23**
	Z:Y	-0.27	-8.97	-7.76	**-5.67**
	Z:Z	-27.22	-6.17	-16.65	**-16.68**
	Average % Change	**-13.39**	**-7.92**	**-10.27**	

Table 35: Percentage Change in Amplitude of First Natural Frequency of Test Cells Evaluated to USABC Procedure 10 Profile by SOC and Orientation

		SOC			
		25 %	50 %	75 %	Average % Change
Axis	Z:X	-5.40	-34.30	-3.60	**-14.43**
	Z:Y	-8.50	11.20	35.90	**12.87**
	Z:Z	-24.40	-1.70	6.00	**-6.70**
	Average % Change	**-12.77**	**-8.27**	**12.77**	

Table 36: Percentage Change in Frequency of First Natural Frequency of Test Cells Evaluated to WMG-MPG Profile by SOC and Orientation

		SOC			
		25 %	50 %	75 %	Average % Change
Axis	Z:X	-0.16	-6.88	-3.37	**-3.47**
	Z:Y	-2.97	-0.29	-3.14	**-2.13**
	Z:Z	-0.74	-0.70	-0.82	**-0.75**
	Average % Change	**-1.29**	**-2.63**	**-2.44**	

Table 37: Percentage Change in Acceleration of First Natural Frequency of Test Cells Evaluated to WMG-MPG by SOC and Orientation

		SOC			
		25 %	50 %	75 %	Average % Change
Axis	Z:X	-20.10	-11.90	-25.30	**-19.10**
	Z:Y	-1.70	-3.60	-24.70	**-10.00**
	Z:Z	-31.20	7.20	79.60	**18.53**
	Average % Change	**-17.67**	**-2.77**	**9.87**	

More specifically, for the cells which underwent the USABC Procedure 10 vibration profiles, the cell orientated along the Z:Z axis and pre-conditioned at 25 % SOC exhibited the greatest change in natural frequency, 27.22 %. Likewise, the cell orientated along the Z:Y axis and pre-conditioned at 25 % SOC exhibited the least change in natural frequency, 0.27 %. In addition, it was observed that the cell positioned along the Z:Y axis and pre-conditioned at 75 % SOC and the cell positioned along the Z:Z axis and pre-conditioned to 50 % SOC showed the greatest and least change in amplitude, 35.9 % and 1.7 %, respectively. For the cells that underwent the WMG-MPG vibration profile, the cell placed along the Z:Z axis and

pre-conditioned at 50 % SOC exhibited the greatest change in natural frequency, 6.9 %. Similarly, the cell orientated along the Z:X axis and pre-conditioned at 25 % SOC exhibited the least change in natural frequency, 0.2 %. Table 36 also shows that the shift in resonance frequency for the cells which underwent the WMG-MPG vibration profile is less pronounced than that observed for cells subjected to the USABC Procedure 10 vibration profile. Furthermore, Table 37 illustrates that the cell positioned along the Z:Z axis and pre-conditioned at 75 % SOC and the cell positioned along the Z:Y axis and pre-conditioned to 25 % SOC showed the greatest and least change in amplitude, 79.6 % and 1.7 %, respectively.

5.5 **Results – Investigation 2 – NCA Samples**

The following section identifies the trends in the observed measurements taken throughout the durability testing on the cells when subject to the USABC Procedure 10 standard. It highlights trends relating to the impact of vibration on cell performance and any possible causality between cell orientation and the susceptibility of the cell to vibration induced degradation. Salient results are presented that illustrate the trend in cell performance evaluated at EOT.

Unlike investigation 1 presented in Section 5.4, Analysis of Variance (ANOVA) against the control samples was conducted on the results to determine the significance of the impact of vibration. This was due to the larger sample size per test orientation and SOC.

5.5.1 Post-Test External (Visual) Condition of Cells

At EOT, no significant mechanical damage or degradation was observed on any of the test samples. No leaking or expulsion of electrolyte was witnessed or any external fatigue cracking or delamination noted. The consistent observation at EOT, at the point where the cells were clamped within the test fixture, was the compression of the external insulation wrapped around the cell. The results showed no significant difference as a result of different cell orientations.

5.5.2 1C Discharge Capacity Results

All samples (including control samples) show a reduction in capacity post vibration testing within the range of 0.30 to 0.39 Ah. It is however evident that the reduction in capacity observed in the control samples is comparable to that observed within the tested samples. This indicates that the reduction in capacity is likely to be a function of environmental conditions as opposed to the effects of vibration. This hypothesis is also supported when the mean change in cell capacity of each cell orientation is compared to the mean of the control samples. It is also further supported by the ANOVA analysis (shown in Table 38) that clearly shows that the mean change in the control and tested samples are similar at the 95 % confidence level, confirming that any change capacity reduction cannot be uniquely attributed to the vibration applied to the cells.

Table 38: Change in Capacity of Test Cells

Cell sample No	Orientation	SOT (Ah)	EOT (Ah)	Change from SOT and EOT (Ah)	Percentage change (%)
1	Z:Z	3.04	2.72	-0.32	-10.53
2	Z:Z	3.07	2.69	-0.38	-12.38
3	Z:Z	3.08	2.73	-0.35	-11.36
4	Z:X	3.06	2.70	-0.36	-11.76
5	Z:X	3.05	2.73	-0.32	-10.49
6	Z:X	3.06	2.69	-0.37	-12.09
7	Z:Y	3.08	2.70	-0.38	-12.34
8	Z:Y	3.07	2.71	-0.36	-11.73
9	Z:Y	3.05	2.66	-0.39	-12.79
10	Control	3.07	2.70	-0.37	-12.05
11	Control	3.03	2.73	-0.30	-9.90
12	Control	3.07	2.70	-0.37	-12.05
Mean change					
Orientation				**Mean change (Ah)**	**Mean change (%)**
Mean change capacity- Z:X				-0.350	-11.45
Mean change capacity- Z:Y				-0.377	-12.28
Mean change capacity- Z:Z				-0.350	-11.42
Mean change capacity- Control				-0.347	-11.34
ANOVA analysis					
Orientation				**ANOVA p-value against control - Null hypothesis: Mean of vibrated cells and control cells are equal. Reject null hypothesis if p < 0.05**	
Z:X orientation				0.911	
Z:Y orientation				0.295	
Z:Z orientation				0.914	

5.5.3 Pulse Power Results

All samples displayed a reduction in the pulse power performance post vibration testing. Table 39 illustrates the change in R_{DC} inferred from the pulse power test results. Based on research conducted by [152] the standard error (the confidence in the sample mean resulting from the experiment due to past confidence with experiment/cells) is 0.62 % [152]. The experimental error of the samples tested was calculated to be ± 0.53 % indicating a high confidence in the repeatability of the pulse power measurements undertaken.

It can be seen from Table 39 the worst performing cell was sample 4 (Z:X) which displayed a 5.34 % increase in R_{DC}. The cell with the least increase in DC resistance post vibration was sample 7 (vibrated in the Z:Y axis) that had a 3.70 % increase.

The percentage change in R_{DC} of sample 7 and sample 3 are comparable to that of the control samples within this evaluation, supporting the hypothesis that it is not possible to isolate cell degradation (defined as in increase in cell ohmic resistance) due to vibration.

Table 39: Change in Pulse Power Performance – R_{DC}

Cell sample No	Orientation	DC resistance (SOT) (mΩ)	DC resistance (EOT) (mΩ)	Change in DC resistance (mΩ)	Percentage change in DC resistance - difference between SOT and EOT (%)
1	Z:Z	45.32	47.31	1.99	4.39
2	Z:Z	45.20	47.16	1.96	4.34
3	Z:Z	44.65	46.34	1.69	3.78
4	Z:X	44.59	46.97	2.38	5.34
5	Z:X	45.14	47.16	2.02	4.47
6	Z:X	44.85	46.95	2.10	4.68
7	Z:Y	44.83	46.49	1.66	3.70
8	Z:Y	45.00	47.19	2.19	4.87
9	Z:Y	44.59	46.43	1.84	4.13
10	Control	44.80	46.34	1.54	3.44
11	Control	45.47	46.49	1.02	2.24
12	Control	44.73	46.32	1.59	3.55
Mean change					
Orientation				**Mean change (mΩ)**	**Mean change (%)**
Mean change in R_{DC} - Z:X				2.17	4.83
Mean change in R_{DC} - Z:Y				1.90	4.23
Mean change in R_{DC} - Z:Z				1.88	4.17
Mean change in R_{DC} - Control				1.38	3.08
ANOVA analysis					
Orientation				**ANOVA p-value against control - Null hypothesis: Mean of vibrated cells and control cells are equal. Reject null hypothesis if p < 0.05**	
Z:X orientation				0.024	
Z:Y orientation				0.099	
Z:Z orientation				0.077	

Within all samples subject to vibration, an increase in R_{DC} was observed which may indicate a decrease in contact area between active material and current collector resulting from the delamination or cracking of internal surfaces [82]. However a mean increase in R_{DC} of 3.08 % was observed within the control samples (compared to a mean of 4.83 %, 4.23 % and 4.17 % for the Z:X, Z:Y and Z:Z samples

respectively) suggesting that the environmental conditions had a comparable impact on the R_{DC} of the cells.

ANOVA of the significance of the mean change in R_{DC} of the tested cells in relation to the control samples was also performed. The results of this analysis are shown in Table 39. The ANOVA assessment indicates that only cells subject to vibration along the Z:X axis have a statistically significant increase in R_{DC} as a result of the vibration when assessed at the 95 % confidence level. The Z:Y and Z:Z orientations show no significant change when compared to the control samples.

5.5.4 OCV Results

Assessing the results shown in Appendix M it can be confirmed that no significant change in the OCV measurements were observed between SOT and EOT. It is also noteworthy that due to the low values witnessed (no greater than ± 0.026 % change) that any observed difference within the OCV measurements are potentially within the error range of the measurement method. This supports the results presented in [80, 81] that also note that OCV is not adversely affected by vibration loading. The mean change in OCV is equal for all cell orientations. These results imply that there is no clear orientation that performs significantly worse or better than another. No ANOVA analysis was conducted due to the near negligible difference in OCV for both the test and control samples.

5.5.5 EIS Results

Table 40 and Table 41 show the R_O and the R_{CT} of the cells at SOT and EOT as measured through EIS.

Table 40 highlights that all cells (including the reference samples) exhibit an increase in R_O at EOT. For the cells that underwent the USABC Procedure 10 vibration profile, sample 4 (Z:X) exhibited the greatest change in R_O - 2.02 mΩ (8,73 %). Moreover, cell sample 2 orientated along the Z:Z axis exhibited the least change in R_O - 1.83 mΩ (5.12 %). An increase in R_O typically originates from an increase in cell contact resistance or delamination of the material layers [143, 151]. However the mean change in R_O resistance for the control samples is 1.42 mΩ (6.03 %), compared to 1.72 mΩ (7.32 %), 1.84 mΩ (7.90 %) and 1.52 mΩ (6.55 %) for the Z:X, Z:Y and Z:Z orientations respectively. An ANOVA analysis of the results was conducted to determine if there was significant change in R_O due to vibration. Based on this statistical analysis, there is no significant change in R_O for any of the three cell orientations at the 95 % confidence level.

Table 40: Start and End of Test Ro Measurements

Cell sample No	Orientation	SOT (mΩ)	EOT (mΩ)	Change from SOT and EOT (mΩ)	Percentage change (%)
1	Z:Z	23.62	25.17	1.55	6.56
2	Z:Z	23.82	25.04	1.22	5.12
3	Z:Z	23.00	24.83	1.83	7.96
4	Z:X	23.15	25.17	2.02	8.73
5	Z:X	23.64	25.32	1.68	7.11
6	Z:X	23.68	25.13	1.45	6.12
7	Z:Y	23.18	24.78	1.60	6.90
8	Z:Y	23.46	25.44	1.98	8.44
9	Z:Y	23.23	25.17	1.94	8.35
10	Control	23.51	25.15	1.64	6.98
11	Control	23.92	24.98	1.06	4.43
12	Control	23.20	24.75	1.55	6.68
Mean change					
Orientation				**Mean change (mΩ)**	**Mean change (%)**
Mean change R_O - Z:X				1.72	7.32
Mean change R_O - Z:Y				1.84	7.90
Mean change R_O - Z:Z				1.53	6.55
Mean change R_O - Control				1.42	6.03
ANOVA analysis					
Orientation				**ANOVA p-value against control - Null Hypothesis: Mean of vibrated cells and control cells are equal. Reject null hypothesis if p < 0.05**	
Z:X orientation				0.309	
Z:Y orientation				0.120	
Z:Z orientation				0.676	

The R_{CT} results presented in Table 41 highlight significant variation in results between the items subjected to vibration and those designated as control samples. What is noticeable from these results is that the control samples all exhibit a significant increase in R_{CT} (between 16.90 % to 29.90 % increase), whereas samples exposed to vibration have a wide variation of results, with the mean value of R_{CT} actually decreasing in some orientations (e.g. Z:X and Z:Y). Samples evaluated in the Z:Z orientation show a similar change in R_{CT} as the control samples have a significantly higher mean change of 18.55 % than Z:X (1.08 %) and Z:Y (-0.66 %).

This difference between the Z:Z and the two horizontal orientations of Z:X and Z:Y is also confirmed within the ANOVA analysis for the mean value of R_{CT}. Table 41 illustrates that there is a significant difference at the 95 % confidence level for the horizontal cell orientations. A possible explanation for the significant increase in R_{CT}

in the Z:Z samples and the control items may be due to the electrolyte distribution caused by the orientation of the cells. This hypothesis is supported by a study undertaken by [87] which found evidence to indicate that cell orientation can impact the electrical cycling performance of the cell. It is therefore hypothesized that samples laying in either of the two horizontal planes and subjected to vibration result in greater electrolyte spread than samples mounted in the vertical axis where the electrolyte would be eventually pushed towards the base of the cell. This hypothesis may be further supported as the control samples were stored in the Z orientation within the manufacturers supplied shipping carton during testing. Further testing is required to fully explore and affirm the validity of this hypothesis.

Table 41: Start and End of Test R_{CT} Measurements

Cell sample No	Orientation	SOT (mΩ)	EOT (mΩ)	Change from SOT and EOT (mΩ)	Percentage change (%)
1	Z:Z	5.80	7.05	1.25	21.55
2	Z:Z	5.62	7.06	1.44	25.62
3	Z:Z	5.78	6.27	0.49	8.48
4	Z:X	6.10	6.82	0.72	11.80
5	Z:X	6.22	5.72	-0.50	-8.04
6	Z:X	5.89	5.86	-0.03	-0.51
7	Z:Y	6.37	6.38	0.01	0.16
8	Z:Y	6.04	6.05	0.01	0.17
9	Z:Y	6.07	5.93	-0.14	-2.31
10	Control	5.83	7.28	1.45	24.87
11	Control	6.47	7.56	1.09	16.85
12	Control	5.72	7.43	1.71	29.90
Mean change					
Orientation				**Mean change (mΩ)**	**Mean change (%)**
Mean change R_{CT} - Z:X				0.06	1.08
Mean change R_{CT} - Z:Y				-0.04	-0.66
Mean change R_{CT} - Z:Z				1.06	18.55
Mean change R_{CT} - Control				1.42	23.87
ANOVA analysis					
Orientation				**ANOVA p-value against Control - Null hypothesis: Mean of vibrated cells and control cells are equal. Reject null hypothesis if p < 0.05**	
Z:X orientation				0.027	
Z:Y orientation				0.001	
Z:Z orientation				0.355	

5.5.6 Mechanical Characterisation Results

The change in frequency and amplitude of the first natural frequency observed within each cell between the SOT and EOT are shown in Table 42 and Table 43. Because the control samples were not evaluated for resonance behaviour via an EMS frequency sweep to limit their exposure to mechanical excitation, it is not possible to conduct an ANOVA analysis with regard to the control samples.

From the results presented in Table 42, it is noticeable that the majority of cells show no statistically significant change in natural frequency between the SOT and EOT. In the majority of the cells evaluated a change of frequency no greater than ± 0.78 % was observed. Changes in this range are within the error measurement range of the test method as the accelerometers were removed and reapplied between start and end of test resonance measurements. Two cells evaluated in the Z:X orientation display a noticeable change in their first natural frequency. These are sample 4 (2.5 % increase) and sample 6 (13.14 % decrease) that potentially indicates a change in material properties of the cell.

Table 42: Summary of Change in Frequency of Observed First Cell Resonance

		First resonant frequency			
Cell sample No	**Orientation**	**SOT**	**EOT**	**Change (Hz)**	**Change (%)**
1	Z:Z	3070	3070	0	0.00
2	Z:Z	3700	3700	0	0.00
3	Z:Z	3575	3557	-18	-0.50
4	Z:X	3604	3694	90	2.50
5	Z:X	3327	3353	26	0.78
6	Z:X	3363	2921	-442	-13.14
7	Z:Y	3074	3070	-4	-0.13
8	Z:Y	3074	3070	-4	-0.13
9	Z:Y	3574	3594	20	0.56
Mean change					
Orientation				**Mean change (Hz)**	**Mean change (%)**
Mean change first Resonant frequency - Z:X				-108.67	16.12
Mean change first Resonant frequency - Z:Y				4.00	0.10
Mean change first Resonant frequency - Z:Z				-6.00	-0.17

With regard to the amplitude of the first resonant frequency (shown in Table 43), there is a significant change for the majority of cells. As discussed within Section 5.4.6 one reason for this could be attributed to the amount of petro wax used between the accelerometer and the cell surface, between SOT and EOT resonance measurements. The greatest change in amplitude was observed within sample 4

(Z:X), which had an increase of 40.3 %, highlighting a reduction in cell damping. However, a reduction of amplitude was also noted post testing in sample 3, 7 and 9 which indicates an increase in cell damping characteristics. One possible explanation for this could be due to a redistribution of electrolyte within the cells due to vibration. Further research to fully define the validity of this hypothesis and the potential causality between cell vibration and internal electrochemical changes within the cell are discussed in Section 5.6.

Table 43: Summary of Change in Amplitude of Observed First Cell Resonance

		Amplitude at first resonance			
Cell sample No	**Orientation**	**SOT**	**EOT**	**Change (g_n)**	**Change (%)**
1	Z:Z	1.35	1.35	0.00	0.00
2	Z:Z	1.23	1.27	0.04	3.25
3	Z:Z	1.30	1.22	-0.08	-6.15
4	Z:X	1.34	1.88	0.54	40.30
5	Z:X	1.26	1.26	0.00	0.00
6	Z:X	1.49	1.61	0.12	8.05
7	Z:Y	1.31	1.11	-0.20	-15.27
8	Z:Y	1.17	1.29	0.12	10.26
9	Z:Y	1.28	1.24	-0.04	-3.13
Mean change					
Orientation				**Mean change (g_n)**	**Mean change (%)**
Mean change in amplitude in first resonance - Z:X				0.22	16.12
Mean change in amplitude in first resonance - Z:Y				-0.04	-2.71
Mean change in amplitude in first resonance - Z:Z				-0.01	-0.97

5.6 **Discussion**

5.6.1 Discussion of Investigation 1 – NMC 18650 Cells

The primary conclusion from this study is that both the electrical performance and the mechanical properties of the NMC 18650 lithium-ion cells are affected by exposure to vibration energy that is commensurate with a typical vehicle life. Experimental data suggests that the rate of degradation is not uniform and varies considerably with respect to cell SOC and orientation to the applied axis of vibration. Further, these investigation highlights, that even cells that have comparable characteristics at SOT, key measures of performance, such as impedance, diverge considerably after the application of vibration energy. However, the results do not show a consistent trend. Consequently, the magnitude and spread of that performance change is unpredictable. This is highlighted by Table 44.

Table 44: Comparison of Cell Performance Ranking by Assessment

Sample No.	Test Profile	SOC	Orien - tation	Capacity	Pulse Power R_{DC}	OCV	EIS: R_o	EIS: R_{CT}	Resonance Frequency	Resonance Amplitude
10	USABC	25%	Z:Z	12	11	15	14	16	1	7
11	USABC	25%	Z:X	4	7	13	9	17	3	14
12	USABC	25%	Z:Y	14	3	15	8	18	17	11
13	USABC	50%	Z:Z	6	15	15	15	13	9	17
14	USABC	50%	Z:X	15	12	15	11	12	5	3
15	USABC	50%	Z:Y	5	6	13	3	14	4	10
16	USABC	75%	Z:Z	1	1	10	1	1	2	13
17	USABC	75%	Z:X	8	2	10	6	8	8	16
18	USABC	75%	Z:Y	2	8	9	7	2	6	2
19	WMG-MPG	25%	Z:Z	10	9	6	2	7	14	4
20	WMG-MPG	25%	Z:X	9	4	7	5	9	18	8
21	WMG-MPG	25%	Z:Y	11	10	10	12	3	12	18
22	WMG-MPG	50%	Z:Z	3	13	3	16	4	15	12
23	WMG-MPG	50%	Z:X	17	16	3	13	5	7	9
24	WMG-MPG	50%	Z:Y	18	14	2	17	6	16	15
25	WMG-MPG	75%	Z:Z	16	5	3	4	15	13	1
26	WMG-MPG	75%	Z:X	7	17	7	10	10	10	5
27	WMG-MPG	75%	Z:Y	13	18	1	18	11	11	6

Ranking Key

Greatest reduction in performance																	Least reduction in performance
1	2	3	4	5	6	7	8	9	10	11	12	13	14	15	16	17	18

Table 44 shows that a series of complex interactions are potentially triggered whilst the cells are undergoing a vibration load that activates several failure modes and/or degradation mechanisms. The implications of these observations are further explored in Section 5.6.4, where the implication of this research for the design of RESS for future EV applications is discussed in greater detail.

With respect to the EIS results, the observed aging mechanism with regard to the change in R_O is significantly different to that observed with electrical cycling [143, 153], where there is typically a change in R_{CT} behaviour. It is therefore hypothesised from these results that if a battery cell was both electrically cycled and simultaneously subjected to vibration, such as the conditions associated with EV operation, then a combination of these aging mechanisms would be observed.

Table 45 collates the electromechanical EOT results and highlights, for each test-type, the individual cell ranking with respect to effect of vibration cycle on cell orientation. For cells subjected to the USABC Procedure 10 vibration profiles, the greatest overall change in electrical performance was experienced by the cell placed in the Z:Y orientation. Similarly, for the WMG-MPG dataset, the results suggest that cells orientated in the Z:Z axis experienced the greatest overall amount of electrical performance degradation. This cell behaviour is not present in the change of the natural frequency or amplitude of the cells. The differences in cell behaviour, when exposed to the different vibration profiles, may be attributed to the difference in acceleration levels within the profiles. This in turn is related to the amount of time compression applied to synthesis the vibration standard from measured vehicle data [26]

Table 45: Assessment Ranking of Orientation by Test

Assessment	Test	Orientation Ranking by Assessment and Test Profile		
		Least Change ⇨		Greatest Change
Electrical characterisation				
Capacity—1C discharge	USABC	Z:X	Z:Y	Z:Z
	WMG-MPG	Z:Y	Z:X	Z:Z
Pulse Power	USABC	Z:Z	Z:X	Z:Y
	WMG-MPG	Z:Y	Z:X	Z:Z
OCV	USABC	Z:Z	Z:X	Z:Y
	WMG-MPG	Z:X	Z:Y	Z:Z
EIS (R_o)	USABC	Z:Z	Z:X	Z:Y
	WMG-MPG	Z:Y	Z:X	Z:Z
EIS (R_{CT})	USABC	Z:Z	Z:Y	Z:X
	WMG-MPG	Z:Z	Z:X	Z:Y
Mechanical characterisation				
Resonance (change in frequency)	USABC	Z:Y	Z:X	Z:Z
	WMG-MPG	Z:Z	Z:Y	Z:X
Resonance (change in amplitude)	USABC	Z:Y	Z:Z	Z:X
	WMG-MPG	Z:Z	Z:Y	Z:X

Table 46 collates the electromechanical EOT results and presents the ranking with respect to the different values of SOC used to pre-condition each cell prior to subject them to the different vibration excitations. The results for the USABC Procedure 10 vibration profile show that the cells pre-conditioned to 75 % SOC experienced the greatest level of electrical performance degradation. Similarly, the results obtained from the WMG-MPG profile highlight that the cells pre-conditioned to 25 % SOC displayed the greatest electrical performance degradation. Conversely, the cells pre-conditioned to 50 % SOC typically exhibit the lowest levels of electrical performance degradation. It has previously been shown that a potential reason for this difference can be attributed to the changes that occur within the mechanical structure of the cell at the different levels of SOC [154, 155]. However, Table 44 indicates that no correlation can be established between the measured data for changes in

mechanical properties and the degradation in electrical performance. This initial conclusion is supported by related research that reported the difficulty in correlating electromechanical ageing mechanisms [82, 104, 124, 155-157]. This may indicate that there are limitations in the measurement method employed to record these parameters. These may include the accuracy of the attachment of accelerometers to the cells or the amount of Petro wax used to attach the accelerometers to the cells. Equally, it may indicate an actual change in material properties which may not correlate with electro-chemical ageing. It is acknowledged that to determine conclusively the causality of the observed aging from these experiments, that forensic analysis of the cells which is outside of the scope of this thesis, is required. A more conclusive analysis that aims to determine the root cause of the results is outlined in 7.2.3. A study investigating the changes in the surface films of the cells evaluated in investigation 1 (Section 5.4) is presented in [40].

Table 46: Assessment Ranking of SOC by Test

Assessment	Test	Orientation Ranking by Assessment and Test Profile		
		Least Change ⇨		Greatest Change
Electrical characterisation				
Capacity—1C discharge	USABC	25 %	50 %	75 %
	WMG-MPG	50 %	75 %	25 %
Pulse Power	USABC	50 %	25 %	75 %
	WMG-MPG	75 %	50 %	25 %
OCV	USABC	50 % = 25 %		75 %
	WMG-MPG	25 %	75 %	50 %
EIS (R_o)	USABC	25 %	50 %	75 %
	WMG-MPG	50 %	75 %	25 %
EIS (R_{CT})	USABC	25 %	50 %	75 %
	WMG-MPG	75 %	25 %	50 %
Mechanical characterisation				
Resonance (change in frequency)	USABC	50 %	75 %	25 %
	WMG-MPG	25 %	75 %	50 %
Resonance (change in amplitude)	USABC	75 %	50 %	25 %
	WMG-MPG	75 %	50 %	25 %

5.6.2 Discussion of Investigation 2 – NCA 18650 Cells

The primary conclusion from this study is that both the electrical performance and the mechanical properties of the NCA lithium-ion cells are relatively unaffected when exposed to vibration energy that is commensurate with a typical vehicle life. In the majority of the EOT cell measurements, a similar change in electrical performance was observed within the control samples. This indicates that the measured degradation was likely to have been influenced by other environmental conditions as opposed to being a function of the mechanical excitation of the applied vibration. ANOVA analysis of the mean results confirmed (with a 95 % confidence) the effects of vibration did not change the cells R_O and capacity.

For the mechanical characterisation of the cells, two thirds of the cells showed no significant change with regard to the shift in the natural frequency of their first resonance. This correlates with the electrical characterisation results, indicating that vibration energy has a minimal impact on the performance of these cells. Changes in R_{CT} followed an unusual trend however. Samples vibrated within the Z:Z orientation degraded at a similar rate to the control samples, whilst cells tested in the horizontal conditions did not degrade. As R_{CT} relates to the electrochemical charge transfer dynamics of the cell; based on the theory presented in [158-161] it is hypothesised that this behaviour is a result of the electrolyte distribution. A similar level of degradation was also observed within the control samples which were continually stored in the Z axis within the manufacturers shipping carton.

Reviewing the performance of each cell from each characterisation activity; samples 1, 4 and 8 demonstrate some correlation between R_{DC}, R_O, energy capacity and a change in resonance. However, overall there is a limited correlation between electrical cell characterization and changes in the cell's natural frequency.

As discussed within Section 5.6.1 there is some concern with regard to the effect on the amount of petro wax material employed between the accelerometer and the surface of the cell on the measured amplitude between SOT and EOT measurements. If the resonance search testing is to be repeated on future tests, it is recommended that the frequency sweep evaluations on the 18650 cells are conducted using light weight accelerometers that utilize a stud fastener and a machined cell surface-bonded collar (as presented in Section 6.3.5.2). Despite a considerable amount of care being taken to ensure that the accelerometers were installed onto the same location of the cell at each frequency sweep measurement and levelled via an inclinometer, the use of petro wax is susceptible to user error. Ensuring the accelerometer is semi-permanently bonded to the radial surface of the cell; in a (perfectly true) vertical orientation can result in different quantities of petro wax being used for each accelerometer installation. It is hypothesised that this may introduce subtle changes in vibration transmissibility from the cell to the accelerometer.

Whilst the data set was increased within this study when compared to that discussed in 5.4, it is acknowledged that a larger data set is required to confirm the findings discussed.

5.6.3 Comparison of Results from NMC and NCA 18650 Investigations

Table 47 compares the measured post-test difference of all samples from the NCA 18650 study with NMC samples conditioned to 75 % SOC from investigation 1. Reviewing the pulse power results from the NCA cells it is noticeable that the R_{DC} from the pulse power measurement of the NCA samples is consistent and has a far smaller spread than that observed within the 75 % SOC samples from the NMC investigation. A similar observation with regard to the value of R_O for the NMC and NCA cells is noticeable.

Table 47: Comparison of Change of NCA Vs. Change in NMC 18650 Cells Evaluated at 75% SOC and in Accordance to USAB Procedure 10

		Electrical characterisation - Pre and post-test change					Mechanical characterisation - Pre and post-test change	
Cell sample No	**Orientation**	**Pulse power - change in R_{DC} (mΩ)**	**EIS change in R_o (mΩ)**	**EIS change in R_{CT} (mΩ)**	**OCV - change in voltage (V)**	**Change in capacity (Ah)**	**Resonance frequency - change in Hz**	**Resonance amplitude - change in g_n**
1	Z:Z	1.99	1.55	1.25	0.001	-0.32	0	0.00
2	Z:Z	1.96	1.22	1.44	-0.001	-0.38	0	0.04
3	Z:Z	1.69	1.83	0.49	0.000	-0.35	-18	-0.08
16 †	Z:Z	95.23	*	*	0.001	-0.27	-566	0.2
4	Z:X	2.38	2.02	0.72	0.000	-0.36	90	0.54
5	Z:X	2.02	1.68	-0.50	0.000	-0.32	26	0.00
6	Z:X	2.1	1.45	-0.03	0.000	-0.37	-442	0.12
17 †	Z:X	89.09	96.90	-7.00	0.001	-0.02	-124	-0.07
7	Z:Y	1.66	1.60	0.01	0.000	-0.38	-4	-0.20
8	Z:Y	2.19	1.98	0.01	0.000	-0.36	-4	0.12
9	Z:Y	1.84	1.94	-0.14	0.000	-0.39	20	-0.04
18 †	Z:Y	58.18	94.70	-8.40	0.002	-0.15	228	1.06
10	Control	1.59	1.55	1.71	0.000	-0.37	N/A	N/A
11	Control	1.54	1.64	1.45	-0.001	-0.37	N/A	N/A
12	Control	1.02	1.06	1.09	0.000	-0.30	N/A	N/A
8 †	Control	-0.68	0.00	-8.90	0.000	-0.10	N/A	N/A

Note: † indicates that the sample was a NMC 18650 cell from study defined in 5.4. ***** indicates that data could not be recorded from that cell due to the post-test degradation.

The R_{CT} results from the two cell manufacturers show that the NCA cells do not illustrate the same level of degradation when oriented in any of the three test positons. In fact, the NMC cells from Section 5.4 illustrate a reduction in R_{CT} post vibration testing. This trend is not witnessed within the NCA samples. However both the NCA reference cells and Z:Z oriented items shown similar changes in R_{CT} as the NMC cells.

The OCV data from both studies does not highlight any significant change irrespective of orientation, cell chemistry or manufacturer. The voltage difference recorded is within the tolerance of the error of the equipment. This supports the results presented in [80, 81] that also noted that OCV is not adversely affected by vibration loading.

With regard to capacity, it is noticeable that the measured amount of capacity fade within the NCA cells is typically greater than that noted within the NMC items. However, unlike the NMC cells, the NCA 18650's have a smaller spread of results. The reference samples for the NCA cells also illustrate the same level of capacity

fade indicating that this reduction is a function of laboratory climatic conditions, as opposed to vibration excitation. In terms of absolute change between SOT and EOT, the worst performing NMC sample (sample 16) has a comparable capacity fade to that of the typical NCA item.

With respect to the mechanical characterization results, it must be noted that with the NCA samples, the first resonance was less than 2 g_n (typically between 1.20 to 1.90 g_n) pre and post testing. In comparison to the NMC cells results presented in Section 5.4, the NCA items display significantly less degradation in vibration response. No resonance at either pre or post testing was greater than twice the excitation force indicating that the NCA cells have both a greater damping coefficient and a stiffer construction than the NMC items. These characteristics may explain how the NCA cells have displayed less relative vibration aging than the NMC cells from the previous study.

With regard to visual condition, both types of 18650 cell showed no significant external degradation, other than marks from the clamp faces of the fixtures post testing. Comparing the overall results for the NMC samples evaluated to USABC Procedure 10 and comparing them to the NCA cells, there is a correlation between the two different cell chemistries. Both types of 18650 cells typically show the least degradation when oriented in the Z axis of the cell with respect to the Z axis of the vehicle (Z:Z condition) when assessed to the USABC standard.

5.6.4 Implications for Vehicle Design

The results presented suggest that as part of the technology selection process, OEM's should study the susceptibility of their chosen cell technology to mechanically induced vibration profiles at different "vehicle to cell" orientations to mitigate their effects through improved system design. Within these two studies there has been a considerable difference of behaviour with the two cell chemistries. Whilst typically the NCA cells evaluated are typically unaffected by a representative 100,000 mile road vibration excitation, there were some specific aging behaviour (such as an observed increase in DC resistance, derived from pulse power testing, in Z:X oriented samples) identified. Any aging behaviour as a function of vibration would have to be characterized to ensure effective battery management system (BMS) development and to maximise useful service life. A study investigating the effects of NMC vibration aged cells from the investigation presented in Section 5.4 on a BMS strategy is discussed in [39].

The results from this study also show that both the electrical performance and the mechanical properties of lithium-ion cells can be affected by exposing the cell to vibration energy that is representative of a typical vehicle life. Whilst this is evident from the data presented within Section 5.4, the underlying causality is not yet clear. As a result, it is not possible to quantify the relationship that defines cell ageing caused by vibration excitation. Irrespective of this limitation, both the electrical and mechanical data show that NMC cells subject to vibration have a much greater

spread in the internal resistance, energy capacity and natural frequency. Managing this diversity may potentially drive further complexity in the systems engineering functions required to scale individual cells into a complete RESS. A number of articles discuss the need to minimise cell-to-cell variations within the system as a mean to reduce the differential current flows and heat generation with the pack. This research highlights that even for a RESS that is initially well designed; the impact of vibration-induced ageing may require greater levels of cell balancing and thermal management for this chemistry type.

The results summarised in Table 44 to Table 47 highlight that both the SOC and orientation are as important parameters to consider when designing a RESS as the contribution of the vibration induced profile. It is expected that variations in SOC within the RESS will be observed, especially for a BEV, where a large depth of discharge (DOD) is required to maximise vehicle range. Consequently, SOC may be a parameter that engineers consider more greatly than orientation. However, to maximize the volumetric energy density and minimise the footprint of the RESS, engineers may need to account for the impact of cell orientation on the performance of the RESS. Consequently, the author suggests that as part of the technology selection process, OEMs should study the susceptibility of the chosen cells to mechanically induced vibration profiles at different SOC and cell orientation to mitigate their effects through improved system design.

5.7 **Conclusions**

This study developed a test methodology, testing practices, test fixtures and safety protocols to allow for the evaluation of two different 18650 lithium-ion cell chemistries to vibration that was representative of 100,000 miles of customer durability. Unlike the previous studies identified within Chapter 2, these investigations evaluated the electrical and mechanical performance of the cells via impedance, capacity, OCV and natural frequency measurements at the SOT and EOT. The findings of this study have been published within [36, 37]. Additional studies utilising the cells and results from this study that are outside the scope of this thesis, have also been published. These studies, which are presented in [39, 40], include an investigation into the impact of vibration aged cells on a BMS strategy and the effect of vibration on surface layers.

Both vibration profiles employed within this study, which were devised to represent 100,000 miles of vehicle operation, resulted in a performance decrease within the NMC 18650 cells. However, the two different vibration profiles of USABC Procedure 10 and WMG-MPG resulted in two different results with respect to the effect of SOC and cell orientation. Of the NMC samples evaluated to USABC Procedure 10, cells in the Z:Z orientation typically displayed the least amount of degradation, whilst cells in the Z:Y orientation displayed the greatest. Whilst samples evaluated to the Z:X and Z:Z orientation displayed the least and greatest amount of degradation when

exposed to the WMG-MPG profile, respectively. Of the samples evaluated to USABC Procedure 10, items conditioned to 75 % SOC displayed the greatest degradation, whilst WMG/MBK, items conditioned to 25 % SOC displayed the greatest degradation. Samples conditioned to 50 % SOC typically displayed the least degradation regardless of the test profile.

Typically, both the electrical performance and the mechanical properties of the NCA 18650 lithium-ion cells were relatively unaffected when evaluated in accordance with USABC Procedure 10. No external damage or electrolyte leakage was observed in any of the test cells post vibration testing. No significant change in R_O, or cell capacity was observed as a result of vibration at the 95 % confidence level. OCV was not affected by vibration within this investigation. Cell degradation as a function of vibration was observed within the R_{DC} of the cells oriented in the Z:X axis. However no significant change in the R_{DC} resistance was noted at the 95 % confidence level in either the Z:Y and Z:Z oriented samples. Samples tested in the horizontal orientations of Z:X or Z:Y did not illustrate an increase in R_{CT}, which was observed to increase within both the Z:Z and control samples. A similar reduction in energy capacity, increase in R_O and increase in R_{DC} was witnessed within the reference samples. These results indicate that the change in these electrical attributes is a function of other environmental conditions.

When comparing the orientation results of the NCA samples assessed in investigation 2 to the NMC items from investigation 1, no significant correlation in performance was observed. Drawing on the literature review presented in Chapter 2 and the experimentation undertaken, at this stage, the underlying causality between the application of vibration energy and cell orientation is not fully understood. It is recommended that the definition of these relationships is the focus of on-going research, using novel cell imaging and autopsy methods, to quantify changes in material composition and structure as per the study presented in [40]. Expanding the experimental programme to also include cells of different form-factor and chemistries will identify if the experimental results presented here are transferable to other cell technologies.

In conclusion, the experimental results highlight that depending on cell chemistry the potential for key electrical and mechanical properties within the cell to diverge, over time, due to the application of vibration energy that is consummate with a typical road vehicle life. Unless this phenomenon is well understood at the design stage of the vehicle, it may drive further complexity into design of the RESS in addition to causing in-service warranty claims.

6 Study 4 - Vibration Durability Behaviour of EV Batteries via Multi-Axis Testing Techniques

6.1 Introduction

This study investigates if the electromechanical attributes of NCA 18650 battery cells and a Tesla Model S module (composed of the same 18650 cell type and chemistry) are adversely affected by exposure to vibration commensurate with that experienced by EVs through road induced excitation. The vibration excitation employed within this study is underpinned through real-world vehicle measurements sequenced to represent 10 years of vehicle European structural durability. Unlike the investigation presented in Chapter 5, this study applied the vibration to the test items in six degrees of freedom (6DOF) using a multi-axis shaker table (MAST). This method of real-world mechanical testing is known to be more representative of the vibration experienced by automotive components, as 6 motions of vibration (X, Y, Z, roll, pitch and yaw) are applied simultaneously. Similar to the studies presented in Chapter 5, cell and module characterisation within the electrical domain is performed via quantification of impedance, the open-circuit potential of the DUT and its energy capacity. Conversely, the mechanical properties of the test items are inferred through measurement of the cell's natural frequency, or impact excitation modal analysis, in the case of the Tesla module. Experimental results are presented that highlight that the electromechanical performances of the 18650 NCA cells do not, in the main, display statistically significant degradation when subjected to vibration representative of a typical 10-year European vehicle life.

Unlike the studies presented in Chapter 5, which apply vibration to each axis sequentially and uni-axially within the frequency domain via the use of PSD profiles, this study applies the measured vibration within the time domain. The advantage of this methodology is that errors resulting from test time compression are avoided [33]. Also, because the vibration motion is applied in the time domain, it is more representative of real-world *in-vehicle* loading. As discussed within [3, 162, 163] within the context of traditional vehicle testing and component evaluation, the application of combined axial motions will often highlight additional failure modes that would otherwise not be observed through single-axis testing.

Due to the challenge accessing test equipment of this type, within a University context to undertake doctoral research, this study was performed at MPG within the Component Test Laboratory (CTL) Cube 2 test facility.

This Chapter is structured as follows; the objective and aims of this study are defined in Section 6.2. Section 6.3 presents the test methodology and associated theory. Sections 6.4 and 6.5 introduce and analyse the test result for the 18650 cells and Tesla Model S module respectively, whilst the discussion and conclusions are given in Sections 6.6 and 6.7.

6.2 Objective and Aims of Study

6.2.1 Objective

To determine if NCA 18650 battery cells and a current productionised Tesla Model S 18650 battery module can be electrochemically and mechanically aged by mechanical induced vibration. This shall be performed via the use of a multi axis shaker table and measurements from a Smart ED RESS, replicated in the time domain, that are representative of a 10 year durability life. The study investigates if orientation influences the observed degradation within the 18650 battery cells resulting from vibration.

6.2.2 Aims

- To determine if vibration applied in 6DOF that is representative of approximately 10 years of European customer EV usage can age NCA 18650 battery cells and a Tesla Model S module.
- To measure if cell orientation in relation to the vehicle axis can affect the vibration durability life of the NCA 18650 battery cells.
- To compare the vibration degradation of NCA 18650 cells with the observed degradation trends observed from the previous study defined in Chapter 5.

6.3 Method of Vibration Durability Testing in 6DOF of 18650 Cells and Tesla Model S Module

This Chapter defines the test method employed to determine the durability and aging behaviour of 18650 NCA cells and a Tesla Model S module when subjected to vibration in 6DOF. The test process and structure of this Chapter is summarised in Figure 57.

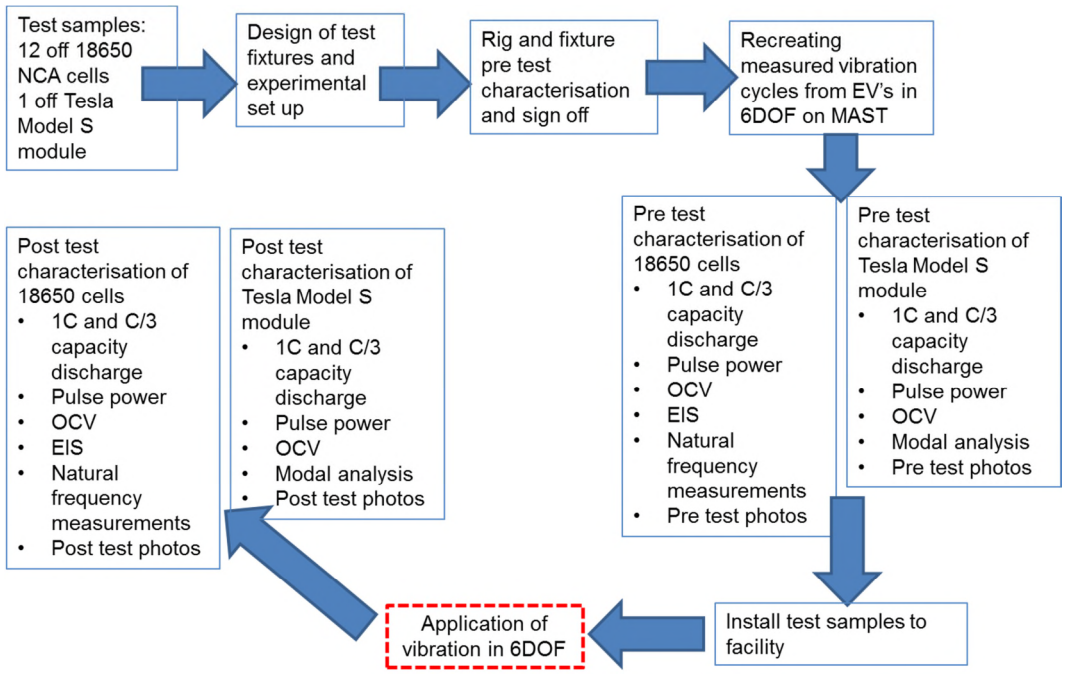

Figure 57: Schematic of Test Process for Cells and Module

6.3.1 Test Samples

The details of sample preparation, sample reference number, SOC and orientation are defined in Table 48.

Table 48: Test Sample Information

Sample Reference No	SOC (%)	Test Profile	Orientation for Test
18650 NCA Cells			
2991	75 %	Data from Smart ED sequenced to 10 years European customer structural durability	Z
2994			Z
2996			Z
2997			Y
2998			Y
2999			Y
3000			X
3001			X
3005			X
2995			Control
3003			Control
3004			Control
Tesla Model S Module			
3	25 %	Data from Smart ED sequenced to 10 years European customer structural durability	Vehicle orientation

Twelve 18650 NCA cells were evaluated during this test program. During this investigation the 18650 cells were assessed at 75 % SOC. 75 % SOC was identified in Section 5.4 as a charge state where increased cell degradation was observed when cells were evaluated to USABC Procedure 10. The cells were then divided into 2 batches. One batch comprised of 9 cells and was subjected to vibration in 6DOF. The remaining 3 cells were allocated as control samples. The control samples were placed into storage at 10 °C for the duration of the testing at the University of Warwick. Control samples (which were not subjected to vibration) were included within this experiment to determine what aging had been caused through vibration. Because battery cells are typically packaged in different orientations within battery pack assemblies, this study evaluated the effect of the three different X, Y and Z axis cell orientations (defined in Figure 58).

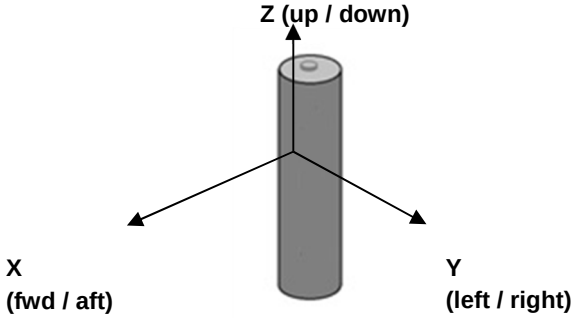

Figure 58: The Three Cell Orientations Evaluated within this Study

A single Tesla Model S module was also assessed in parallel to the 18650 cells on the MAST facility. The module was an item that had been removed from a low mileage (approximately 20,000 miles) UK specification Tesla Model S P85D, JLR evaluation vehicle. The vehicle had been involved in several JLR performance benchmarking studies (by JLR and the University of Warwick). Due to the embedded energy within this test item and the safety concerns of evaluating a module within an enclosed laboratory environment, all vibration testing on the Tesla module was conducted at 25 % SOC. This was in accordance with the risk assessment developed for this study, which is presented in Appendix O.

6.3.2 Design of Test Fixtures and Experimental Set Up

This section discusses the test fixtures and test arrangement developed to conduct vibration durability testing of the test samples within this study. The engineering drawings and assembly processes for the test fixtures are presented in Submissions 3 and 6. As discussed within 5.3.2, all vibration durability and assessment fixtures employed within this study were constructed from 6082-T6 grade aluminium, due to the high Poisson's ratio associated with this material (circa: 0.33) [130].

6.3.2.1 18650 Cell Fixtures

The three cell-mounting fixtures presented in Section 5.3.2 were utilised within the 6DOF study. A new fixture mounting plate (with the correct hole pattern) was fabricated to allow for the attachment of the durability fixture to the MAST. The complete fixture including test instrumentation is presented in Figure 59.

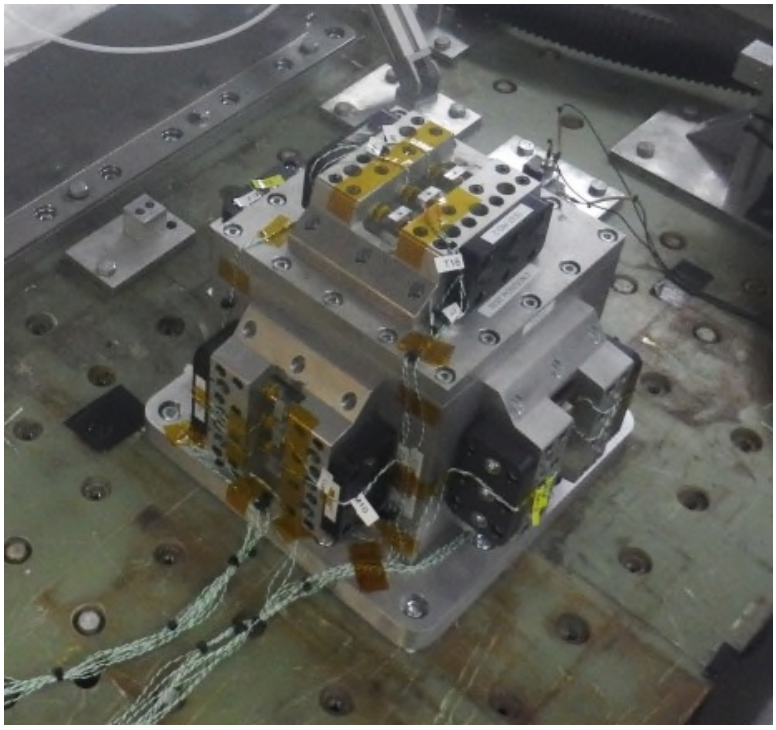

Figure 59: 18650 Durability Fixture Installed onto Multi-Axis Shaker Table (MAST). Note Mounting Locations to Achieve Cell Orientations in Relationship to Application of Vibration

6.3.2.2 Tesla Model S Module Fixture

Figure 60 illustrates the fixture that was designed to conduct the durability testing on the Tesla Model S module.

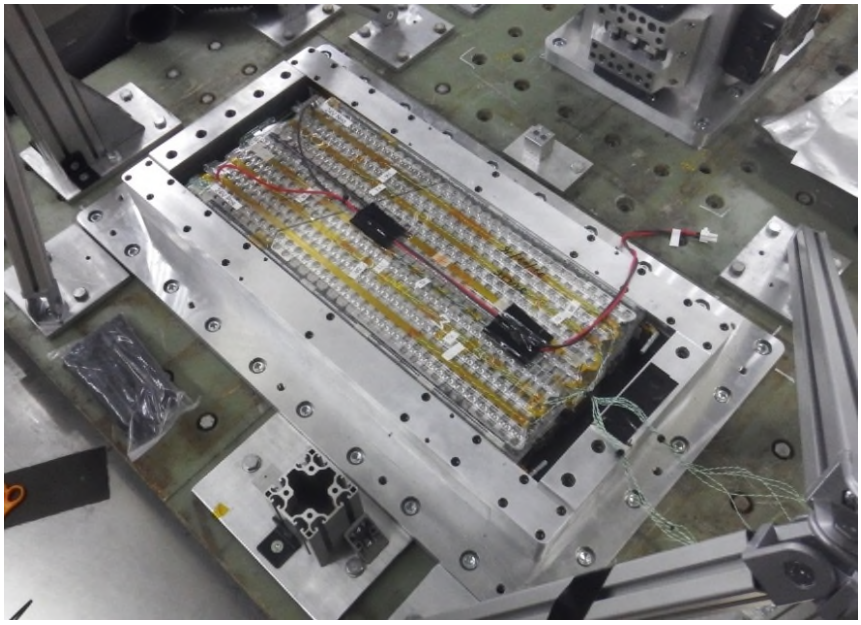

Figure 60: Tesla Model S Durability Fixture Installed onto 6DOF MAST

This fixture was fabricated to recreate a dimensionally accurate “in-pack” mounting condition for a single Tesla Model S module assembly. The internal dimensions of the fixture mimicked the internal dimensions of a Tesla Model S battery assembly and employed the same module retention method via clamping side rails. Within this study, only the design intent orientation of the module was assessed.

6.3.2.3 Test Facility and Setup

The test rig employed a TEAM Cube MAST at MPG. The specification and performance details of the TEAM Cube are shown in Appendix N.

The TEAM cube was installed under a Design Environmental climatic chamber which, in turn, was connected to an L.Kel remote air conditioning (RAC) unit. During this test program the environment was conditioned to 21 °C ±3 °C. The complete test facility is shown in Figure 61.

Within the test environment, K-type thermocouples and vibration sensors were employed to provide suitable test accuracy and safety. To facilitate closed-loop vibration control, 9 DJB Instruments A/130/V accelerometers were installed at key locations on the shaker table (discussed in greater detail in Section 6.3.4). A Labview PXie-1075 chassis with an integrated Ni-PXIe-8133 controller and input modules for 32 thermocouple sensors (NI PXIe-4353), 4 channels for accelerometer measurements (NI PXI-4462) and a multifunctional data module (Ni PXIe-6363) was used for additional sample safety monitoring during the test. The Cube itself was

controlled by a Moog CC02310-301 test controller (Serial No 0069) and associated Moog multi axis vibration software.

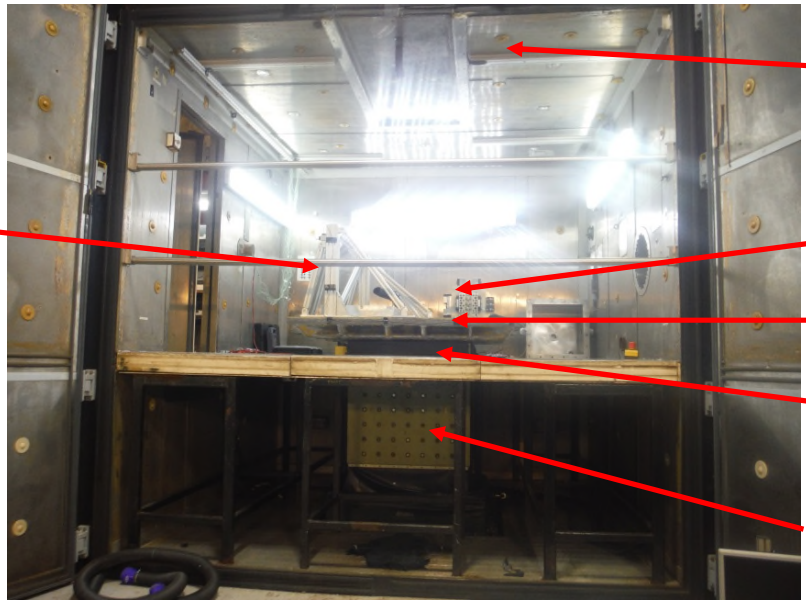

Figure 61: "Cube 2" Vibration Test Facility at Millbrook Proving Ground

The safety aspects of the test plan were discussed with colleagues at WMG and agreed with MPG senior engineers prior to testing. As a result, several safety measures were included within the test set up. To mitigate against any potential risk of catastrophic cell or module failure during vibration testing, the test fixtures were installed within stainless steel fire proof enclosures. These enclosures were fabricated from 2 mm thick 304 grade stainless steel with a 6 mm thick base flange to insure a suitable clamping force could be obtained when it was bolted to the MAST head expander. A gas Nitrogen injection system was installed to each enclosure so that the test item could be placed into an inert environment if a significant increase in test item temperature was detected. Integrated with the enclosure was a PLC monitoring system which that would automatically activate an alarm if either the surface temperature of the cells or the bus bars of the Tesla module were greater than 60 °C. It would also activate if a test item temperature change of greater than 4 °C/s was observed (in accordance with WMG safety protocols and the developed risk assessment presented in Appendix O and P). All thermocouples were attached to the test items by being sandwiched between several layers of polyimide tape to ensure that the risk of an earth path from the DUT through the instrumentation was minimised

A remotely activated gas extraction system was also installed to the climatic chamber and the test enclosures to allow for the forced extraction of potentially harmful gases (if detected) from the facility. The gas monitoring of the test chamber and each fixture enclosure was performed remotely through air sampling via a RKI Instruments Eagle gas analyser (Serial No (04-021-118) which did so every

30 seconds. This system would also output an audible alarm if hazardous quantities of hydrofluoric gas (> 1 part per million), unsafe oxygen levels (< 20 %) or any hydrocarbons were detected.

The base plates of the fixtures were fabricated from 25 mm thick aluminium tool plate and contained cast nylon inserts. This was to reduce the risk of an earth path being created from the test item to the shaker table head expander in the event of a sample fault. 10 mm thick G10 sheeting was also placed between the test fixtures and shaker table head expander. This was performed to reduce the risk of heat transfer to the cast magnesium alloy components of the shaker table during a thermal incident and to also add an extra layer of electrical insulation between the test items and metal components of the shaker facility.

The test was monitored by technicians and the researcher 24 hours a day 7 days a week. It could also be viewed remotely via a web cam. The full risk assessment developed for this test program developed in partnership with specialist engineers at MPG is presented in Appendix O, whilst the incident management flow chart is presented in Appendix P. The complete test arrangement is illustrated in Figure 62.

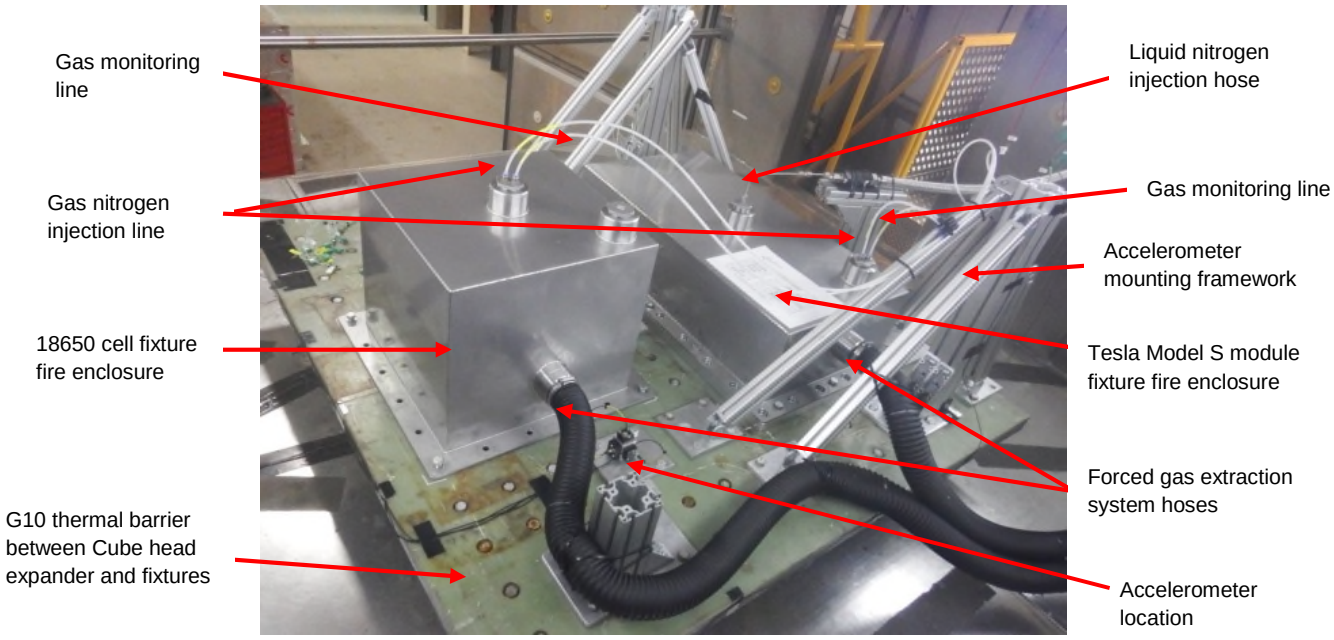

Figure 62: Multi Axis Shaker Rig Assembly

6.3.3 Rig and Fixture Pre-Testing Characterisation and Sign Off

As discussed in 5.3.3, the primary requirement for a durability test rig is to ensure that the vibration profile demanded by the electronic controller is faithfully applied to the samples under test. This is achieved by designing the experimental fixture to maximise the transmissibility of the vibration energy from the shaker table to the sample whilst concurrently minimising unrepresentative cross-axis behaviour of the durability fixture. It is recognised good test practice to evaluate the vibration response characteristics of fixtures prior to any durability test [89, 131, 164]. All fixtures within this study were evaluated in accordance with BS EN 60068 and

ensured that the maximum vibration amplitude in any axis perpendicular to the specified axis did not exceed 50 % of the specified amplitude up to 500 Hz [134].

Prior to evaluating the fixtures, and prior to commencing any vibration study [132-134], it is also necessary to fully understand the frequency response of the shaker. This is to ensure that the MAST does not exhibit a resonance within the frequency range of the durability test (which in the case of this study was 0 to 110 Hz due to the equipment capabilities) or exhibit any vibration spectra which could create unrepresentative failure modes to occur within the DUT.

This section discusses and presents the results from the pre-testing shaker, rig and fixture characterisation activity. This was conducted as follows:

- Assessment of MAST for resonances in X, Y and Z at 1 g_n over a frequency range of 3 – 110 Hz at 1 octave/minute in the Z axis.
- Assessment of 18650 fixtures and resonance search plate when evaluated in accordance with BS EN 60068
- Assessment of Tesla Model S module fixture when evaluated in accordance with BS EN 60068

6.3.3.1 Response of Multi-Axis Shaker

The vibration response of the multi-axis shaker was measured using a swept sine wave of amplitude 1 g_n over a frequency range of 3 – 110 Hz at 1 octave/minute prior to testing in the Z Axis. Accelerometers were placed in the X, Y and Z axis across the head expander of the TEAM Cube MAST on aluminium accelerometer mounting blocks. The table was excited in the Z axis and the cross axis motion was measured by the accelerometers.

Upon analysing the response of the Cube MAST used in this study, no significant resonances or cross axis motion was identified that would detrimentally impact the accuracy of the durability test programme. An example of the response of the bare MAST is shown in Figure 63. This figure shows that when the table is excited in a pure Z axis at 1 g_n that the X and Y response of the head expander is typically ± 0.1 g_n, indicating a desirable low cross axis motion.

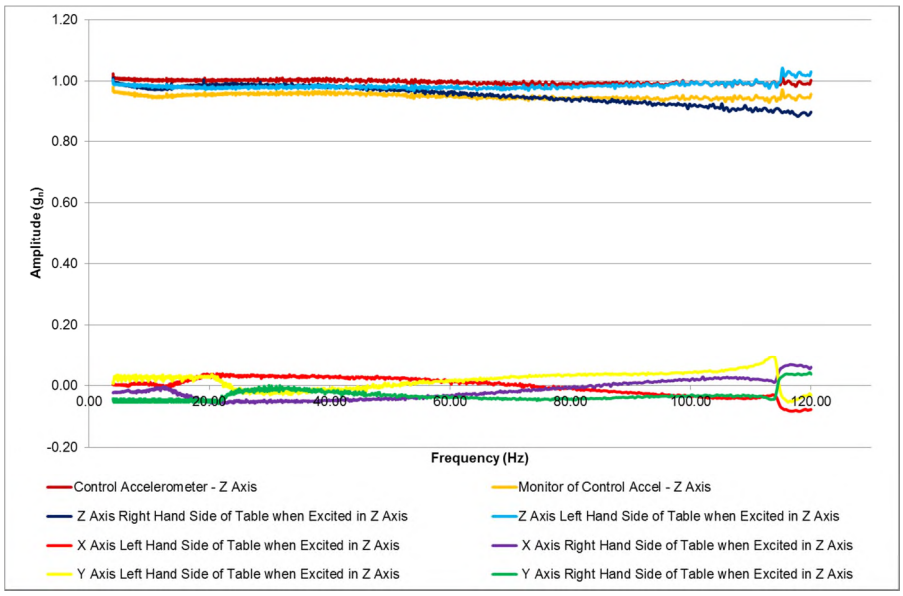

Figure 63: Response of Bare TEAM Cube Head Expander from 3 to 120 Hz in Pure Z Excitation

6.3.3.2 Vibration Response of 18650 Fixtures and Resonance Search Plate

The 18650 fixtures and resonance search plate from the studies defined in Chapter 5 were reassessed in accordance with BS EN 60068 to ensure they were still within specification following the testing presented in Chapter 5. The fixtures met the requirements of this evaluation and showed no significant change in performance from the evaluation defined in Section 5.3.3.

6.3.3.3 Vibration Response of Tesla Model S Fixture

The results from this measurement activity are presented in Figure 64 and Figure 65.

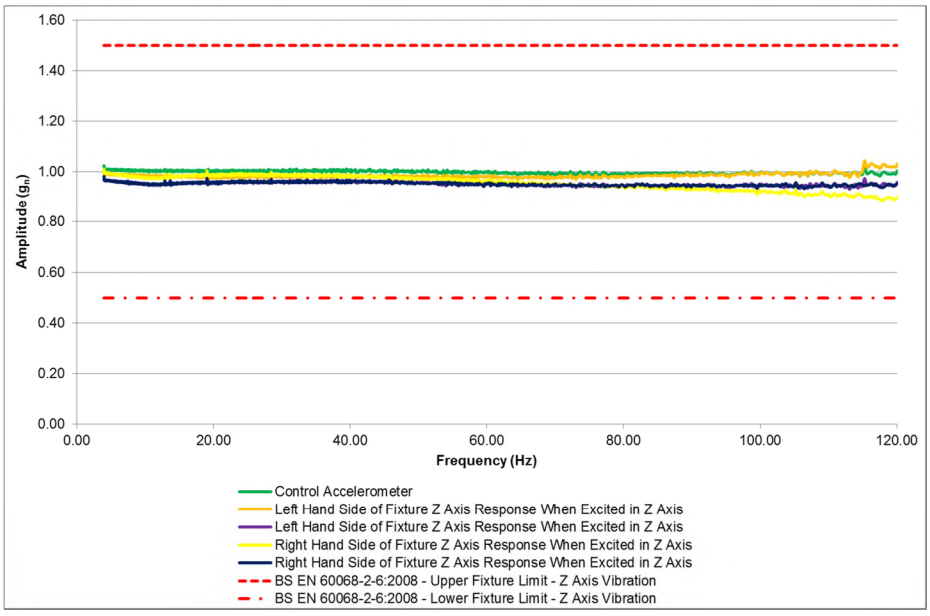

Figure 64: BS EN 60068 Resonance Evaluation of Tesla Model S Module Durability Fixture (Z - Axis of Fixture)

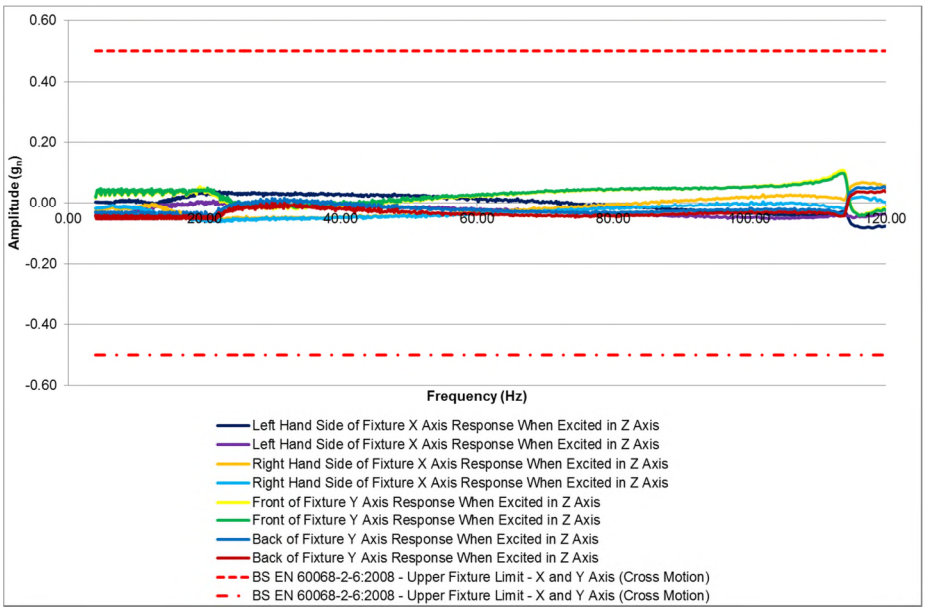

Figure 65: BS EN 60068 Resonance Evaluation of Tesla Model S Module Durability Fixture (X and Y-Axis of Fixture)

The Tesla Model S fixture was evaluated on the TEAM cube MAST in accordance with BS EN 60068 from 3 to 120 Hz at 1 g_n. The measurement locations are presented in Submission 6. The Tesla Model S module fixture met the requirements of BS EN 60068 from 3 to 120 Hz.

6.3.4 Recreating Measured Vibration Cycles from BEV's in 6DOF on a MAST

With 6DOF vibration tests, measured vibration signals are applied in the time domain to the DUT. Within this study, it was decided to use the vibration measurements from the Smart ED which were recorded for the study discussed in Chapter 3. These measurements included the response of the battery assembly as the vehicle was subjected to specific durability surfaces at MPG. The vibration signals from the Smart ED were chosen for the 6DOF durability study, as its compact dimensions and suspension geometry results in high levels of vibration energy at frequencies below 5 Hz. Also, the X and Y axis vibration loads are significantly higher than other current production BEVs measured within Chapter 3. Furthermore, the Smart ED has a battery assembly constructed of 18650 type cells, which therefore has a greater correlation to the test samples under assessment within this investigation. The battery assembly was also developed by Tesla, on behalf of Mercedes Benz Smart. However, it must be highlighted that the major assumption with using this data is that smaller A-segment vehicles (such as the Smart ED) will be operated in a similar manner to that of premium executive "E-segment" vehicles (such as the Tesla Model S) within urban, rural and motorway environments. In reality this may not be the case due to the dynamic differences associated with these products.

The results presented in Chapter 5 evaluating the effect of vibration on 18650 cells, have used random vibration test spectra to assess the durability of the test items.

These apply vibration to the test items using compressed PSD plots which replicate 100,000 miles of vibration in 16 hours to 150 hours per axis depending on the test specification utilised (discussed further in Chapter 3 and [26, 45, 70, 105]). Whilst testing using a PSD methodology is desirable for standardised test specifications designed for multiple applications, testing in the time domain in 6DOF eliminates time compression uncertainty of PSD tests. It is also a closer representation of the in-vehicle condition. Within this study to run 100,000 miles of Smart ED vibration in the time domain would take approximately 2500 hours in 6DOF. Due to the MAST facility hire costs the test was limited to a total run time of 150 hours. To maximise the vibration applied to the samples the Millbrook Structural Durability test frame work was utilised [115]. Unlike standards utilised in the previous cell vibration durability studies (as discussed in Chapter 5) this standard defines life in years as opposed to mileage. However approximately 15,000 miles of proving ground driving represents 10 year typical European customer structural degradation. A summary of surface repeats required for the standard procedure is shown in Table 49.To ensure that the desired number of surfaces could be replicated within 150 hours on the MAST facility; the recorded signals were optimised for time. To achieve this, significant periods of “non-damaging” vibration (vibration that was less than 0.1 g_n) were edited from each of the signals. This is a common method with regard to reducing the test time, of vibration tests conducted in the time domain [165]. This process is illustrated in Figure 66.

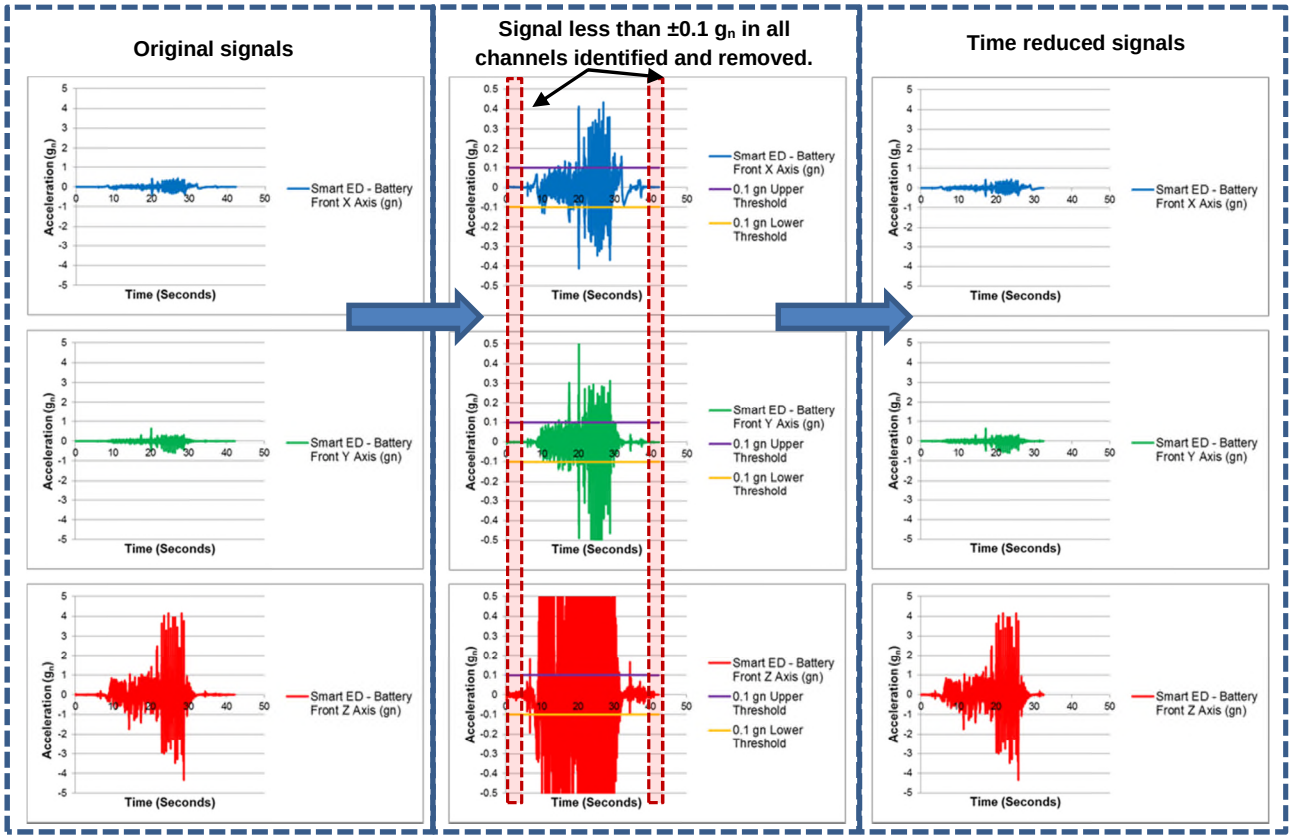

Figure 66: Example of the Removal of Content with Acceleration Less than 0.1 g_n Within an Example Data Set

Subsequently some signals such as the mile straight accelerations at wide open and part throttle were removed completely due to the low levels of vibration acceleration experienced during these measurements. To maximise the available test time, additional surface repeats for the hill route, handing circuit and high speed circuit were added to the test schedule. The revised number of surfaces and associated number of repeats are defined in Table 49.

Table 49: Surface Repeats for 10 Years European Structural Durability

Surface	Repeats of Surface Required for 10 Years European Structural Durability	Revised Number of Repeats for 10 Years European Structural Durability	Number of repeats of surface for 1 loop (total 300 loops required)	Edited duration of surface (seconds)	Total duration of surface with surface repeats for one loop (seconds)
Hill route (loop 1)	3365	3600	12	22	264
City course	6570	6600	22	13	286
Twist humps	1800	1800	6	33	198
Sine waves	1204	1200	4	34	136
Random waves	1200	1200	4	85.5	342
Belgian pave	600	600	2	134	268
Cats eyes – 30 mph	600	600	2	29	58
Cats eyes – 50 mph	600	600	2	57	114
HSC	420	600	2	11	22
Handling circuit	219	600	2	110	110
Pot holes*	54	60	1*	32	32
Mile Straight – Wide open throttle	1200	0	0	0	0
Mile Straight – Part open throttle	1200	0	0	0	0
Total		**-**	**-**	**-**	**1830**

Note: This sequence is repeated 300 times to achieved 150.36 hours test duration (approximately 10 years European EV customer usage) * = perform once every 5 loops of surfaces

To ensure a representative even loading of surfaces was achieved and to warrant that no surface was repeated for a significant duration (approximately no greater than 10 minutes) the signals were replicated in “loops”. A loop was a block of multiple surfaces which lasted approximately 30 minutes and contained a weighted number of repeats for each surface (as defined in Table 49). Each loop of signals was repeated 300 times to achieve approximately 150 hours of vibration.

Prior to starting the test, the FDS and SRS (as discussed in Chapter 3 and Appendix A and B) of the edited surface measurements for the Smart ED (as shown in Table 49) were compared to the FDS and SRS for USABC Procedure 10 and the derived random profiles defined in 3.4.6. The Z axis FDS and SRS analysis are presented in Figure 67 and Figure 68, whilst the complete analysis is shown in Submission 7.

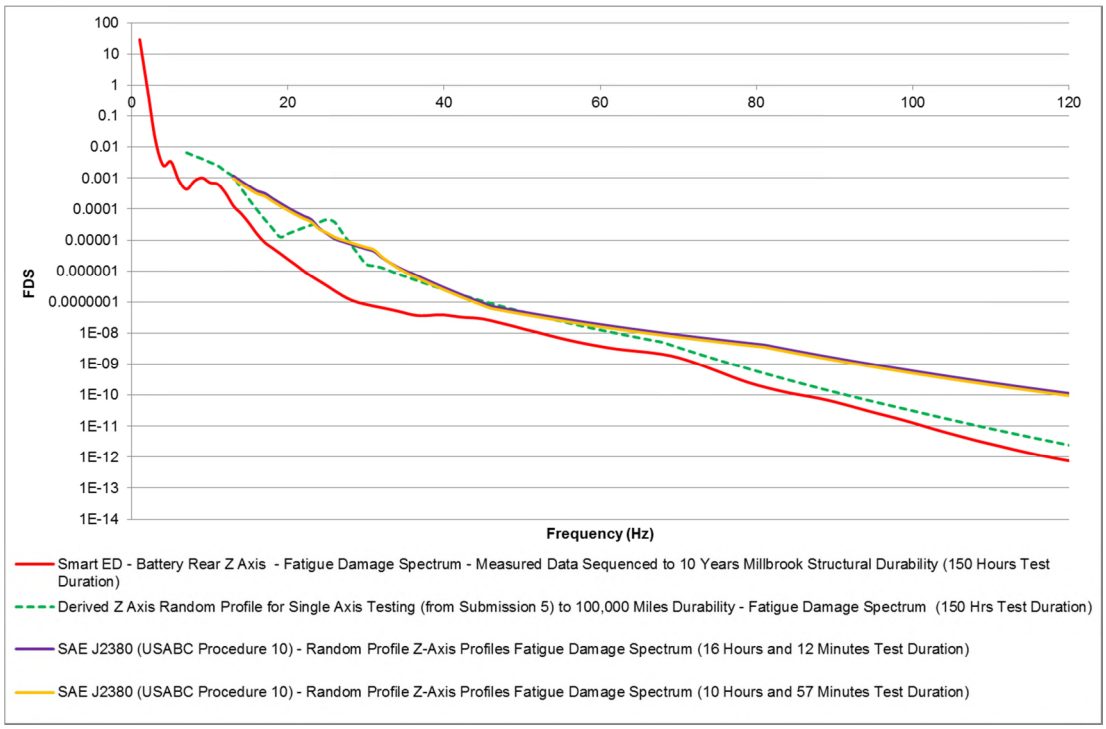

Figure 67: FDS Comparison

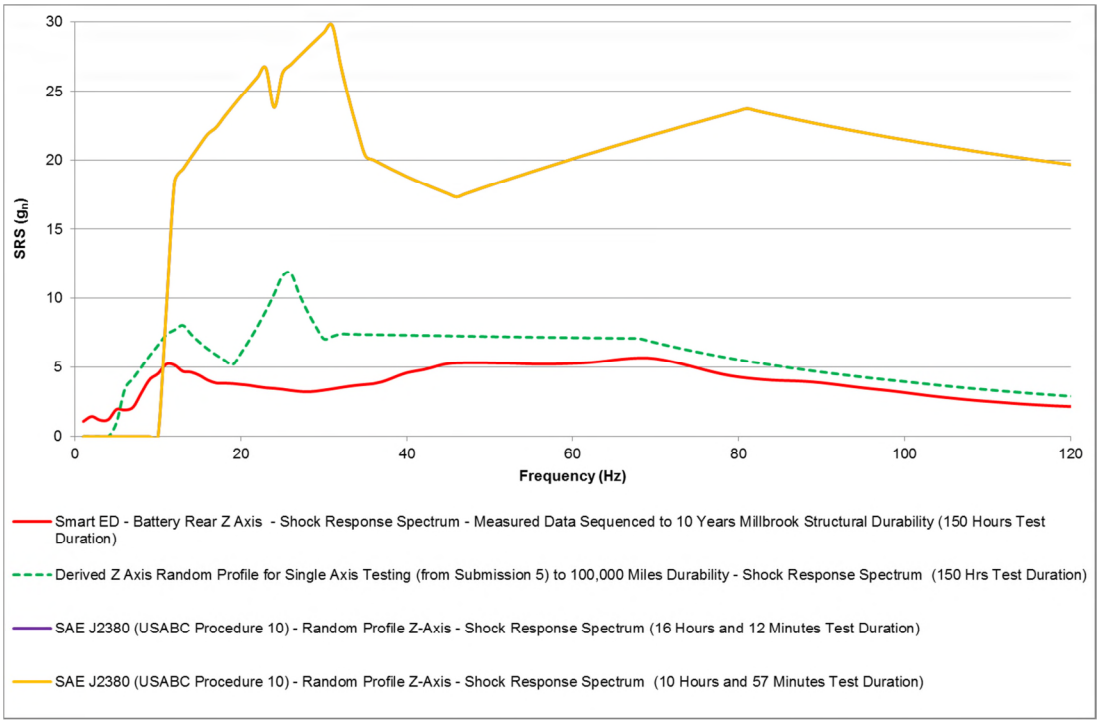

Figure 68: SRS Comparison

This analysis shows that compared to the previous single axis testing, the FDS loading is approximately 15 % of that of USABC Procedure 10 and 100,000 miles of BEV driving from 5 to 120 Hz. However, this investigation has a FDS and SRS loading at frequencies below 5 Hz which have been omitted within the single axis studies conducted in Chapter 5 and contemporary literature [82, 83, 90] due to the displacement capabilities of EMS test equipment.

Further, the SRS analysis showed that the shock loading within this study is approximately 50 % to 16 % of 100,000 miles of BEV driving and USABC Procedure 10 respectively. However, this analysis does not take into account the cross-axis fatigue damage and shock loading which occurs within a 6DOF test due to the additional roll, pitch and yaw moments.

When replicating recorded data in the time domain on any shaker system, (especially when the data is being replicated in 6DOF), it is necessary to ensure that the control accelerometers are installed in the same X, Y and Z locations on the rig to that of the measurement vehicle. Within this study the top, front right hand corner mounting hole on the cube head expander was taken as the 0:0:0 coordinate origin for the X:Y:Z measurement for the accelerometers. The locations of the accelerometers of the measurement vehicle (shown in Appendix Q) which used the front right hand wheel centre as the X, Y, Z origin were transposed to the cube head expander. A frame work was constructed around the test pieces to ensure the accelerometers were installed in the correct locations in space to mimic the in-vehicle measurement locations. This frame work was suitably ridged to ensure that no control disrupting resonances within the frame work itself occurred within the desired test frequency range of 0 to 110 Hz.

An example of the typical response of the Cube against the original measured signal is shown in Figure 69.

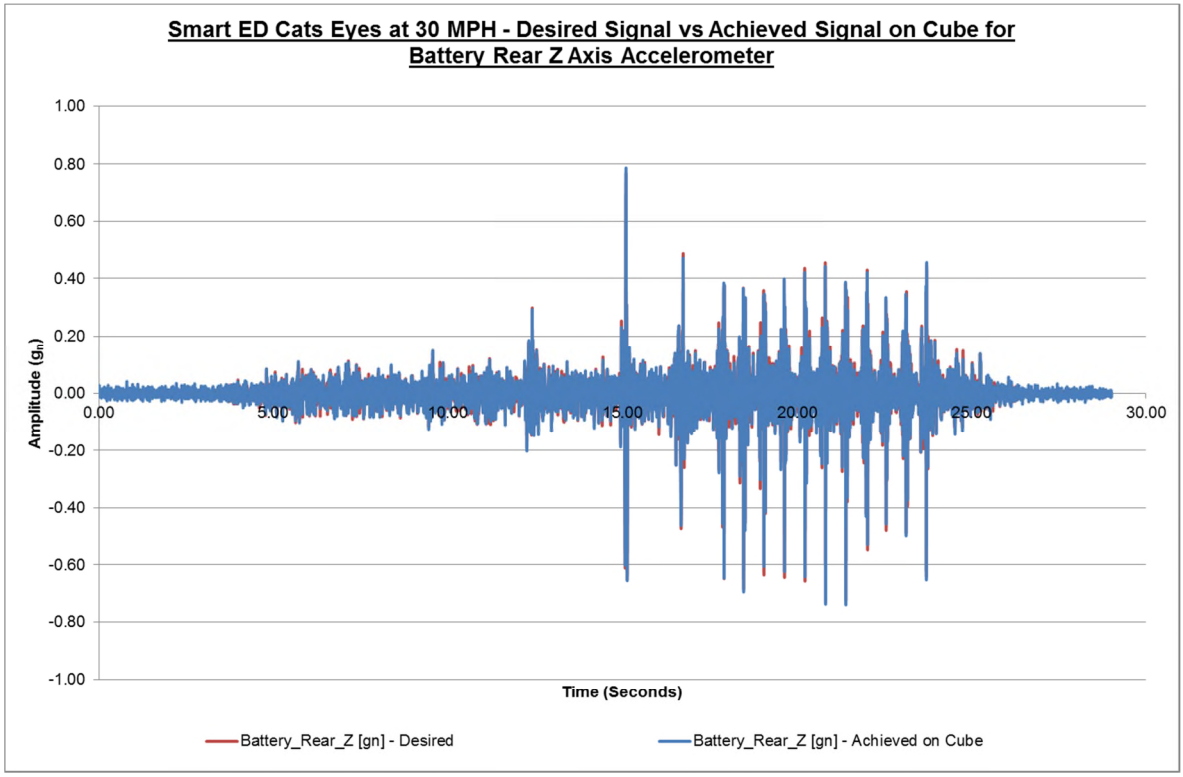

Figure 69: Smart ED – Cats Eyes at 30 MPH – Desired Signal vs Achieved Signal – Z Axis

The vibration signals were filtered with a low pass filter (with a cut-off frequency of 110 Hz) during the Iteration process. Within the pave signal file, a large 8 g_n spike

was noted which was clipped to 3 g_n in-line with the capabilities of the shaker system. The 8 g_n spike was typical of that associated with signal noise or an impact to the measurement accelerometer (such as that from a stone). Comparisons of the measured signals versus the replicated signals on the Cube MAST are illustrated in Submission 7.

6.3.5 Pre Test Electrical and Mechanical Characterisation of 18650 Cells

The following tests were performed on the cells at the SOT. All electrical tests were conducted at temperature of 21 °C ± 0.5 °C whilst the mechanical characterisation was conducted at temperature of 21 °C ± 3 °C.

6.3.5.1 Pre Test Electrical Characterisation

Pre-test electrical characterisation of capacity discharge, pulse power, OCV, and EIS was conducted in accordance with the method defined in Section 5.3.4. However, within this study capacity discharge was performed at C/3 as well as at 1C. This difference of procedure was as follows: The cells were fully charged using the CC-CV process defined in Section 5.3.4.1. The cells were allowed to rest for 4 h prior to being discharged at 1C to the manufacturer's defined cut-off voltage of 2.75 V. The energy extracted was recorded as a measure of the cell's 1C energy capacity. After a 4 hour rest the process was repeated, but the discharge current was reduced to C/3 and to lower voltage limit of 2.75 V. The energy extracted was recorded as a measure of the cell's C/3 energy capacity.

6.3.5.2 Pre-Test Mechanical Characterisation

The natural frequency of each cell was measured by fastening the respective cell to a VP85 EMS table and applying a swept sine wave from 5 to 3700 Hz, of amplitude 1 g_n at a rate of 1 octave/minute. The response of the cell in relation to this 1 g_n excitation, was recoded via a lightweight, single axis, accelerometer as shown in Figure 70. The measurement accelerometers (model PCB 352C65) were secured to the centre of the cell via a threaded aluminium collar which was bonded to the cell surface. These were attached to the cell via the use of HBM X60 adhesive. A strip of polyimide tape was placed between the cell and the adhesive to enable removal of the adhesive and collar post testing whilst minimising the risk of damage to the cell wall. This test arrangement resulted in a combined additional weight of approximately 2.6 g (approximately 6 % additional mass for each cell). Their inclusion within the experimental set-up was not deemed to have any significant impact on test accuracy through the addition of mass. When the cells were installed into their associated fixtures prior to testing, the collars were levelled using a small digital inclinometer. This was to ensure that no "off axis" errors could occur from the accelerometer being installed off centre from the vertical. To ensure transmissibility errors were reduced (as discussed within [166]) the accelerometers were tightened to a torque of 1 Nm on their respective collars prior to measuring the natural frequency of the cells. It is noteworthy, that this revised measurement methodology was introduced to overcome the issues discussed within Chapter 5 with respect to

the petro wax bonding method. The bonded collar arrangement was developed and trialled prior to being used within this study. A comparison of the repeatability of the two accelerometers mounting techniques are presented in Appendix R.

Two control accelerometers (model PCB 352A24) were secured at opposite ends on the top of the test fixture, but close to the specimens (as shown in Figure 70) using petro wax. An averaging control strategy was employed during the natural frequency measurement. Data was recorded at 2.5 times the desired peak frequency in accordance with Niquest rate guidelines [107]. Each sweep was performed three times and an average response was recorded.

Post natural frequency measurement each cell was allowed to rest for a minimum of 4 hours before any additional testing activities to ensure the test samples could electromechanically stabilise.

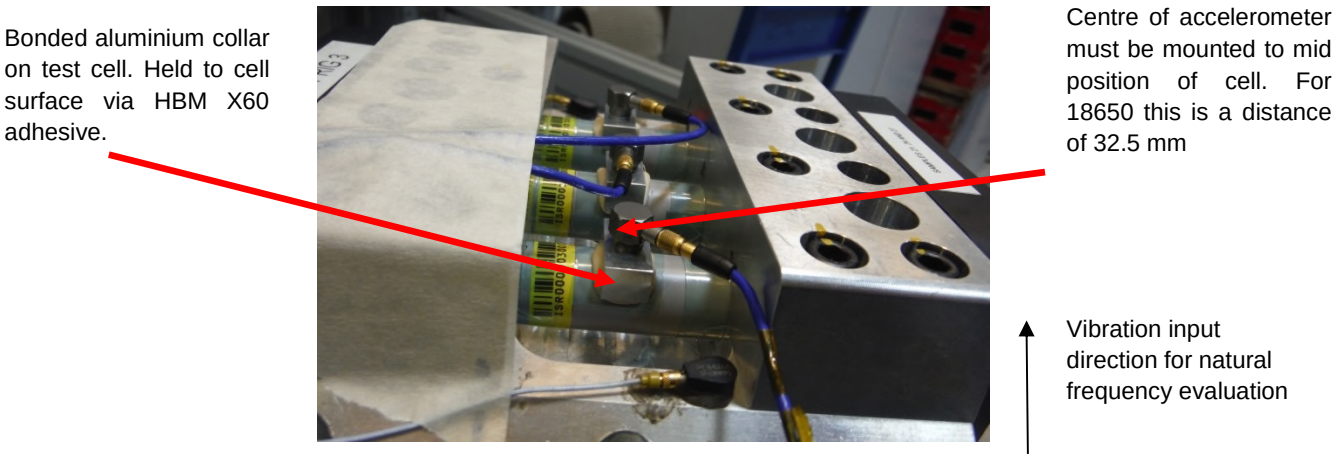

Figure 70: Location of Cell Accelerometer for Natural Frequency Measurement via Swept Sine Frequency Sweep.

6.3.6 Pre Test Electrochemical and Mechanical Characterisation of Tesla Model S Module

The following tests were performed on the Tesla Model S Module at SOT. All electrical tests were conducted at temperature of 21 °C ± 0.5 °C whilst the mechanical characterisation was conducted at temperature of 21 °C ± 3 °C.

6.3.6.1 SOC Adjustment of Tesla Model S Module

The Tesla Model S module SOC was adjusted by fully charging the device with a constant current of 202 A to 25.2 V followed by a constant voltage phase at 25.2 V until the current fell to 0.05 A. At the end of charge, the module was allowed to rest for 4 hours prior to being discharged at 1C for the desired time (e.g. 45 min, to achieve 25 % SOC). The cells were allowed to reach equilibrium for 4 hours.

6.3.6.2 1C and C/3 Capacity of Tesla Model S Module

Initially the module was fully charged using a CC phase of 220 A to 25.2 V followed by a CV phase at 25.2 V until the current fell to 4 A. The module was allowed to rest

for 4 hours prior to being fully discharged at 1C to 15 V (the manufacturer defined cut-off voltage).

With regard to the C/3 assessment, the module was initially conditioned using a CC phase of 220 A to 25.2 V followed by a CV phase at 25.2 V until the current fell to 4 A. Like the 1C assessments the cells were allowed to rest for 4 hours prior to being fully discharged at C/3 to 15 V.

6.3.6.3 Pulse Power Discharge Resistance of Tesla Model S Module

To determine the R_{DC}, a series of pulses was applied to the module after it was conditioned to 50 % SOC. Each current pulse was 10 seconds in length and the pulse current magnitude was 20 %, 40 %, 60 %, 80 % and 100 % of the modules rated pulse discharge current of 707 A (approximately 3.2 C). Each discharge pulse at a current level was followed by a 30 minute rest period prior to performing the charge pulse at the same current level. The R_{DC} of the cell was calculated as described in Equation 15. An average was calculated from all five pulses to determine the average R_{DC} of the test sample as per Equation 16.

6.3.6.4 Modal Analysis of Tesla Model S Module

The modal analysis of the Tesla module is a continuation of the test methodology developed for the evaluation of pouch cells as discussed in Chapter 4. Whilst the relevant test methodology is outlined within this section, additional modal analysis theory is discussed within Chapter 4 of this document and Submission 2.

The method of experimental modal analysis chosen for the evaluation of the Tesla Model S module was “hammer survey” via a Single Input Multiple Output (SIMO) method. With this method several measurement accelerometers are attached to the DUT at multiple locations. The input excitation is applied to the DUT at a single location via a calibrated nylon tipped impact hammer (with built-in load cell). Each point is assessed individually before being combined to determine the modal behaviour of the DUT.

The test sample was marked with twenty one measurement locations which resulted in a three by seven grid pattern across the test item. A schematic of the grid pattern is presented in Figure 71. This grid density was chosen to ensure that enough measurements were recorded to accurately determine the mode shapes of the DUT.

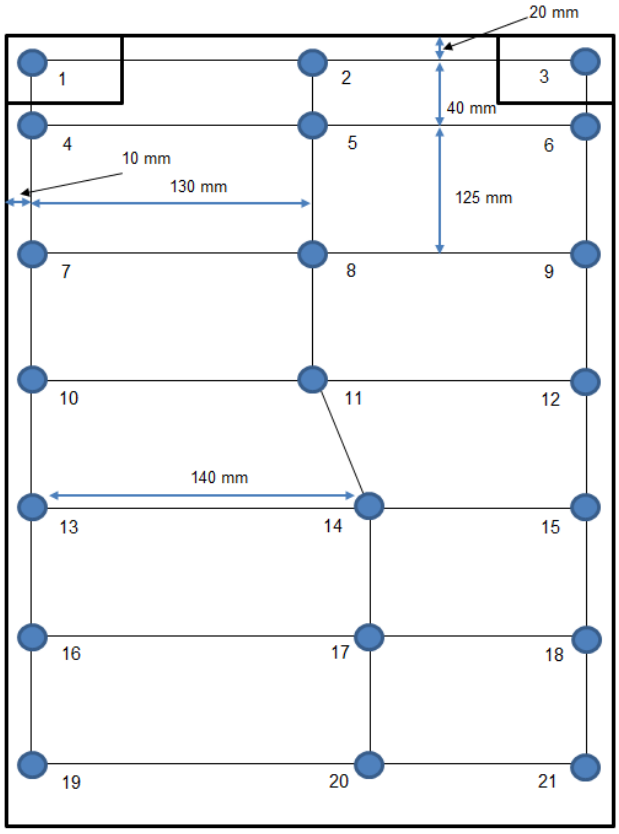

Figure 71: Test Grid Pattern

The measurements were recorded using the same equipment, free-free condition and by the author both pre and post testing. A picture of the twenty one impact locations and the test equipment are shown below in Figure 72 to Figure 73.

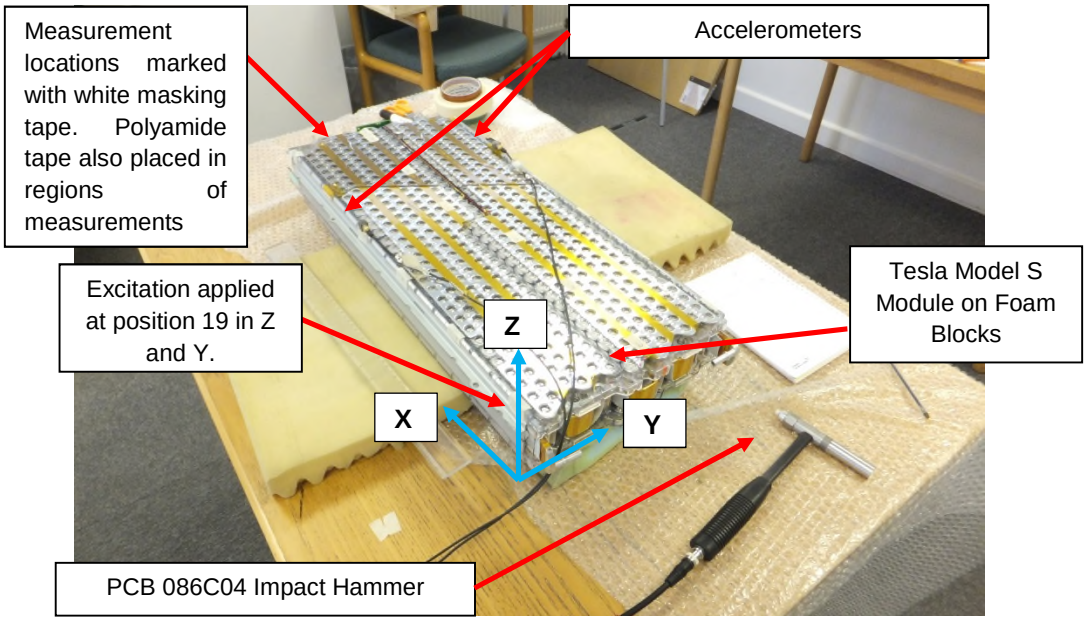

Figure 72: Sample Test Set Up

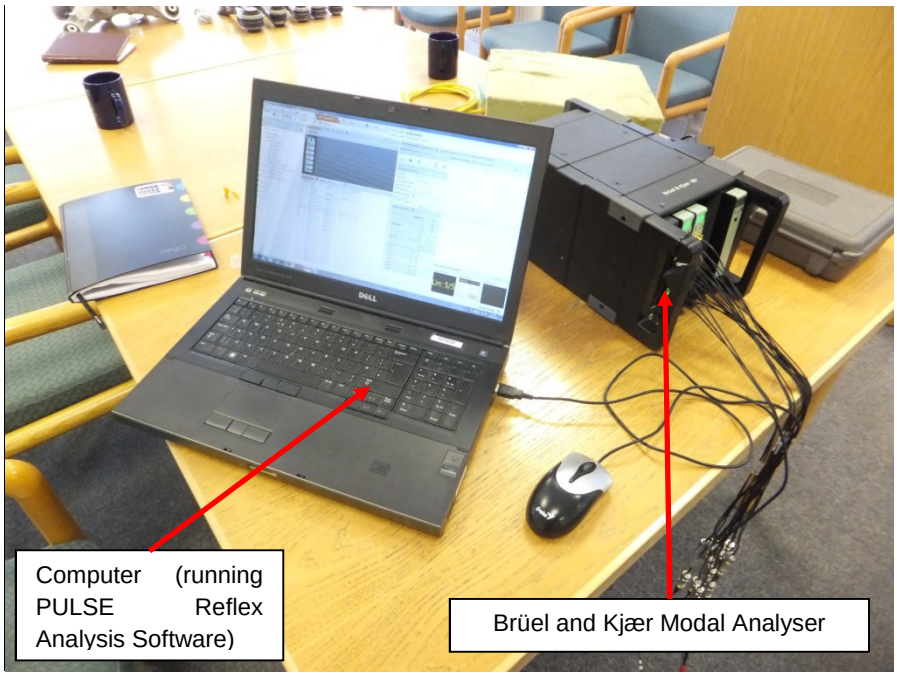

Figure 73: Data Logging and Modal Analyser Set Up

The testing was conducted in an air conditioned room at a temperature of 21 °C +/- 3 °C. The test sample was allowed to thermally stabilise in the office environment for approximately 3 days before testing commenced. The DUT was checked prior to testing using a Fluke Ti20 thermal imager to ensure it was within the desired temperature range.

For safety reasons, and to eliminate the risk of a short circuit during the modal analysis, the bus bars and terminals) were covered using insulating polyimide tape.

The testing was conducted using a 160 g “PCB 086C04” impact hammer with a “PCB 084A08” head extender which added an additional 100 g of head weight to the impact hammer. This was used in conjunction with two single multi axis “Brüel and Kjær TEDS 4524B” accelerometers. The data logger analyser used within this experiment was a “Brüel and Kjær 3053-B-12/0 Input Output Controller” within a “Brüel and Kjær 3660 type C chassis”.

The excitation hammer, response accelerometer and data logger were all within their yearly calibration. The measuring equipment was also calibrated as a system prior to testing via applying a known shaker excitation (1 g_n) to the measurement devices and ensuring the response of the system was within manufacturers tolerances. The impact hammer was checked for calibration tolerance via a static application of a known mass.

The 0.25 kg hammer with a nylon tip provided a measurement frequency range of approximately 0-800Hz. The reason why this frequency band was chosen was so that the primary modes could be determined, but also to assess if the natural frequencies of the module were within the region of typical road induced vibration as

identified in [32]. The data was sampled at 3.2 times the desired peak frequency in accordance with Shannon's sampling theorem.

The weight of the accelerometers mounted to the DUT was no greater than 0.0004 % of the total weight of the module, thus minimising the result of experimental error by the introduction of additional weight to the DUT. The accelerometer was fixed via the use of "petro wax" so that no surface or structural change was introduced by the application of permanent adhesives.

Finally, because the measurement surface of the module was the live bus bars, several extra layers of polyimide tape were placed in regions of measurements to reduce the risk of the test item creating an earth pathway via the measurement equipment. The mounting of accelerometers via petro wax assisted the insulation properties of the instrumentation.

The sample was placed on two blocks of polyurethane foam. These blocks were positioned under the two ends of the test sample. Each location (defined within Figure 71) on the test item was subjected to five impact excitations in both the Z and Y axis. Each measurement was averaged to generate a single input and single output response for the given test location for both the Z and Y axis.

Prior to measuring the Tesla module modal behaviour, the response of the DUT mounted on the foam pads was assessed for a *free-free* test condition. The lowest natural frequency of the module occurred at approximately 240 Hz, whereas the highest resonance of DUT mounted on the foam pad occurred at approximately 120 Hz. As discussed in Chapter 4 this level of frequency separation between the mounting medium and the cell, confirms the required degree of separation of approximately 100 Hz between the ridged body modes and flexible body modes required for a *free-free* test condition.

Within this investigation, the data was post processed using the "PULSE Reflex" software within the Brüel and Kjær modal analyser to generate the desired information for the module. A single FRF from each test position was evaluated together using its global curve fitting application to generate a single FRF trace which represented the modal performance of the whole module. The modal properties of natural frequency and modal damping were extracted by the PULSE Reflex software. Mode shapes were also estimated from the FRF's using the PULSE Reflex software. Additional information with regard to curve fitting techniques and methodology associated with experimental modal analysis from the perspective of an end user is included in Submission 2.

6.3.7 Application of Vibration

The vibration was applied to the test items in 6DOF for 150 hours in accordance with the surface repeats as defined in Table 49. The samples were checked every four hours for any significant changes in temperature (greater than 4 °C) or any emission of gases via the remote monitoring systems discussed in Section 6.3.2.3.

6.3.8 Cell and Module Post-Test Characterisation

At the end of the vibration profile, the cells were left to stabilise for a minimum of 4 hours prior to visual inspection. Post testing the cells and module were re-characterised as per the methods discussed in Sections 6.3.5 and 6.3.6.

6.4 **Results Part 1 – 18650 Cells**

The following section identifies the trends in the observed measurements taken throughout the multi-axis durability testing on the NCA 18650 cells subjected to 150 hours of vibration. It highlights trends relating to the effect of vibration on cell performance, and identifies if cell orientation can result in vibration durability related ageing. Only the results that illustrate the trends in cell performance change post vibration are presented in this section. However, a complete data set is supplied in Submission 7.

6.4.1 Post-Test External (Visual) Condition of Cells

Post testing, no significant mechanical damage or degradation was observed on any of the test samples. No leaking or expulsion of electrolyte was witnessed. A summary of the EOT visual condition of the cells is shown below in Appendix S. One of the most consistent observations at the EOT was damage to the insulation of the cell. Some damage was sustained through the removal of the bonded aluminium accelerometer mounting collar; however, it must be noted that this was not attributable to the application of vibration.

With regard to vibration sustained damage; compression of both the additional external insulation (polyamide tape applied to mitigate the risk of voltage drain to the aluminium fixture during testing) and the grey insulation of the cell itself, was observed at the point where the cell was clamped within the test rig. The results from the external inspection of the cells show no significant difference in performance with respect to orientation as all test samples have a visually similar condition at EOT. However, fretting of the positive terminal was observed in the Z-axis sample ISR 2994 (shown in Figure 74) and a surface defect was noted in the casing of Y-axis sample ISR 2997 (shown in Figure 75), however this was observed prior to testing.

Figure 74: Fretting Observed on Positive Terminal of ISR 2994 Post Testing

Figure 75: Surface Defect Noted on Casing of ISR 2997

6.4.2 1C Discharge Capacity Results

All samples (including control samples) illustrated a reduction in capacity post vibration testing. The results from the 1C discharge evaluation are shown in Table 50. It is evident from these results, that the reduction in capacity observed in the control samples is greater than that observed within the tested samples. This hypothesis is also supported when the mean change in cell capacity of each cell orientation is compared to the mean of the control samples.

When reviewing the ANOVA analysis of the Y-axis samples, it indicates that there is a significant change in capacity performance, as a result of vibration. However, this is due to the greater degradation of capacity performance observed in the control samples. Therefore, in this instance, the significant effect of the vibration is actually a positive one. Due to this significance within the Y axis oriented samples, the effect of 1C capacity discharge by in pack orientation can be summarised as follows: Y < X = Z.

Table 50: Ranked Change in Capacity of All Test Cells

Cell ID	Orientation	SOT (Ah)	EOT (Ah)	Change from SOT and EOT (Ah)	Percentage Change (%)	Overall Ranking 1 = Worst 9 = Best
2991	Z	2.97	2.88	-0.09	-3.03	1
2994	Z	2.98	2.90	-0.08	-2.68	5
2996	Z	2.94	2.92	-0.02	-0.68	= 9
2997	Y	2.98	2.91	-0.07	-2.35	6
2998	Y	2.97	2.94	-0.03	-1.01	7
2999	Y	3.01	2.92	-0.09	-2.99	3
3000	X	2.95	2.87	-0.08	-2.71	4
3001	X	2.99	2.90	-0.09	-3.01	2
3005	X	2.94	2.92	-0.02	-0.68	= 9
2995	Control	3.06	2.92	-0.14	-4.58	-
3003	Control	3.08	2.94	-0.14	-4.55	-
3004	Control	3.07	2.97	-0.10	-3.26	-
				Mean Change (mΩ)	**Mean Change (%)**	**Ranking**
Mean Change in (Ah) – X				-0.06	-2.13	=1
Mean Change in (Ah)- Y				-0.06	-2.12	2
Mean Change in (Ah) – Z				-0.06	-2.13	=1
Mean Change in (Ah) – Control				-0.13	-4.13	-
ANOVA Analysis						
Orientation				**ANOVA p-value against Control Null Hypothesis: Mean of vibrated cells and control cells are equal. Reject null hypothesis if p < 0.05)**		
X				0.0687		
Y				0.0457		
Z				0.0687		

6.4.3 C/3 Discharge Capacity Results

Like the 1C capacity discharge results discussed in Section 6.4.2, all samples (including the control items) display a reduction in C/3 capacity measurement post testing. This is illustrated in Table 51.

Table 51: Ranked Change in C/3 Capacity of All Test Cells

Cell ID	Orientation	SOT (Ah)	EOT (Ah)	Change from SOT and EOT (Ah)	Percentage Change (%)	Overall Ranking 1 = Worst 9 = Best
2991	Z	2.98	2.90	-0.08	-2.68	3
2994	Z	3.03	2.95	-0.08	-2.64	4
2996	Z	3.03	2.98	-0.05	-1.65	7
2997	Y	2.98	2.92	-0.06	-2.01	5
2998	Y	3.02	2.97	-0.05	-1.66	6
2999	Y	3.08	2.95	-0.13	-4.22	2
3000	X	2.91	2.88	-0.03	-1.03	8
3001	X	3.07	2.93	-0.14	-4.56	1
3005	X	2.95	2.92	-0.03	-1.02	9
2995	Control	3.02	2.90	-0.12	-3.97	-
3003	Control	3.09	2.94	-0.15	-4.85	-
3004	Control	3.04	3.01	-0.03	-0.99	-
				Mean Change (mΩ)	**Mean Change (%)**	**Ranking**
Mean Change in (Ah) – X				-0.07	-2.20	3
Mean Change in (Ah)- Y				-0.08	-2.63	1
Mean Change in (Ah) – Z				-0.07	-2.32	2
Mean Change in (Ah) – Control				-0.10	-3.27	-
ANOVA Analysis						
Orientation				**ANOVA p-value against Control Null Hypothesis: Mean of vibrated cells and control cells are equal. Reject null hypothesis if p < 0.05)**		
X				0.552		
Y				0.673		
Z				0.468		

A noteworthy observation is that the C/3 performance of the Y axis samples is on average, the worst performing orientation. Where in the 1C discharge, the Y axis samples were the best performing. This is likely to be as a result of sample ISR 2999 which has a high capacity degradation (-4.22 %) when assessed at C/3 discharge.

The control samples (like the 1C discharge results) have a higher reduction in capacity post testing than the samples that were tested. This indicates that from a capacity reduction perspective there may be some evidence to suggest that cells excited to vibration in 6DOF may degrade at a slower rate than cells left in a static condition. However, further testing is required to confirm this hypothesis.

The ANOVA analysis presented in Table 51 highlights that there is no significant effect to C/3 capacity for any of the orientations as a result of vibration in 6DOF. In summary, the performance of each orientation can be defined as follows: X = Z =Y.

6.4.4 Pulse Power Results

Table 52 illustrates the change in pulse power of all test samples together (including reference samples). The results presented were conducted at 50 % SOC.

The worst performing cell was ISR 3001 (X) which displayed an 8.77% increase in DC resistance. The cell with the least degradation in DC resistance post vibration was ISR 3005 (X) which had a 5.10 % increase.

With all samples subjected to vibration, an increase in pulse power resistance was observed which indicates a decrease in contactor area, possibly as a result of delamination or cracking of internal surfaces [82]. A mean increase in DC resistance of 2.45 % was observed within the control samples (compared to a mean of 7.07 %, 6.19 % and 6.75 % for the Z, Y and X oriented samples respectively) suggesting that vibration had a significant effect on the cells performance. This is confirmed by the ANOVA analysis presented in Table 52. Based on the ANOVA analysis the following hierarchy of orientation performance is determined from these results at the 95 % confidence level: Y < X < Z.

Table 52: Change in Pulse Power Performance – R_{DC}

Cell ID	Orientation	DC Resistance (SOT) (mΩ)	DC Resistance (EOT) (mΩ)	Change in DC Resistance (mΩ)	Percentage Change in R_{DC} Between SOT and EOT (%)	Ranking Worst to Best 1 = Worst 9 = Best
2991	Z	40.56	43.51	2.95	7.28	3
2994	Z	40.82	43.80	2.98	7.31	2
2996	Z	40.64	43.33	2.69	6.62	5
2997	Y	41.08	43.36	2.28	5.55	8
2998	Y	40.91	43.45	2.54	6.22	7
2999	Y	40.38	43.13	2.75	6.81	4
3000	X	41.32	43.95	2.63	6.37	6
3001	X	40.00	43.51	3.51	8.77	1
3005	X	41.32	43.42	2.11	5.10	9
2995	Control	41.90	42.98	1.08	2.58	-
3003	Control	42.22	42.92	0.70	1.66	-
3004	Control	41.37	42.66	1.29	3.11	-

	Mean Change (mΩ)	Mean Change (%)	Ranking
Mean Change in Pulse Power R_{DC} - X	2.75	6.75	2
Mean Change in Pulse Power R_{DC} - Y	2.52	6.19	3
Mean Change in Pulse Power R_{DC} - Z	2.88	7.07	1
Mean Change in Pulse Power R_{DC} - Control	1.02	2.45	-

ANOVA Analysis	
Orientation	**ANOVA p-value against Control Null Hypothesis: Mean of vibrated cells and control cells are equal. Reject null hypothesis if p < 0.05)**
X	0.018
Y	0.002
Z	0.001

6.4.5 OCV Results

Assessing the results illustrated in Appendix T, no significant change in the OCV measurements were observed between start and end of test as no change is greater than 0.05 % (0.002 V). The low values witnessed, mean that any observed difference within the OCV measurements are potentially within the error of the measurement method. This supports the results presented in [80, 81] that also noted that OCV is not adversely affected by vibration loading.

This assertion is supported by the ANOVA analysis presented in Appendix T which shows that there is no significant change in OCV as a result of vibration at the 95 % confidence level between the tested cells and the control items.

Given the measurement error associated with this measurement, the mean change in OCV is equal for all orientations. This results in no clear orientation performing significantly worse or better than another. Therefore the following hierarchy of orientation performance is determined from these results: X = Y = Z.

6.4.6 EIS Results

Table 53 and Table 54 show the R_O and the R_{CT} of the cells at SOT and EOT as measured by EIS. Figure 76 presents a typical Nyquist plot of the cells pre and post vibration test. Additional EIS plots are presented in Submission 7 [167].

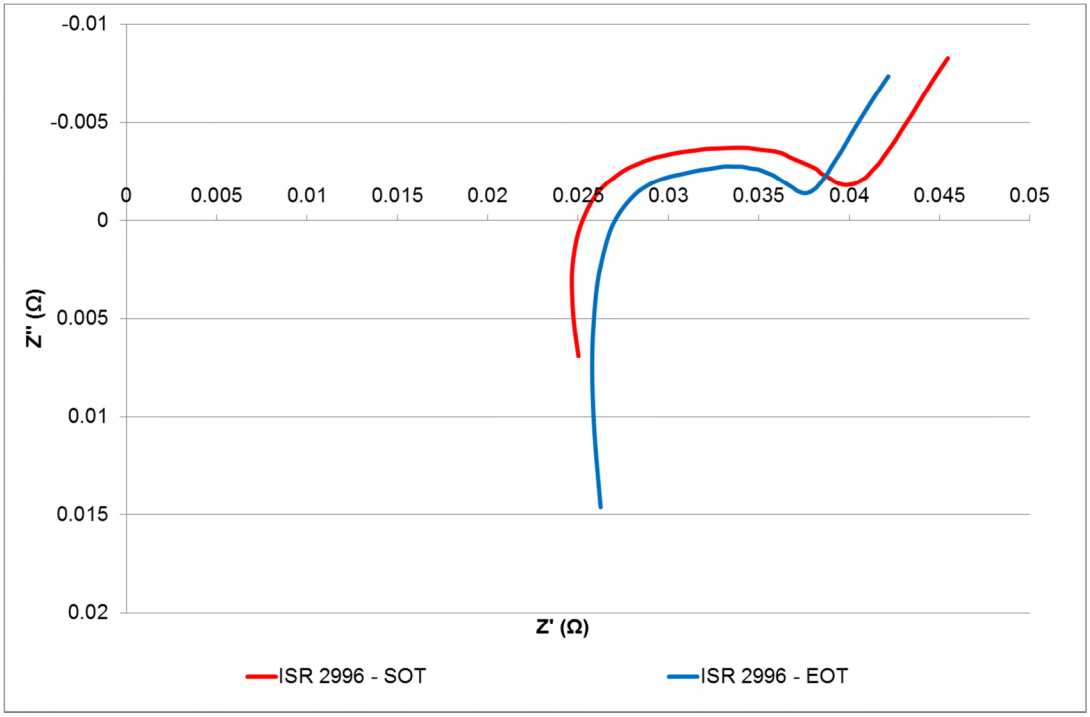

Figure 76: Typical Pre and Post Test EIS Curves for 18650 NCA Test Samples

Table 53 highlights that all the cells (including the reference samples) exhibit an increase in R_O at EOT. ISR 2999 (Y Axis sample) exhibited the greatest change in R_O of 2.12 mΩ (9.39 %). However ISR 2997 which was also orientated in the Y axis exhibited the least change in R_O of 0.99 mΩ (4.20 %). An increase in R_O typically originates from an increase in cell contact resistance, possibly through delamination of the material layers [149, 151] or due to damage to the current collectors. However the mean change in R_O resistance for the control samples is 1.59 mΩ (6.92 %), compared to 1.57 mΩ (6.89 %), 1.49 mΩ (6.47 %) and 1.53 mΩ (6.62 %) for the X,

Y and Z orientations respectively. This indicates that whilst vibration may have had an effect on this electromechanical property, it is likely that the majority of the observed increase is a function of the test accuracy. This hypothesis is confirmed when reviewing the error associated with this type of electrical measurement. For 18650 cells EIS ohmic resistance has an experimental error of ±1.25 mΩ [152] and a standard error of 1.26 %.

Table 53: Start and End of Test R_O Measurements

Cell ID	Orientation	SOT (mΩ)	EOT (mΩ)	Change from SOT and EOT (mΩ)	Percentage Change (%)	Overall Ranking 1 = Worst 9 = Best
R_O Results						
2991	Z	22.99	24.45	1.47	6.39	4
2994	Z	23.12	24.90	1.78	7.68	3
2996	Z	23.26	24.60	1.34	5.78	6
2997	Y	23.57	24.56	0.99	4.20	9
2998	Y	23.25	24.61	1.35	5.82	5
2999	Y	22.58	24.70	2.12	9.39	1
3000	X	23.24	24.57	1.33	5.74	7
3001	X	22.35	24.43	2.09	9.33	2
3005	X	23.23	24.54	1.31	5.62	8
2995	Control	22.66	24.12	1.45	6.41	-
3003	Control	23.27	24.89	1.62	6.96	-
3004	Control	22.77	24.46	1.69	7.41	-
				Mean Change (mΩ)	**Mean Change (%)**	**Ranking**
Mean Change in R_O – X				1.57	6.89	1
Mean Change in R_O – Y				1.49	6.47	3
Mean Change in R_O – Z				1.53	6.62	2
Mean Change in R_O – Control				1.59	6.93	-
ANOVA Analysis						
Orientation				**ANOVA p-value against Control Null Hypothesis: Mean of vibrated cells and control cells are equal. Reject null hypothesis if p < 0.05)**		
X				0.967		
Y				0.786		
Z				0.718		

ANOVA analysis of the significance of the mean change in ohmic resistance of the tested cells in relation to the control samples is shown in Table 53. Based on the above statistical analysis, there is no significant change in R_O for any of the three

cell orientations at the 95 % confidence level as a result of the application of vibrations in 6DOF. Therefore, the following hierarchy of orientation performance is determined from these results: Y = Z = X

The R_{CT} results presented in Table 54 demonstrate that all samples (except ISR 3000), including the control samples, show a decrease in R_{CT} post testing.

Table 54: Start and End of Test R_{CT} Measurements

Cell ID	Orientation	SOT (mΩ)	EOT (mΩ)	Change from SOT and EOT (mΩ)	Percentage Change (%)	Overall Ranking 1 = Worst 9 = Best
R_{CT} Results						
2991	Z	14.38	11.44	-2.94	-20.47	6
2994	Z	15.64	13.97	-1.67	-10.68	4
2996	Z	15.64	13.88	-1.76	-11.24	5
2997	Y	16.57	12.79	-3.78	-22.83	7
2998	Y	17.42	12.04	-5.38	-30.86	9
2999	Y	16.46	12.52	-3.95	-23.99	8
3000	X	12.26	12.38	0.12	0.95	1
3001	X	13.73	12.50	-1.24	-9.01	3
3005	X	17.33	16.67	-0.66	-3.79	2
2995	Control	21.31	16.27	-5.04	-23.64	-
3003	Control	22.25	14.62	-7.63	-34.31	-
3004	Control	19.03	16.20	-2.83	-14.86	-
				Mean Change (mΩ)	**Mean Change (%)**	**Ranking**
Mean Change in R_{CT} – X				-0.59	-3.95	1
Mean Change in R_{CT} - Y				-4.37	-25.89	3
Mean Change in R_{CT} – Z				-2.12	-14.13	2
Mean Change in R_{CT} – Control				-5.17	-24.27	-
ANOVA Analysis						
Orientation				**ANOVA p-value against Control Null Hypothesis: Mean of vibrated cells and control cells are equal. Reject null hypothesis if p < 0.05)**		
X				0.033		
Y				0.618		
Z				0.103		

This reduction in R_{CT} could be a function of improved anode and cathode “wetting” over the duration of the test. However, given that the control samples displayed a similar improvement, this proposed mechanism is unlikely to be a function of the applied vibration.

Samples evaluated in the Y orientation show a similar average reduction in R_{CT} as the control samples. They also have a significantly higher mean change of -25.89 % than the X axis oriented items (-3.95 %). The Z axis oriented samples have a lower improvement to that of the Y oriented samples and the controls of -14.13 %.

Reviewing the ANOVA analysis results presented in Table 54, samples mounted in the X axis orientation showed a significant difference in R_{CT} performance as a result of vibration when compared to the control samples. Whilst it must be noted that the R_{CT} had reduced in all samples post testing, the reduction was lower in X-axis items, resulting in a "significant effect of vibration" within these samples.

In summary, assessing the mean change with regard to R_{CT}, the performance of cell orientation can be summarised as follows: Y = Z < X.

6.4.7 Mechanical Characterisation Results

The purpose of conducting this test was to determine if a mechanical change had occurred within a given test cell which had resulted in a change in natural frequency between the SOT and EOT. The change in frequency and amplitude of the first natural frequency observed within each cell between the start and end of test are shown in Table 55 and Table 56. An example of a typical start and end of test vibration response of the test cells from this study is presented in Appendix U. A full data set is shown in Submission 7 [167].

Table 55: Summary of Change in Frequency of Observed First Cell Resonance for Samples

		First Resonance Frequency				
ISR number	**Orientation**	**SOT**	**EOT**	**Change (Hz)**	**Change (%)**	**Ranking**
2991	Z	3700	3700	0.00	0.00	=
2994	Z	3700	3700	0.00	0.00	=
2996	Z	3700	3700	0.00	0.00	=
2997	Y	3700	3700	0.00	0.00	=
2998	Y	3700	3700	0.00	0.00	=
2999	Y	3700	3700	0.00	0.00	=
3000	X	3700	3700	0.00	0.00	=
3001	X	3700	3700	0.00	0.00	=
3005	X	3700	3700	0.00	0.00	=
				Mean Change (Hz)	**Mean Change (%)**	**Ranking**
Mean Change First Resonance Frequency - X				0.00	0.00	=
Mean Change First Resonance Frequency - Y				0.00	0.00	=
Mean Change First Resonance Frequency- Z				0.00	0.00	=

Reviewing the results presented in Table 55, all cells showed no change in natural frequency between the start and end of test. Assessing the mean change with

regard to the first natural frequency, the performance of cell orientation can be summarised as follows: X = Y = Z.

Whilst it is likely that no significant mechanical degradation occurred which could have affected the natural frequency, it must be noted that the resonance of the cells was greater than the frequency range capabilities of the EMS table which was used for the natural frequency measurement activity. Subsequently the natural frequency at the start and end of test was logged at 3700 Hz.

With regard to the amplitude of the “first resonant frequency” (shown in Table 56), there is a significant change in the majority of cells indicating a change in damping of the cell assembly.

The greatest change in amplitude was observed within ISR 2999 (Y-axis), which had an increase of 39.22 %, highlighting a reduction in damping of the cell. Generally, Y axis oriented cells a greater reduction in damping characteristics than the other cell orientations. A possible explanation for this observation could be due to a redistribution of electrolyte within the cells material layers due to vibration, which would correlate with the improved wetting hypothesis. However further studies and investigations would have to be conducted to determine the cause for this change.

Table 56: Summary of Change in Amplitude of Observed First Cell Resonance for Samples

		Amplitude at First Resonance				
ISR number	**Orientation**	**SOT**	**EOT**	**Change (g_n)**	**Change (%)**	**Ranking**
2991	Z	1.66	1.82	0.16	9.64	4
2994	Z	1.61	1.68	0.07	4.35	8
2996	Z	1.70	1.81	0.11	6.47	6
2997	Y	1.80	1.97	0.17	9.44	5
2998	Y	1.70	2.24	0.54	31.76	2
2999	Y	2.04	2.84	0.80	39.22	1
3000	X	1.70	1.78	0.08	4.71	7
3001	X	1.54	1.70	0.16	10.39	3
3005	X	1.89	1.90	0.01	0.53	9
				Mean Change (g_n)	**Mean Change (%)**	**Ranking**
Mean Change in Amplitude in First Resonance - X				0.08	5.21	3
Mean Change in Amplitude in First Resonance - Y				0.50	26.81	1
Mean Change in Amplitude in First Resonance - Z				0.11	6.82	2

Assessing the mean change with regard to the amplitude of the first natural frequency, the performance of cell orientation can be summarised as follows: X < Z < Y.

ANOVA analysis could not be performed for the mechanical characterisation results as the control samples were not subjected to a resonance search. This was due to the possible mechanical stress associated with the test method, which could impact the electrical characteristics of the control items.

6.5 **Results Part 2 – Tesla Model S Module**

The following section identifies the trends in the observed measurements taken throughout the durability testing on a Tesla Model S module subjected to 150 hours of vibration. This vibration was reproduced on a multi-axis shaker from signals recorded from a Smart ED. These signals were applied to the item under evaluation in 6DOF. It highlights trends relating to the effect of vibration the modules performance

6.5.1 Post-Test External (Visual) Condition of Tesla Model S Module

Post testing there was no significant external damage or degradation noted within the Tesla Model S Module. The only noted observation was that the positive terminal when unbolted showed a slightly greater gap condition than at SOT which indicated a relaxing of materials in this area.

6.5.2 Post-Test Electrical Characterisation Results

The pre and post testing electrical characterisation results are presented in Table 57.

Table 57: Pre and Post Testing Electrical Characterisation Results for Tesla Model S Module

Test	Pre-Test	Post Test	Change	Change in %
OCV (V)	24.91	24.88	-0.03	-0.12
1C Capacity Discharge (mA)	221.82	221.55	-0.27	-0.12
C/3 Discharge (mA)	223.65	222.05	-1.60	-0.72
DC Resistance (mΩ)	5.22	5.36	0.14	2.73

What is noticeable from these measurements is that both the OCV and capacity of the module was unaffected by the vibration with each of these measurements showing a change that was less than 0.75 % post testing. The internal resistance of the module however, did show an increase of 2.73 % post application of vibration. However, this was a significantly lower increase than that observed within the single cells, which indicates that the increased damping of the packaging of the module assembly may have an effect on reducing the degradation of the cells caused by vibration excitation. It cannot be determined at this time whether this resistance increase is a result of damage to the module or the cells within the assembly. There is some evidence to suggest from this experiment that the electrical performance of the module is unaffected by vibration applied in 6DOF.

6.5.3 Post-Test Mechanical Characterisation Results

Whilst the module was excited in both the Y and Z axis during this study, only the Z-axis results are presented due to the correlation between these data sets. The full data set is presented in Submission 7 [167].

The natural frequency, damping and mode shapes, both pre and post testing are presented in this Chapter. Whilst measurements of the module were recorded up to 1600 Hz, only the modes from 0 to 800 Hz are presented due to the average coherence being typically less than 0.95 for the Z-axis. A graphical representation of the average coherence for the module assembly for the Z-axis measurements for the SOT and EOT is presented in Figure 77.

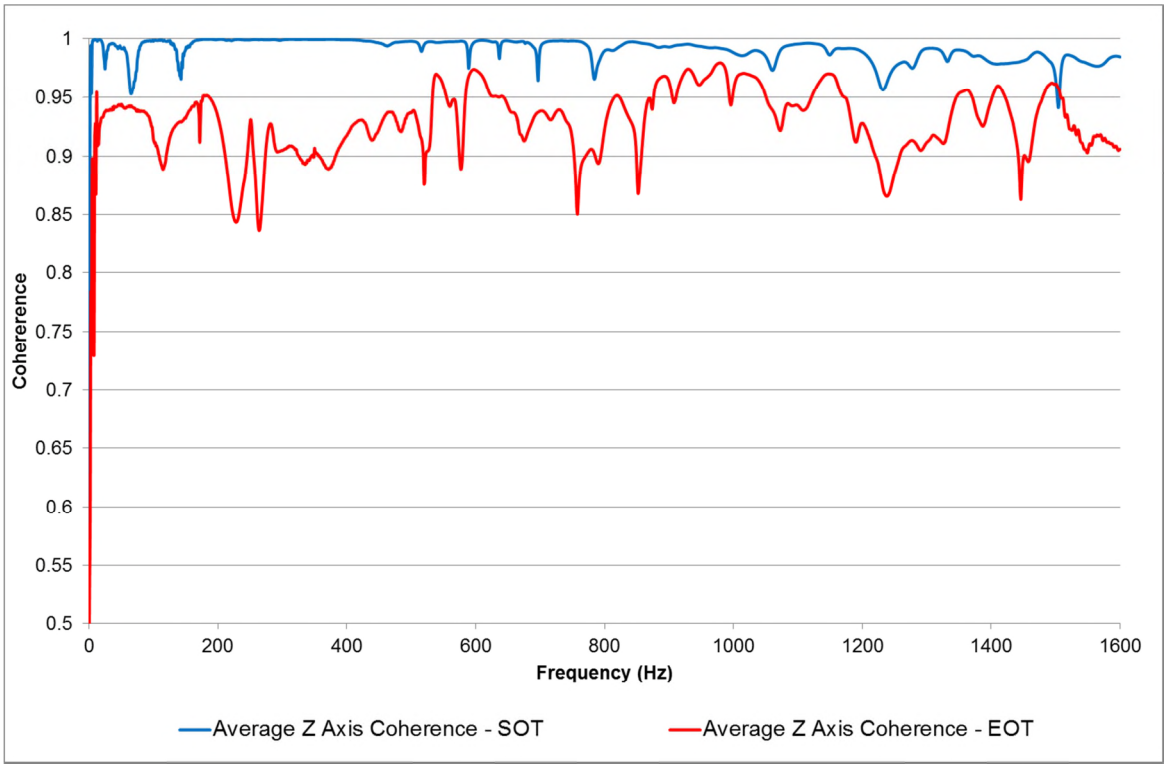

Figure 77: Average Z-Axis Coherence for Hammer Survey Measurements from Tesla Model S Module

The modes shapes are presented in Appendix V. Table 58 presents the natural frequencies of the Tesla Model S module when excited in the Z axis in the free-free condition at the SOT and EOT. Whilst Table 59 presents the damping of each of the modes witnessed. When the Tesla Module was excited in the Z axis, ten modes were observed within the 0 to 800 Hz range at the SOT and EOT. The first mode was observed at 249 Hz (both at the SOT and EOT). The first mode is outside the range of typical road induced vibration. Reviewing the results from Table 58 it is noticeable that there is very little change between with the first two modes between start and end of test with respect to the observed natural frequency. Interestingly the third mode is where the greatest change in one single natural frequency occurs. With the third mode there is a reduction in frequency of -26.19 Hz (-8.50 %) which

indicates a significant change in stiffness to an area of the module assembly. In this instance, this area is the positive terminal assembly, which was observed to have lifted slightly post testing.

Table 58: Modal Analysis with Z-Axis Excition – Natural Frequencies and Associated Mode Shapes at SOT and EOT

Mode	SOT Mode Z Axis (Hz)	EOT Mode Z Axis (Hz)	Change in Frequency	Percentage Change	Mode Shape
1	249.08	249.08	0.00	0.00	First Bending
2	262.26	262.63	0.38	0.14	First Torsion
3	308.04	281.85	-26.19	-8.50	Localised Bending (Terminal)
4	387.16	393.52	6.36	1.64	Second Torsion
5	511.28	500.98	-10.31	-2.02	Third Torsion
6	531.21	526.97	-4.24	-0.80	Forth Torsion
7	573.94	561.67	-12.27	-2.14	Combined Torsion and Bending
8	620.01	630.92	10.91	1.76	Second Bending
9	732.80	731.41	-1.39	-0.19	Combined Torsion and Bending
10	740.05	745.00	4.95	0.67	Combined Torsion and Bending

This reduction in stiffness for the third mode is also supported by Table 59 which shows a percentage change in damping of -35.47 % between SOT and EOT for the third mode.

Table 59: Modal Analysis with Z-Axis Excition – Percentage Damping of Each Mode and Associated Mode Shapes at SOT and EOT

Mode	SOT Damping of Mode Z Axis (%)	EOT Damping of Mode Z Axis (%)	Change in Damping (%)	Percentage Change between SOT and EOT	Mode Shape
1	1.69	1.61	-0.07	-4.22	First Bending
2	1.73	1.90	0.17	9.69	First Torsion
3	8.13	5.24	-2.88	-35.47	Localised Bending (Terminal)
4	9.37	2.47	-6.90	-73.60	Second Torsion
5	2.35	1.68	-0.67	-28.70	Third Torsion
6	5.05	2.07	-2.99	-59.13	Forth Torsion
7	1.42	1.28	-0.14	-9.93	Combined Torsion and Bending
8	1.75	1.79	0.04	2.35	Second Bending
9	2.67	2.11	-0.56	-20.86	Combined Torsion and Bending
10	1.81	1.52	-0.29	-16.12	Combined Torsion and Bending

However, with respect to the damping of modes, the forth mode (which is the third observed torsional mode) has the greatest reduction in damping of -73.60 % between SOT and EOT. Whilst these modes are outside the range of road induced vibration, if they are excitable by on-board power electronics a significant reduction in damping might result in possible noise issues being transmitted. It may also result in acceleration in degradation of the module.

6.6 **Discussion**

6.6.1 Effect of Vibration in 6DOF on 18650 NCA Lithium-ion Cells

Table 60 presents the average change for each cell orientation for the 18650 NCA cells subjected to vibration in 6DOF. The primary conclusion from this study is that both the electrical performance and the mechanical properties of the NCA lithium-ion cells are relatively unaffected when exposed to vibration energy that is commensurate with a typical vehicle life. However, there are some nuances within the data that must be highlighted.

Table 60: Average Change for Each Test Attribute by Cell Orientation Post Vibration Testing in 6DOF

Orienta-tion	Pulse Power - Change in R_{DC} (mΩ)	EIS Change in R_o (mΩ)	EIS Change in R_{CT} (mΩ)	OCV - Change in Voltage (V)	Change in 1C Capacity (Ah)	Change in C/3 Capacity (Ah)	Resonance Frequency - Change in Hz	Resonance Amplitude - Change in g_n
Z	2.87	1.53	-2.12	-0.001	-0.06	-0.07	0.00	0.11
X	2.75	1.58	-0.59	-0.001	-0.06	-0.07	0.00	0.08
Y	2.52	1.49	-4.37	0.000	-0.06	-0.08	0.00	0.50
Control	1.02	1.59	-5.17	0.000	-0.13	-0.10	N/A	N/A

It is noticeable from Table 60 (and the ANOVA analysis in Section 6.4.4) that the R_{DC} performance was significantly impacted by the vibration applied in 6DOF when compared to the control samples. This indicates that the cells may have some degree of damage to the current collector or cell material layers as a result of the multi-axis vibration loading. However, this finding is not confirmed by the degree of change observed within the measurement of $R_{O.}$ Like R_{DC}, R_O is also an indication of current collector condition and material layer integrity. Whilst there is also degradation within the observed average values for each orientation, the difference between the control and tested items is minimal. This limited difference between the control and tested items results in the vibration being the non-significant contributor to the increase in $R_{O.}$ To fully understand what may be occurring within these cells with respect to these two attributes requires further testing via non-destructive testing (such as CT scanning) followed by chemical and microscopic analysis of the cell layers. Example methods that may be appropriate are discussed further within

[82]. However, it must be noted that R_{DC} is an average value calculated from multiple discharge pulses whilst R_O is a measured resistance.

R_{DC}, R_O and capacity (in both 1C and C/3) all show linear degradation post testing regardless of orientation. In the investigations conducted in Chapter 5 and [82] there has been a significant difference in the performance of the different cell orientations. However, unlike these previous studies (where cells have had a separate vibration profile applied for each vehicle axis and the cells have been subsequently rotated on a rig to achieve the correct loading), this study has applied the vibration in a more representative manner where the all axis of vibration are applied simultaneously. Also, another explanation for this even loading with regard to R_{DC}, R_O and capacity is that cross axis motion (roll, pitch and yaw) are also applied within this experiment which is likely to accelerate damage within the cell assembly.

One observation from this study concerns the decrease in R_{CT}. As discussed in Section 6.4.6 given that the control samples also displayed a significant increase it is unlikely that this reduction is a result of vibration. It is possible that this is result of a specific characteristic of this sample of cells. It is therefore recommended that this is investigated further through forensic techniques. However, if a decrease in R_{CT} is confirmed within future testing of 18650 cells, it would indicate that vibration has the potential to improve the performance of this attribute. Furthermore, it may require an adaptive BMS strategy over the life of the battery assembly.

As observed within Section 5.6 the OCV shows no significant change post testing regardless of changes to the other measured attributes.

Within the mechanical characterisation of the cells, none of the cells showed a significant change in natural frequency. This supports the general finding of the electrical characterisation data, indicating that the vibration had minimal impact on the cells degradation. However, as highlighted in Section 6.4.7 the natural frequency of the cells was outside the capability of the shaker table used for the natural frequency assessment of the cells.

With regard to the change of amplitude of the cells it must be noted that a change in damping was observed indicating some change in the structural stiffness. However it must be noted that the accelerometer mounting collars remained attached to the cells for the duration of the test and it is entirely possible that the X60 adhesive may have degraded during the evaluation as this was the first test that this mounting methodology had been applied for the measurement of natural frequency.

Table 61 shows the ranked performance of each cell from the eight sets of characterisation data. Interestingly within this study there is some evidence of consistently poor performing cells when ranked per test. For example, ISR3005 (tested in the X orientation) is typically one of the best performing cells in all the assessments. Conversely ISR2999 (tested in the Y orientation) generally is the worst performing cell. There is also some mild correlation between the electrical characterisation performance and the change in amplitude which has not been

witnessed in any of the previous 18650 vibration durability studies presented in Chapter 5. Likely factors for an increase in the level of correlation within this test between electrical and characterisation methods are that; firstly the vibration within this study is applied in the time domain as opposed to using random a PSD which is applied in the frequency domain. The signals within this study are repeated regularly and are a replication of actual BEV battery measurements. The vibration spectra within the experiments defined in Chapter 5 are applied in a random nature within given spectral parameters which may result in a greater variation in degradation. Another factor which could be attributable to the cause of this improved correlation between mechanical and electrical testing is that the test items within this study are evaluated with respect to gravity. Within the investigations defined in Chapter 5 a single axis vertical shaker was used and the samples were rotated on the fixture to achieve the desired loading. Whilst this is industry practice, this methodology may result in unrepresentative loading as the effect of gravity is not considered. Finally, the vibration loading within this study was applied with 6DOF of movement. It is likely to be far more damaging due to the simultaneous axial loads than the experiments performed in Chapter 5. Within these studies the vibration for the three, major axis of vibration were applied sequentially.

Table 61: Comparison of Cell Performance Ranking by Post Test Assessment

		Electrical Characterisation						Mechanical Characterisation	
Cell	Orientation	Pulse Power Results Ranking	EIS Results Ranking R_o	EIS Results Ranking R_{CT}	OCV Results Ranking	Capacity Results Ranking 1C	Capacity Results Ranking C/3	Resonance Results - Frequency Ranking	Resonance Results - Amplitude Ranking
2991	Z	3	4	6	1	5	3	No change	4
2994	Z	2	3	4	2	3	4	No change	8
2996	Z	5	6	5	2	8	7	No change	6
2997	Y	8	9	7	9	3	5	No change	5
2998	Y	7	5	9	7	5	6	No change	2
2999	Y	4	1	8	2	1	2	No change	1
3000	X	6	7	1	2	7	8	No change	7
3001	X	1	2	3	2	2	1	No change	3
3005	X	9	8	2	7	8	9	No change	9

Ranking Key:

Greatest reduction in performance								Least reduction in performance
1	2	3	4	5	6	7	8	9

With respect to the performance of the cells with regard to in vehicle orientation, Table 62 presents a summary of each assessment for each potential packaging axis. The data illustrated in Table 62 suggests that there is no clear overriding orientation that is consistently worse with respect to degradation. What is noticeable

from this tabulated data set is that the effect is equal in a large section of the performance tests. This indicates that the cells are robust regardless of in vehicle packaging orientation.

Overall the characterisation results typically indicated that post vibration, a similar change in electrical performance was observed within the control samples. This indicates that the measured degradation was influenced to a greater extent by the laboratory conditions as opposed to the mechanical excitation of the applied vibration. This result is comparable to the results from the study on NCA cells presented in Section 5.5. However, given the combination of cross axial motions applied to the test samples within this experiment, it was assumed prior to testing that the effect of the vibration would be the most significant cause of degradation within this experiment.

Table 62: Assessment Ranking of Orientation by Test

Assessment	Test	Orientation Ranking By Assessment		
		Least Change	⇨	Greatest Change
Electrical Characterisation				
Pulse Power	6DOF	Y	X	Z
EIS (Ro)	6DOF	X = Y = Z		
EIS (R_{CT})	6DOF	Y = Z		X
OCV	6DOF	X = Y = Z		
Capacity - 1C Discharge	6DOF	Y	Z = X	
Capacity – C/3 Discharge	6DOF	X = Y = Z		
Mechanical Characterisation				
Resonance (Change in Frequency)	6DOF	X = Y = Z		
Resonance (Change in Amplitude)	6DOF	X	Z	Y

6.6.2 Comparison to Results from Previous 18650 NCA Study Chapter 5

Table 63 compares the measured average change with respect to axis of all NCA 18650 samples from this study and those evaluated to USABC Procedure 10 as defined in Section 5.5.

Table 63: Comparison of Change of NCA 18650 Cells Evaluated in 6DOF Vs. NCA 18650 Cells Evaluated to USABC Procedure 10 from Chapter 5. Samples Conditioned to 75% SOC

Orienta-tion	Test Profile	Pulse Power - Change in R_{DC} (mΩ)	EIS Change in R_O (mΩ)	EIS Change in R_{CT} (mΩ)	OCV - Change in Voltage (V)	Change in 1C Discharge Capacity (Ah)	Resonance Frequency - Change in Hz	Resonance Amplitude - Change in g_n
Z	USABC	1.88	1.53	1.06	0.000	-0.35	-6.00	-0.01
Z	6DOF	2.87	1.53	-2.12	-0.001	-0.06	0.00	0.11
X	USABC	2.17	1.72	0.06	0.000	-0.35	-108.67	0.22
X	6DOF	2.75	1.58	-0.59	-0.001	-0.06	0.00	0.08
Y	USABC	1.90	1.84	-0.04	0.000	-0.38	4.00	-0.04
Y	6DOF	2.52	1.49	-4.37	0.000	-0.06	0.00	0.50
Control	USABC	1.38	1.42	1.42	0.000	-0.35	N/A	N/A
Control	6DOF	1.02	1.59	-5.17	0.000	-0.13	N/A	N/A

Reviewing the results presented in Table 63, a comparable increase in R_O for each orientation regardless of testing regime was observed. Generally a greater degree of change in R_{DC} is observed within the samples that were evaluated using vibration in 6DOF. This could indicate an increase in damage to the contact area or cell tabs within the cell assembly due to the combined axial loading associated with this method of vibration testing. However as discussed within Section 6.6.1 further analysis is required on the samples that were evaluated in 6DOF to understand the difference between R_{DC} and R_O.

With regard to R_{CT} and capacity significant differences between the single axis assessment of USABC Procedure 10 and the 6DOF testing were observed. The R_{CT} of the cells assessed using a 6DOF vibration test methodology displayed a significant reduction in this attribute post testing. Given that this effect was also observed within the control sample, it is likely that this is due to specific electrode characteristic associated with this batch of 18650 NCA cells. It could also be a result in the environmental conditions that the cells were subjected to between characterisation and SOT or even during shipping. This hypothesis is supported by studies which have observed changes in electrical attributes of cells (including R_{CT}) as a result of calendar aging and storage trials [168-171].

The OCV data from both studies do not highlight any significant change irrespective of orientation or test methodology. The voltage difference recorded is within the tolerance of the error of the equipment. This supports the results presented in [80, 81] that also noted that OCV is not adversely affected by vibration loading.

Table 64 presents the packaging orientation ranking of the cells from the two studies. It is noticeable that there is little consistency between the two test methods with respect to the cell orientation. It is likely these differences are a result of the mechanical excitation and that the 6DOF test applies vibration with respect to gravity.

Table 64: Comparison of Orientation Results of Pansonic NCA vs – Note C/3 Discharge Omitted Due to only 1C Discharge being Performed within Chapter 5

Assessment	Test	Orientation Ranking By Assessment and Test Profile		
		Least Change	⇨	Greatest Change
Electrical Characterisation				
Pulse Power (R_{DC})	USABC Procedure 10	Z	Y	X
	6DOF	Y	X	Z
EIS (Ro)	USABC Procedure 10	Z	X	Y
	6DOF	X = Y= Z		
EIS (R_{CT})	USABC Procedure 10	Y	X	Z
	6DOF	Y	Z	X
OCV	USABC Procedure 10	X = Y= Z		
	6DOF	X = Y = Z		
Capacity - 1C Discharge	USABC Procedure 10	Z	X	Y
	6DOF	Y	Z = X	
Mechanical Characterisation				
Resonance (Change in Frequency)	USABC Procedure 10	Z	Y	X
	6DOF	X = Y = Z		
Resonance (Change in Amplitude)	USABC Procedure 10	Z	Y	X
	6DOF	X	Z	Y

6.6.3 Effect of Vibration in 6 DOF on Tesla Model S Module

The electrical performance of the Tesla module displayed little electrical degradation as a result of 6DOF vibration that was representative of 10 years of European customer use.

Table 65 presents the percentage change observed within the Tesla Model S module compared against the 18650 NCA cells evaluated in this study. The percentage change in R_{DC} and the capacity is far lower than that observed within the separate 18650 cells. As discussed in Section 6.5.2 the likely explanation for this observation is the damping provided by the casing, electrical isolation and the combined effect of the aggregated cells within the module assembly. The change in OCV is greater than that observed within the separate cells. Also given that it is still a small reduction of -0.12 % it is still not an indication of any significant effect of the applied vibration. However, because only one sample of Tesla Model S module was assessed within this study (due to the financial costs associated with sourcing multiple Tesla Model S modules), it cannot be concluded whether the observed changes are an effect of other laboratory conditions. As only one sample was evaluated the spread of the results cannot be determined. Therefore, it is recommended that future testing is conducted on additional samples (with a supporting control item) to confirm the results.

Table 65: Percentage Change of Tesla Module Compared Against 18650 Cells - Tested in 6DOF

Sample / Orientation	R_{DC} – Percentage Change (%)	OCV - Percentage Change (%)	Capacity at 1C - Percentage Change (%)	Capacity at C/3 - Percentage Change (%)
Tesla / Vehicle Orientation (Z)	2.73	-0.12	-0.12	-0.72
18650 NCA / Z	7.07	-0.03	-2.13	-2.32
18650 NCA / X	6.75	-0.02	-2.13	-2.20
18650 NCA / Y	6.19	0.00	-2.12	-2.63
18650 NCA /Control	2.45	-0.01	-4.13	-3.27

Another limitation of the testing is that the sample was not new and had been subjected to circa: 20,000 miles worth of battery cycles by JLR as part of a separate internal benchmarking and measurement study. This initial 20,000 miles worth of electrical and mechanical degradation, which may or may not be the greatest loss of performance within the total life of this component, is unaccounted for within these results. It is recommended that a future test is performed on new modules to validate the findings from this study.

The testing of the Tesla module has provided impact to the academic and industrial community through the development and execution of vibration durability tests on high energy BEV modules. This study has also proved that it is possible to accurately conduct impact excitation modal analysis on modules.

6.6.4 Implications for Vehicle Design

This study has provided additional evidence to suggest that the susceptibility of cells to vibration is technology dependant. This study has also provided evidence to suggest that the effect of vibration of cells is reduced when they are assembled into a module. This is due to the damping provided by the assembly and surrounding packaging.

One of the main findings from this 6DOF vibration study is that the effect of cell packaging orientation on this type of NCA cell has minimal impact of the degradation caused by vibration.

This study has highlighted that a difference of results between vibration evaluation methods can be observed between vibration durability methodologies. The 6DOF test was rated for 10 years European customer use and the sequential single axis USABC Procedure 10 test standard utilised in Section 5.5 is comparable to 100,000 miles of North American customer use. Relying on the results from just the single axis test may have highlighted issues (or a favourable cell orientation) that would have resulted in unnecessary cost implications to a vehicle development program. It is argued that the 6DOF test within this study is more realistic of the vibration environment that an BEV battery cell / assembly would be subjected to during its life

time. This is because the dynamic motion for the X-axis, Y-axis, Z-axis, roll, pitch and yaw are applied to the DUT simultaneously in the time domain. Also the test vibration is recorded from actual vehicle structural measurements, as opposed to the application of a compressed approximation of a combination of different vibration measurements in the form of a PSD. However it must also be highlighted for a true comparison between the studies defined in Chapter 5 and the 6DOF test, should be repeated for a 100,000 miles of proving ground durability as opposed to 10 years European customer use, which equates to 15,000 miles of proving ground durability.

6.7 **Conclusions**

This thesis presents the first study undertaken to determine the effects electromechanical excitation on 18650 cells and modules when exposed to multi-axis vibration in 6DOF. It has defined a new test methodology as well as safety practices that could be further employed by engineers and researchers investigating the durability of EV RESS to mechanical excitation. This findings and test methodology have also been published within [38]

This study has quantified the effect that vibration has on the electromechanical properties of NCA 18650 battery cells and a Tesla Model S 18650 battery module when applied in 6DOF. Both the electrical performance and the mechanical properties of the 18650 lithium-ion cells within this study typically showed no statistically significant degradation when subjected to multi axis vibration, representative of 10 years customer use. Furthermore, no particular cell orientation consistently displayed a significantly greater reduction in cell electromechanical performance. A statistically significant change in R_{DC} was observed post vibration testing on all NCA 18650's for all three cell orientations. The remainder of electrical attributes employed to characterise cell performance (capacity, R_O, R_{CT} and OCV) all indicate either no statistically significant change or a reduction in performance that may not be attributed directly to vibration loading of the cell. With regard to mechanical integrity, no significant external damage or electrolyte leakage was observed in any of the tested cells post vibration. No change in sample natural frequency was also observed. However, samples oriented in the Y-axis displayed a significant reduction in natural frequency amplitude post vibration indicating a possible change in cell stiffness.

With regard to the Tesla Model S module; the results indicate that vibration does not impact the electromechanical performance of this module design. Reductions in 1C and C/3 capacity discharge were 0.12 % and 0.72 % post testing, whilst OCV reductions were no greater than 0.12 %. However an increase in R_{DC} of 2.73 % was observed. A total of 10 modes were observed when the module was excited in the Z axis within the frequency range of 0 to 800 Hz. The first bending and torsion modes observed within the Tesla Module did not change between the SOT and EOT when excited in the Z-axis via impact excitation. Modes above 263 Hz post testing

typically reduced in frequency and damping post application of vibration. The first mode of the Tesla module was outside the range of road load excitation. This is also the first study to characterise a module via hammer survey modal analysis.

In conclusion, the results presented in this study highlight that this particular cell chemistry and design, one that is already being used or investigated by many leading vehicle manufacturers, is largely robust to vibration excitation that is commensurate with a typical 10-year European vehicle life when evaluated as a singular item and when assessed in a module configuration.

7 Reflective Review

The following Chapter is a reflective review of the research undertaken during this research programme. It defines the strengths of the studies undertaken and the opportunities for further work.

7.1 **Strengths of Research**

7.1.1 Strengths of Research Defining the In-Service Environment and Development of Test Standards

Via the methodology derived in Sections 3.3 and 6.3.4, in-vehicle vibration measurements from three contemporary BEV's products were synthesised to specific vehicle lives of 100,000 miles and 10 years of UK customer use. Unlike the previous research in this domain (presented in [27, 71]), this doctorate has provided a full break down of the synthesised test profile and the methodology in which it was generated. It also employed measurements from multiple different customer driving scenarios as opposed to relying on deriving a profile from a single highly damaging event (as undertaken within [71]). As well as enabling accurate durability testing of battery assemblies, this full disclosure of the provenance of the presented EV vibration durability profiles removes uncertainty from future studies wishing to validate a product for an A or C segment BEV application (for 100,000 miles UK durability). The developed profile from this study has a specific vibration profile for each of the three-major vehicle axis, overcoming the inaccuracies of contemporary standards which typically validate in just the Z-axis or via a single profile for the horizontal axis.

Another strength of the research is that the derived profile was utilised to determine how representative contemporary legislative and duty of care EV vibration test standards are for the determination of durability life. The presented process of comparing test standards via FDS and SRS has overcome the uncertainty and inaccuracies of comparing profiles by acceleration levels. It also allows swept sine and random profiles to be compared. Limitations of contemporary EV vibration procedures, from the perspective of durability evaluations have been identified. Subsequently recommendations for the development of future vibration durability tests have been defined. Many of the presented recommendations have been adopted by organisations such as the NHTSA / SAE within the development of their new future standards [172, 173]. Finally, the derived test profile and stages of the test profile development process have been published in [32-34].

Finally, this programme has applied the synthesised vibration profiles to durability tests of 18650 cells, to confirm their effectiveness as a method of determining the durability of EV components.

7.1.2 Strengths of Research Defining Natural Vibration Characteristics of EV Components

The studies undertaken to characterise the natural vibration characteristics of battery modules and cells have proven that hammer survey modal analysis techniques can successfully be applied to pouch cells and battery modules to determine their natural vibration characteristics. The studies presented within this thesis are also the first to fully define damping, stiffness, and mode shapes for each of the natural frequencies present from 0 to 800 Hz within pouch cells and a Tesla Model S module. Another significant strength of this research is that it is the first to quantify the changes in natural frequency, stiffness and damping of laminate pouch cells resulting from changes in charge state. The characterisation data from the modal analysis of laminate pouch cells, has also been made available to the wider academic community within [35].

7.1.3 Strengths of Research Defining the Vibration Durability Performance of EV Components via Both Single and Multi-Axis Techniques

This research has developed new repeatable test practises and underpinning methods to determine the durability of EV battery cells, module and pack assemblies. It has devised methodologies for conducting live cell and module tests on different EMS and hydraulic MAST systems and has developed risk assessments and safety protocols to abate identified hazards. Subsequently this research presents testing pathways and practical testing solutions which are transferable to other EV components or RESS devices. The presented data also supports the investigations by future engineers and researchers, wishing to characterise the effects of vibration on the reliability of future EV battery assemblies.

This study has also overcome issues associated with previous testing activities which undermined the accuracy of the test results. Firstly, all test fixtures employed during this study were characterised prior to testing in accordance with BS EN 60068 to ensure that they did not have any resonances within the test frequency range. In addition this research study defined the mounting condition of the test items and took significant care within the design of the test fixtures to ensure a representative in-vehicle mounting condition was replicated.

Unlike previous vibration studies ([8, 80-82, 90, 93]), a suite of electrical and mechanical measurements were undertaken at the start and end of test to fully characterise the effect of vibration on cell and module performance. Full data sets of the electrical and mechanical measurements have been made available to the wider research community through the publications presented in [36-38].

This doctorate contains the first study which fully defines a multi-axis vibration testing method and provides both electrical and mechanical data which determines how a Tesla Model S and 18650 NCA cells are affected by vibration that is commensurate with a 10 year UK life. It also provides evidence to suggest that the effect of vibration is likely to be technology dependant. However as discussed in

greater detail in Section 7.2, this is assertion requires additional investigation into the mechanical assembly of the cells evaluated via forensic techniques.

7.1.4 Other Strengths of Research

The results from this research programme provide further impact to academia and industry through collaborative studies with other researchers. Data from cell durability experiments have been used within studies investigating factors that cause aging within battery cells, as well as defining how external mechanisms influence the control parameters of battery management software. The findings of these collaborative studies have been published within [40] and [39] respectively.

Overall, this research has identified best in class engineering procedure with respect to conducting vibration measurement, characterisation and durability testing on EV RESS components. It provides impact by applying state-of-the-art vibration characterisation and testing techniques to the novel field of EV battery cells and modules, within a single research program

7.2 **Opportunities for Further Work**

Table 66 defines the work undertaken within this thesis.

Table 66: Summary of Research Undertaken and Areas for Further Investigation

Description	Defining the In-Service Environment	Natural Vibration Behaviour of EV Components	Vibration Durability	
			Single Axis Durability	Multi Axis Durability (6DOF)
Cells				
Cylindrical Cells (18560)		✓**	✓	✓
Pouch Cells		✓		
Prismatic Cells				
Modules				
Assembled from Cylindrical Cells (18560)		✓		✓
Assembled from Pouch Cells				
Assembled from Prismatic Cells				
Pack				
Assembled from Cylindrical Cells (18560)	✓*			
Assembled from Pouch Cells	✓*			
Assembled from Prismatic Cells	✓*			

Note:
*= Additional analysis presented in Table 67
**= Not defined via modal analysis

It highlights the gaps that exist in the existing knowledge with respect to the three key areas that are required to define the vibration durability of an EV RESS. Opportunities for further work in each of these areas are discussed in greater detail.

7.2.1 Opportunities for Further Work with Respect to Defining the In-Service Environment and Development of Test Standards

As highlighted in Section 3.6 the in-vehicle measurement data used within this study was derived from A and C segment vehicles. Whilst the experiments performed have illustrated trends with regard to the robustness of 18650 cells and modules, the conclusions with respect to the durability life can only be attributable to city and medium size cars. Table 67 illustrates the measurement data for the different pack constructions vs market segments.

Table 67: Summary of Vehicle Pack Type Measured by Vehicle Segment

Vehicle Segment Classification	Cylindrical Cell Pack	Pouch Cell Pack	Prismatic Cell Pack
A Segment Vehicles (City Cars)	✓		✓
B Segment Vehicles (Small Cars)			
C Segment Vehicles (Medium Cars)		✓	
D Segment Vehicles (Large Cars)			
E Segment Vehicles (Executive Cars)			
F Segment Vehicles (Luxury Vehicles)			
J Segment Vehicles (Sports Utility Vehicles and 4 x 4)			
M Segment Vehicles (Multi-Purpose Vehicles)			
S Segment Vehicles (Sports Cars)			

This table clearly illustrates that just for measurement data from the pack itself, there are 24 permutations of pack construction and vehicle segment that require measurement to be able to determine the variations in operational loading that a battery assembly could witness within a BEV application. The data collated within this study have been recorded from a small sample size of vehicles from the A and C classes. As a result the synthesised profiles may display some behaviour that is unique to the vehicles or vehicle class that may not be suitable for RESS destined for larger vehicles such as SUV's or luxury products. Therefore, it is recommended to perform a future measurement study with a larger fleet size of different evaluation vehicles from different vehicle classes. This fleet should also include HEV so that the differences in vibration loading associated with the typical battery locations

associated with these products can be defined and understood. In addition, an opportunity exists for a study to focus if there are differences, if any, between the batteries installed in HEV application compared to that in a BEV function.

The road load data utilised in this investigation evaluated the vibration experienced by the battery casing of three current production BEV's when subjected to a range of proving ground surfaces. Whilst these measurement locations will undoubtedly support the development of future standards and test methods, an understanding of the internal vibration conditions of the battery assembly could be used to improve EV cell standards. Therefore it is recommended that a future study is performed where accelerometers are placed upon the internal components (such as cells and bus bars) of RESS and the response of these items to proving ground durability surfaces are recorded.

The main limitation of the derived profiles is that they use surface weightings based on an adapted ICEV structural durability schedule. Whilst it could be argued that future BEV usage will be comparable to that of ICEV customers due to improvements in product range, a study does need to be performed that determines the exact 90^{th} percentile customer usage for EV's and that fully defines the acceleration loading with regard to discreet events to eliminate uncertainty from the processing method.

Further, this study has focused on European usage, and has not considered the implications of different markets on the durability requirements for RESS. Therefore it would be beneficial if future surface weightings also considered regional variances with regard to measured accelerations and customer usage.

This study focused on deriving a set of vibration profiles that could be performed on a wide range of shaker systems. Subsequently the derived profiles applied vibration within the frequency range of 5 to 200 Hz. It may be beneficial to perform an additional set of synthesised profiles that define spectra outside of this bandwidth so that the DUT could be excited at frequencies below 5 Hz and above 200 Hz on suitable facilities.

The critical review of standards highlighted that an opportunity exists for a standard to be developed that in a single rig based test combines vibration, dynamic charge discharge (such as that from a legislative drive cycle) and climatic cycling. However further vehicle data and research is required to determine how these different ageing mechanisms interact to allow for suitable time compression of these attributes within a single test.

7.2.2 Opportunities for Further Work with Regard to Defining Natural Vibration Characteristics of EV Components

To reaffirm the results presented it is necessary to do further tests. These tests will evaluate the same cell for different SOC values. This would highlight any possible relationship between SOC and natural frequency without the impact of cell-to-cell

variations introducing uncertainty to the results obtained. While this initial study focused on the SOC range of 10 % - 90 %, a further study will characterise the cell at the extremes of operation that will be experienced within an EV, namely less than 10 % SOC and greater than 90 % SOC. Introducing temperature as another variable to the experimental set-up that could yield interesting results for the vehicle manufacturer or battery systems integrator. While this study has concluded that there is little evidence to suggest that SOC impacts the frequency response of a NMC 25 Ah laminate pouch cell, further investigation is required to identify if these results are transferable to other cell chemistries and form-factors currently being investigated by the automotive industry. As discussed in Section 4.6, a further investigation should be undertaken to determine the vibration witnessed by cells when a battery enclosure is excited by either road induced vibration or on-board ancillaries within a BEV or HEV. For such a study, a grounded (rather than a free-free) test method may be more appropriate since this will allow the evaluation of the cell within the correct orientation and restraint for the battery pack design under investigation.

With regard to the modal analysis of modules, further modal analysis work into other types of EV module construction methods, such as those employing cylindrical and prismatic cells should be conducted. This would help obtain a wider understanding of the natural vibration characteristics of these assemblies. This would ultimately help improve FEA modelling and would increase the knowledge of vibration behaviour of module and battery assemblies employed within the automotive industry. Currently there is limited peer reviewed data to quantify the results of FEA modelling, which must be validated by physical testing to determine their accuracy of simulating the real-world environment.

7.2.3 Opportunities for Further work with Respect to Vibration Durability Testing of EV Components via Both Single and Multi-Axis Techniques

One of the limitations of the methodology employed within the studies presented in Chapters 5 and 6 is that electrical and mechanical characterisation data was only measured at SOT and EOT. As a result, no discussion or conclusions can be made about the rate of degradation throughout the vehicle's life. It is recommended that a future study should characterise the cells at intermediate points during the test programme, e.g. intervals that are representative of 10,000 miles / 1 year of vehicle use. Not only would this facilitate further investigation into both the absolute value of degradation, but also the expected in-service rate of capacity and power fade over the life of the vehicle.

The electromechanical condition and assembly of the cells after EOT characterisation should be assessed using novel cell imaging and autopsy methods, as discussed within [40, 82]. This is firstly to quantify the changes that occur within the material composition and structure of the cell post vibration and also to determine why the cells from this study displayed significantly less degradation than

the cell technology evaluated within [82]. Whilst initial investigations have been conducted into the effects of vibration on the surface films of the NMC cells subjected to the USABC Procedure 10 profiles by Somerville et al. [40] additional investigations on the aging effects at a electrochemical level should be performed on NCA samples evaluated within the single and multi-axis studies to determine the cause of the reduction in R_{DC} and improvement in R_{CT} witnessed.

Whilst there is evidence within this study to suggest that NCA chemistry cells are more resilient to vibration than NMC, it would be undesirable to make this conclusion as this study does not consider the variability of different manufacturing and assembly processes employed by the two different cell suppliers (such as the binder, the film thickness etc.), which could impact the cell vibration performance. Therefore the author proposes a future study in which cells of different chemistries are selected from the same manufacturer and are assessed when subjected to the same vibration durability conditions. However it must be noted that it will be challenging within this proposed study to make any definitive conclusions, since cell manufacturers rarely fully disclosed their manufacturing processes. Therefore it is also recommended that a further experiment is conducted using cells that have been specially manufactured by a specialist cell fabricator so that data on cells with a known construction provenance can be obtained.

With respect to the single axis testing defined in Chapter 5, the durability assessment was conducted using a single axis EMS. As a result, the cells were not tested with respect to gravity. This could have caused unrepresentative loading due to the effects of mass loading associated with rotating the samples on the durability fixture. It is therefore recommended that future single axis experiments are conducted using either a MAST or single axis shaker with slip table capability.

Within the study presented in Chapter 6, only one Tesla module was evaluated. Also this item had undergone 20,000 miles of evaluation miles within a vehicle prior to the vibration test. Therefore it is plausible that the initial 20,000 miles worth of electrical and mechanical degradation (which may or may not be the greatest loss of performance) was unaccounted for within the results presented. It is recommended that a future test is performed on new modules to validate the findings from this study. In addition, this study only evaluated one Tesla module and did not allocate a control sample. Subsequently the spread and confidence of the observed findings cannot be fully substantiated at this time. Therefore it is recommended a repeat test is performed on multiple samples of the same module design.

8 Conclusions

This research programme has provided new knowledge that allows manufacturers to understand the effect of vibration on the mechanical durability and performance of contemporary EV cells forms.

Knowledge of how the durability of battery assemblies are affected by vibration was generated through investigations within three areas that define the impact of vibration on the durability on EV components. Firstly the research focused on quantifying the “in-service” vibration environment of BEV RESS assemblies. This was attained through the analysis of vibration measurements from contemporary BEV products and current state of the art legislative and best practice test standards. This study subsequently defined a new vibration test profile for single axis vibration testing which is representative of 100,000 miles of UK BEV durability and is suitable for the evaluation of A and C segment vehicles. Unlike contemporary standards this profile was derived from real world BEV measurements and BEV customer usage data. The derived profile and methodology employed to synthesise this new test method are published within [32-34]. It has also been adopted by the sponsoring organisation within the Catapult Test Procedure CAT-C-140 [102]. The recommendations and knowledge from this study have supported the development of future federal homologation tests [172]. Innovation has been provided to industry and academia through the delivery of a new vibration profile which provides engineers and researchers with a repeatable life representative test method for vibration durability evaluations.

The second aim was to determine the natural vibration and modal response behaviour of EV RESS components. This was to understand their behaviour to vibration excitation and to ultimately provide characterisation data to assist the development of CAE models. This aim was accomplished through the application of state of the art modal analysis techniques to characterise the mechanical behaviour of lithium-ion pouch cells and a Tesla model S module. This novel testing practice also defined the effect of SOC on the stiffness, damping, natural frequencies and mode shapes of the lithium-ion pouch cells. The data sets from these studies have been utilised by JLR in the mechanical modelling of EV battery assemblies and have been made available to the wider research community via the publication [35]. This was also the first study to fully define the natural vibration characteristics and the associated mechanical properties of battery cells and modules, via modal analysis techniques.

The final aim was to determine the durability behaviour of EV components and assemblies by subjecting them to vibration that is representative of a 100,000 miles or 10 years durability to define the resulting changes in performance characteristics. This was accomplished by investigating the effect of vibration on the electromechanical performance of two different lithium-ion chemistries of 18650 cells, and a Tesla Model S module. Statistically significant electromechanical

degradation from vibration applied via both uniaxial and multiaxial techniques for both of 100,000 miles and 10 years of customer use. The effect of SOC and cell packaging orientation on the susceptibility of the 18650 cell form to vibration was also ascertained. Prior to these investigations, published research had failed to correlate electrical and mechanical decay resulting from vibration excitation, in both cells and modules, to vehicle mileage or service life. These are the first studies to characterise the effect that vibration has on the performance of 18650 cells and a module, when excited using 6DOF excitation techniques. The results from these studies have been published within [36-38].

As well as providing mechanical and electrical data on the effect that vibration has on cells and modules, this research has provided further innovation through the definition of practical requirements with respect to vibration durability assessments. It has identified industry best practice with regard to the design, fabrication and assessment of vibration fixtures, and presents health and safety requirements for conducting HV battery vibration on modern shaker table facilities. The testing practices developed during this research programme have been published within [32-37, 39, 40] and have been adopted by the sponsoring organisation and MPG.

In summary, the research presented within this thesis provides knowledge and novel testing techniques that allow manufacturers to understand the durability performance of EV battery assemblies, with respect to the effects of vibration. It provides transferable methodology for conducting durability and characterisation testing of a RESS and their associated components. In addition, it provides quantification of physical behaviour in areas of battery research where only a qualitative understanding previously existed. It provides impact to both the sponsoring organisation and the wider UK automotive industry through the provision of vibration characterisation data sets and new evaluation procedures.

9 References

1. Parry-Jones, R., *Driving Success – A Strategy for Growth and Sustainability in the UK Automotive Sector*. 2013, Automotive Council UK: 1 Victoria Street, London, SW1H 0ET. p. 1-87.
2. Ikezoe, M., Hirata, N., Amemiya, C., Miyamoto, T., Watanabe, Y., Hirai, T., and Sasaki, T., *Development of High Capacity Lithium- Ion Battery for NISSAN LEAF (2012-01-0664).* SAE International, 2012(2012-01-0664): p. 1-7.
3. Dodds, C., *Structural Testing of Complete Vehicles , Aggregates and Components in the Laboratory*. 2007, Dodds and Associates: Edinburgh, Scotland. p. 1-103.
4. Dasgupta, A., Choi, C., and Habtour, E., *Simulation and Test Vibration - Nonlinear Dynamic Effects in Vibration Durability of Electronic Systems*, in *8th International Conference on Integrated Power Systems*. 2014, University of Maryland, College Park, MD 20742, USA: Nuremberg, Germany.
5. Halfpenny, A., *Methods for Accelerating Dynamic Durability Tests*, in *9th International Conference on Recent Advances in Structural Dynamics*. 2006: Southamption. p. 1-19.
6. Avdeev, I. and Gilaki, M., *Structural Analysis and Experimental Characterization of Cylindrical Lithium-ion Battery Cells Subject to Lateral Impact.* Journal of Power Sources, 2014. **271**: p. 382-391.
7. Zhang, X. and Wierzbicki, T., *Characterization of Plasticity and Fracture of Shell Casing of Lithium-ion Cylindrical Battery.* Journal of Power Sources, 2015. **280**: p. 47-56.
8. Choi, H.Y., Lee, J.S., Kim, Y.M., and Kim, H., *A Study on Mechanical Characteristics of Lithium-Polymer Pouch Cell Battery for Electric Vehicle*. 2013, Hongik University: Seoul, South Korea. p. 1-10.
9. Berla, L., Woo Lee, S., Cui, Y., and Nix , W., *Mechanical Behavior of Electrochemically Lithiated Silicon.* Journal of Power Sources, 2015. **273**: p. 41-51.
10. Greve, L. and Fehrenbach, C., *Mechanical Testing and Macro-Mechanical Finite Element Simulation of the Deformation, Fracture, and Short Circuit Initiation of Cylindrical Lithium-ion Battery Cells.* Journal of Power Sources, 2012. **214**: p. 377-385.
11. Oh, K.-Y., Siegel, J., Secondo, L., Kim, S.U., Samad, N., Qin, J., Anderson, D., Garikipati, K., Knobloch, A., Epureanu, B., Monroe, C., and Stefanopoulou, A., *Rate Dependence of Swelling in Lithium-ion Cells.* Journal of Power Sources, 2014. **267**: p. 197-202.
12. Sahraei, E., Meiera, J., and Wierzbicki, T., *Characterizing and Modeling Mechanical Properties and Onset of Short Circuit for Three Types of Lithium-ion Pouch Cells.* Journal of Power Sources, 2014. **247**: p. 503-516.
13. Feng, X., Sun, J., Ouyang, M., Wang, F., He, X., Lu, L., and Peng, H., *Characterization of Penetration Induced Thermal Runaway Propagation Process within a Large Format Lithium-ion Battery Module.* Journal of Power Sources, 2015. **275**: p. 261-273.
14. Liu, X., Stoliarov, S., Denlinger, M., Masias, A., and Snyder, K., *Comprehensive Calorimetry of the Thermally-Induced Failure of a Lithium-ion Battery.* Journal of Power Sources, 2015. **280**: p. 516-525.

15. Spinner, N., Field, C., Hammond, M., Williams, B., Myers, K., Lubrano, A., Rose-Pehrsson, S., and Tuttle, S., *Physical and Chemical Analysis of Lithium-ion Battery Cell-to-Cell Failure Events Inside Custom Fire Chamber.* Journal of Power Sources, 2015. **279**: p. 713-721.
16. United Nations, *ECE R100 - Battery Electric Vehicles with Regard to Specific Requirements for the Construction, Functional Safety and Hydrogen,* 2002, United Nations,
17. Economic and Social Council *Proposal for the 02 series of amendments to Regulation No. 100 (Battery electric vehicle safety),* ECE/TRANS/WP.29/2012/102, 2013, Economic and Social Council 1-54
18. *The Tests Explained*. 2015 [cited 2015 9th February 2015]; Available from: http://www.euroncap.com/testprocedures.aspx.
19. United Nations, *Transport of Dangerous Goods - Manual of Tests and Criteria - Fifth Edition - Amendment 1,* 2011, United Nations, New York, 62
20. Somerville, L., *Submission 1: A Gentle Introduction Followed by a Very Practical Approach to Ageing of Lithium-ion Cells*. 2013, WMG: University of Warwick. p. 1-65.
21. Svens, P., Lindstrom, J., Gelin, O., Behm, M., and Lindbergh, G., *Novel Field Test Equipment for Lithium-Ion Batteries in Hybrid Electrical Vehicle Applications.* Energies, 2011. **4**: p. 741-757.
22. Cropley, S., *UK Car Manufacturing Hits 17-Year High - JLR and Nissan Rank Top*, in *Autocar*. 2017, Haymarket: Twickenham, UK.
23. Goss, A. *Jaguar Land Rover is Britain's Biggest Car Manufacturer for a Second Year*. 2017 [cited 2017 7th June 2017]; Available from: http://www.jaguarlandrover.com/news/2017/01/jaguar-land-rover-britains-biggest-car-manufacturer-second-year.
24. Saunders, M., *Jaguar I-Pace: First Drive of Electric SUV Concept*, in *Autocar*. 2017, Haymarket: Twickenham, UK. p. 26-31.
25. Wilkinson, L., *Range Rover Hybrid Review* in *The Telegraph*. 2013, Telegraph Media Group: London, SW1W 0DT, UK.
26. Hooper, J., *Study into the Vibration Inputs of Electric Vehicle Batteries*, in *School of Engineering*. 2012, Cranfield University: Cranfield University. p. 1-116.
27. Martin, D., Hiebl, A., and Krueger, L., *Electromobility - Challenges for Structural Durability.* Materialwissenschaft und Werkstofftechnik, 2011. **42**(10): p. 958-963.
28. Risam, G.S., Balakrishnan, S., Patil, M.G., Kharul, R., and Antonio, S., *Methodology for Accelerated Vibration Durability Test on Electrodynamic Shaker (2006-32-0081).* SAE International, 2006. **1**: p. 1-9.
29. Shafiullah, A.K.M.W., Christine Q;, *Generation and Validation of Loading Profiles for Highly Accelerated Durability Tests of Ground Vehicle Components.* Engineering Failure Analysis, 2013. **33**: p. 1-16.
30. Lei, B., Li, X., Liu, Z., Morisset, C., and Stolz, V., *Robustness Testing for Software Components.* Science of Computer Programming, 2010. **75**: p. 879-897.
31. Winter, R., *Handbook for Robustness Validation of Automotive Electrical/Electronic Modules*. 2013, Frankfurt, Germany: German Electrical and Electronic Manufacturers‘ Association. 130.

32. Hooper, J. and Marco, J., *Characterising the in-Vehicle Vibration Inputs to the High Voltage Battery of an Electric Vehicle.* Journal of Power Sources, 2014. **245**: p. 510-519.
33. Hooper, J. and Marco, J., *Defining a Representative Vibration Durability Test for Electric Vehicle (EV) Rechargeable Energy Storage Systems (RESS)*, in *Electric Vehicle Show 29 (EVS29)*. 2016, EVS29: Montreal, Canada. p. 1-6.
34. Hooper, J. and Marco, J., *Understanding Vibration Frequencies Experienced by Electric Vehicle Batteries*, in *HEVC 2013 - 4th Hybrid and Electric Vehicles Conference*. 2013, IET: London, England. p. 1-6.
35. Hooper, J. and Marco, J., *Experimental Modal Analysis of Lithium-ion Pouch Cells.* Journal of Power Sources, 2015(285 (2015)): p. 247 to 259.
36. Hooper, J., Marco, J., Chouchelamane, G., and Lyness, C., *Vibration Durability Testing of Nickel Manganese Cobalt Oxide (NMC) Lithium-Ion 18650 Battery Cells.* Energies, 2016. **9**(52): p. 27.
37. Hooper, J., Marco, J., Chouchelamane, G., Lyness, C., and Taylor, J., *Vibration Durability Testing of Nickel Cobalt Aluminum Oxide (NCA) Lithium-Ion 18650 Battery Cells.* Energies, 2016. **9**(281): p. 1-18.
38. Hooper, J., Marco, J., Chouchelamane, G., Chevalier, J., and Williams, D., *Multi-Axis Vibration Durability Testing of Lithium ion 18650 NCA Cylindrical Cells.* Journal of Energy Storage, 2018(15): p. 103–123.
39. Bruen, T., Hooper, J., Marco, J., Gama, M., and Chouchelamane, G., *Analysis of a Battery Management System (BMS), Control Strategy for Vibration Aged Nickel, Manganese Cobalt Oxide (NMC) Lithium-Ion 18650, Battery Cells.* Energies, 2016. **9**(255): p. 1-20.
40. Somerville, L., Hooper, J., Marco, J., McGordon, A., Lyness, C., Walker, M., and Jennings, P., *Impact of Vibration on the Surface Film of Lithium-Ion Cells.* Energies, 2017. **10**(741): p. 1-12.
41. Society of Automotive Engineers International, *SAE J670e Vehicle Dynamics Terminology* 2008, Society of Automotive Engineers International, Warrendale, PA, 1-74
42. Harrison, T., *An Introduction to Vibration Testing*. 2014, Naerum, Denmark: Bruel and Kjaer Sound and Vibration Measurement 11.
43. Harrison, T., *Sine Vibration Theory*. 2014, Naerum, Denmark: Bruel and Kjaer Sound and Vibration Measurement. 27.
44. Harrison, T., *Random Vibration Theory*. 2014, Naerum Denmark: Bruel and Kjaer Sound and Vibration Measurement.
45. Hooper, J., *Vibration Durability Testing and Aging of Lithium Nickel Manganese Cobalt Oxide (NMC) Lithium Ion 18650 Cylindrical Cells*, in *Vehicle Electrification and Energy Storage*. 2015, University of Warwick: Coventry, Warwickshire, UK. p. 244.
46. *QC/T 743-2006 - Lithium-ion Batteries for Electric Vehicles* 2006,
47. International Electrotechnical Commission, *IEC 62281: Safety of Primary and Secondary Lithium Cells and Batteries During Transport,* IEC62281, 2012, International Electrotechnical Commission, Geneva, Switzerland, 33
48. International Electrotechnical Commission, *IEC 62133: Secondary Cells and Batteries Containing Alkaline or Other non-Acid Electrolytes - Safety Requirements for Portable Sealed Secondary Cells, and for Batteries Made from them, for use in Portable Applications,* 2012, International Electrotechnical Commission, Geneva, Switzerland,

49. United States Advanced Battery Consortium, *Electric Vehicle Battery Test Procedures Manual,* 1996, United States Advanced Battery Consortium, 129
50. Institute of Electrical and Electronics Engineers, *IEEE 1625-2008: IEEE Standard for Rechargeable Batteries for Multi-Cell Mobile Computing Devices* IEEE 1625, 2008, Institute of Electrical and Electronics Engineers, New Jersey, USA,
51. Institute of Electrical and Electronics Engineers, *IEEE 1725-2011: IEEE Standard for Rechargeable Batteries for Cellular Telephones* IEEE 1725, 2011, Institute of Electrical and Electronics Engineers, New Jersey, USA,
52. Sandia National Laboratories, *SAND2005-3123 - FreedomCAR Electrical Energy Storage System Abuse Test Manual for Electric and Hybrid Electric Vehicle Applications,* 2006, Sandia National Laboratories, California 94550, 1-47
53. Underwriters Laboratories, *UL1642 - Lithium Batteries,* 2009, Underwriters Laboratories, 1-30
54. Underwriters Laboratories, *UL2580: Standard for Batteries for Use in Electric Vehicles,* UL2580, 2011, Underwriters Laboratories,
55. Underwriters Laboratory, *UL2054 - Household and Commercial Batteries,* 2009, Underwriters Laboratory, 1-46
56. Underwriters Laboratory *UL2271: Batteries for Use in Light Electric Vehicle (LEV) Applications* UL2271, 2010, Underwriters Laboratory
57. United Nations, *Recommendations on the Transport of Dangerous Goods,* UN38.3, United Nations, 44-51
58. United Nations, *Recommendations on the Transportation of Dangerous Goods - Manual of Tests and Criteria - Fourth Edition,* UN38.3, 2008, United Nations, 43 to 51
59. Battery Saftey Organisation, *BATSO 01: Manual for the Evaluation of Energy Systems for Light Electric Vehicles - LEV - Secondary Lithium Batteries,* BATSO 01, 2011, Battery Saftey Organisation, Berlin, Germany, 41
60. Society of Automotive Engineers, *J2380: Vibration Testing of Electric Vehicle Batteries,* J2380, 2009, Society of Automotive Engineers, Warrendale, PA, 1-7
61. Society of Automotive Engineers, *J2380: Vibration Testing of Electric Vehicle Batteries,* J2380-12, 2013, Society of Automotive Engineers, Warrendale, USA, 1-7
62. Society of Automotive Engineers, *J2929: Safety Standard for Electric and Hybrid Vehicle Propulsion Battery Systems Utilizing Lithium-based Rechargeable Cells,* (SAE J2929-2013), 2013, Society of Automotive Engineers, Warrendale, USA,
63. British Standard, *BS 62660-2:2011: Secondary Lithium-ion Cells for the Propulsion of Electric Road Vehicles. Reliability and Abuse Testing (British Standard),* BS 62660-2:2011, 2011, British Standard, London, UK,
64. Automotive Industry Standards (AIS), *AIS-048: Battery Operated Vehicles - Safety Requirements of Traction Batteries,* AIS 048, 2009, Automotive Industry Standards (AIS), India, 18
65. ANSI & NEMA, *American National Standard – for Portable Rechargable Cells and Batteries - ANSI C18.2m Part 2 – 2007,* 2007, ANSI & NEMA, Rosslyn, VA, USA, 51

66. British Standards, *BS ISO 12405-2:2012 -Electrically Propelled Road Vehicles — Test Specification for Lithium-ion Traction Battery Packs and Systems Part 2: High-Energy Applications,* 2012, British Standards, 1-60
67. Japanese Industrial Standards, *JIS C 8714:2007: Safety Tests for Portable Lithium-ion Secondary Cells and Batteries for use in Portable Electronic Applications* JIS C 8714, 2007, Japanese Industrial Standards,
68. Underwriters Laboratories, *UL1642 (Fifth Edition): Lithium Batteries,* UL1642, 2012, Underwriters Laboratories, 31
69. Ministry of Industry and Information Technology of the Peoples Republic of China, *GB/T 31486-2015 - Electrical Performance Requirements and Test Methods for Traction Batteries of Electric Vehicles* 2015, Ministry of Industry and Information Technology of the Peoples Republic of China, Peoples Republic of China, 1-9
70. Hooper, J., *Definition of a New EV RESS Vibration Durability Test Via a Critical Review of Current Test Standards*, in *Vehicle Electrification and Energy Storage*. 2016, University of Warwick: University or Warwick, Coventry, CV4 7AL. p. 108.
71. Kjell, G. and Lang, J.F., *Comparing Different Vibration Tests Proposed for li-ion Batteries with Vibration Measurement in an Electric Vehicle*, in *EVS27*. 2013, e of Sweden, Dept of Structural and Solid Mechanics: Barcelona, Spain. p. 1-11.
72. British Standards, *BS ISO 12405-1:2011 - Electrically Propelled Road vehicles - Test Specification for Lithium-ion Traction Battery Packs and Systems - Part 1: High-Power Applications* BS 12405-1:2011, 2011, British Standards, London, England,
73. Moore, *UN38.3 Lithium-ion Battery Testing - Vibration and Shock Testing Requirements*. 2008, UN Informal Working Group Meeting: Washington, DC, USA.
74. International Electrotechnical Commission, *IEC 60068-2-64:2008 - Vibration Broadband Random and Guidance,* IEC 60068-2-64:200, 2008, International Electrotechnical Commission, Geneva, Switzerland, 39
75. Lee, J.H., Mok Lee, H., and Ahn, S., *Battery Dimensional Changes Occurring During Charge/Discharge Cycles—Thin Rectangular Lithium-ion and Polymer Cells.* Journal of Power Sources, 2003: p. 833–837.
76. Siegel, J., Stefanopoulou, A., Hagans, P., Ding, Y., and Gorsich, D., *Expansion of Lithium Ion Pouch Cell Batteries: Observations from Neutron Imaging.* Journal of The Electrochemical Society, 2013. **160**(8): p. A1031-A1038.
77. Pohl, D., *Lithium Iron Phospahate: What Factors Influence the Durability of Storage Systems*, in *Solar Energy Storage*, A. Levran, Editor. 2014.
78. Suttman, A., *Lithium Ion Battery Aging Experiments and Algorithm Development for Life Estimation*. 2011, The Ohio State University: Ohio, USA. p. 122.
79. Kleiner, K., Dixon, D., Jakes, P., Melke, J., Yavuz, M., Roth, C., Nikolowski, K., Liebau, V., and Ehrenberg, H., *Fatigue of LiNi0.8Co0.15Al0.05O2 in Commercial Li-ion Batteries.* Journal of Power Sources, 2015. **273**: p. 41-51.
80. Chapin, J.T., Alvin, W., and Carl, W., *Study of Aging Effects on Safety of 18650-Type LiCoOx Cells*. 2011, Underwriters Laboratory Inc.: Northbrook, Illinois, US.

81. Wu, A., *Study on Aging Effects on Safety of 18650 Type LICOOX Cells*. Product Safety Engineering Society / UL.
82. Brand, M., Schuster, S., Bach, T., Fleder, E., Stelz, M., Glaser, S., Muller, J., Sextl, G., and Jossen, A., *Effects of Vibrations and Shocks on Lithium-ion Cells.* Journal of Power Sources, 2015(288): p. 62-69.
83. Svens, P., *Methods for Testing and Analyzing Lithium-Ion Battery Cells intended for Heavy-Duty Hybrid Electric Vehicles*, in *Department of Chemical Engineering and Technology*. 2014, KTH Royal Institute of Technology: Stockholm, Sweden. p. 87.
84. Flodberg, G. and Gällstedt, M. *Barrier Lab*. 2015 [cited 2015 19th March 2015]; Available from: http://www.innventia.com/en/Our-Ways-of-Working/Measurement-and-testing/Packaging-and-materials-testing/The-barrier-lab/.
85. ASTM International, *F1249-06(2011): Standard Test Method for Water Vapor Transmission Rate Through Plastic Film and Sheeting Using a Modulated Infrared Sensor,* F1249-06(2011), 2006, ASTM International,
86. Ball, R., *CAT-P-096-A-Nissan Leaf Battery tear-down*. 2013, WMG, University of Warwick: University of Warwick, Coventry. p. 1-25.
87. Ratnakumar, B., Smart, M., Ewell, R., Whitcanack, L., Chin, K., and Surampudi, S., *Lithium-Ion Rechargeable Batteries on Mars Rovers*, in *2nd International Energy Conversion Engineering Conference*. 2004, American Institute of Aeronautics and Astronautics.
88. Hong, S.-K., Epureanu, B., and Castanier, M., *Parametric Reduced-Order Models of Battery Pack Vibration Including Structural Variation and Pre-Stress Effects (2013-01-2006).* SAE International, 2013. **1**(2013-01-2006): p. 1-12.
89. Coe, S., *Fixtures for Vibration Testing*. 2013, Data Physics: Hailsham, East Sussex, UK. p. 1-47.
90. Kelty, K., *Tesla - The Battery Technology Behind the Wheel*. 2008, Tesla Motors: Palo Alto, CA. p. 1-41.
91. Preistley, N., *Vibration Testing of Batteries.* Environmental Engineering, 1992. **5**(4): p. 8-11.
92. Ye, B. and Zhang, S., *Modeling and Analysis of the Battery Packs and Modules in A123 Systems*. 2012, A123. p. 1-25.
93. Choi, Y., Jung, D., Ham, K., and Bae, S., *A Study on the Accelerated Vibration Endurance Tests for Battery Fixing Bracket in Electrically Driven Vehicles.* Procedia Engineering, 2011. **10**: p. 851-856.
94. Lu, G.-Y., *Random Frequency Response Analysis of Battery Systems Using 'Virtual Shaker Table' (2011-01-0665).* SAE International, 2011(1): p. 1-5.
95. Halfpenny, A., *Accelerated Vibration Testing Based on Fatigue Damage Spectra.* nCode International, www. ncode. com: p. 1-9.
96. Wynn, A. *Reliability and Safety of New Electric Vehicle Technology is put to the Test at Millbrook*. 2014 [cited 2014 20th March 2014]; Available from: http://www.renewableenergyfocus.com/view/36222/reliability-and-safety-of-new-electric-vehicle-technology-is-put-to-the-test-at-millbrook/.
97. Marchington, E., *Electric Vehicle Regulatory Reference Guide (Draft 1)*. 2013, United Nations Economic Commission for Europe: 7th Electric Vehicles and the Environment (EVE) Informal Working Group (IWG) meeting, 17th October 2013, Beijing, China. p. 36.

98. The California Air Resources Board (ARB), *Zero-Emission Vehicle Standards for 2009 Through 2017 Model Year Passenger Cars, Light Duty Trucks and Medium-Durty Vehicles,* 2012, The California Air Resources Board (ARB), California, USA, 1-32
99. *Same Difference*, in *Environmental Engineering*. 2013, Concorde Publishing Ltd London, UK. p. 30-32.
100. Fisher, G., Grubisic, V., Gu, B.L., Lu, S.C., and Li, M., *Determination of Design and Test Spectra for Vehicle Components Under Operational Conditions in China*, in *Proc. 25th. FISITA Congress*. 1994, FISITA: Beijing, China.
101. Sener, A.S., *Determination of Vehicle Components Fatigue Life Based on FEA Methods and Experimental Analysis.* Internation Journal of Electronics, Mechanical and Mechatornics Engineering, (1): p. 133-145.
102. Hooper, J., *Study into the Effect of Vibration*. 2014, WMG: Warwick University, Coventry, England. p. 34.
103. Harrison, T., *"Dos and Don'ts" in Vibration Testing*. Vibration Testing Vol. 18. 2014, Naerum, Denmark: Bruel and Kjaer Sound and Vibration Measurement. 35.
104. Sujatha, C., *Vibration and Acoustics*. 1st ed. 2010, Dehli, India: Tata McGraw Hill Education Private Ltd. 513.
105. Hooper, J., *Experimental Modal Analysis of Lithium Nickel Manganese Cobalt Oxide (NMC) Laminate Pouch Cells*, in *Vehicle Electrification and Energy Storage*. 2015, University of Warwick: Coventry, Warwick, CV4 7AL. p. 117.
106. Bilošová, A., *Modal Testing*. 2011, Investments in Education Development. p. 1-120.
107. Coe, S., *Vibration and Signal Processing*. 2006, Data Physics: Hailsham, East Sussex, UK. p. 1-33.
108. Burgess, A., *Transient Response of Mechanical Structures Using Modal Analysis Techniques*, in *Department of Mechanical Engineering*. 1988, Imperial College London: London.
109. Meade, M. and Dillon, C., *Signals and Systems*. 2nd ed, ed. G. Bloodworth, A. Dorey, and J. Fidler. 1994, London, UK: Chapman and Hall. 167.
110. *The Cube*. 2015 [cited 2015 30th March 2015]; Available from: http://www.teamcorporation.com/The-CUBE.
111. *Hydraulic Simulation Tables*, MOOG, Editor. 2014, MOOG: Luton, Bedfordshire, UK. p. 1-12.
112. *LDS V8 - Medium Force Shaker*. 2015 [cited 2015 26th May 2015]; Available from: http://www.bksv.com/Products/shakers-exciters/lds-vibration-test/shakers/medium-force/V8ElectrodynamicShaker?tab=accessories.
113. Halfpenny, A. and Walton, T., *New Techniques for Vibration Qualification of Vibrating Equipment on Aircraft*, in *Aircraft Airworthiness & Sustainment 2010*. 2010, nCode: Austin, Texas, USA. p. 1-18.
114. Halfpenny, A. and Walton, T., *Using the Fatigue Damage Spectrum (FDS) to Determine Flight Qualification of Vibrating Components on Helicopters*, in *Astelab 2009*. 2009, nCode: Paris, France. p. 1-13.
115. Millbrook Proving Ground, *Millbrook Structural Durability Procedure,* 2012, Millbrook Proving Ground, Millbrook, Bedfordshire, England,
116. Birrell, S., *Electric Vehicle Usage Behaviour*. 2014: University of Warwick.

117. Rao, J. and Gupta, K., *Introductory Course on Theory and Practice of Mechanical Vibrations*. 2nd ed. 1999, Dehli, India: New Age International. 539.
118. United States of America Department of Defence, *MIL-STD-810-F: Environmental Engineering Considerations and Laboratory Tests,* MIL-STD-810F, 2000, United States of America Department of Defence, 539
119. Williams, A., *EV Battery Vibration Testing and JLR Internal Standards – 30th September 2013*, J. Hooper, Editor. 2013, Jaguar Land Rover: Warwick University, Coventry. p. 1.
120. Schwartz, B. and Richardson, M., *Experimental Modal Analysis.* CSI Reliability Week,, 1999: p. 1-12.
121. Harrison, T., *Experimental Modal Analysis*. 2003, Brüel & Kjær Sound & Vibration Measurement: Royston, Hertfordshire. p. 1-84.
122. Avitabile, P., *Experimental Modal Analysis - A Simple Non-Mathematical Presentation.* Sound and Vibration, 2001(January 2001): p. 3-11.
123. *PCB Impact Hammer - Model: 086C01*. 2014 [cited 2014 14th October 2014]; Available from: http://www.pcb.com/Products.aspx?m=086C01.
124. Bono, R., *Transducer Mounting and Test Setup Configurations*, in *IMAC XXVI: Conference & Exposition on Structural Dynamics - Technologies for Civil Structures*. 2011, The Modal Shop.
125. https://www.endevco.com/download/TP312.pdf, *Guide to Adhesively Mounting Accelerometers*. 2014, Endevco. p. 1 - 7.
126. http://zone.ni.com/reference/en-XX/help/372416F-01/svtconcepts/svfreqresponse/. *Frequency Response (Sound and Vibration)*. 2014 [cited 2014 25th May 2014]; Available from: http://zone.ni.com/reference/en-XX/help/372416F-01/svtconcepts/svfreqresponse/.
127. http://zone.ni.com/reference/en-XX/help/372416A-01/svtconcepts/use_freq_ana_vis/. *Using the Frequency Analysis VIs (Sound and Vibration Measurement Suite)*. 2009 [cited 2014 25th May 2014]; Available from: http://zone.ni.com/reference/en-XX/help/372416A-01/svtconcepts/use_freq_ana_vis/.
128. Avitabile, P., *Teaching Modal Analysis*. University of Massachusetts: University of Massachusetts Lowell. p. 1-12.
129. Moon, S.-I., Cho, I.-J., and Yoon, D., *Fatigue Life Evaluation of Mechanical Components Using Vibration Fatigue Analysis Technique.* Journal of Mechanical Science and Technology, 2011. **25**(3): p. 611-637.
130. Kaw, A., *Mechanics of Composite Materials* 2ed. 2006, CRC Press, Taylor and Francis Group, Florida, 33487-2742, USA: CRC Press 475.
131. Buckley, K. and Chiang, L., *Design Principles for Vibration Test Fixtures*. 2011, MIT Lincoln Laboratory. p. 1-12.
132. Harrison, T., *Resonance*. Vibration Testing. Vol. 5. 2014, Naerum, Denmark: Bruel and Kjaer. 11.
133. Harrison, T., *A Practical Guide to Vibration Testing*. 2014, Brüel & Kjær Royston, Hertfordshire. p. 11.
134. British Standards, *BS EN 60068 Environmental Testing,* British Standards,
135. Srinivas Reddy and Vijaya Kumar Reddy, *Design and Analysis of Vibration Test Bed Fixtures for Space Launch Vehicles.* Indian Journal of Science and Technology, 2010. **3 No. 5**(6): p. 592-595.

136. Harrison, T., *Basic Fixture Design*. Vibration Testing. Vol. 12. 2014, Naerum, Denmark: Bruel and Kjaer. 15.
137. Avitabile, P., *Why You Can't Ignore Those Vibration Fixture Resonances.* Sound and Vibration, 1999(3): p. 20-26.
138. NASA, *General Environmental Verfication Standard (GEVS) - For GSFC Flight Programs and Projects,* 2013, NASA, NASA Goddard Space Flight Centre, Greenbelt, Maryland 20771, USA,
139. Department of Defence - United States of America, *MIL-STD-810F,* 2000, Department of Defence - United States of America, Belvoir, VA, 1-539
140. Ministry of Defence, *Ministary of Defence Standard 00-35, Environmental Handbook for Defence Materiel, Part 3 - Issue 4 Publication Date 18 Sept 2006,* 2006, Ministry of Defence, Glasgow, Scotland,
141. University of Warwick / WMG, *CAT_C_183_A: Snapshot Tests for Vibration Ageing Test (J2380 and Millbrook 100,000 Miles),* 2014, University of Warwick / WMG, University of Warwick, Coventry, CV4 7AL,
142. International Electrotechnical Commission, *IEC 62660-1: Secondary Lithium-ion Cells for the Propulsion of Electric Road Vehicles - Part 1: Performance Testing* 2012, International Electrotechnical Commission, Geneva, Switzerland,,
143. Barai, A., Chouchelamane, G.H., Guo, Y., McGordon, A., and Jennings, P., *A Study on the Impact of Lithium-ion Cell Relaxation on Electrochemical Impedance Spectroscopy.* Journal of Power Sources, 2015. **280**: p. 74-80.
144. Barai, A., Uddin, K., Widanalage, W.D., McGordon, A., and Jennings, P., *The Effect of Average Cycling Current on Total Energy of Lithium-ion Batteries for Electric Vehicles.* Journal of power sources, 2016. **303**: p. 81-85.
145. Barai, A., Widanage, W.D., Marco, J., McGordon, A., and Jennings, P., *A Study of the Open Circuit Voltage Characterization Technique and Hysteresis Assessment of Lithium-ion Cells.* Journal of Power Sources, 2015. **295**: p. 99-107.
146. Anderman, M., *The Tesla Battery Report. Tesla Motors: Battery Technology, Analysis of the Gigafactory, and the Automakers' Perspectives*. 2014, Advanced Automotive Batteries: Oregon House, CA, USA. p. 1-39.
147. Rawlinson, P.D., *Integration System for A Vehicle Battery Pack*, T.M. Inc, Editor. 2012, Tesla Motors Inc. p. 1-21.
148. Harrison, T., *The Vibration System*. 2014, Naerum, Denmark: Bruel and Kjaer Sound and Vibration Measurement. 15.
149. Chouchelamane, G., *Electrochemical Impedance Spectroscopy*. 2013, WMG: University of Warwick. p. 1-24.
150. Schweiger, H.-G., Obeidi, O., Komesker, O., Raschke, A., Schiemann, M., Zehner, C., Gehnen, M., Keller, M., and Birke, P., *Comparison of Several Methods for Determining the Internal Resistance of Lithium Ion Cells.* Sensors, 2010. **10**: p. 5604-5625.
151. Birkl, C. and Howey, D., *Model Identification and Parameter Estimation for LiFePO4 Batteries*, in *Hybrid and Electric Vehicles Conference 2013 (HEVC 2013)*. 2013, IET: London. p. 1-6.
152. Taylor, J., *Uncertainty / Error Measurement of Electrical Characterisation Methods*, J. Hooper, Editor. 2015, WMG: WMG, University of Warwick, Coventry, CV4 7AL. p. 1-3.

153. La Mantia, F., *Characterization of Electrodes for Lithium-Ion Batteries through Electrochemical Impedance Spectroscopy and Mass Spectrometry*. 2008, ETH Zurich: Zurich. p. 164.
154. Wanga, J., Liua, P., Hicks-Garnera, J., Shermana, E., Soukiaziana, S., Verbruggeb, M., Tatariab, H., Musserc, J., and Finamorec, P., *Cycle-Life Model for Graphite-LiFePO4 Cells.* Journal of Power Sources, 2010. **196**: p. 3942–3948.
155. Bourlot, S., Blanchard, P., and Robert, S., *Investigation of Aging Mechanisms of High Power Li-ion Cells used for Hybrid Electric Vehicles.* Journal of Power Sources, 2011. **196**: p. 6841-6846.
156. Jeevarajan, J., Duffield, B., and Orieukwu, J. *Safety of Lithium at Different States of Charge*. in *Space Safety is No Accident: The 7th IAASS Conference*. 2014. Friedrichshafen, Germany: Springer.
157. Ramadass, P., Haran, B., White, R., and Popov, B.N., *Mathematical Modeling of the Capacity Fade of Li-ion Cells.* Journal of Power Sources, 2003. **123**: p. 230-240.
158. Jin An, S., Li, J., Daniel, C., Mohanty, D., Nagpure, S., and Wood, D.L., *The State of Understanding of the Lithium-ion-Battery Graphite Solid Electrolyte Interphase (SEI) and its Relationship to Formation Cycling.* Carbon, 2016(105): p. 52-76.
159. Rexach, S., *Measurement Method for Characterising the Wetting Behavior of Electrodes and Separators in Lithium-ion Cells*. 2014, Technische Universität München: München. p. 154.
160. Sheng, Y., *Investigation of Electrolyte Wetting in Lithium Ion Batteries: Effects of Electrode Pore Structures and Solution*. 2015, University of Wisconsin Milwaukee: Milwaukee, Wisconsin, USA. p. 146.
161. Sheng, Y., Fell, C., Son, Y.K., Metz, B., Jiang, J., and Church, B., *Effect of Calendering on Electrode Wettability in Lithium-ion Batteries.* Frontiers in Energy Research, 2014. **2**(56): p. 1-8.
162. Tustin, W., *Sumultaneous Multiple Axis Vibration Testing.* The AMMTIAC Quarterly. **3**(4): p. 13-14.
163. Kim, C.-J., Kang, Y.J., and Lee, B.-H., *Generation of Driving Profile on a Multi-Axial Vibration Table for Vibration Fatigue Testing.* Mechanical Systems and Signal Processing, 2012. **26**: p. 244-253.
164. *Fixtures for B&K Exciters*. 1987, Bruel Kjaer: Naerum, Denmark. p. 1-24.
165. Vertua, A., Halfpenny, A., and Kihm, F., *Proving Ground Optimisation based on Fatigue Damage Spectra*, in *French Society for Metallurgy and Materials - SF2M, Journées de Printemps 2011*. 2011, nCode. p. 1-13.
166. Harrison, T., *Care and Use of Accelerometers*. 2014, Bruel and Kjaer Sound and Vibration Measurement: Naerum, Denmark. p. 1-7.
167. Hooper, J., *Six Degree of Freedom (6DOF) Vibration Durability Testing and Aging of Lithium Ion 18650 Cylindrical Cells and Modules*, in *Vehicle Electrification and Energy Storage*. 2017, University of Warwick: Coventry, UK.
168. Kassem, M., Bernard, J., Revel, R., Pelissier, S., Duclaud, F., and Delacourt, C., *Calendar Aging of a Graphite/LiFePO4 Cell.* Journal of Power Sources, 2012. **212**: p. 296-305.

169. Keil, P. and Jossen, A., *Calendar Aging of NCA Lithium-Ion Batteries Investigated by Differential Voltage Analysis and Coulomb Tracking.* Journal of The Electrochemical Society, 2017. **164**(1): p. A6066-A6074.
170. Uddin, K., Perera, S., Widanage, W.D., Somerville, L., and Marco, J., *Characterising Lithium-Ion Battery Degradation through the Identification and Tracking of Electrochemical Battery Model Parameters.* Batteries, 2016. **2**(13): p. 1-17.
171. Keil, P., Schuster, S.F., Wilhelm, J., Travi, J., Hauser, A., Karl, R.C., and Jossena, A., *Calendar Aging of Lithium-Ion Batteries - Impact of the Graphite Anode on Capacity Fade.* Journal of The Electrochemical Society, 2016. **163**(9): p. A1872-A1880.
172. *Vibration and Thermal Cycling Test - (Procedures, Appendices, and Warwick Peer Review)*. 2014, NHTSA: Washington DC, USA. p. 1158 - 1247.
173. Hooper, J., *A Critical Review of Society of Automotive Engineers (SAE) Draft Test Procedure: "Vibration with Thermal Cycling Version 6"*, in *WMG*. 2014, University of Warwick: University of Warwick, Coventry, CV4 7AL. p. 25.
174. Biot, M., *Theory of Elastic Systems Vibrating Under Transient Impulse, with an Application to Earthquakeproof Buildings.* Proceedings of the National Academy of Science, 1933. **19**(2): p. 262-268.
175. Miles, J., *On Structural Fatigue Under Random Loading.* Journal of Aeronautical Sciences, 1954.
176. Lalanne, C., *Les Vibrations Aleatoires*, in *Cours ADERA*. 1978.
177. Rice, S. *Mathematical Analysis of Noise*. in *Selected Papers on Noise and Stochastic Processes*. 1954. New York: Dover.
178. Halfpenny, A., *A Frequency Domain Approach for Fatigue Life Estimation from Finite Element Analysis*, in *International Conference on Damage Assessment of Structures (DAMAS 99) Dublin.* 1999, nCode: Dublin, Ireland. p. 1-9.

Appendix

Appendix A: Calculation of SRS

To explain the theory behind SRS within the context of an automotive component development program, the example of a prototype automotive head lamp is presented in Figure 78. This example was selected from current academic literature due to it being an automotive electrical component that is formed of a multiple materials and assembly processes. It is likely that during the development of a head lamp, that the measured acceleration from the lamp itself will not be available [5]. This will be due to that fact that this component is typically a sub component of the front body architecture and will not have been measured due to cost, manpower, equipment and time restrictions [5]. In addition, the test schedules and regimes for component testing are typically fixed before a prototype vehicle. Therefore engineers must rely on more generic data [5]. The most likely source of data will be from acceleration measurements recorded on the chassis of a similar vehicle or early development prototype. It is necessary to therefore find a way of using this data as a means to establish the test specification [5]. Taking this measured chassis acceleration, it is possible to determine the acceleration witnessed by the lamp assembly. For this calculation it is necessary to know the frequency response of the lamp and its associated bracket components. Taking the assumption that the system responds linearly, acceleration levels witnessed by the lamp unit can be established by filtering input acceleration by a frequency transfer function [5]. However in practise, determining the frequency response is usually quite complicated without a prototype component or robust CAE model [5]. Therefore it is necessary to assume the component of interest behaves as a SDOF system.

In the early 1900's the American engineer Biot et al. [174] was researching and analysing the effect of earthquakes via the assumption of a simple SDOF response [5, 113]. This response function for the lamp assembly example is shown in Figure 78. Within the SDOF model, the response is dominated by a single peak located at the natural frequency [5]. At frequencies below the natural frequency the component behaves quasi-statically while at frequencies exceeding the natural frequency the response is significantly attenuated [113].

Within his research, Biot reasoned that despite not understanding the actual natural frequency of the item or component of interest it was possible to create a spectrum of response by sweeping the frequency and plotting the maximum response over a range of natural frequencies [113]. Subsequently the absolute maximum response of the mass of the lamp is plotted as a function of the resonance frequencies [71].

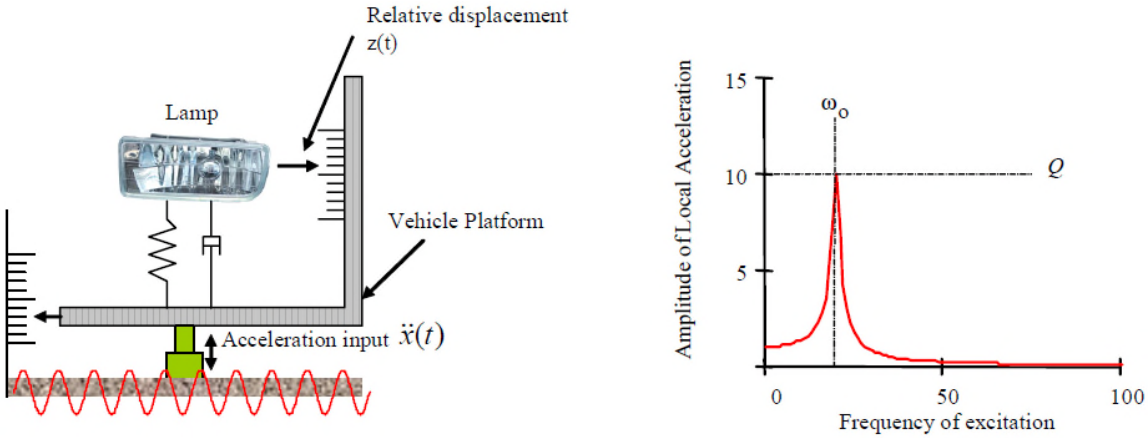

Figure 78: Single Degree of Freedom (SDOF) System Example

To compute the SRS the measured acceleration signal is initially filtered by a SDOF transfer function centred on a specified natural frequency f_n [113]. This is illustrated in Figure 79. The maximum value of the filtered response is then calculated and this represents a single point in the SRS plot [113]. This calculation is repeated over a whole range of frequencies to create the entire SRS [113].

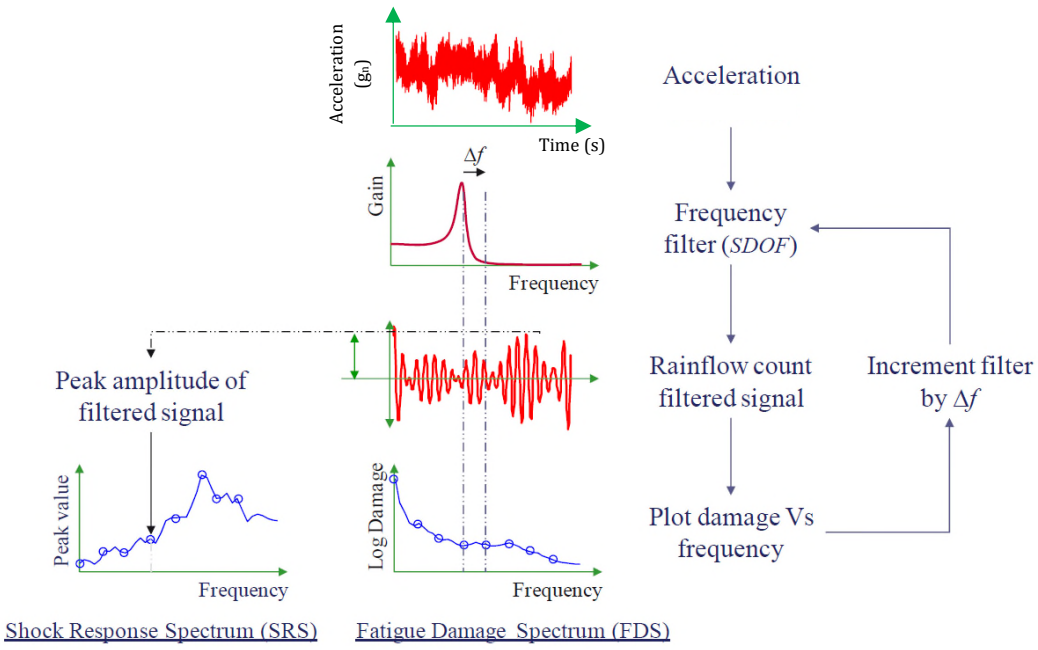

Figure 79: Schematic Flowchart Illustrating the SRS and FDS Calculation Process

As highlighted by [5] the SDOF response function is dominated by a single spike located at the natural frequency f_n. At frequencies below the natural frequency, the component behaves quasi-statically [$Gain(f<f_n)$ 1], while at frequencies exceeding the natural frequency, the response is significantly attenuated [$Gain(f >> fn)$ 0] [5, 113]. Around the natural frequency the component will respond dynamically and will become greatly amplified with its maximum response being limited only by the damping in the system [$Gain(f = f_n) = Q$] [5, 71, 113]. The formula for the SDOF

filter function is illustrated in Equation 18 . The filter function defined in Equation 18 will return a SRS in terms of acceleration vs. frequency fn [113].

$$Gain_{accel}(f) = \frac{1}{\sqrt{\left(1 - \left(\frac{f}{f_n}\right)^2\right)^2 + \frac{1}{Q^2}\left(\frac{f}{f_n}\right)^2}}$$

Equation 18

$Gain_{accel}(f)$ is the SDOF filter with respect to frequency f, and f_n is the natural frequency; both are expressed in *Hz*. The ratio of the maximum dynamic response to the static response is known as the 'dynamic amplification' Q factor [5, 71, 113]. Where ς is the relative damping of the SDOF system [71].

$$Q = \frac{1}{2\varsigma}$$

Equation 19

It is possible to fit the amplification factor Q to the particular component being tested; however, established procedure assumes 5% structural damping factor, which results in a value of Q = 10 for comparative analysis [5, 71, 113]. However, whilst this methodology is suitable for calculating the SRS from a time signal of a given acceleration input, for random vibration data (that presents the acceleration loading by means of a PSD) it is necessary to apply a different calculation to determine an accurate shock response. In [175] Miles et al. presents Equation 20 which allows for the calculation of the RMS acceleration [113].

$$RMS_{accel}(f_n) = \sqrt{\frac{\pi}{2} f_n \, Q \, G(f_n)}$$

Equation 20

Using the formula expressed in Equation 20 Miles et al. derived a spectrum of the RMS acceleration response to a random PSD applied to a SDOF system of natural frequency f_n [175]. $G\ (f_n)$ is the PSD of acceleration in g_n^2/Hz at frequency f_n, and Q is the dynamic amplification factor [113, 175].

This equation determines the RMS acceleration response for a particular natural frequency. In order to determine the maximum likely response (i.e. the SRS), Miles et al. suggested multiplying the RMS spectrum by a factor of 3 (i.e. 3 standard deviations) [113, 175]. Theoretically the maximum response can be higher as typically random vibration shaker controllers utilise a '3 sigma clipping" control when applying random vibration to test items (discussed in greater detail in Submission 3).

However Lalanne et al. [176] proposed a refinement to Miles' equation. In research conducted by Rice et al. [177] it was determined that for a narrow-band frequency response, typical of a SDOF system, the amplitude distribution was found to be

Rayleigh and not Gaussian as proposed by Miles. Within [177] the authors therefore re-derived Equation 20 substituting the Rayleigh probability function as follows for random PSD's.

$$ERS_{accel}(f_n) \cong \sqrt{\pi\, f_n\, Q\, G(f_n) \ln(f_n\, T)}$$

Equation 21

The resulting Equation 21 is known as the extreme response spectrum (ERS). It represents the most likely extreme amplitude response witnessed by a SDOF system through exposure to a random PSD excitation of duration T seconds [113]. The ERS is comparable to the time domain SRS and in simplistic terms is an SRS for PSD excitation. However, whereas the SRS is usually used to determine the maximum response to a highly damaging transient shock, the ERS represents the expected response witnessed over long term vibration loading [113]. The term SRS is usually replaced with the term ERS when it has been derived using statistical means from a PSD for a random vibration test [5]. However it must be noted that for the remainder of this Submission paper the term SRS is used to encompass both SRS and ERS to avoid over complication within the analysis of the results [5].

With respect to a vibration loading via a swept sine input, the SRS in terms of acceleration can be calculated via Equation 22.

$$SRS_{accel}(f_n) \cong Q\, A(f_n)$$

Equation 22

Where $A(f_n)$ is the amplitude of the sine sweep in g_n at frequency f_n in Hz.

Appendix B: Calculation of FDS

When the SDOF system (presented in Figure 80 and consisting of a mass, a spring and a viscous damper) is excited by the motion x(t) the mass starts to oscillate [71]. The oscillation can be described either as the relative motion of the spring, z(t) or as the absolute motion of the mass, y(t) [71]. This model assumes fatigue to be caused by (or proportional to) the relative motion z(t) in the structure. If a cycle count of the obtained motion z(t) is performed, the damage due to the excitation x(t) can be estimated [71]. If such cycle counting is done for SDOF systems with different resonance frequencies and the resulting damage plotted as a function of the resonance frequency, the FDS is obtained [113]. When calculating the FDS the damping of the SDOF system must be specified in order to determine the amplitude of the response [71].

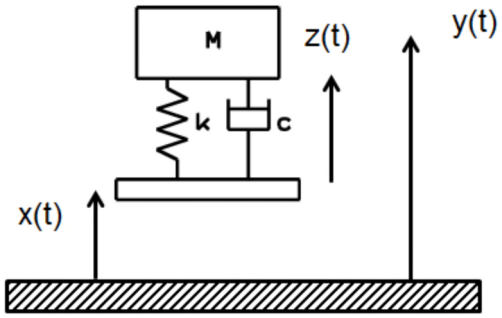

Figure 80:Single Degree of Freedom Dynamic System Model [71]

Within the calculation of the FDS it is assumed that the fatigue damage varies exponentially with the stress and relative displacement) [71]. Figure 81 represents a typical S/N (or Wöhler) curve which relates stress range S to the number of cycles to failure N_f. The curve follows a straight line when plotted on log axes and was described by Basquin using the power-law relationship as defined in Equation 23.

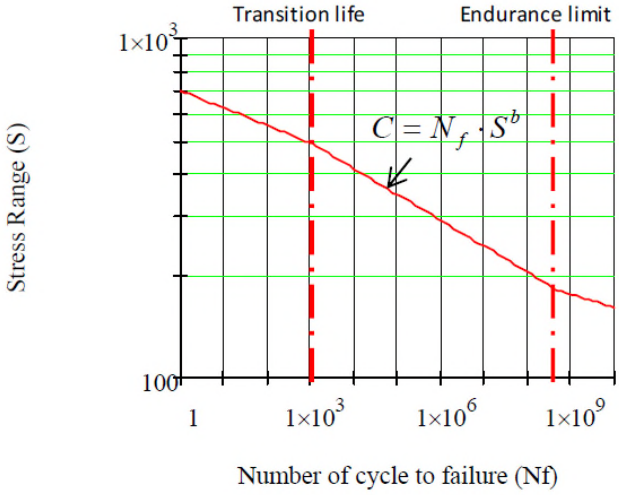

Figure 81: Typical fatigue S/N curve for Aluminium Alloy 6082 in the T6 condition [113]

$$C = S^b N_f$$

Equation 23

Where N_f is the life-length, and the stress, S, is obtained from

$$S = Kz(t)$$

Equation 24

Within Equation 23 and Equation 24 the Basquin coefficient (intercept of the SN curve with the y axis) is defined by C, S is the stress range (twice the amplitude of the sinusoidal stress), N_f is the number of sinusoidal cycles to failure and b is the Basquin exponent (gradient of the SN curve in log space as illustrated within Figure 81) [113]. The Basquin exponent material parameter b can vary between 3 and 10 [71]. MIL-STD-810F recommends using a value of b = 8 where the loading profile is mainly broadband random, and b = 6 where the loading profile is mainly sinusoidal [113, 139].However in practice many engineers assume a value of b = 4 which leads to a more conservative test [71, 113]. It must be noted however that the Basquin exponent b can have a significant effect on the FDS analysis. For traditional fatigue analysis b is obtained from fatigue tests on the material (as per Figure 81) and is then modified to account for geometrical stress concentrations, etc. As long as only comparisons between FDS for different tests or measurements are done, these values are not important [71].

The total damage D in a given time signal is obtained by summing the damage from each stress cycle applying Miner's linear damage accumulation rule [113] as discussed in [178]. This is obtained from Equation 25.

$$D = \sum \frac{1}{N_f} = \sum \frac{S^b}{C}$$

Equation 25

Appendix C: Description of Measured Proving Ground Surfaces [32]

Road surface	Road surface classification	Road surface description
Belgian pave	Urban	Industry-standard surface for evaluating vehicle's noise vibration and harshness and durability. 1.45 km of block granite paving.
City course	Urban	Level asphalt paved surface with multiple tight turns, speed hump and posted speed limits typical of an urban driving environment.
Pot holes	Urban	Two large simulated pot holes, made of cast iron laid into the concrete surface of the road.
Random waves	Urban	Undulating surface out of phase, inducing maximum suspension travel and high amplitude low frequency input to vehicle structure.
Sine waves	Urban	Sine waves out of phase, for high frequency input to the vehicle interior and structure.
Twist humps	Urban	Series of 10 handed angled humps of tarmac construction that has been developed to apply torsional chassis inputs.
Cats eyes (30 mph)	Rural	44 cats eyes along a 90 m length of track
Cats eyes (50 mph)	Rural	44 cats eyes along a 90 m length of track
Handling circuit	Rural	A concrete paved 6 m wide track with varying camber. Typical of rural roads.
Hill route (loop 1)	Rural	A simulated alpine road which has numerous assents, descents and bends with changing camber.
High Speed Circuit (HSC)	Motorway	A circular constant radius banked concrete paved track constructed to simulate motorway driving conditions.
Mile straight (part throttle)	Motorway	Long, precisely levelled surface with fast approach and departure lanes.
Mile straight (wide open throttle)	Motorway	Long, precisely levelled surface with fast approach and departure lanes.

Appendix D: Test Vehicle Details / Specifications

Vehicle	Smart ED	Mitsubishi iMiEV	Nissan Leaf
Vehicle Registration	BF60UDZ	WX10JTU	BW11CCO
Vehicle Hand	RHD	RHD	RHD
Kerb Weight	820 kg	1110 kg	1521 kg
Length	2695 mm	3475 mm	4445 mm
Width	1560 mm	1475 mm	1770 mm
Height	1542 mm	1610 mm	1550 mm
Wheel Base	1867 mm	2250 mm	2700 mm
Track Width Front	1283 mm	1310 mm	1539 mm
Track Width Rear	1384 mm	1270 mm	1534 mm
Ground Clearance (Lowest Point on Vehicle)	140 mm	150 mm	160 mm
Battery Length	460 mm	1500 mm	1540 mm
Battery Width	1065 mm	980 mm	1150 mm
Location of Battery	750 mm from front of Wheel Centre	720 mm from front of wheel centre	800 mm from front of wheel centre

Appendix E: Summary of nCode Parameters for FDS and SRS Calculation

Parameter	Setting or Value	Comments
Q	10	None
Basquin exponent material parameter, b	4	
K	1	
Basquin coefficient, c	1	
ERS Method	Narrow band	
FDS Method	Rayleigh	
S/N Coefficient Format	C	
Number of Bins	4096	For PSD
Interpolation Method	Log	For PSD
Frequency Step	1Hz	For Swept Sine and PSD

Appendix F: 1C Discharge Capacity Performance of 18650 NMC Cells – Section 5.4

Sample No	Test profile	SOC (%)	Orientation	Cell capacity at SOT (Ah)	Cell capacity at EOT (Ah)	Percentage change in Ah (%)
16	USABC	75 %	Z:Z	2.21	1.94	-12.22
18	USABC	75 %	Z:Y	2.21	2.06	-6.79
22	WMG-MPG	50 %	Z:Z	2.18	2.08	-4.59
11	USABC	25 %	Z:X	2.15	2.10	-2.33
15	USABC	50 %	Z:Y	2.18	2.14	-1.83
13	USABC	50 %	Z:Z	2.23	2.19	-1.79
26	WMG-MPG	75 %	Z:X	2.10	2.07	-1.43
17	USABC	75 %	Z:X	2.15	2.13	-0.93
20	WMG-MPG	25 %	Z:X	2.12	2.12	0.00
19	WMG-MPG	25 %	Z:Z	2.11	2.11	0.00
21	WMG-MPG	25 %	Z:Y	2.09	2.09	0.00
10	USABC	25 %	Z:Z	2.19	2.19	0.00
27	WMG-MPG	75 %	Z:Y	2.09	2.09	0.00
12	USABC	25 %	Z:Y	2.18	2.19	0.46
14	USABC	50 %	Z:X	2.15	2.17	0.93
25	WMG-MPG	75 %	Z:Z	2.07	2.10	1.45
23	WMG-MPG	50 %	Z:X	2.05	2.13	3.90
24	WMG-MPG	50 %	Z:Y	1.92	2.12	10.42
8	USABC	75 %	Reference	2.16	2.06	-4.63
2	USABC	25 %	Reference	2.20	2.13	-3.18
9	WMG-MPG	75 %	Reference	2.13	2.12	-0.47
3	WMG-MPG	25 %	Reference	2.14	2.14	0.00
5	USABC	50 %	Reference	2.18	2.19	0.46
6	WMG-MPG	50 %	Reference	1.92	2.09	8.85

	SOT	EOT
Standard deviation for USABC Procedure 10 samples (Ah)	0.03	0.08
Mean for USABC Procedure 10 samples (Ah)	2.18	2.12
Standard deviation for WMG-MPG samples (Ah)	0.07	0.02
Mean for WMG-MPG samples (Ah)	2.08	2.10

Appendix G: Pulse Power Performance of 18650 NMC Cells - Section 5.4

Sample No	Test profile	SOC (%)	Orientation	DC resistance (SOT) (mΩ)	DC resistance (EOT) (mΩ)	Percentage change in R_{DC} between SOT and EOT (%)
16	USABC	75 %	Z:Z	74.32	169.55	128.1
17	USABC	75 %	Z:X	73.41	162.50	121.4
12	USABC	25 %	Z:Y	72.73	151.59	108.4
20	WMG-MPG	25 %	Z:X	72.27	142.95	97.8
25	WMG-MPG	75 %	Z:Z	73.18	142.95	95.3
15	USABC	50 %	Z:Y	71.82	138.18	92.4
11	USABC	25 %	Z:X	72.27	131.82	82.4
18	USABC	75 %	Z:Y	73.18	131.36	79.5
19	WMG-MPG	25 %	Z:Z	72.27	126.59	75.2
21	WMG-MPG	25 %	Z:Y	72.05	121.36	68.5
10	USABC	25 %	Z:Z	71.14	117.05	64.5
14	USABC	50 %	Z:X	72.73	116.36	60.0
22	WMG-MPG	50 %	Z:Z	72.73	115.00	58.1
24	WMG-MPG	50 %	Z:Y	72.05	109.32	51.7
13	USABC	50 %	Z:Z	70.45	102.27	45.2
23	WMG-MPG	50 %	Z:X	71.82	93.64	30.4
26	WMG-MPG	75 %	Z:X	73.64	90.00	22.2
27	WMG-MPG	75 %	Z:Y	73.18	85.91	17.4
5	USABC	50 %	Reference	75.23	86.14	14.5
2	USABC	25 %	Reference	72.27	73.64	1.9
3	WMG-MPG	25 %	Reference	71.14	71.82	1.0
6	WMG-MPG	50 %	Reference	72.05	72.05	0.0
9	WMG-MPG	75 %	Reference	73.18	72.73	-0.6
8	USABC	75 %	Reference	74.09	73.41	-0.9

	SOT	EOT
Standard deviation for USABC Procedure 10 samples (mΩ)	1.19	22.35
Mean for USABC Procedure 10 samples (mΩ)	72.45	135.63
Standard deviation for WMG-MPG samples (mΩ)	0.63	21.48
Mean for WMG-MPG samples (mΩ)	72.58	114.19

Appendix H: OCV Performance of 18650 NMC Cells - Section 5.4

				Voltage (V)		
Sample No	**Test profile**	**SOC**	**Orientation**	**SOT**	**EOT**	**Percentage change (%)**
27	WMG-MPG	75 %	Z:Y	3.882	3.891	0.23
24	WMG-MPG	50 %	Z:Y	3.658	3.666	0.22
25	WMG-MPG	75 %	Z:Z	3.878	3.885	0.18
22	WMG-MPG	50 %	Z:Z	3.663	3.670	0.19
23	WMG-MPG	50 %	Z:X	3.661	3.668	0.19
3	WMG-MPG	25 %	Reference	3.588	3.595	0.2
19	WMG-MPG	25 %	Z:Z	3.584	3.590	0.17
20	WMG-MPG	25 %	Z:X	3.587	3.590	0.08
26	WMG-MPG	75 %	Z:X	3.883	3.886	0.08
18	USABC	75 %	Z:Y	3.897	3.899	0.05
5	USABC	50 %	Reference	3.678	3.676	0.05
21	WMG-MPG	25 %	Z:Y	3.581	3.580	0.03
16	USABC	75 %	Z:Z	3.894	3.895	0.03
17	USABC	75 %	Z:X	3.895	3.896	0.03
2	USABC	25 %	Reference	3.599	3.598	0.03
15	USABC	50 %	Z:Y	3.674	3.675	0.03
6	WMG-MPG	50 %	Reference	3.668	3.669	0.03
11	USABC	25 %	Z:X	3.591	3.590	0.03
8	USABC	75 %	Reference	3.897	3.897	0
9	WMG-MPG	75 %	Reference	3.889	3.889	0
13	USABC	50 %	Z:Z	3.674	3.674	0
14	USABC	50 %	Z:X	3.674	3.674	0
10	USABC	25 %	Z:Z	3.599	3.599	0
12	USABC	25 %	Z:Y	3.598	3.598	0

	SOT	**EOT**
Standard deviation for USABC Procedure 10 samples (V)	0.13	0.14
Mean for USABC Procedure 10 samples (V)	3.72	3.72
Standard deviation for WMG-MPG samples (V)	0.13	0.13
Mean for WMG-MPG samples (V)	3.71	3.71

Appendix I: EIS R_O Performance of 18650 NMC Cells - Section 5.4

Sample No	Test profile	SOC	Orientation	SOT (mΩ)	EOT (mΩ)	Percentage change (%)
16	USABC	75 %	Z:Z	*	*	*
19	WMG-MPG	25 %	Z:Z	46.7	167.1	257.82
15	USABC	50 %	Z:Y	46.4	164.5	254.53
25	WMG-MPG	75 %	Z:Z	46.8	155.0	231.20
20	WMG-MPG	25 %	Z:X	46.9	153.5	227.29
17	USABC	75 %	Z:X	46.2	143.1	209.74
18	USABC	75 %	Z:Y	46.5	141.2	203.66
12	USABC	25 %	Z:Y	47.7	135.5	184.07
11	USABC	25 %	Z:X	46.9	126.0	168.66
26	WMG-MPG	75 %	Z:X	47.0	114.3	143.19
14	USABC	50 %	Z:X	47.3	114.2	141.44
21	WMG-MPG	25 %	Z:Y	46.1	102.2	121.69
23	WMG-MPG	50 %	Z:X	46.4	90.0	93.97
10	USABC	25 %	Z:Z	45.9	86.9	89.00
13	USABC	50 %	Z:Z	46.0	84.0	82.61
22	WMG-MPG	50 %	Z:Z	50.0	84.9	69.80
24	WMG-MPG	50 %	Z:Y	46.8	66.8	42.74
27	WMG-MPG	75 %	Z:Y	47.0	64.9	38.09
5	USABC	50 %	Reference	49.6	60.8	22.58
2	USABC	25 %	Reference	46.2	49.3	6.71
9	WMG-MPG	75 %	Reference	46.3	47.5	2.60
3	WMG-MPG	25 %	Reference	46.7	47.3	1.40
6	WMG-MPG	50 %	Reference	46.2	46.8	1.30
8	USABC	75 %	Reference	47.5	47.5	0.00

	SOT	EOT
Standard deviation for USABC Procedure 10 samples (mΩ)	0.64	28.05
Mean for USABC Procedure 10 samples (mΩ)	46.61	124.43
Standard deviation for WMG-MPG samples (mΩ)	1.13	39.02
Mean for WMG-MPG samples (mΩ)	47.08	110.97

*= No data available due to cell issue

Appendix J: EIS R_{CT} Performance of 18650 NMC Cells - Section 5.4

Sample No	Test profile	SOC	Orientation	SOT (mΩ)	EOT (mΩ)	Percentage change (%)
16	USABC	75 %	Z:Z	*	*	*
18	USABC	75 %	Z:Y	23.90	15.50	35.15
21	WMG-MPG	25 %	Z:Y	24.08	15.75	34.59
22	WMG-MPG	50 %	Z:Z	24.50	16.10	34.29
23	WMG-MPG	50 %	Z:X	23.73	15.73	33.71
24	WMG-MPG	50 %	Z:Y	23.90	16.06	32.80
19	WMG-MPG	25 %	Z:Z	22.43	15.67	30.14
17	USABC	75 %	Z:X	24.50	17.50	28.57
20	WMG-MPG	25 %	Z:X	21.64	15.47	28.51
26	WMG-MPG	75 %	Z:X	22.90	16.43	28.25
27	WMG-MPG	75 %	Z:Y	22.56	16.20	28.19
14	USABC	50 %	Z:X	24.70	18.20	26.32
13	USABC	50 %	Z:Z	23.10	17.40	24.68
15	USABC	50 %	Z:Y	23.70	18.00	24.05
25	WMG-MPG	75 %	Z:Z	21.50	16.51	23.21
10	USABC	25 %	Z:Z	23.72	18.70	21.16
11	USABC	25 %	Z:X	23.00	18.23	20.74
12	USABC	25 %	Z:Y	22.80	19.10	16.23
9	WMG-MPG	75 %	Reference	28.89	16.38	43.30
2	USABC	25 %	Reference	28.80	16.70	42.01
6	WMG-MPG	50 %	Reference	25.44	15.73	38.17
8	USABC	75 %	Reference	24.60	15.70	36.18
3	WMG-MPG	25 %	Reference	22.51	15.25	32.25
5	USABC	50 %	Reference	24.40	17.50	28.28

	SOT	EOT
Standard deviation for USABC Procedure 10 samples (mΩ)	1.15	0.91
Mean for USABC Procedure 10 samples (mΩ)	23.04	16.40
Standard deviation for WMG-MPG samples (mΩ)	0.70	1.36
Mean for WMG-MPG samples (mΩ)	23.59	17.27

Appendix K: Change in Frequency Performance of 18650 NMC Cells - Section 5.4

				First Natural Frequency Greater Than 2 g_n (Hz)		
ISR number	**Test Profile**	**SOC %**	**Orientation**	**SOT (Hz)**	**EOT (Hz)**	**Percentage Change (%)**
10	USABC	25 %	Z:Z	2579	1877	27.2
16	USABC	75 %	Z:Z	3400	2834	16.6
11	USABC	25 %	Z:X	2335	2039	12.7
15	USABC	50 %	Z:Y	3200	2913	9.0
14	USABC	50 %	Z:X	3189	2914	8.6
18	USABC	75 %	Z:Y	2937	3165	7.8
23	WMG-MPG	50 %	Z:X	1962	2097	6.9
17	USABC	75 %	Z:X	1940	1816	6.4
13	USABC	50 %	Z:Z	3209	3011	6.2
26	WMG-MPG	75 %	Z:X	3354	3467	3.4
27	WMG-MPG	75 %	Z:Y	3700	3584	3.1
21	WMG-MPG	25 %	Z:Y	3061	2970	3.0
25	WMG-MPG	75 %	Z:Z	3182	3156	0.8
19	WMG-MPG	25 %	Z:Z	3641	3614	0.7
22	WMG-MPG	50 %	Z:Z	3700	3674	0.7
24	WMG-MPG	50 %	Z:Y	3061	3070	0.3
12	USABC	25 %	Z:Y	2572	2579	0.3
20	WMG-MPG	25 %	Z:X	3694	3700	0.2

	SOT	**EOT**
Standard Deviation for USABC Procedure 10 Samples (Hz)	488.77	522.61
Mean for USABC Procedure 10 Samples (Hz)	2817.89	2572.00
Standard Deviation for WMG-MPG Samples (Hz)	558.97	514.99
Mean for WMG-MPG Samples (Hz)	3261.67	3259.11

Appendix L: Summary of Change in Amplitude performance of 18650 NMC Cells - Section 5.4

				Amplitude of First Natural Frequency Greater Than 2 g_n (g_n)		
ISR number	**Test Profile**	**SOC (%)**	**Orientation**	**SOT (g_n)**	**EOT (g_n)**	**Percentage Change (%)**
25	WMG-MPG	75 %	Z:Z	1.62	2.91	79.6
18	USABC	75 %	Z:Y	2.95	4.01	35.9
14	USABC	50 %	Z:X	2.89	1.90	34.3
19	WMG-MPG	25 %	Z:Z	5.03	3.46	31.2
26	WMG-MPG	75 %	Z:X	2.96	2.21	25.3
27	WMG-MPG	75 %	Z:Y	4.09	3.08	24.7
10	USABC	25 %	Z:Z	3.32	2.51	24.4
20	WMG-MPG	25 %	Z:X	4.52	3.61	20.1
23	WMG-MPG	50 %	Z:X	2.61	2.30	11.9
15	USABC	50 %	Z:Y	2.85	3.17	11.2
12	USABC	25 %	Z:Y	1.99	1.82	8.5
22	WMG-MPG	50 %	Z:Z	3.63	3.89	7.2
16	USABC	75 %	Z:Z	3.31	3.51	6.0
11	USABC	25 %	Z:X	2.02	1.91	5.4
24	WMG-MPG	50 %	Z:Y	2.80	2.70	3.6
17	USABC	75 %	Z:X	1.97	1.90	3.6
13	USABC	50 %	Z:Z	2.34	2.30	1.7
21	WMG-MPG	25 %	Z:Y	3.01	2.96	1.7

	SOT	**EOT**
Standard Deviation for USABC Procedure 10 Samples (g_n)	0.55	0.81
Mean for USABC Procedure 10 Samples (g_n)	2.63	2.56
Standard Deviation for WMG-MPG Samples (g_n)	1.06	0.57
Mean for WMG-MPG Samples (g_n)	3.36	3.01

Appendix M: Start and End of Test OCV Measurements of all NCA Cells Evaluated – Section 5.5

		Voltage (V)			
Cell sample No	**Orientation**	**SOT**	**EOT**	**Change from SOT and EOT**	**Percentage change (%)**
1	Z:Z	3.838	3.839	0.001	0.026
2	Z:Z	3.839	3.838	-0.001	-0.026
3	Z:Z	3.840	3.840	0	0
4	Z:X	3.838	3.838	0	0
5	Z:X	3.839	3.839	0	0
6	Z:X	3.840	3.840	0	0
7	Z:Y	3.840	3.840	0	0
8	Z:Y	3.840	3.840	0	0
9	Z:Y	3.838	3.838	0	0
10	Control	3.842	3.841	-0.001	-0.026
11	Control	3.834	3.834	0	0
12	Control	3.839	3.839	0	0

Mean change		
Orientation	**Mean change (V)**	**Mean change (%)**
Mean change in OCV - Z:X	0	0
Mean change in OCV - Z:Y	0	0
Mean change in OCV - Z:Z	0	0
Mean change in OCV – Control	-0.00033	-0.00867

Appendix N: TEAM Cube Multi-Axis Shaker Specification

Shaker Model	TEAM Cube - Hydraulic Shaker Table
Serial Number	3
Maximum Thrust	62 kN in each axis – peak sine 31 kN rms in each axis – peak random
Maximum Acceleration	8 g_n (sine)
Maximum Displacement	+/- 50 mm (100 mm Peak to Peak) in Z +/- 23 mm (46 mm peak to peak) in X and Y +/- 6° roll, pitch and yaw.
Frequency Range	< 0.1Hz to < 300 Hz
Typical Payload Range (Note - Dependant on Test Profile)	25-500 Kg

Appendix O: Risk Assessment for 6DOF Study

Risk	Likelihood	Impact	Risk Management Approach/Mitigating Actions	Action
Personnel and Training				
Lack of understanding giving rise to cell handling errors/thermal events.	Low	High	All staff engaged in test activities to have necessary skills and competence. No unnecessary personnel to handle cells or enter test area.	Written into operating procedures
Test area is potentially hazardous	High	High	PPE should be worn when in test area. PPE includes safety shoes, nitrile or latex gloves, laboratory coat, and safety glasses. No jewellery to be worn when handling cells or module.	Written into test procedure
			Emergency PPE equipment to be available in laboratory such as safety hook.	Items to be ordered and installed into test area.
			Ensure exits are not obstructed in the event of a hazardous incident. Access to laboratory must be limited to necessary personnel.	Written into test procedure. Laboratory can only be accessed via swipe card. Assess to Millbrook site regulated by security. Doors to laboratory must be kept closed during testing. Lock cube doors during test.
Risk to personnel of cell/module rupture	Low	High	Test area must be cleared of unnecessary personnel prior to setting up or commencing test.	Written into test procedure
			Test cell to be free of personnel and locked during testing. No entry signs to be displayed	Written into test procedure. Test cell to be clear of people during testing and locked.
			Testing to be conducted in area which has gas expansion relief	Test cell is not completely sealed. Volume of test cell is approximately 22 m^3 (22,000 litres).
			18650 cell forms tested have "pressure venting" built into design.	Ensure cells can release pressure when assembled within fixture and module assembly prior to testing
			Test fixture must contain blast protection within its design	Design test fixture with blast protection and relief
			Temperature monitoring system to be incorporated into fixture that outputs an alarm when cells exceed 60 °C or display an increase in cell temperature >4 °C a second	Fire alarm and cell monitoring system to be incorporated into rig design

Risk	Likelihood	Impact	Risk Management Approach/Mitigating Actions	Action
Personnel and Training				
Risk of cell / module fire	Low	High	Test area must be cleared of unnecessary personnel prior to setting up or commencing test.	Written into test procedure
			Test cell to be free of personnel and locked during testing. No entry signs to be displayed	Written into test procedure
			Test fixture must be designed in a manner which would contain a cell and module fire for a limited period of time to allow for evacuation	Design test fixture with compartmentalisation using fire retardant materials
			Facility / rig to incorporate fire alarm	Ensure smoke/gas detection and alarms are installed in facility. Laboratory is manned 24 hours a day for at least 6 days a week. With 16 hours manned on the Sunday
				Temperature monitoring system to be incorporated into fixture that outputs an alarm when cells exceed 60°C or display an increase in cell temperature >4°C a second
			Incorporate fire extinguishing system into facility / rig	Test facility to incorporate suitable Li-ion fire suppression system such as liquid nitrogen, argon or nitrogen injection. Fire and first aiders on-site.
Risk to personnel of gasses from venting cells.	Low	High	Test to be conducted in well-ventilated area.	Test facility air extraction to be running continuously during testing
			Chemistry of test item(s) to be defined prior to testing so that the correct clean up procedure can be prepared before testing.	Written into test procedure
			Chemistry of test item(s) to be defined prior to testing so that the correct HF cream can be ordered prior to testing and installed into medical cabinet in test laboratory	Written into test procedure
			Test area must be cleared of unnecessary personnel prior to setting up or commencing test.	Written into test procedure
			Test cell to be free of personnel and locked during testing. No entry signs to be displayed	Written into test procedure
			Suitable gas detection and audible alarm to be installed in pedestrian and test cell areas	Incorporate gas detection system into facility
			Gases from test items to be managed by a method of suction that vents to atmosphere away from personnel or any form of office ventilation or air conditioning inlet or opening. Nitrogen and/or compressed air purge to be available into facility chamber and fire enclosures	Incorporate extraction system into facility / fixture design. Nitrogen / compressed air purge system to be incorporated into facility

Risk	Likelihood	Impact	Risk Management Approach/Mitigating Actions	Action
Personnel and Training				
Risk of electrocution	Low	High	Test area must be cleared of unnecessary personnel prior to setting up or commencing test.	Written into test procedure
			Test cell to be free of personnel and locked during testing. No entry signs to be displayed	Written into test procedure
			Testing to be conducted on items with a voltage no greater than 50 volts.	Written into test procedure
			Testing to be conducted on items with an Ah rating greater than 70 Ah, to be performed at 25 % SOC	Written into test procedure
			All staff engaged in test activities to have necessary skills and competence. No necessary personnel to handle cells or enter test area.	Written into operating procedures
			Voltage and temperature monitoring of test items to be conducted during testing.	Written into test procedure
			All module terminals to be insulated and protected - impedance monitoring of head expander and fixtures to be conducted	Written into test procedure
			Suitable insulation must be installed to eliminated electrical pathways into test fixture and test facility / equipment	Written into test procedure. Fixture design must incorporate suitable electrical insulation.
Equipment and Facilities				
E/M shaker may make an unplanned shut down during test	Low	Low	Equipment should be inspected and operated prior to test set-up. Only authorised trained personnel are in the test area during testing. Equipment failure will result in loss of vibration input and so is “Fail safe”	Written into test procedure
Risk of test item fire igniting equipment and facilities	Low	High	Thermal barrier of FR4, G10 or similar high temperature composite must be installed between test item and any magnesium alloy components of the shaker facility.	Written into test procedure
			Fixture to limit risk of fire spreading from test items to facility / equipment through physical thermal barriers / compartmentalisation	Design test fixture with blast protection and relief along with fire limitation and compartmentalisation
			Incorporate fire mitigation system into facility	Test facility to incorporate suitable Li-ion fire suppression system such as liquid nitrogen, argon or nitrogen injection. Fire and first aiders on-site. 24 hour monitoring / onsite fire crew.
Cell / Module Handling				
Possibility of shorting cell terminals or puncturing cell	Low	High	Cells/modules to remain in transport packaging until ready for test set-up.	Written into test procedure
			Jewellery to be removed or covered with insulating tape. Care to be taken with tools when connecting cells/modules in test area.	Written into test procedure
Possible injury from lifting items	Med	Med	Rigs, modules, test assemblies and boxes greater than 10kg must be lifted and handled using suitable equipment such as cranes, pallet trucks etc.	Written into test procedure
Box of cells may present a manual handling risk	Med	Med	Routes should be carefully assessed and, where possible, sack or pallet trolleys should be used.	Written into test procedure

Risk	Likelihood	Impact	Risk Management Approach/Mitigating Actions	Action
Cell / Module Preparation				
Cell may be inadvertently shorted or punctured during test set-up.	Low	High	Training of personnel. Test area should have clear exit routes and be well ventilated during test set-up.	Standard Catapult Operating Procedure
Cell / module event may cause other cells / modules to vent	Low	High	Cells not undergoing test should be kept in a separate area and within their transport packaging.	Written into test procedure
			Cells / modules within test rig must be separated.	Ensure fixture design incorporates cell / module separation and compartmentalisation
Test Set-up				
Thermal event mitigation	Low	High	Thermal barrier of FR4, G10 or similar high temperature composite must be installed between test item and any magnesium alloy components of the shaker facility.	Written into test procedure
	Low	High	Thermocouples to be installed onto test item to monitor temperature. Any temperature in excess of 60 °C or a rate of temperature change greater than 4 °C per minute must trigger an alarm during testing and activate a fire mitigation system. Thermocouples must also be installed in base of fixtures to monitor fixture base to head expander temperature, as well as thermocouples monitoring enclosure temperature.	Written into test procedure
	Low	High	Voltage and impedance monitoring of test items to be conducted during testing.	Written into test procedure
	Low	High	All module terminals to be insulated and protected	Written into test procedure
Trip or fall hazards may be present.	Med	Med	Good housekeeping should be practiced. All tools/equipment should be kept in the appropriate place and, if not immediately required, stored away safely.	Written into test procedure
Unauthorised personnel may enter the test area during test set-up or execution.	Med	Low/Med	Laboratory exclusion zone must be in place on all exits of laboratory to restrict access to laboratory and to also ensure exits are not obstructed in the event of a hazardous incident.	Written into test procedure. Barrier bar or cones to be available in laboratory to ensure eclusion zone can be enforced.
			Main test cell doors to be locked when test in progress. Fire escape panic bar to be installed on test cell door so that it can be locked from outside, but still allow for quick exit by personnel during set-up activities. Signs warning that unauthorised personnel are prohibited are clearly displayed.	Test facility prevents unauthorised entry. Fire escape panic bar to be installed on test cell door so that it can be locked from outside, but still allow for quick exit by personnel during set-up activities.

Risk	Likelihood	Impact	Risk Management Approach/Mitigating Actions	Action
Test Set-up				
Test profiles unrepresentative and too severe causing a hazard that is not conducive to the desired test conditions	Med	Med	Test profiles utilised for testing are derived from EV durability data and are specifically devised not to replicate abuse conditions or events	Ensure test profiles that are representative of "normal, on-road" EV durability conditions are selected for testing.
			Random profiles will be run with 6dB abort limits which will stop the testing in a controlled manner if vibration levels exceed desired test values.	Written into test procedure
			Random profiles will be run with 3dB alarm limits which will inform the user that the test vibration levels have started to exceed desired test values.	Written into test procedure
			Vibration testing to be conducted in a control loop, with at least two control accelerometers which are to be set to an averaging control strategy. Control accelerometers must be fixed to the test rig via a mechanical fastening method.	Written into test procedure
			Control accelerometers to be checked for accuracy, calibration and functionality prior to testing	Written into test procedure
			Test profiles to be run first on bare fixtures to ensure control effectiveness prior to testing	Written into test procedure
Test rig not bolted down to the shaker facility correctly	Low	Med	All fasteners to be paint marked post tightening to a specified torque (to be written into fixture assembly procedure) to allow for monitoring of fastener loosening and as a check condition that they have been tightened prior to testing.	Written into test procedure
Tools and loose bolts and washer left on shaker table during EMS start up	Med	Low/Med	Prior to starting testing EMS armature, head expanders, slip table and surrounding area to be check for unused washers, bolts and tools	Written into test procedure
Post Testing				
Risk of thermal event due to internal damage sustained during testing	Med	Med	Test items to be quarantined and monitored for 7 days prior to being shipped post vibration testing.	Written into test procedure. Quarantine area to be set aside near test area.

Appendix P: Incident Management Flow Chart for 6DOF Study

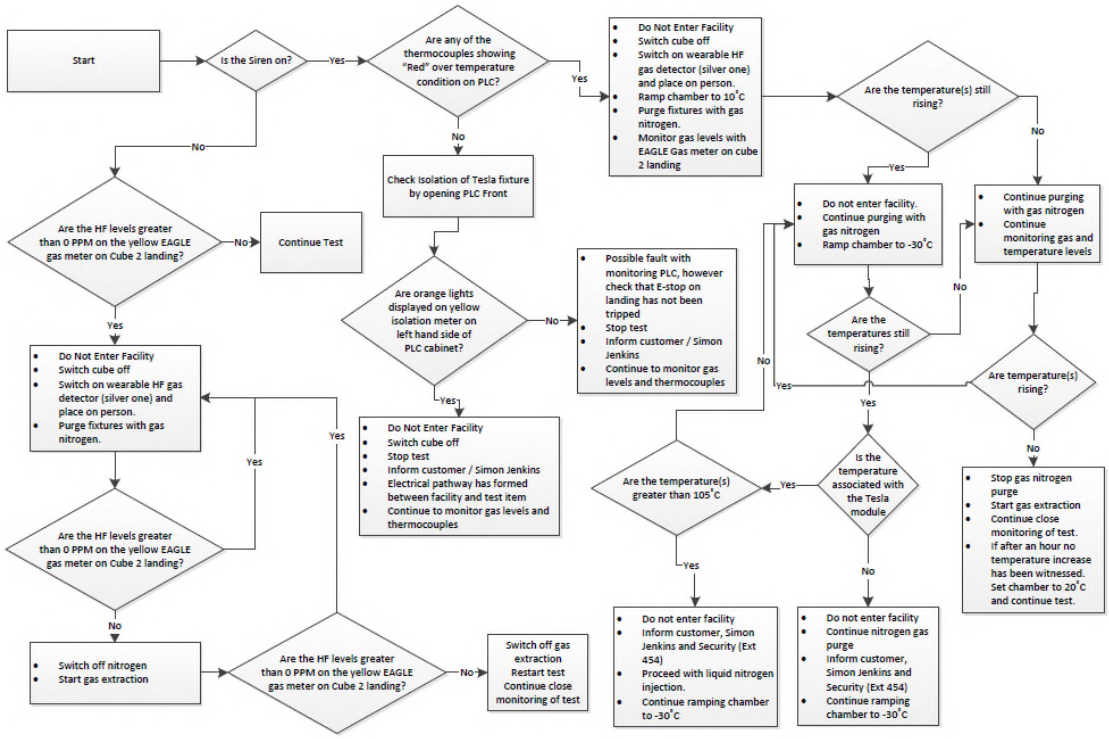

Appendix Q: Accelerometer Locations for 6 DOF Study and Schematic

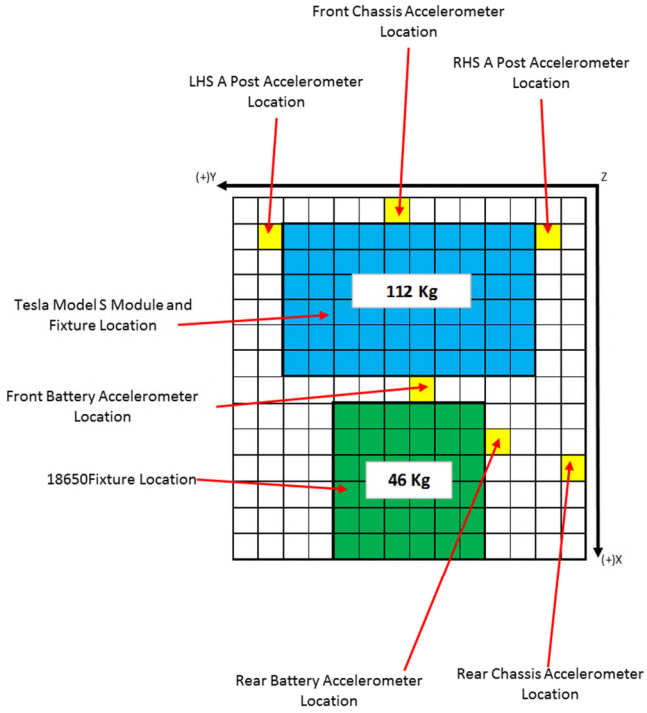

Schematic of Accelerometer Locations and Fixture Positions on Cube Head Expander

Location of Accelerometers on Cube Head Expander to Replicate Locations on Measurement Vehicle

Axis	Measurement (mm)
RHS A Post Accelerometer	
Y	0
X	0
Z	530
LHS A Post Accelerometer	
Y	1260
X	0
Z	525
Front Battery Accelerometer	
Y	550
X	580
Z	0
Rear Battery Accelerometer	
Y	190
X	840
Z	0
Front Chassis Accelerometer	
Y	705
X	-100
Z	60
Rear Chassis Accelerometer	
Y	-10
X	980
Z	160

Appendix R: Repeatability Trials of Bonded Collar Mounted Accelerometer Results

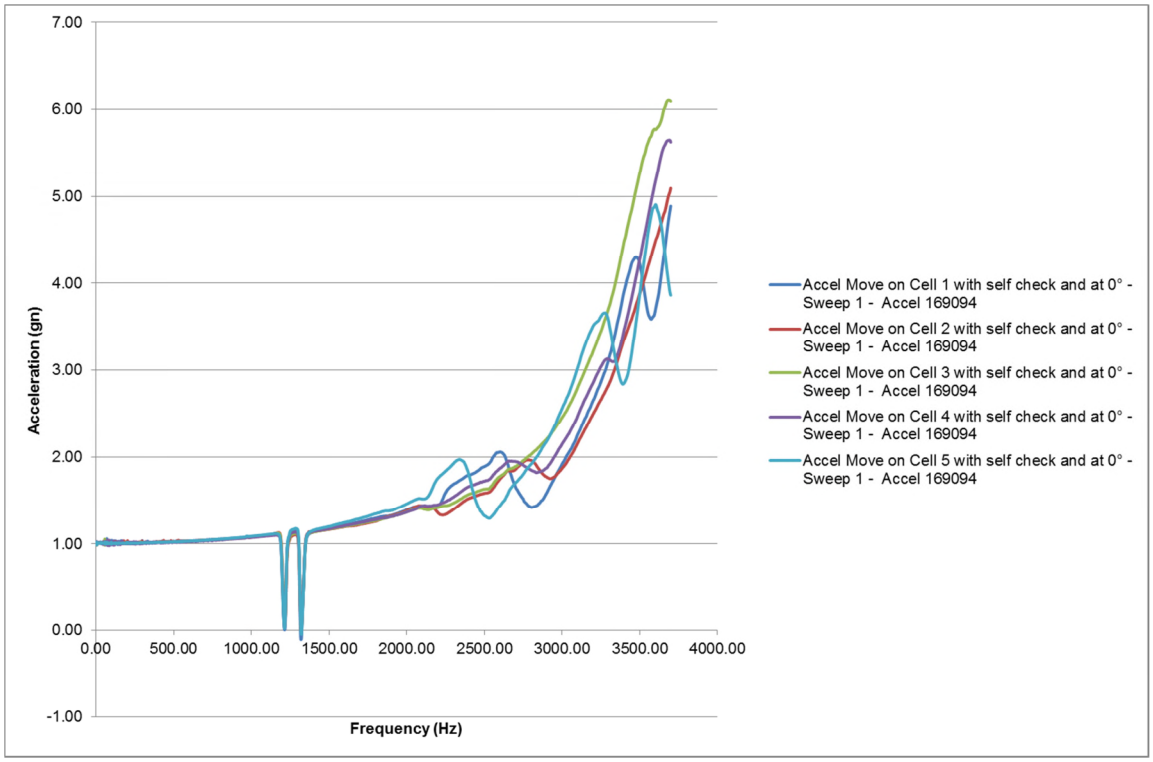

Repeatability of Petro Wax Attachment Method

Repeatability of Bonded Collar Attachment Method

Appendix S: Post Test Visual Observations in Test Cells

Cell ID	Orientation	Observations / Comments
2991	Z	Witness marks from fixture clamping. Some insulation damage from removal of accelerometer X60 bonding - damage not a result of vibration.
2994	Z	Fretting observed on positive terminal of cell. Witness marks from fixture clamping.
2996	Z	Witness marks from fixture clamping. Some insulation damage from removal of accelerometer X60 bonding - damage not a result of vibration.
2997	Y	Some insulation damage from removal of accelerometer X60 bonding - damage not a result of vibration. Surface defect noted on casing of sample post testing.
2998	Y	Witness marks from fixture clamping. Some insulation damage from removal of accelerometer X60 bonding - damage not a result of vibration.
2999	Y	Witness marks from fixture clamping. Some insulation damage from removal of accelerometer X60 bonding - damage not a result of vibration.
3000	X	Witness marks from fixture clamping.
3001	X	Witness marks from fixture clamping.
3005	X	Witness marks from fixture clamping. Some insulation damage from removal of accelerometer X60 bonding - damage not a result of vibration.
2995	Control	None
3003	Control	None
3004	Control	None

Appendix T: Start and End of Test OCV Measurements of all Cells Evaluated

Cell ID	Orientation	SOT (V)	EOT (V)	Change from SOT and EOT (V)	Percentage Change (%)	Overall Ranking 1 = Worst 9 = Best
2991	Z	3.902	3.900	-0.002	-0.051	No change
2994	Z	3.906	3.905	-0.001	-0.026	No change
2996	Z	3.904	3.903	-0.001	-0.026	No change
2997	Y	3.901	3.902	0.001	0.026	No change
2998	Y	3.902	3.902	0	0.000	No change
2999	Y	3.906	3.905	-0.001	-0.026	No change
3000	X	3.898	3.897	-0.001	-0.026	No change
3001	X	3.905	3.904	-0.001	-0.026	No change
3005	X	3.900	3.900	0	0.000	No change
2995	Control	3.903	3.902	-0.001	-0.026	-
3003	Control	3.906	3.906	0	0.000	-
3004	Control	3.904	3.904	0	0.000	-

	Mean Change (mΩ)	Mean Change (%)	Ranking
Mean Change in OCV - X	-0.0007	-0.0171	= 1
Mean Change in OCV - Y	0.0000	0.0000	= 1
Mean Change in OCV - Z	-0.0013	-0.0342	= 1
Mean Change in OCV - Control	-0.0003	-0.0086	-

ANOVA Analysis

Orientation	ANOVA p-value against Control Null Hypothesis: Mean of vibrated cells and control cells are equal. Reject null hypothesis if p < 0.05)
X	0.409
Y	0.375
Z	0.447

Appendix U: Typical Pre-Post Test Vibration Response for 18650 Cell

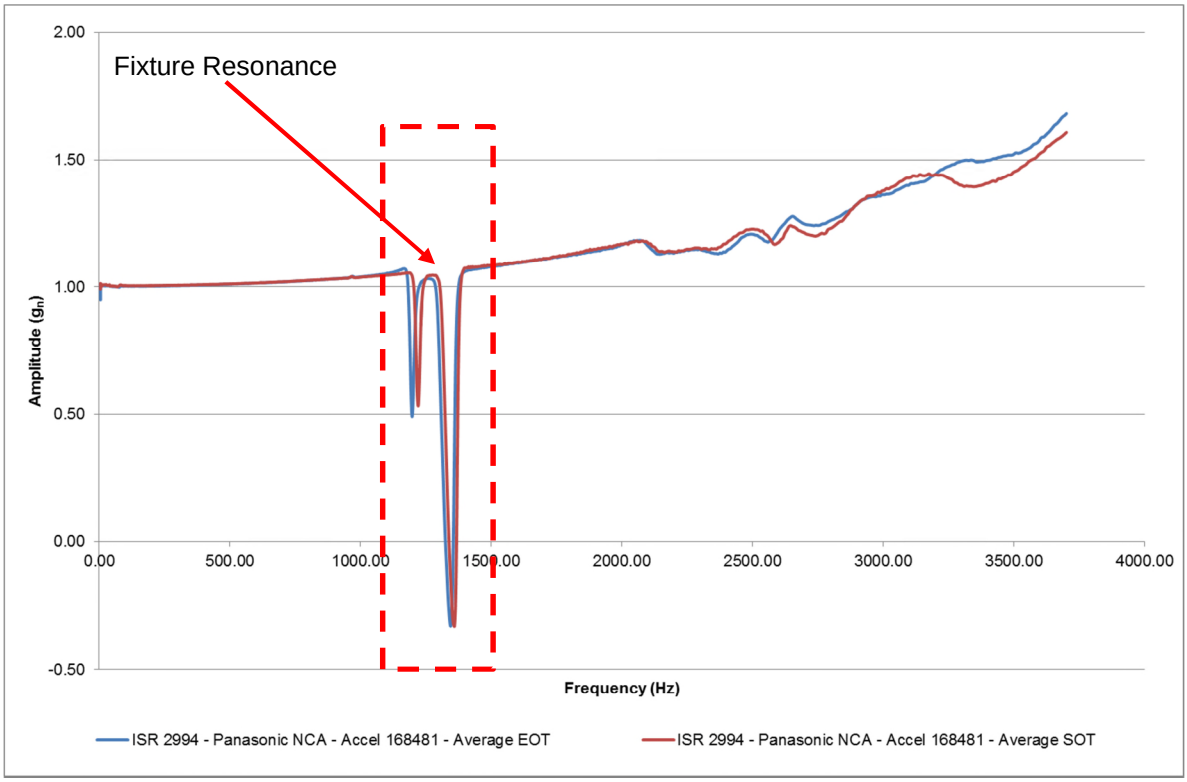

Start and End of Test Frequency Response for ISR 2994 – Z Orientation

Appendix V: Tesla Model S Mode Shapes

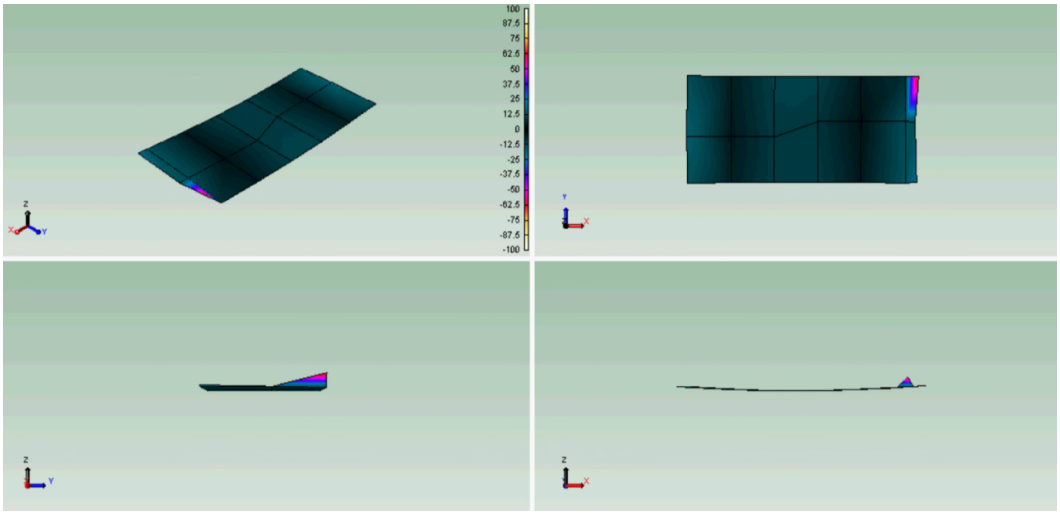

Z Axis Excitation - First Bending Mode

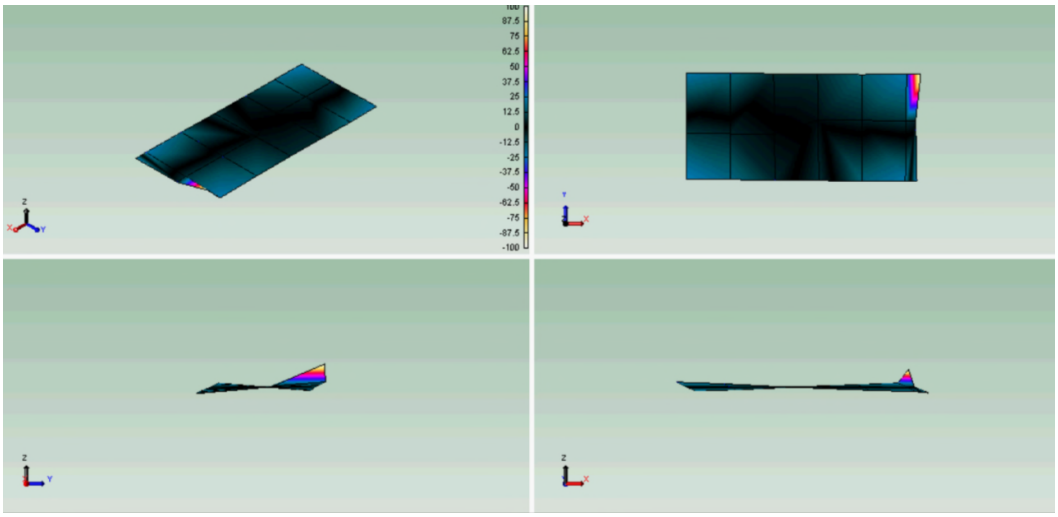

Z Axis Excitation - First Torsional Mode

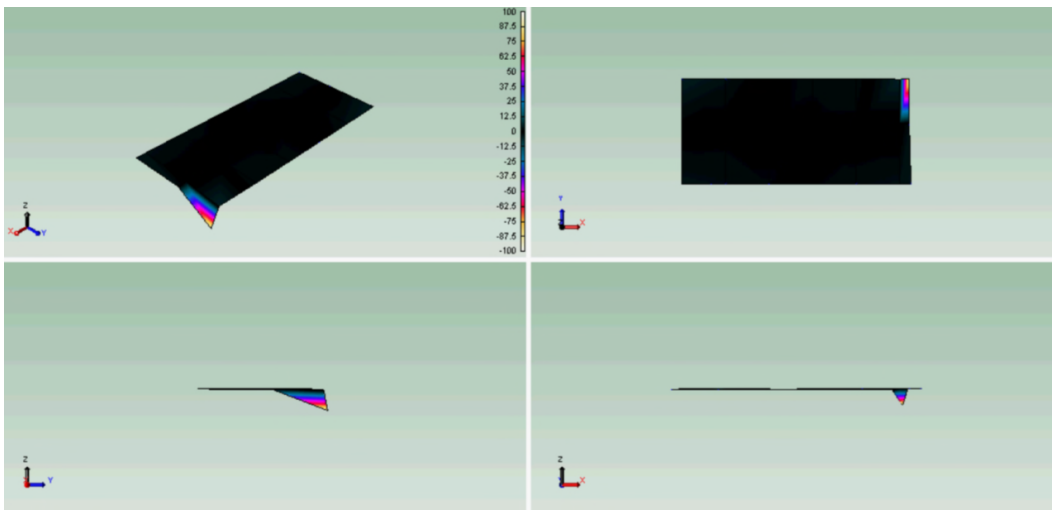

Z Axis Excitation - Localised Bending (Terminal)

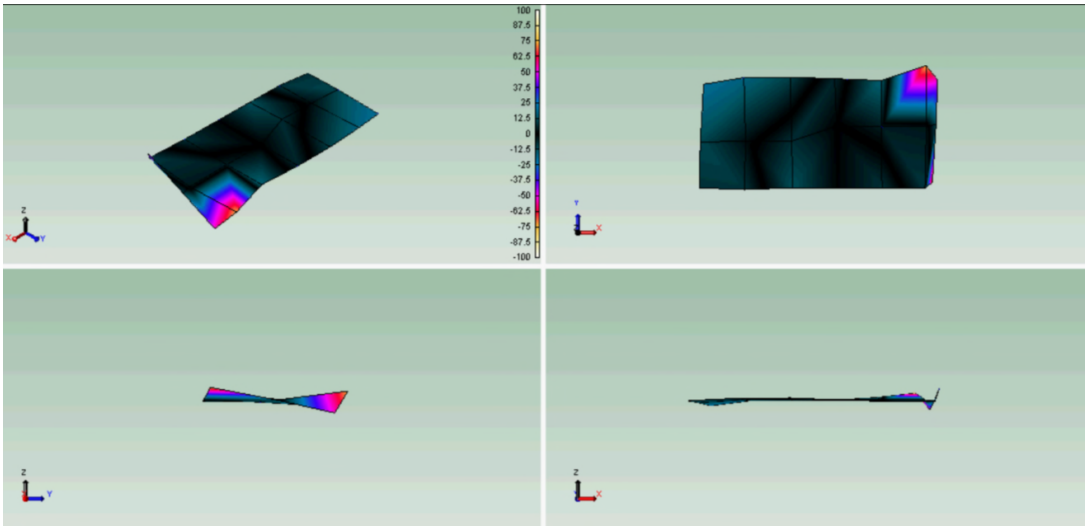

Z Axis Excitation - Second Torsional Mode

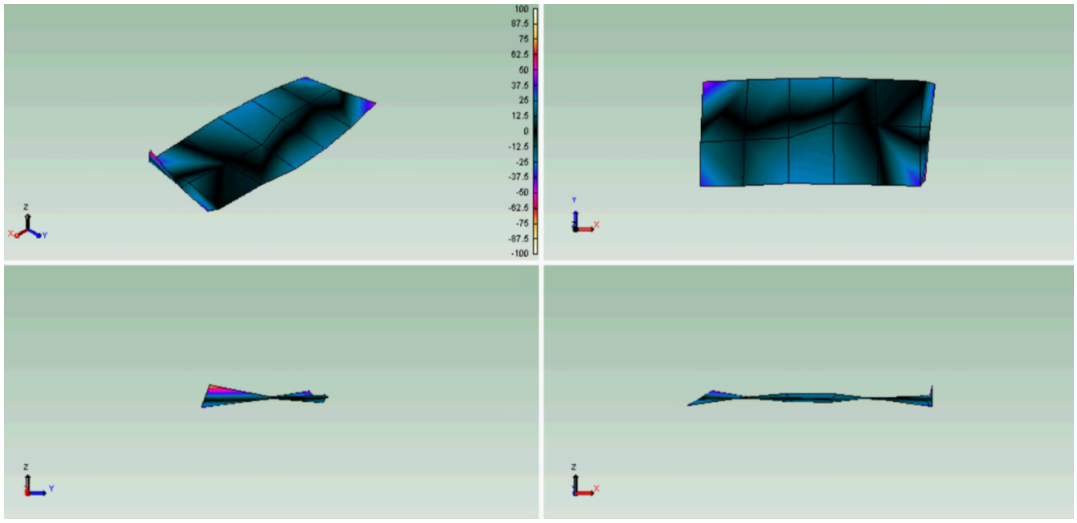

Z Axis Excitation - Third Torsion

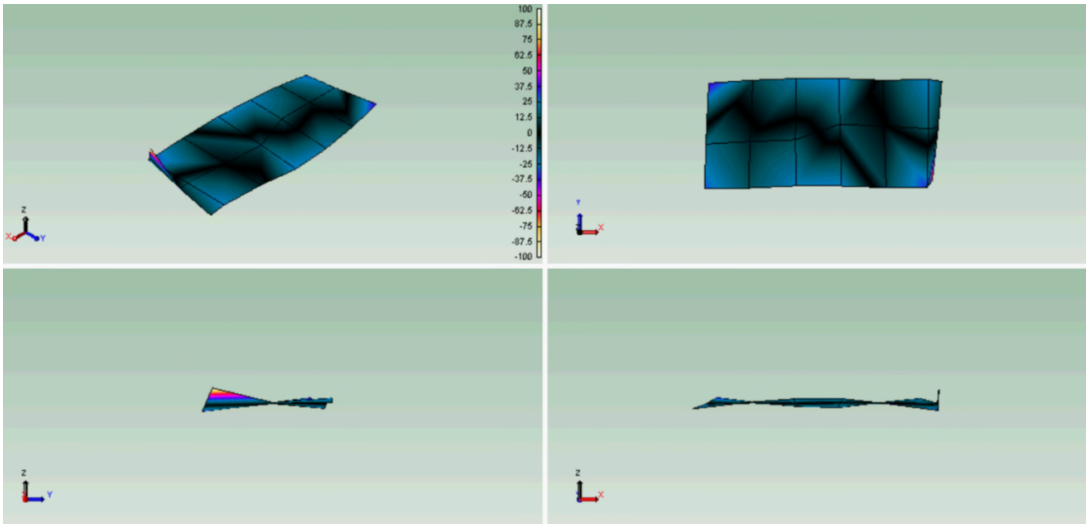

Z Axis Excitation - Forth Torsion

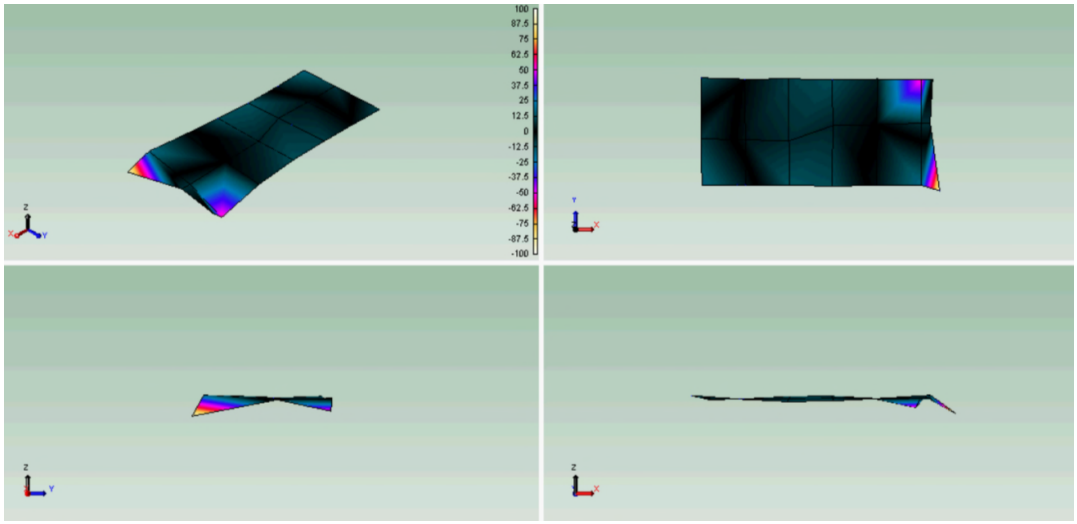

Z Axis Excitation - Combined Torsion and Bending

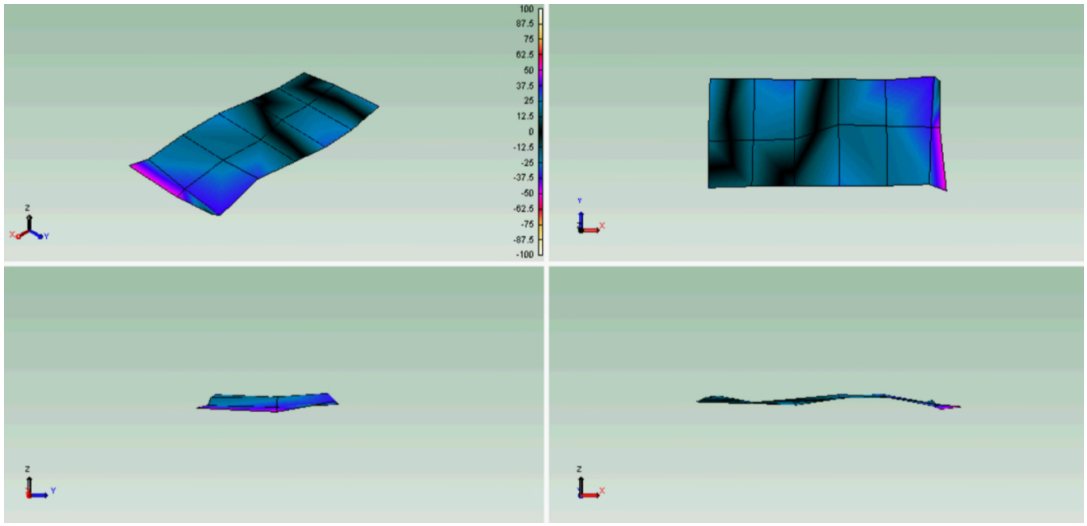

Z Axis Excitation - Second Bending

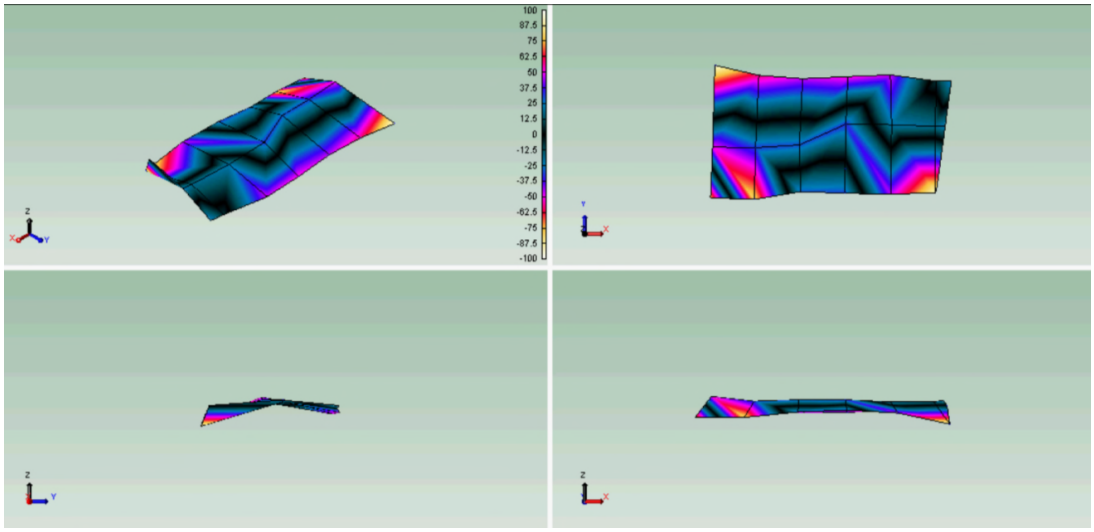

Z Axis Excitation - Combined Torsion and Bending 2

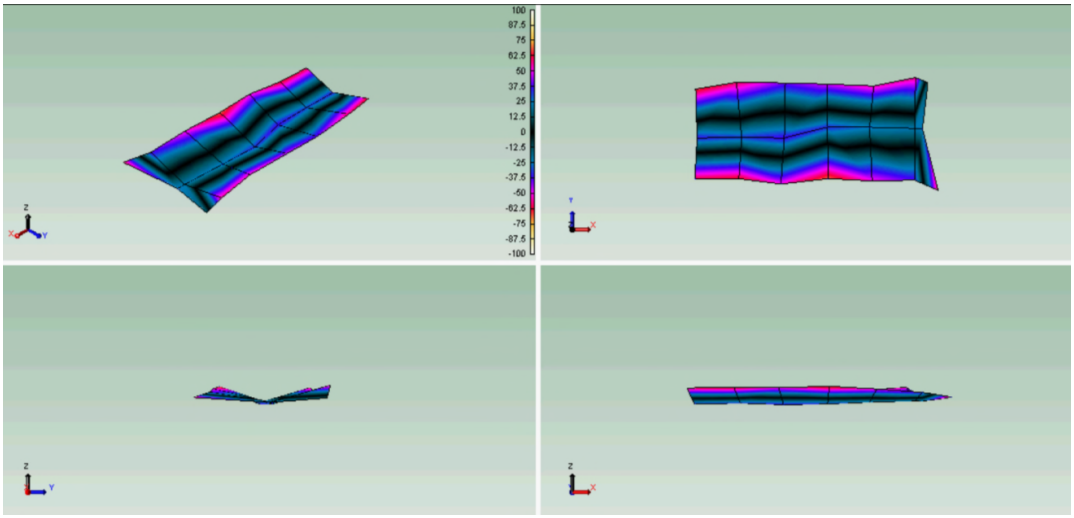

Z Axis Excitation - Combined Torsion and Bending 3